

N° d'ordre :

Année 2005

THESE

Présentée

Devant l'**ECOLE CENTRALE DE LYON**

Ecole Doctorale de Chimie

Pour l'obtention

Du Diplôme de Doctorat

(arrêté du)

Spécialité : **Chimie**

Présenté et soutenue publiquement le 16 Novembre 2005

Par

Mlle Yanxia HOU

<p>ELABORATION ET CARACTERISATION DE BIOFILMS POUR MICRO- ET NANOBIOCAPTEURS OLFACTIFS</p>

Directrice de Thèse : Nicole JAFFREZIC-RENAULT

Commission d'examen composée de :

Pr. Jean-Louis MARTY

Pr. Roland SALESSE

Dr. Hubert PERROT

Pr. Nicole JAFFREZIC-RENAULT

Pr. Aidong ZHANG

Rapporteur

Rapporteur

Directeur de thèse

Co-directeur de thèse

Acknowledgements

First, I wish to express my deep gratitude to my supervisor Prof. Nicole Jaffrezic-Renault, directrice de recherche au CNRS, for accepting me in her group for my thesis and stage during the study for master's degree. I am so grateful for all her kind help, her confidence in me, her gentleness and generosity, as well as for all opportunities she has given me during these years. I will never forget international adventures we had together.

I would like to thank Prof. Aidong Zhang, vice-president in college of chemistry at Central China Normal University, for being co-supervisor of the thesis and initiator of my connection to France, and for all his valuable help. I wish to thank Prof. Claude Martelet for all fruitful discussions and priceless advices during these years. I am grateful to Dr. Abdelhamid Errachid for accepting me in his laboratory for two very interesting stages, for his gentleness, all valuable help and advices as a "grand frère".

I am so grateful to Jean-Louis Marty, professor at Université de Perpignan, Roland Salesse, directeur de recherche au INRA, and Dr. Hubert Perrot, charge de recherche au CNRS, for accepting to judge this work.

Special thanks to all people who gave me kind help during these three years in different laboratories: Monique Lacroix who offers us comfortable working conditions; Dominique Vincentelli (our maman Dominique) who gave me a lot of help; Henri Jaffrezic for his kind help on literature searching and X-ray reflectivity measurements; Bernard Beaugiraud for SEM observations. I would like to thank also Prof. Daniel Tréheux, Denise, Jean-Michel, Thérèse and Dudu (F7), Jean (D5) for their gentleness. Special thanks also to all members in CEGELY, particularly to Laurent Nicolas, Josiane, Philippe, Gilles, Daniel, Laure, Claude, Ricardo, Alice for their kindness and all their help.

I would like to thank all the "Spot-Nosed members", particularly Josep Samitier, Roland Salesse, Edith Pajot, Jasmina Minic, Lino Reggiani, Cecilia Pennetta, Gabiel Gomila, Oscar Ruiz for their kind collaboration and help. I want also to thank Dr. L  ic Briand for his careful correction on the chapter IV in this thesis.

Finally, I want to thank all my friends in laboratories. I will never forget nice moments I had with them. It is from them that I know more about the world and different cultures. They are: my Lebanese friends: Frida, Rita, Walid, Tunisian friends: Saloua, Mouna, Amira, Chaker, Lotfi, Houssine, Ahlem, Omrani, Fadhila, Sonia; Algerian friend Messaoud; Chinese friends: Li Liu, Xuejiang Wang, Zhongzhe Xiao, Kun Peng, Fusheng Sui; Dongxiong Ling, Xuguang Lan,

Ukrainian friends: Alexey, Sergei, Valentyna, Slava, Olga, Iryna; French friends: Anne-Laure, Pierrot, Anne-Gaelle, Anne; Brezilian friends: Raquel, Lougas; Vietnamese friends: Höai, Tuan; Cameroonian friend: Temga and all other postdoc and trainees. Special thanks to Saloua for showing me how to manipulate “Voltalab” with great patience, for being always there when I need help, to Chaker for all his help and collaboration.

I would like to take the opportunity to thank all people I know in Barcelona Science Park, in particular, Isabelle for being so kind and also for her nice guide in Coimbra.

To end on my private matters, I want to thank my “French family” for accepting and supporting me with so much love during these years. Very special thanks to Jérôme, who shares all happy and hard moments with me, and supports me unconditionally for my work. Last but not least I would like to thank all my family, particularly my parents who made me who I am and support me to realize my dreams; as well as my sisters Xiaoxia and Yanjie, my little brother Nanjie whom I love so much.

CONTENTS

INTRODUCTION	1
CHAPTER I: BIOSENSORS	5
1. GENERAL INTRODUCTION ON BIOSENSORS	5
1.1. Definition	6
1.2. Classification of biosensors	7
2. IMMOBILIZATION TECHNIQUES.....	8
2.1. Immobilization criteria	8
2.2. Immobilization techniques	9
2.2.1. Adsorption.....	9
2.2.2. Microencapsulation.....	10
2.2.3. Entrapment	10
2.2.4. Cross-linking	12
2.2.5. Covalent binding	13
2.2.6. Langmuir-Blodgett technique.....	13
3. TRANSDUCERS.....	15
3.1. Electrochemical transducers	16
3.1.1. Amperometric	16
3.1.2. Potentiometric.....	17
3.1.3. Conductimetric.....	17
3.1.4. Impedimetric	18
3.1.4.1. Theoretical background.....	18
3.1.4.2. Data presentation	21
3.1.4.3. Application for biosensor	22
3.2. Optical transducers	23
3.3. Calorimetric transducers.....	24
3.4. Piezoelectric transducers.....	25
3.5. Magnetic transducers	26
4. NANOTECHNOLOGY AND BIOSENSORS	27
4.1. Nanostructures for biosensors construction	27
4.1.1. Nanoparticles.....	27
4.1.2. Nanowires, nanofibers and nanorods.....	28
4.1.3. Nanotubes and porous nanostructures	29
4.1.4. Nanoelectrodes and nanoarrays	29
4.2. Microcontact printing	29

5. ELECTRONIC NOSES	32
6. GENERAL OBJECTIVE OF THE THESIS	34
REFERENCES.....	35
 CHAPTER II: TWO IMMOBILIZATION TECHNIQUES: LANGMUIR-BLODGETT AND SELF-ASSEMBLED MONOLAYERS	
1. LANGMUIR-BLODGETT TECHNIQUE	43
1.1. History.....	43
1.2. Langmuir films	44
1.2.1. Amphiphilic molecules	45
1.2.2. Principle of surface tension measurement	46
1.2.3. Instrument.....	48
1.2.4. Surface pressure-molecular area isotherm	48
1.3. Langmuir-Blodgett films.....	49
1.3.1. Principle	49
1.3.2. Type of deposition	50
1.3.3. Transfer ratio	51
1.4. The mixed amphiphile/protein LB films	51
1.4.1. Different methods for preparation of the mixed amphiphile/protein LB films	51
1.4.1.1. Adsorption of proteins under the compressed amphiphile monolayer	51
1.4.1.2. Injection of proteins under the compressed amphiphile monolayer	52
1.4.1.3. Adsorption of proteins under non-compressed amphiphile monolayer.....	53
1.4.2. Structure of the mixed monolayer at the air/water interface.....	54
1.4.3. Application of LB technique for biosensor elaboration	55
2. SELF-ASSEMBLED MONOLAYERS	56
2.1. Introduction	56
2.1.1. Definition of self-assembled monolayers.....	56
2.1.2. Types of self-assembled monolayers on electrode	56
2.1.3. Advantages of self-assembled monolayers.....	57
2.2. Preparation of self-assembled monolayers	58
2.2.1. Preparation of SAMs on gold substrates	58
2.2.1.1. Pretreatment of gold substrates	58
2.2.1.2. Formation of the SAMs on gold substrate	60
2.2.2. Pretreatment and formation of SAMs on silver substrates.....	61
2.3. Kinetics and mechanism of formation of SAMs	62
2.4. Structure of SAMs on gold and silver substrate	63
2.5. Protein immobilization by SAMs.....	63
2.5.1. Protein modification	64
2.5.2. Substrate modification	65
2.5.2.1. Non-covalent binding.....	66

2.5.2.2. <i>Cross-linking</i>	66
2.5.2.3. <i>Direct covalent attachment</i>	66
2.5.2.4. <i>Direct affinity attachment</i>	68
2.6. Application of SAMs to biosensor elaboration	69
3. CHARACTERIZATION OF SAMs AND LB FILMS	70
REFERENCES	73
 CHAPTER III: ELABORATION OF AN IMPEDIMETRIC IMMUNOSENSOR BY LANGMUIR-BLODGETT TECHNIQUE	 78
1. GENERAL INTRODUCTION ON ANTIBODY IgG	78
1.1. Structure of antibody IgG	78
1.2. Antibody specificity and affinity	79
1.3. Kinetics of antibody-antigen interaction.....	80
2. STUDY OF MIXED LANGMUIR-BLODGETT FILMS OF IMMUNOGLOBULIN G/AMPHIPHILE AND THEIR APPLICATION FOR IMMUNOSENSOR ENGINEERING	82
2.1. Introduction	83
2.2. Materials and methods	84
2.2.1. Biomaterials and chemicals.....	84
2.2.2. The fabrication of silver substrate	85
2.2.3. Self-assembled monolayers and modification of silver substrates.....	85
2.2.4. Langmuir-Blodgett films	86
2.2.5. Impedance measurements	87
2.3. Results and discussion	87
2.3.1. Adsorption of antibody IgG to amphiphile monolayer at the air/water interface.....	87
2.3.2. Surface pressure-molecular area isotherms	90
2.3.3. The stability of the mixed IgG/amphiphile monolayer	92
2.3.4. Impedance measurements	95
2.4. Conclusion	97
REFERENCES	98
 CHAPTER IV: ELABORATION OF AN ODORANT BIOSENSOR BASED ON ODORANT-BINDING PROTEINS BY LANGMUIR-BLODGETT TECHNIQUE	 100
1. INTRODUCTION ON ODORANT-BINDING PROTEINS	100
2. STUDY OF LANGMUIR AND LANGMUIR-BLODGETT FILMS OF ODORANT-BINDING PROTEIN/AMPHIPHILE FOR ODORANT BIOSENSORS	103
2.1. Introduction	104
2.2. Materials and methods	106
2.2.1. Materials	106
2.2.2. Gold substrate and monolayer preparation	106

2.2.3. Langmuir and Langmuir-Blodgett films.....	107
2.2.4. Equilibrium with volatile odorant.....	108
2.2.5. Langmuir-Blodgett films characterization	109
2.2.5.1. <i>Scanning Electron Microscopy</i>	109
2.2.5.2. <i>Atomic Force Microscopy</i>	109
2.2.6. Electrochemical Impedance Spectroscopy	109
2.3. Results and discussion	110
2.3.1. Adsorption of protein at the air/water interface.....	110
2.3.2. Surface pressure-molecular area isotherms	111
2.3.3. Stability of the mixed protein/amphiphile monolayer	114
2.3.4. Transfer of Langmuir-Blodgett films	115
2.3.5. Characterization of Langmuir-Blodgett films for odorant biosensor applications	117
2.3.5.1. <i>Atomic force microscopy</i>	117
2.3.5.2. <i>Non Faradaic electrochemical impedance spectroscopy</i>	119
2.4. Conclusion	122
REFERENCES.....	124
 CHAPTER V: DEVELOPMENT OF A NEW IMMOBILIZATION TECHNIQUE BASED ON SELF-ASSEMBLED MULTILAYER FOR G PROTEIN-COUPLED RECEPTORS	 127
1. INTRODUCTION ON RHODOPSIN.....	127
1.1. Vision	127
1.2. Structure of rhodopsin	129
2. IMMOBILIZATION OF RHODOPSIN ON A SELF-ASSEMBLED MULTILAYER AND ITS SPECIFIC DETECTION BY ELECTROCHEMICAL IMPEDANCE SPECTROSCOPY	131
2.1. Introduction	132
2.2. Materials and methods	133
2.2.1. Biomaterials and chemicals.....	133
2.2.2. Fabrication and pre-treatment of gold substrate	134
2.2.3. Formation and deposition of LB films of rhodopsin	135
2.2.4. Preparation of self-assembled multilayer	135
2.2.5. Electrochemical measurements	136
2.2.6. Atomic force microscopy	136
2.3. Results and discussion	136
2.3.1. Study of Langmuir films of rhodopsin	136
2.3.1.1. <i>Characteristics of rhodopsin monolayer at the air/water interface</i>	136
2.3.1.2. <i>Stability of rhodopsin monolayer at the air/water interface</i>	137
2.3.2. Study of self-assembled multilayer formation.....	139
2.3.2.1. <i>Electrochemical characteristics of self-assembled multilayer formation by CV</i>	139
2.3.2.2. <i>Electrochemical characteristics of self-assembled multilayer formation by EIS</i>	140

2.3.2.3. <i>Self-assembled multilayer formation characterized by AFM</i>	143
2.3.2.4. <i>Recognition properties of the self-assembled multilayer</i>	144
2.4. Conclusion	147
REFERENCES	148
 CHAPTER VI: A NOVEL DETECTION STRATEGY OF ODORANTS BASED ON	
OLFACTORY RECEPTORS IMMOBILIZED ON IMPEDIMETRIC BIOSENSORS 151	
1. INTRODUCTION ON OLFACTORY RECEPTORS	151
1.1. Smell	151
1.1.1. Olfactory system.....	152
1.1.2. Olfactory signal transduction	152
1.2. OR I7 and structural characteristics of its specific ligands	153
2. A NOVEL DETECTION STRATEGY FOR ODORANT MOLECULES BASED ON A CONTROLLED	
BIOENGINEERING OF RAT OLFACTORY RECEPTOR I7	155
2.1. Introduction	156
2.2. Materials and methods	157
2.2.1. Biomaterials and chemicals.....	157
2.2.2. Preparation of odorant solutions	158
2.2.3. Experimental setup.....	158
2.3. Results and discussion	158
2.3.1. Efficiency of binding bioreceptor OR I7	159
2.3.2. Detection of odorants	162
3. MICROELECTRODE	166
3.1. Microelectrode 1	166
3.1.1. Structure of the microelectrode 1	166
3.1.2. Electrochemical characteristics of the microelectrode 1	166
3.2. Microelectrode 2	168
3.2.1. Structure of the microelectrode 2	168
3.2.2. Electrochemical characteristics of self-assembled multilayer formation on microelectrode	
2 by EIS	168
3.3. Conclusion	169
REFERENCES:	170
CONCLUSION	172
ANNEXES	176
ANNEXE I: CONTACT ANGLE	176
ANNEXE II: ATOMIC FORCE MICROSCOPE	179
ANNEXE III: SCANNING ELECTRON MICROSCOPE	183
ANNEXE IV: LIST OF PUBLICATIONS	185

INTRODUCTION

Biosensors witnessed extraordinary progress over the past 20 years. Due to their advantages such as easy-to-use, robust, rapid, portable, and relatively inexpensive, biosensors can be considered as a potential alternative to conventional analytical techniques. In the more recent years important advances in biotechnology and nanotechnology have taken place, opening a new way to elaborate sensors based on the mimic of the animal sensing system, such as electronic nose, which has potential impact on increasing the quality of life, health and safety of citizens.

This thesis is based on two related projects: “Concerted Action: Biocapteur olfactif” and EC project “single protein nanobiosensor grid array (SPOT-NOSED)” with the aim of elaborating olfactory micro- and nanobiosensors for development of the electronic noses. The overall objective of the thesis is to elaborate and to characterize the biofilms of odorant-binding proteins (OBPs) and olfactory receptors (ORs) on electrode for construction of the olfactory micro- and nanosensors.

A very critical point on elaboration of the biosensor is to choose a proper immobilization technique, by which the bioreceptors retain their recognition properties, their stability, and their specificity. In our study, two types of immobilization techniques: Langmuir-Blodgett (LB) and another one based on self-assembled monolayers (SAMs) were investigated to build up ultrathin films on electrode.

This thesis includes six chapters. In the **chapter I**, after a general introduction on biosensors, we have reviewed immobilization and transduction techniques which are commonly used for elaboration of biosensors. In addition, we have briefly introduced the recent development of nanotechnology and its application on biosensors, as well as electronic noses. In the **chapter II**, we have presented in detail the two immobilization techniques used in this thesis: LB and SAMs, and their application to the construction of biosensors.

In the **chapter III**, as a preliminary study, a commercially available antibody IgG is chosen to study mixed LB films of biomolecule/amphiphile and their possible application on elaboration of biosensor, since antibody/antigen constitute the well known immune

system. In the **chapter IV**, after validation of the technique presented in the **chapter III**, LB technique is applied to construct odorant biosensors based on the mixed odorant-binding proteins/amphiphile LB films which are characterized by Atomic Force Microscopy (AFM) and Electrochemical Impedance Spectroscopy (EIS).

As referred above, the other part of this thesis is to transfer olfactory receptor on solid substrate for elaborating olfactory nanosensor. In **chapter V**, rhodopsin is first studied as a model since it is the only G-protein coupled receptors (GPCRs) whose crystal structure is available. In this part, rhodopsin in its membrane fraction is immobilized on gold electrode either by LB technique or by building up self-assembled multilayer. It is demonstrated that LB technique is not suitable for the immobilization of rhodopsin, however, by self-assembled multilayer rhodopsin can be immobilized efficiently, specifically, quantitatively and stably on the gold electrode. Therefore, in the **chapter VI** we use this new developed method to immobilize olfactory receptors (rat OR I7) on the gold electrode to develop olfactory biosensors. Finally, for the first time, the dose-dependent detection of OR I7 (in its membrane fraction) for odorant molecules is performed by EIS.

(Français)

Ces vingt dernières années témoignent de l'extraordinaire progrès des biocapteurs. Dotés d'avantages certains comme leur facilité d'utilisation, leur robustesse, leur rapidité de réponse, leur portabilité, et leur faible coût, les biocapteurs sont considérés comme une alternative potentielle aux techniques analytiques conventionnelles. Plus récemment, d'importantes avancées en biotechnologie et nanotechnologie ont ouvert la voix à l'élaboration de capteurs imitant le système sensoriel animal, entre autres le nez électronique, avec comme impact potentiel, l'amélioration de la qualité de vie, de la santé et de la sécurité de la personne.

Cette thèse s'appuie sur deux projets, "Action Concertée: Biocapteur olfactif" et projet Européen "single protein nanobiosensor grid array (SPOT-NOSED)", visant à élaborer des micro et nanobiocapteurs olfactifs pour le développement de nez électroniques. L'objectif de ce travail est de réaliser et de caractériser des biofilms des protéines spécifiques d'espèces odorantes et de récepteurs olfactifs sur électrodes pour la réalisation de micro- et nanobiocapteurs olfactifs.

Le principal enjeu dans l'élaboration des biocapteurs est de choisir la technique d'immobilisation appropriée afin que le biorécepteur conserve ses propriétés de reconnaissance, de stabilité et de spécificité. Pour notre étude, nous avons exploré deux types de techniques de transfert de couches ultraminces sur électrodes: couches Langmuir-Blodgett et monocouches auto-assemblée.

Le manuscrit se compose de six chapitres. Le **chapitre I** est une introduction générale aux biocapteurs et une revue des techniques d'immobilisation et de transduction couramment utilisées pour leur élaboration. Nous y introduisons également le récent développement des nanotechnologies appliquées aux biocapteurs ainsi que le nez électronique. Le **chapitre II** décrit les deux types de techniques, LB et SAMs, utilisées pour ce travail ainsi que leur application pour la fabrication de biocapteurs.

Le **chapitre III** présente une étude préliminaire sur l'anticorps IgG, connu et commercialisé, pour valider l'utilisation des couches LB (IgG/amphiphile) pour l'élaboration des biocapteurs. Le **chapitre IV** montre l'application de cette technique LB pour fabriquer un biocapteur d'odorant basé sur des couches mixtes de LB composées d'une protéine spécifique d'espèce odorante et d'un amphiphile et caractérisées par Microscopie à Force Atomique et Spectroscopie d'Impédance Electrochimique.

Les chapitres suivants traitent du transfert de récepteurs olfactifs sur support solide

pour la réalisation d'un biocapteur olfactif. Le **chapitre V** montre l'étude préliminaire sur le seul modèle de GPCRs dont la structure cristalline est connue : la rhodopsine. La molécule dans sa fraction membranaire a été immobilisée sur électrode d'or par la technique LB puis par une technique de multicouche auto-assemblée basée sur les SAMs. Après avoir démontré que la technique LB n'était pas adapté, nous avons développé la seconde technique pour obtenir une immobilisation efficace, spécifique, quantitative et stable. Enfin dans le **dernier chapitre**, nous utilisons cette nouvelle méthode pour immobiliser les récepteurs olfactifs (rat OR 17) sur électrode d'or et pour la première fois la détection des molécules d'odorant par les OR 17 (dans leur fraction membranaire) est réalisée par EIS.

CHAPTER I: BIOSENSORS

1. GENERAL INTRODUCTION ON BIOSENSORS

In 1962, Clark and Lyon reported the elaboration of the first biosensor. (1) They constructed an “enzyme electrode”, comprising immobilized enzymes on an electrochemical detector, and hence a sensor that could respond to the substrate concentration of the enzyme. Since then, the field of biosensors has greatly expanded due to advances in signal transduction technologies and also to huge advances in the receptor technology used for the fabrication of sensing elements. Today, there is an increasing need for more easy-to-use, robust, rapid, portable, and relatively inexpensive technologies as biosensors.

As referred in “Biosensors and bioelectronics 20 years on” by Turner (2), in 1985, the world market for biosensors was \$ 5 millions and today it is a little over \$ 5 billions. Most of this three orders of magnitude growth has been in the field of home blood glucose monitors. Newman and Turner have reviewed the commercial developments in the home blood glucose biosensors. (3) Publication in the field of biosensors has apparently lagged behind the strong commercial growth of the sector as measured in dollars but has still shown a forty fold increase in activity in the field over the past 20 years. A simple search of the ISI Web of knowledge using the term biosensor(s) shows 35 hits for 1985 and 1391 for 2005. On the website of science direct 5490 articles can be found searching with the term of biosensor.

The extraordinary success of this subject must surely be due to the strategic nature of this type of research, which combines imaginative fundamental studies with a clear practical objective to improve quality of life. A further attraction is the multidisciplinary nature of work in this area, which demands not only chemistry, physics, biology, and engineering skills, but full understanding of the application areas of biosensors in health care, pharmaceuticals, food and process control, environmental monitoring, defence and security.

1.1. Definition

Biosensors are analytical devices containing immobilized biological sensitive materials in contact with or integrated within a transducer, which ultimately converts a biological signal into a quantitatively measurable electrical signal.

From the concept we can see that a biosensor is composed of two essential components: a bioreceptor and a transducer. Figure I.1 shows schematic view of a biosensor.

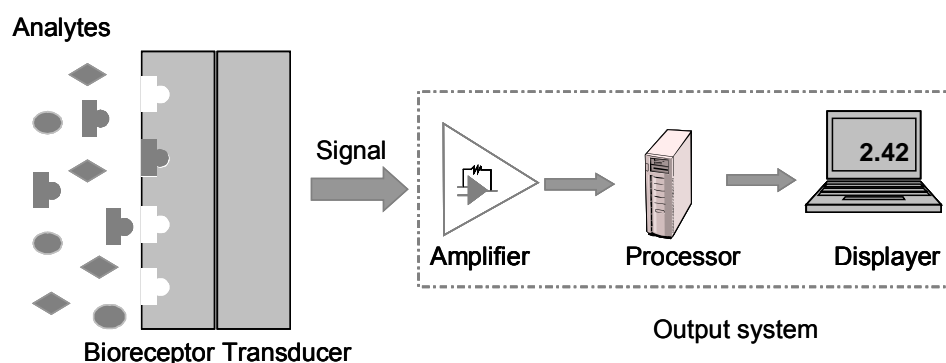


Figure I.1: Schematic view of a biosensor.

A bioreceptor is the most ultimate component of a biosensor. It is responsible for the selective recognition of the analytes, generating the physicochemical signal monitored on the transducer. Ultimately, it determines the sensitivity of the device. There is a wide range of naturally produced molecules from plants, animals, and microorganisms that can be used as the receptor in biosensors elaboration.

Receptors	Transducers
Enzymes	Optical
Antibodies	Electrochemical
Organelles	Thermometric
Cell receptors	Piezoelectric
Tissues	Magnetic
Microorganisms	
Nucleic acids	
Synthetic receptors	

Table I.1: Fundamental components used for biosensor construction.

A transducer is the another crucial component for the biosensor, which converts a specific biological response to an useful electronic output, and must also be suitable for the receptor immobilization on, or close to, its surface. The output system involves amplifying, processing and displaying the signal in an appropriate format. In the Table I.1, the most frequently used sensing elements and transducers in the construction of biosensors are listed.

1.2. Classification of biosensors

Biosensors can be classified according to three criteria:

- the bioreceptor type, e.g. an immunosensor, enzyme biosensors, etc.,
- the physics of the transduction process, e.g. an impedimetric sensor, amperometric biosensors, optical biosensors, etc.,
- the application field, e.g. a medical biosensor.

Sometimes a combination of the first two elements is used, e.g. impedimetric immunosensor.

2. IMMOBILIZATION TECHNIQUES

For designing a biosensor, the biological component has to be properly attached to the transducer. This process is known as immobilization. One key point in biosensor fabrication is the development of immobilization technologies for stabilizing biomolecules and tethering them to surfaces. The usual aim is to produce a thin film of immobilized biologically active material on or near the transducer surface which responds only to the presence of one or a group of materials or substances requiring detection.

2.1. Immobilization criteria

There are a number of requirements that the immobilization technique must satisfy if biosensors are made for practical uses: (4)

- the biological film must retain substantial biological activity when attached to the sensor surface;
- the biological film must remain tightly associated with the sensor surface while retaining structure and function of the bioreceptor;
- the immobilized biological film should have a long-term stability and durability;
- the biological material must keep high degree of specificity to a particularly biological component.

Some other important factors have to be taken into account for developing a suitable immobilization method. First, the biological films should be assembled by reproducible procedures, and once form, the films should be adaptable to different environments. Second, biosensor sensitivity, which is especially important for an efficient and effective biosensor, depends on both the sensitivity of the detection system and the density of distribution and/or orientation of the biological material close to the sensor surface. Therefore, the immobilization technique should provide the desired distribution and/or orientation of biological molecules on the transducer. Although a high surface density of the bioreceptors is required for a sensitive device, overloading of the surface should be avoided, particularly for affinity-based systems. Since overloading has the potential for blockage or inactivation of the active sites of the immobilized biomolecules. Third, uniform layering and structure of the bioreceptor on the sensor surface is critical for production of an optimal biosensor surface. The protein molecules should be attached

to the sensor surface, leaving the active sites exposed. In practice, many biosensors suffer from the non-specific binding. Usually a blocking agent is introduced to eliminate such effect, bovine serum albumin (BSA) is often used for immunosensing applications. Moreover, after immobilization, the bioreceptors should not desorb during the use of the biosensor.

2.2. Immobilization techniques

The commonly used immobilization methods are described as follows. (5, 6)

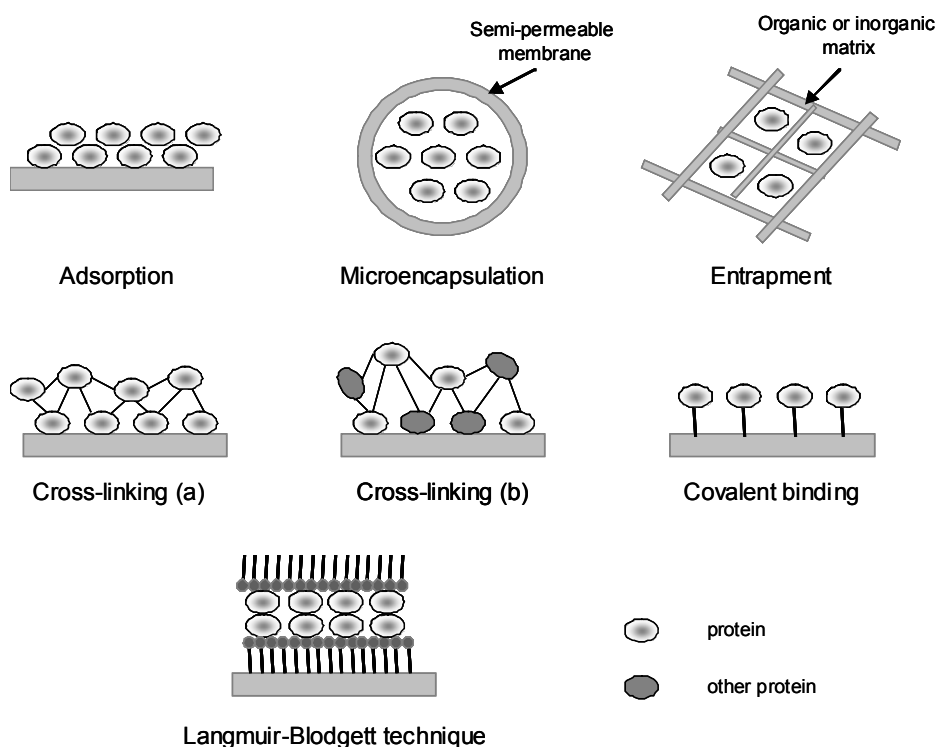


Figure I.2: Immobilization techniques commonly used for elaboration of biosensors.

2.2.1. Adsorption

Adsorption of a bioreceptor from solution onto an insoluble support (or electrode) can proceed via either physical or chemical interactions. Physical adsorption takes place by ionic, polar, hydrophobic forces or van der Waals forces. However, for chemisorption a chemical bond forms by sharing or transferring electron.

Adsorption is a very simple immobilization method and it requires minimal preparation. However, biomolecules immobilized through adsorption exhibit a certain degree of reversibility. With few exceptions, the forces involved in the binding are not very strong. Hence, adsorbed biomaterial is very sensitive to changes in pH, temperature, ionic strength and the substrate. Moreover, irregular distributions of

randomly oriented proteins are commonly observed on the surface. Hence biosensors employing adsorbed biomolecules are mostly insensitive and display a large degree of non-specificity. This method is only suitable for short-term investigations.

2.2.2. Microencapsulation

The biomaterial is held in place behind a membrane, giving close contact between the bioreceptor and the transducer.

Such a method was used in early biosensors. Since the bioreceptor is in the solution, its activity keeps maximal. This method is adaptable and reliable. Unfortunately, its preparation is very complicated, therefore, it is not popular.

2.2.3. Entrapment

An alternative method for the immobilization of the bioreceptors is entrapment in glasses and other inorganic materials using sol-gel methods. In the sol-gel procedure, the biological molecules are entrapped in an aqueous microenvironment in a porous matrix, such as a polymeric oxo-bridged SiO_2 network. The matrices are porous, wet gel is formed by the hydrolysis and condensation-polymerization of metal and semimetal alkoxides, mostly SiO_2 materials (7). The sol-gel has several advantages: it can be performed at room temperature; biomolecules keep their activity as well as their chemical, thermal, and structural stabilities. However, it suffers from low reproducibility and poor spatial control for the bioreceptor deposition.

Another method based on entrapment of the bioreceptor onto the transducer surface is realized by using an electropolymerized film. Since the pioneering work of Foulds and Lowe (8), Umana and Waller (9), Bartlett and Whitaker (10), the immobilization of the biomolecules in electropolymerized films is obtaining increasingly attention and has proven to be well suited for the preparation of biosensors. Recently Serge Cosnier reviewed the biomolecule immobilization on electrode surfaces by electrochemically polymerized films. (11) Most of the electrochemically deposited polymer films used are conducting polymer, e.g. polypyrrole, polyacetylene, polythiophene, polyaniline and polyindole. Among them, polypyrrole and its derivatives play the leading role due to their versatile applicability and the wide variety of molecule (redox) species covalently linked to a pyrrole group. Nevertheless, a few biosensors based on insulating electropolymerized films like polyphenols were also reported. (12)

The biomolecules are usually entrapped in a polymer matrix which grows onto the electrode surface from the solution containing the dissolved monomer

and the biomolecules. The monomer is electrochemically oxidized at a fixed potential giving rise to free radicals. These radicals are adsorbed onto the electrode surface and undergo subsequently a wide variety of reactions leading to the polymer network. The process is governed by the electrode potential and by the reaction time which allows control the thickness of the resulting films.

Recently, Cosnier's team has developed a more sophisticated approach involving the adsorption of amphiphilic monomers and the biomolecules before the electropolymerization. (13) Another interesting alternative involves, initially, the electropolymerization of functionalized conducting polymers, then the attachment of biomolecules to the polymer surfaces by chemical grafting or by affinity of the biomolecules at the functional group. (14, 15) The main advantage of this sequential procedure, namely electropolymerization and covalent or affinity binding, lies in the possibility to optimize the experimental conditions for each step. In particular, the initial formation of polymer films can be performed under conditions (in organic solvent, high potential values for the polymerization process, etc.) which are deleterious for biomolecules.

The elaboration of functionalized polymer films has been investigated either by direct electropolymerization of functionalized monomers or by chemical or electrochemical post-functionalization of deposited conducting polymer films. Schuhmann et al. performed a chemical nitration of a polypyrrole film followed by the electrochemical reduction of the in-situ generated groups, providing a polymer film functionalized by amino groups. Then the biomolecules can be immobilized on the polymer film by covalent binding. (14)

The attachment of the biomolecules to the sensor surfaces can also be achieved via an avidin-biotin bridge. Due to the high affinity of the avidin-biotin interaction ($K_a = 10^{15} \text{ M}^{-1}$), this coupling system has been widely used for the biomolecule immobilization. The formation of biotinylated surfaces has been attempted by electropolymerization of a biotin derivative 1 (Figure I.3) functionalized by a phenol group. (16) The first biosensor based on poly(pyrrol-biotin) films was prepared by oxidative polymerization of the biotin derivative 2. (17) Torres-Rodriguez et al. synthesized an electropolymerizable pyrrole (molecule 3 in Figure I.3) with a biotin linked by a long hydrophilic arm (18), which improves the solubility of monomer in water and facilitates its accessibility to the polymerized biotin groups.

However, when the biomolecules are trapped on sensor surfaces by

polymer matrices, they suffer often from instability, diffusion, aggregation, and inactivation.

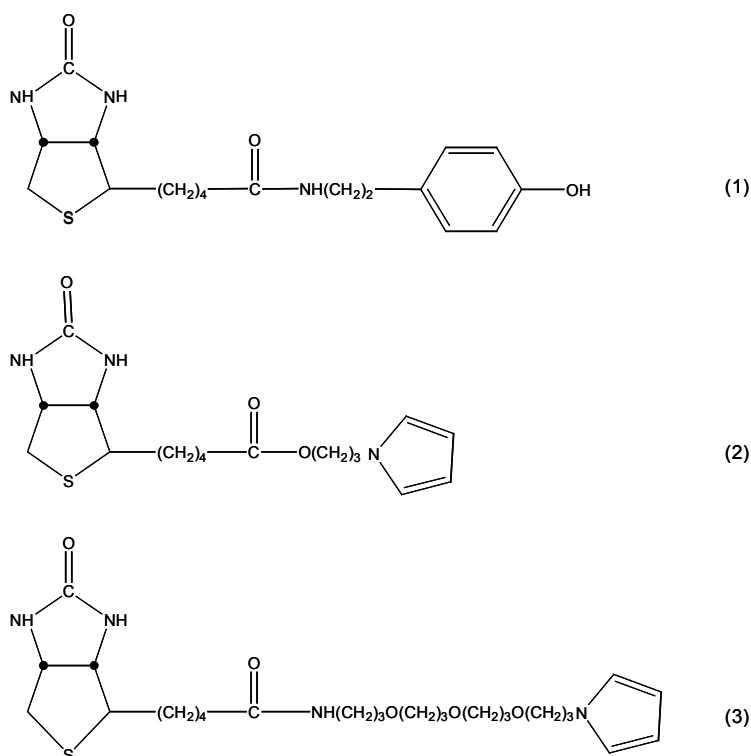


Figure I.3: Structures of the electropolymerizable biotin derivatives.

2.2.4. Cross-linking

With this method, the bioreceptor is intermolecularly crosslinked by bi- or multi-functional reagents. Glutaraldehyde (GA), as the most gentle crosslinking reagent, has been applied with success. The covalent crosslinking occurs because the protein shell contains free amino-groups which may react easily with the bifunctional immobilizing agent.

The protein molecules may be crosslinked with each other (cross-linking a) or with another functionally inert protein (cross-linking b). BSA is usually used as inert protein to dilute the enzyme content in the polymer net in order to enhance the stability and the mechanical properties of the biolayer. The mixture of the enzyme, glutaraldehyde and BSA is placed onto the transducer and then left to dry at room temperature, the cross-linking process will proceed spontaneously.

The advantage of this method is its simplicity as it can be applied on any solid surface. The main drawbacks include: (i) it is difficult to control the reaction; (ii) large amounts of biomolecules are required; (iii) cross-linking can result in multilayers of protein, accordingly, producing low activity of the bioreceptor; (iv) large diffusional

barriers to the transport of the analytes may be resulted.

In order to minimize these drawbacks, Soldatkin et al. optimized the experimental conditions by using glutaraldehyde in a vapour state. The mixed solution of the enzyme and BSA was first deposited on the working ISFET, then the sensor chip was placed in saturated glutaraldehyde vapour for 30 min. Finally, the membranes were dried at room temperature for 10-15 min. (19, 20)

2.2.5. Covalent binding

This method involves a carefully designed bond between a functional group in the bioreceptor and support matrix. Covalent binding of the biomolecules to the surface is a favoured method with minimal loss of the biomolecules. In addition, this method contributes to improve uniformity and reproducibility of the surfaces, and to control density and distribution of the immobilized bioreceptors. A disadvantage of covalent coupling is loss of activities of the biomolecules.

Willner and Katz reviewed the surface functionalization of electrode for covalent binding of enzymes (21). On the one hand, proteins can be covalently bound to the solid support with the availability of functional groups on the surface. For example, metal-oxide materials such as TiO_2 , SnO_2 , In_2O_3 , contain surface hydroxyl groups that are synthetically useful for binding organic materials. Insulating materials, such as SiO_2 , Si_3N_4 can be pretreated to generate the hydroxyl groups. Such a hydroxyl-functionalized electrode can be activated by cyanuryl chloride and subsequently proteins can be linked by amino groups.

On the other hand, carboxylic acid and amine groups directly attached to the support can be used for covalent coupling of complementary amino groups on the lysine residues and carboxylic acid groups of aspartic/glutaric acid residues, respectively. For example, noble metals (Pt, Au, Ag) and insulating substrates (SiO_2 , Si_3N_4) can be functionalized previously by self-assembled monolayers to obtain hydroxyl-, carboxylic acid or amine terminated surface for covalently binding of the proteins.

2.2.6. Langmuir-Blodgett technique

In addition to those mentioned conventional methods, Langmuir-Blodgett technique has been exploited as an useful means of producing well-ordered ultrathin films in which the biomolecules may be immobilized.

Langmuir-Blodgett technique is considered as a desirable

immobilization method for biosensor owing to the advantages: making uniform, ordered and ultra-thin organic films with controllable amount of biocomponents by the number of deposited layers and the packing density of the biological molecules; in addition, preserving the activities and specific recognition properties of the biomolecules. However, since the deposition of LB films on the solid substrate is by hydrophilic and/or hydrophobic interaction, the films are not very stable and are sensitive to the external environment, such as temperature, pH, etc. Usually to overcome this problem, after the deposition of LB films with the biomolecules, the films are stabilized by cross-linking with bifunctional reagent glutaraldehyde.

In practice, the biomolecules are immobilized on the solid surface not only by a single immobilization technique as described above, but also by a combination of different immobilization techniques, just like the combination of LB technique with cross-linking that we have mentioned above.

In this thesis LB and another technique based on self-assembled monolayers were chosen as immobilization methods considering their advantages in elaborating biosensors compared to the other techniques. For example, by these methods the biomolecule deposition can be controlled at molecular level, which is favourable to increase the sensitivity of the biosensors; the biomolecules keep their activities and specific recognition in the ultrathin film; they are economical methods with low biomolecules consumption, they are usually highly reproducible and relatively simple methods. These two immobilization techniques will be described in detail in the Chapter II.

3. TRANSDUCERS

The transducer is a physical element (electrode, optical fibre, quartz crystal, thermistor etc.), which converts the stimulus generated by the bioactive layer, to an electrical signal, amplified by the electronics and converted into analytically useful data. It must be suitable for receptor immobilization on, or close to its surface.

Ideally, the transducer alone is not able to monitor the analyte, but it senses the biochemical event, e.g. formation of the product, or decrease of the reactant concentration. Potential change, electron transfer, light emitted or adsorbed by the product or reactant, heat or mass change etc. can be detected by the transducer. Table I.2 summarizes the principle of transducers and their corresponding output signals used in biosensor construction. In our laboratory the main transduction systems used are electrochemical; in this thesis, electrochemical impedance spectroscopy was chosen as transduction technique. Therefore, electrochemical transducers and their principles are mainly introduced below.

Transducer	Output
<i>Electrochemical (electrode)</i>	
Amperometry	Current
Potentiometry	Voltage
Conductimetry/impedimetry	Conductivity/impedance
<i>Optical (optrodes)</i>	
Colorimetric	Color
Luminescence	Light intensity
Fluorescence	Light intensity
Surface plasmon resonance	Light intensity
<i>Calorimetric</i>	
Thermistor (heat-sensitive sensor)	Temperature
<i>Mass</i>	
Piezoelectric	Frequency shift
Quartz crystal microbalance	Frequency shift
<i>Magnetic</i>	
Paramagnetism	Magnetic field

Table I.2: Principle transduction systems used in biosensor elaboration.

3.1. Electrochemical transducers

Electrochemical transducers are electrodes fabricated with several kinds of materials, such as conductive materials: platinum, gold, glassy carbon, graphite, carbon pastes; insulating materials: SiO_2 , Si_3N_4 ; semiconductive materials: indium tin oxide (ITO) and so on. Biosensors using electrochemical transducers are by far the most commonly reported in the literature (22) and biosensor market has been dominated for many years by electrochemical biocatalytic sensors.

3.1.1. Amperometric

Amperometry is based on measurement of the current resulting from the electrochemical oxidation or reduction of an electroactive species, typically while maintaining a constant applied potential to drive the direction of electron flow to or from the redox molecule to be monitored. The resulting current is directly correlated to the bulk concentration of the electroactive species or their production or consumption rate within the adjacent biocatalytic layer. The first type of biosensor is developed with amperometry and this method is still so popular due to its advantages: simplicity, ease of production, and the low cost of the devices and instrument. Moreover, this method is insensitive to chromogens and sample turbidity, which allows the whole blood samples to be analyzed.

The fundamental measurements system uses three electrodes: a working electrode where the desired reaction occurs, a reference electrode to control the value of the applied potential at this working electrode, and a counter electrode to close the electrochemical circuit.

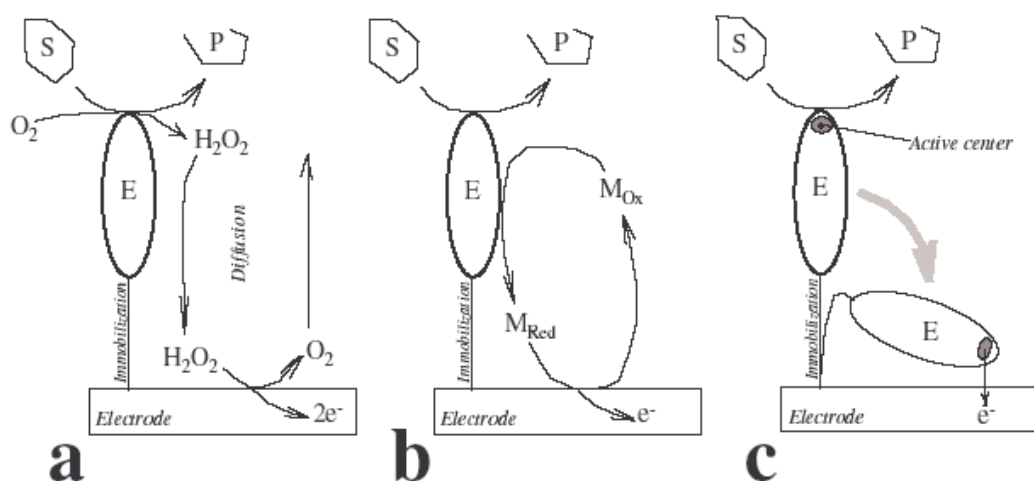


Figure I.4: Three generations of amperometric biosensors based on oxidase. (a): first generation, (b) second and (c) third generation. S – Substrate, P – Product, E – Enzyme. (23)

Since three different electron transfer mechanisms may be observed in amperometric biosensors, three different generations of amperometric biosensors can be constructed, as shown in Figure I.4. The first categories rely on measurement of the product of the enzymatic reaction or on the monitoring of the consumption of the cofactor, i.e. oxygen (see Figure I.4a). The second generation of the amperometric biosensors uses an electron transfer mediator between the enzyme redox center and the electrode surface (see Figure I.4b). Mediators can be inorganic, organic complexes of transition-metals, organic substances and conducting polymers. For the third generation the electron transfer between the active center of the enzyme and the electrode surface can occur directly. Only few enzymes are known to present such a behaviour because the majority of them have the active center surrounded by a “shell” of protein. This shell is a serious barrier for the transfer of electrons.

3.1.2. Potentiometric

A potentiometric sensor operates under conditions of near-zero current flow and measures the difference in potential between the working electrode and the reference electrode. The transducer may be an ion-selective electrode (ISE) which is an electrochemical sensor based on thin films or selective membranes as recognition elements. The output of the potentiometric sensor is a potential difference as a function of time. Potentiometry is less sensitive than amperometry with a detection limit usually being of the order of millimoles.

An important variation of the systems used to determine ion concentrations is the ion-sensitive field-effect transistors (ISFETs). The interest in development of biosensors based on ISFETs is mainly due to their properties: high sensitivity, compatibility with integrated circuit technology, possibility for miniaturisation and multisensing implementations and suitability for large-scale production at a low unit cost. (24)

The operation of an enzyme ISFET is based on the modulation of the gate potential of the ISFET, setting the current through the structure, by pH or ionic change near its surface. This pH or ionic change can be induced by the catalytic reaction in the immobilized enzyme layer on the ISFET surface. In our laboratory a number of investigations based on ISFETs have been performed. (24, 25-28)

3.1.3. Conductimetric

Conductimetric biosensors are based on measuring the time

dependence of the change in conductivity as a result of the receptor recognition of its complementary analyte. The measuring signal reflects the migration of all ions in the biofilm.

A number of investigations have described conductimetric urea sensors. (29-31) In these cases urease immobilized to the electrode surface catalyzes the hydrolysis of urea, which leads to the formation of ammonium, bicarbonate and hydroxide ions. The charged products increase the conductivity of the enzymatic membrane in the vicinity of the sensor surface.

3.1.4. Impedimetric

Electrochemical impedance spectroscopy is a rapidly developing transduction technique for the characterization of biomaterial-functionalized electrodes and biocatalytic transformations at the electrode surfaces. Impedance measurements provide detailed information on resistance/capacitance changes occurring at conductive or semiconductive surfaces. Since only small amplitude perturbing sinusoidal voltage signal is applied to the electrochemical cell, EIS is not destructive for monitoring interfacial phenomena and it was chosen in this thesis as transduction method.

3.1.4.1. Theoretical background

A small amplitude perturbing sinusoidal voltage signal is applied to the electrochemical cell, and the resulting current response is measured. The impedance is calculated as the ratio between the system voltage phase, $U(j\omega)$, and the current phase, $I(j\omega)$, which are generated by a frequency response analyzer during the experiment. The complex impedance can be presented as the sum of the real, $Z_{re}(\omega)$, and imaginary, $Z_{im}(\omega)$, components that originate mainly from the resistance and capacitance of the cell, respectively, as shown in Equation I.1:

$$Z(j\omega) = \frac{U(j\omega)}{I(j\omega)} = Z_{re}(\omega) + jZ_{im}(\omega); \text{ where } \omega = 2\pi f \quad (I.1)$$

Where $j = \sqrt{-1}$, ω and f (excitation frequency) have units of rad.s^{-1} and Hz, respectively.

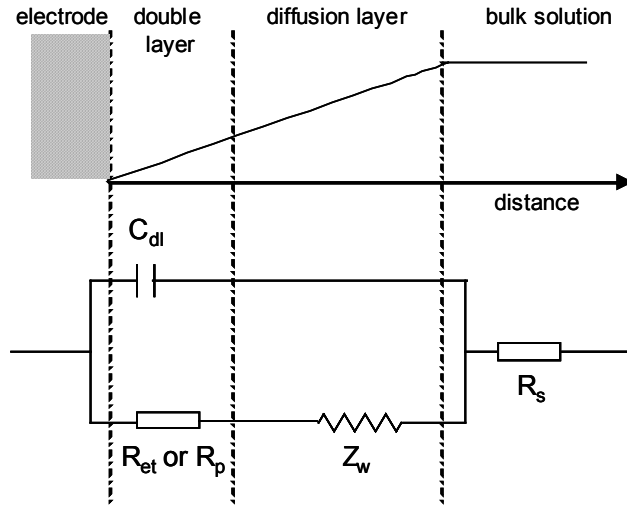


Figure I.5: Electronic equivalent circuit.

Electrochemical transformations occurring at the electrode/electrolyte interface can be modelled by extracting components of the electronic equivalent circuits that correspond to the experimental impedance spectra. A general electronic equivalent circuit (Randles and Ershler model) is shown in Figure I.5. It includes electrolyte resistance R_s ; double layer capacitance, C_{dl} ; electron transfer resistance, R_{et} , which exists when a redox probe is present in the electrolyte solution, or polarization resistance, R_p , which exists when there is no redox probe is present; and the Warburg impedance, Z_w .

(i) Electrolyte resistance

Since all of the current must pass through the electrolyte, uncompensated resistance of the electrolyte solution, R_s , is inserted as a series element in the circuit. It is often a significant factor in the impedance of an electrochemical cell. The resistance of an ionic solution depends on the ionic concentration, type of ions, temperature and the geometry of the area in which current is carried. In a connected electrode with surface area A and length l carrying a uniform current the resistance is defined as Equation I.2:

$$R = \rho \frac{l}{A} \quad (I.2)$$

(ii) Double layer capacitance

When a metal is placed in an electrolyte, a potential is generated owing to the unequal distribution of charge across the interface. Helmholtz suggested that the potential difference lies between two opposite charged layers. The first layer of charges

is located at the metal surface (known as Inner Helmholtz plane) and the second one with equal and opposite charges, is just inside the electrolyte (known as outer Helmholtz plane). This “double layer” of charge existing at the interface behaves as a parallel plate capacitor. This interface capacitance is termed the double layer capacitance C_{dl} . The double layer capacitance depends on the dielectric permittivity introduced into the double charged layer molecules, ϵ_{dl} , for less polar molecules the capacitance should be smaller.

The expression of C_{dl} is given in Equation I.3, where $\epsilon_0 = 8.85 \times 10^{-12} \text{ F m}^{-1}$, it is the dielectric constant of the vacuum, ϵ_p is the effective dielectric constant of the layer separating the ionic charges and the electrode surface, A is the electrode area, and δ is the thickness of the separating layer.

$$C_{dl} = \frac{\epsilon_{dl} A}{\delta} \quad \text{where } \epsilon_{dl} = \epsilon_0 \epsilon_p \quad (I.3)$$

In the equivalent electronic circuit the double layer capacitance can be represented as a sum of a constant capacitance of an unmodified electrode and a variable capacitance originating from the electrode surface modifier. Any electrode modifier of insulating features decreases the double layer capacitance as compared to the pure metal electrode.

When the electrode surface is rough, especially when there are big biomolecules on the surface, the electronic properties of the interface can not be described sufficiently well with a capacitive element, and a constant phase element (CPE) described according to Equation I. 4 is introduced instead of C_{dl} .

$$CPE = A^{-1} (j\omega)^{-n} \quad (I.4)$$

The constant phase element reflects non-homogeneity of the layer, and extent of the deviation from the Randles and Erschler model is controlled by the parameter n in the Equation I.4. The CPE is equivalent to capacitance when $n = 1$.

(iii) Polarisation resistance

Whenever the potential of an electrode is forced away from its value at open circuit, it is referred to as polarizing the electrode. When an electrode is polarized, it can cause current to flow through electrochemical reactions that occur at the electrode surface. The amount of current is controlled by the kinetics of the reactions and the diffusion of reactants both towards and away from the electrode.

(iv) Electron transfer resistance

The electron transfer resistance controls the electron transfer kinetics of the redox probe on the electrode interface. Thus, the insulating modifier on the electrode is expected to hinder the interfacial electron transfer kinetics and to increase the electron transfer resistance.

(v) Warburg impedance

Diffusion of ions to the interface from the bulk of the electrolyte takes place at a finite rate and impedes the current flowing through the electrode system. This impedance created by diffusion, called Warburg impedance. It depends on the frequency of the potential perturbation. At high frequencies the Warburg impedance is small since diffusing reactants do not have to move very far. However, at low frequencies, the reactants have to diffuse farther, therefore, increasing the Warburg impedance.

Among these elements in the electronic equivalent circuits, R_s and Z_w represent bulk properties of the electrolyte solution and diffusion features in solution. Therefore, they are not affected by chemical transformations occurring at the electrode surface. The other two components C_{dl} and R_{et} , depend on the dielectric and insulating features at the electrode/electrolyte interface.

3.1.4.2. Data presentation

A typical shape of impedance spectrum (imaginary part versus real part of impedance) is shown in Figure I.6 presented in the form of an impedance complex plane diagram-Nyquist plot. It includes a semicircle region lying on the axis followed by a straight line. The semicircle portion, at higher frequencies, corresponds to the electron transfer-limited process in Faradaic process, whereas the linear part is characteristics of the lower frequencies range and represents the diffusionally limited electrochemical process.

One of the most important parameters governing the technique is the applied frequencies. At low frequencies, the impedance value is basically determined by the DC-conductivity of the electrolyte solution. At very high frequencies inductance of the electrochemical cell and connecting wires could contribute to the impedance spectra. Thus the analytically meaningful impedance spectra are usually recorded at frequencies where they are mainly controlled by the interfacial properties of the modified electrodes ($10 \text{ mHz} < f < 100 \text{ kHz}$).

However, in the Nyquist plot, when we look at any point on the plot, we can not read at which frequency the point is recorded. Another popular data presentation

for impedance spectra is Bode plot, which contains two graphs: one with the phase of the admittance (the negative phase of the impedance) (φ) on the Y-axis and the logarithmic frequency ($\log_{10}(\omega)$) on the X-axis, the other with the log of the magnitude of the impedance ($\log_{10}|Z(\omega)|$) on the Y-axis and the logarithmic frequency on the X-axis.

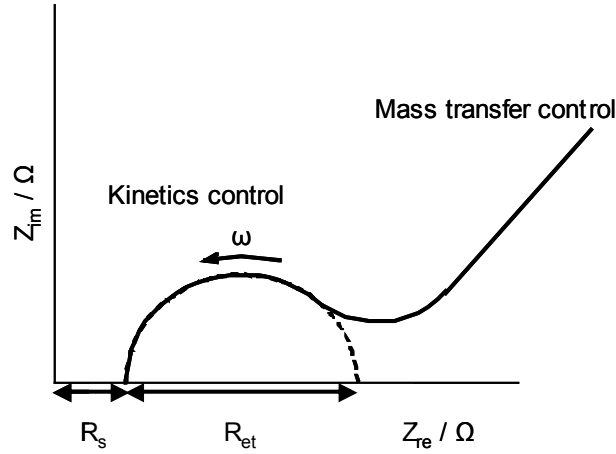


Figure I.6: Impedance spectra presented in the form of a Nyquist plot.

3.1.4.3. Application for biosensor

EIS has been extensively used to various kinds of biosensors, including immunosensors (32-40), DNA-sensors (41-44), and enzyme-based sensors (45). Katz and Willner reviewed recent advances in the application of the impedance spectroscopy to these biosensors. (46, 47) In this thesis EIS was used to study immunosensor system, therefore, here we introduce some problems that we often meet in impedimetric immunosensor.

Electrochemical impedance spectroscopy is an important transduction means of antigen-antibody binding on electrodes. The formation of the complex perturbs the double-charged layer existing at electrode/electrolyte interface, resulting in the increase of its thickness and the insulation of the electrode surface in respect to redox labels added to the solution. This leads to the capacitance change and electron transfer resistance change, respectively.

However, the changes in Faradaic impedance spectrum upon the antigen-antibody complex formation are not always large. If the sensing layer is not well organized and contains many pinholes between the biomolecules, or the redox probe is sufficiently small to freely penetrate through these pinholes, the change observed could be minor. One approach that allows minimize the redox probe penetration through the

pinholes is using a mixed self-assembled monolayer, which can provide better binding of the antigen molecules because the antibody units are diluted and there is less hindrance from the neighbor molecules. (48) Moreover, in the mixed monolayer configuration the impedance measurements do not suffer from the penetration of the redox probe through the pinholes since they are blocked by the non-derivatized thiols. Another method to minimize the penetration of the redox probe makes use of the application of bulky redox molecules such as nicotinamide-adenine dinucleotide (reduced) (NADH), or redox enzymes such as glucose oxidase (GOD). (49)

Another method to amplify the change of the impedance spectra is based on enzyme-labels, which are bound to the components of the immunosensing system. After the antigen-antibody recognition events biocatalytic reactions take place, accordingly, amplify the generated signal. (50-52)

The impedimetric immunosensing can also be amplified by building of an extended network of non-catalytic but very bulky protein molecules after the primary recognition event. Pei et al. used a biotin labelled protein-streptavidin network complex and they found that response signal is really amplified due to the big molecular size of the complex. (53) Moreover, it can be amplified by using enzyme-catalyzed polymer dissolution on the sensing interface. (54, 55) This process results in the decrease of the electron transfer resistance at the sensing interface that is opposite to the formation of the precipitant.

Impedimetric immunosensors suffer often from non-specific adsorption of biomolecules. BSA was often used to co-immobilize in the immunosensing layer in order to eliminate non-specific binding of proteins. (48)

3.2. Optical transducers

Optical transducers use a number of principles, such as the effect of the biological event on light absorption, fluorescence, refractive index, or other optical parameters. These types of transducers become increasingly popular over the last few years due to advantages: their ability to probe surfaces and films in a non-destructive manner; their ability to be miniaturized and so on.

Among them, surface plasmon resonance (SPR) has been receiving continuously growing attention for characterizing and quantifying biomolecular interactions since Nylander and Liedberg demonstrated the application of SPR to gas detection and biosensing in 1982. (56, 57) The main advantages of SPR are real-time

monitoring of binding events and label-free detection of macromolecular interactions. Homola et al. reviewed the developments of the technique and main applications on different fields including biosensing. (58) Earlier works were focused on antigen-antibody interactions (59-63). One of the new areas is the examination of protein-protein or protein-DNA interactions. (64-67)

Surface plasmon resonance occurs under certain conditions when a thin film of metal (gold or silver) is placed inside the laser beam. When the incoming light is monochromatic and p-polarized, the free electrons of the metal will oscillate and absorb energy at a certain angle of incident light. The angle of incidence at which SPR occurs is called the SPR angle. SPR is detected by measurement of the intensity of the reflected light. The refractive index of the sensor surface changes upon binding of macromolecules to the surface. As a result, the SPR wave will change and therefore the angle will change accordingly. There is a linear relationship between the amount of bound material and shift in SPR angle. The SPR angle shift in millidegrees is used as a response unit to quantify the binding of macromolecules to the sensor surface.

3.3. Calorimetric transducers

Thermometric devices operate by measuring enthalpy changes during the biological reaction using one of a range of thermometers, thermopiles (array of thermocouples), or thermistors. Since most reactions include heat producing or consuming, the enthalpy change can be converted to analytical signal to monitor analyte concentrations.

To elaborate a calorimetric biosensor, usually a well thermally insulated column is employed, on which is immobilized the desired enzyme. When substrate flows through the column, the temperature change is monitored by means of strategically placed thermistors and is related to substrate concentration.

In 1974 Mosbach and Danielsson put forward firstly the method of measuring the enzyme reaction using the enzyme thermistor. (68) Harborn et al. evaluated a miniaturized thermal biosensor for the determination of glucose in whole blood. (69) Shimohigoshi et al. developed a novel uric acid and oxalic acid sensors using a bio-thermochip. (70) Zheng et al. elaborated a flow injection calorimetric biosensor for detecting dichlorvos residue. (71) In our laboratory, a glucose sensitive enzymatic thermal sensor was developed based on a pair of commercial microthermal probes by crosslinking the enzymes (glucose oxidase and catalase) with bovine serum albumin

onto the chip surfaces. (72) However, till now calorimetric transducers are not extensively investigated.

3.4. Piezoelectric transducers

Sensors based on piezoelectric principles use the change in the resonant frequency of wave propagation through a piezoelectric material. These principles can be used to measure mass, viscosity, or density changes at the sensor surface.

The use of piezoelectric transducers in biosensors was foreshadowed in the work done by Sauerbrey (1959), who not only pioneered the use of the quartz crystal microbalance (QCM) but thoroughly analysed the physics of the devices. (73) The concern of this work was simply in determining the thickness of thin layers adhering to a surface by microweighing.

QCM consists of a thin disc of AT-cut quartz with thin-film metal electrodes deposited on each face, gold is the electrode choice. With application of an alternating voltage to the electrodes, the crystal oscillates in a thickness shear mode, the plate thickness corresponding to half a wavelength with the crystal faces moving in opposite directions. The resonant frequency is inversely proportional to the crystal thickness. According to the Sauerbrey equation, when the surface of the crystal is subjected to an increase in mass, the change in frequency is given by Equation 1.5:

$$\Delta f = C_Q f^2 \Delta m / A \quad (1.5)$$

Where C_Q is the sensitivity, Δm is the increment of mass, A is the area of the crystal and f is the resonant frequency.

QCMs have traditionally been used in vacuum deposition systems, now they become more and more frequently used in the world of analysis and biosensing, such as gas phase detection, immunosensors, DNA biosensors etc. (74) The first piezoelectric immunosensor was developed by Shons et al. in 1972. In this study the crystal was precoated with nyabar C and BSA and was used to detect BSA antibodies. Since then the field is attracting more and more researchers. All kinds of immobilization techniques have been used to immobilize antibody on crystal surface. Adsorption is a widely used method (75, 76) Protein A and protein G are often used as precoatings to aid antibody immobilization. (77-79) Polymers are also used to immobilize antibody on crystal surface. (80, 81) In addition, Langmuir-Blodgett and self-assembled monolayers were also employed for the elaboration of piezoelectric biosensors. (82-84)

3.5. Magnetic transducers

Magnetic transducer is not as popular as other transduction techniques. However, recently, different kinds of magnetic nanoparticles (Fe_3O_4 , Fe_3S_4 , $\gamma\text{-Fe}_2\text{O}_3$, and various types of ferrites $\text{MeO} \cdot \text{Fe}_2\text{O}_3$, where $\text{Me} = \text{Ni, Co, Mg, Zn, Mn, etc.}$) are increasingly used as powerful and versatile diagnostic tools in biology and medicine.

Richardson et al. developed a magnetic immunoassay technique in which a magnetic field generated by the magnetically labelled targets was detected directly with a magnetometer. (85) Mak et al. developed a high-sensitivity biosensor combining an electrical detection of microbead labelled analytes with a magnetic system for binding strength measurements. (86)

4. NANOTECHNOLOGY AND BIOSENSORS

Today there is a nanotechnology gold-rush. Nearly every major funding agency for science and engineering has announced its own thrust into the field. The actual pioneer of current activities was Nobel laureate Richard Feynman. In 1959 he gave visionary and now often-quoted talk entitled “There’s Plenty of Room at the Bottom”. In this talk he discussed what is possible in principle and anticipated a spectrum of scientific and technical fields that are now well established, such as electron-beam and ion-beam fabrication, nanoimprint lithography, atom-by-atom manipulation etc. His talk has profoundly inspired many of leading scientists in the field of nanotechnology, that’s why we can see Feynman as the father of current nanoactivities.

Nanotechnology involves the study, manipulation, creation and use of materials, devices, and systems typically with dimensions smaller than 100 nm. Nanotechnology is playing an increasingly important role in the development of biosensors. In a research review paper (87) Chen et al. mentioned the advantages that nanotechnology can provide for the construction of biosensors. The use of nanomaterials allows the introduction of many new signal transduction technologies. Due to their submicron dimensions, nanosensors, nanoprobe and other nanosystems allow simple and rapid analyses in vivo. Portable instruments capable of analyzing multiple components are becoming available. Moreover, sensitivity of biosensors can be improved by using nanomaterials.

4.1. Nanostructures for biosensors construction

Various nanostructures have been investigated to determine their properties and possible applications in biosensors. These structures include nanoparticles, nanowires, nanofibers, nanorods, nanotubes and nanostructure self-assembly etc. The application of these nanostructures in elaboration of biosensors will be briefly described here.

4.1.1. Nanoparticles

Functional nanoparticles bound to biomolecules have been used in biosensors to detect and amplify the response signals. Nanoparticles can also be used to enhance the amount of immobilized biomolecules and lower the detection limit of the biosensors. Seydack reviewed application of all kinds of nanoparticles, such as

gold/silver, lanthanides, polymer beads, carbon and organic nanoparticles, to elaboration of optical immunosensors. (88)

Gold nanoparticles are the most stable metal nanoparticles. Nowadays, colloidal gold is readily available with the size in the range of 1-250 nm. Daniel and Astruc gave a review on gold nanoparticles: the discovery, the synthesis, the physical and chemical properties and the application in biology, catalysis, and nanotechnology. (89)

Maxwell et al. developed an optical biosensor by using gold nanoparticles functionalized with oligonucleotide molecules which are labeled with a thiol group at one end and a fluorophore at the other end. (90) Mitchell et al. performed study by using gold nanoparticles to enhance sensitivity and to amplify the signal of SPR biosensing of small molecules. (91)

Moreover, metal nanoparticles have been widely applied to electrochemical biosensors as reviewed by Hernandez-Santos. (92) Cai et al. reported electrochemical DNA biosensors using gold nanoparticle DNA probes. (93, 94) Zhang et al. studied the direct electrochemistry and electrocatalytic behavior of hemoglobin with gold nanoparticles attached to glassy carbon electrode. (95)

4.1.2. Nanowires, nanofibers and nanorods

The electronically switchable properties of semiconducting nanowires provide a direct sensing modality and label-free electrical readout – that is exceptionally attractive for many applications. Devices based on nanowires are emerging as a powerful and general class of ultrasensitive, electrical sensors for the direct detection of biological and chemical species. In a review article entitled “Nanowire, nanosensors” by Patolsky and Lieber, the application of the nanowires to sensors, pH sensing and detection of protein and DNA was discussed. (96) Boron-doped silicon nanowires were reported by Cui et al. for fabricating highly sensitive, real-time electrically based sensors for biological and chemical species. (97)

Sawicka et al. prepared biocomposite nanofibers by electrospinning urease with polyvinylpyrrolidone. (98) And they found the immobilized enzyme remained active. Zhang et al. developed a reagentless uric acid biosensor by immobilizing uricase on ZnO nanorods. (99) By studying direct electrochemistry and thermal stabilities of uricase they reported that the ZnO nanorods derived electrode retained the enzyme bioactivity and can enhance the electron transfer between the enzyme and the electrode.

4.1.3. Nanotubes and porous nanostructures

Recently carbon nanotubes have attracted enormous interest because of their unique structural, mechanical and electronic properties. These properties include high chemical and thermal stability, high elasticity, high tensile strength, and some tubes exhibiting metallic conductivity. (100) There are a number of examples of immobilizing biomolecules onto carbon nanotube modified electrodes for elaborating electrochemical biosensors, including immunosensors, (101) DNA (102-104) and enzyme biosensors (105-107).

In addition to the nanostructures introduced above, novel materials such as porous silicon with pore size compatible with the dimension of the chem.-bio agents have attracted increasing interest for biosensor applications. (108-110) The porous silicon can easily be micromachined, etched, and intergrated with sensor electronics as planar silicon. However, the high internal surface area and the confinement effect of the porous silicon makes the signal per unit area is greatly enhanced. In addition, the stability of a biosensing layer can be greatly enhanced as small molecules can be encapsulated within the porous structure preventing leaching of the biocomponent.

4.1.4. Nanoelectrodes and nanoarrays

With the development of nanotechnology, fabrication of nanometer size objects such as nanoelectrodes and nanoarrays become realizable. These nanoelectrodes and nanoarrays have potential application for the elaboration of electrochemical biosensors. (111-113) In the project "SPOT-NOSED" one of workpackages make an effort to fabricate nanoelectrodes and nanoarrays for elaboration of olfactory nanosensors.

4.2. Microcontact printing

Micro- and nanofabrication are ubiquitous in microelectronics and fabrication of sensors. Microfabrication uses a variety of patterning techniques, the most powerful of these is photolithography. Essentially all intergrated circuits are fabricated using this technology. However, it's known that conventional photolithography is limited by a 100 nm barrier, a critical value in the reduction of feature sizes. Advanced lithography techniques currently being explored as potential substitutes in the regime < 100 nm include extreme UV lithography, soft X-ray lithography, e-beam writing, focused ion beam (FIB), and proximal-probe lithography. These techniques have the capability to generate extremely small features (as small as a few nanometer), but their development

into economical methods for mass-production of nanostructures still requires substantial efforts.

The group of Whitesides developed a set of alternative, non-photolithographic microfabrication methods with soft lithography. These methods share the common feature of using a patterned elastomer as stamp, mold, or mask (rather than a rigid photomask) to generate micropatterns and microstructures. (114) Among them microcontact printing is most widely studied.

Microcontact printing is performed with a relief pattern on the surface of a poly(dimethylsiloxane) (PDMS) stamp to form patterns of SAMs on the surfaces of the substrates by contact. It differs from other printing methods in the use of SAMs to form micropatterns and microstructures of various materials.

The general procedure for μ CP, shown in Figure I.7, involves inking the PDMS stamp with a solution of the surfactant to be printed. As the solvent (typically ethanol) evaporates, the alkanethiolate ink is deposited on the relief structure. The stamp is then brought into conformal contact with a substrate (e.g. gold) for a period ranging from 30 s to several minutes depending on the application. On removing the stamp from surface of the substrate, a pattern is left that is defined by the raised bas-relief structure of the stamp. If required by the application, the rest surface can be filled in with second SAMs simply by dipping the substrate into another alkanethiol solution.

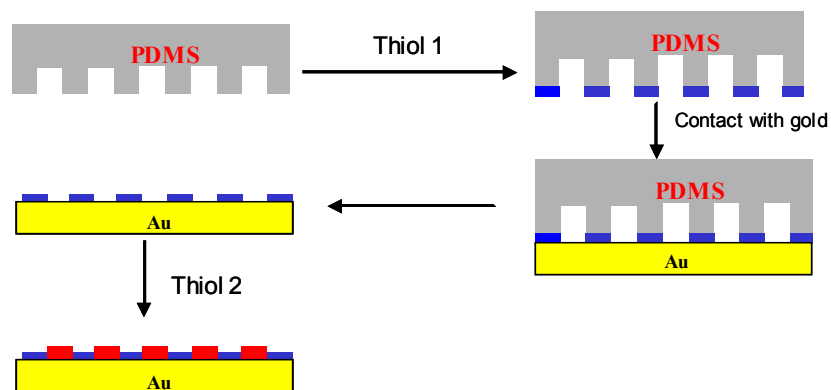


Figure I.7: Schematic procedures for μ CP.

SAMs formed upon the adsorption of omega- substituted alkanethiols on the gold surface, allow control of the surface properties at the molecular scale. μ CP allows SAMs to be patterned, which can generate readily features down to 1 μm in size, and down to 200 nm with difficulty. The convenience, low cost, and widespread application offered by SAMs and μ CP make this combination of the two techniques especially suitable for producing and patterning surfaces relevant to biosensors.

In a review entitled “Patterning self-assembled monolayers using microcontact printing: a new technology for biosensor?” Mrksich and Whitesides predicted the potential application of these techniques to biosensors. (115) In another review Whitesides et al. introduced patterning proteins and cells using soft lithography and they also discussed their application in biosensors. (116)

5. ELECTRONIC NOSES

Today, the human olfactory system is still regarded as the most important “analytical instrument” in many industries to evaluate the flavour of products, such as perfumes, foodstuffs and beverages etc. Although some conventional analytical methods such as gas chromatography and gas chromatography-mass spectrometry are available, they are not only time-consuming, but often inadequate, to some extent.

With the recent development of biotechnology and nanotechnology, biomimetics is now entering the molecular scale. Recently the driving force for research and development in this field is directed towards artificial human senses including electronic noses, eyes, and tongues.

An electronic nose is an instrument that comprises an array of electronic chemical sensors with partial specificity and an appropriate pattern-recognition system, capable of recognition of simple or complex odours. (117) Figure I.8 illustrates the basic components of the human olfactory system and comparison with the construction of an electronic nose. The human olfaction system consists of three essential elements: an array of olfactory receptor cells situated in the roof of the nasal cavity, the olfactory bulb which is situated just above the nasal cavity, and the brain. The electronic nose also has three roughly equivalent elements: the odour sensor array, data pre-processor, and pattern recognition engineering. (118)

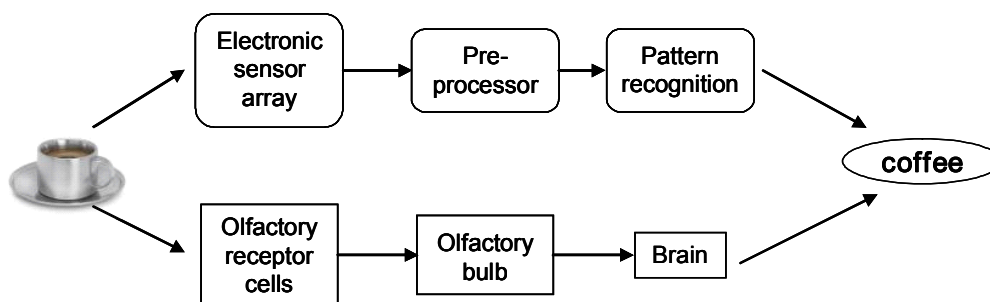


Figure I.8: Diagram showing the three basic elements for an electronic nose and human nose.

The electronic nose represents an exciting area of technology because of its potential applications in many fields. In food processing, electronic noses could be used to monitor food quality and freshness (119-121). In industrial settings, they could be used in process and quality control. In medicine, they could be diagnostic tools (122) and in agriculture, plant growth monitors. In nearly all setting, they could monitor workplace and environmental safety, especially against bioterrorism.

To date, the electronic noses have witnessed great progress. For example, at NASA's Jet Propulsion Laboratory, Dr. Ryan and her team developed an "electronic nose" to monitor air quality on the spacecraft, since trace levels of certain gases can offer early warning of leaks and fire dangers such as overheating electronics. In 1998, they tested the electronic nose on the STS-95 Space Shuttle mission. On that flight, the electronic nose successfully detected ten toxic compounds. (123) However, much more efforts need to be made to increase the quality of our daily life by making use of the electronic noses.

6. GENERAL OBJECTIVE OF THE THESIS

This thesis is based on two related projects: “Concerted Action” and “single protein nanobiosensor grid array (SPOT-NOSED)” formed with the aim at elaborating olfactory micro- and nanobiosensor for development of the electronic noses. Odorant binding proteins and olfactory receptors were chosen as the bioreceptors taking account of their natural properties.

In the project “Concerted Action” we plan to elaborate odorant microbiosensors by using olfactory proteins odorant-binding proteins. The role of our laboratory is to transfer the olfactory proteins on functionalized solid supports and perform detection of odorant molecule by electrochemical measurements such as impedance spectroscopy.

In the European project “SPOT-NOSED” we explore the possibility to develop the first olfactory nano-biosensor array based on the electrical properties of a single olfactory receptor. The nano-biosensor array will integrate a set of nanotransducers, each of which will consist of a functionalized metal nanoelectrode with an anchored olfactory receptor monolayer in between. In order to reach this objective a cross-disciplinary approach is followed in nanolithography, microelectronics, biochemistry and biotechnology. The role of our laboratory in the project is to transfer and characterize olfactory monolayer on micro- and nanoelectrode for construction of olfactory micro- and nanosensors.

In the following chapter, we will present two techniques used in this thesis for transferring olfactory proteins: Langmuir-Blodgett and self-assembled monolayers.

References

- (1) L. C. Jr. Clark, C. Lyon, *Ann. NY Acad. Sci.*, **1962**, 102, 29-45.
- (2) A. P. F. Turner, *Biosensors and Bioelectronics*, **2005**, 20, 2387-2387..
- (3) J. D. Newman, A. P. F. Turner, *Biosensors and Bioelectronics*, **2005**, 20, 2435-2453.
- (4) A. F. Collings, F. Caruso, *Rep. Prog. Phys*, **1997**, 60, 1397-1445.
- (5) K. Wan, Etude de differentes methods de biofonctionnalisation pour la realisation de biocapteurs. Application à la detection de pesticides, Ph.D., *Thesis*, **1999**, Ecole Centrale de Lyon, France.
- (6) M. Provence, Fonctionnalisation de micro-capteurs par la technique de Langmuir-Blodgett application à la detection du glucose, Ph.D., *Thesis*, **1999**, Université Claude Bernard de Lyon, France.
- (7) C. J. Brinker, G. W. Scherer, *Sol-gel Science*, New York Academic, **1990**.
- (8) N. C. Foulds, C. R. Lowe, *J. Chem. Soc. Faraday Trans.*, **1986**, 82, 1259-1264.
- (9) M. Umana, J. Waller, *Anal. Chem.*, **1986**, 58, 2979-2983.
- (10) P. N. Bartlett, R. Whitaker, *J. Electroanal. Chem.*, **1987**, 224, 27-35.
- (11) S. Cosnier, *Biosensors and Bioelectronics*, **1999**, 14, 443-456.
- (12) P. N. Bartlett, D. J. Caruana, *Analyst*, **1992**, 117, 1287-1292.
- (13) S. Cosnier, *Electroanalysis*, **1997**, 9, 894-902.
- (14) W. Schumann, R. Lammert, B. Uhe, H. L. Schmidt, *Sensors and Actuators B*, **1990**, 1, 537-541.
- (15) S. Cosnier, *Electroanalysis*, **1998**, 10, 808-813.
- (16) S. T. Yang, A. Witkowski, R. S. Hutchins, D. L. Scott, L. G. Bachas, *Electroanalysis*, **1998**, 10, 58-60.
- (17) S. Cosnier, A. Le Pellec, *Electrochim. Acta*, **1999**, 44, 1833-1836.
- (18) L. M. Torres-Rodriguez, A. Roget, M. Billon, T. Livache, G. Bidan, *J. Chem. Soc., Chem. Commun*, **1998**, 37, 1993-1994.

- (19) S. V. Dzyadevich, Y. I. Korpan, V. N. Arkhipova, M. Y. Alesina, C. Martelet, A. V. El'Skaya, A. P. Soldatkin, *Biosensors and Bioelectronics*, **1999**, 14, 283-287.
- (20) V. N. Arkhypova, S. V. Dzyadevych, A. P. Soldatkin, A. V. El'skaya, C. Martelet, N. Jaffrezic-Renault, *Biosensors and Bioelectronics*, **2003**, 18, 1047-1053.
- (21) I. Willner, E. Katz, *Angew. Chem. Int. Ed.*, **2000**, 39, 1180-1218.
- (22) J. E. Pearson, A. Gill, P. Vadgama, *Ann. Clin. Biochem.*, **2000**, 37, 119-145.
- (23) M. Pravda, Ph.D., *Thesis*, **1998**, Vrije Universiteit Brussel, Belgium, Chapter II.
- (24) A. P. Soldatkin, J. Montoriol, W. Sant, C. Martelet, N. Jaffrezic-Renault, *Biosensors and Bioelectronics*, **2003**, 19, 131-135.
- (25) Z. Elbhiri, Y. Chevalier, J. M. Chovelon, N. Jaffrezic-Renault, *Talanta*, **2000**, 52, 495-507.
- (26) A. Zhang, Y. Hou, N. Jaffrezic-Renault, J. Wan, A. Soldatkin, J. M. Chovelon, *Bioelectrochemistry*, **2002**, 56, 157-158.
- (27) A. P. Soldatkin, J. Montoriol, W. Sant, C. Martelet, N. Jaffrezic-Renault, *Talanta*, **2002**, 58, 351-357.
- (28) A. P. Soldatkin, V. N. Arkhypova, S. V. Dzyadevych, A. V. El'skaya, J. M. Gravouelle, N. Jaffrezic-Renault, C. Martelet, *Talanta*, **2005**, 66, 28-33.
- (29) D. C. Cullen, R. S. Sethi, C. R. Lowe, *Anal. Chim. Acta*, **1990**, 231, 33-40.
- (30) S. V. Dzydevich, A. A. Shul'ga, A. P. Soldatkin, A. M. Hendji, N. Jaffrezic, C. Martelet, *Electroanalysis*, **1994**, 6, 752-758.
- (31) A. M. Hendji, N. Jaffrezic, C. Martelet, A. A. Shul'ga, S. V. Dzydevich, A. P. Soldatkin, A. V. El'skaya, *Sensors and Actuators B*, **1994**, 21, 123-129.
- (32) M. S. DeSilva, Y. Zhang, P. J. Hesketh, G. Jordan MacLay, S. M. Gendel, J. R. Stetter, *Biosensors and Bioelectronics*, **1995**, 10, 675-682.
- (33) S. Ameer, H. Maupas, C. Martelet, N. Jaffrezic-Renault, H. Ben Ouada, S. Consnier, P. Labbe, *Materials Science and Engineering C*, **1997**, 5, 111-119.
- (34) A. Bardea, E. Katz, I. Willner, *Electroanalysis*, **2000**, 12, 1097-1106.
- (35) H. Gu, A. Yu, H. Chen, *Journal of Electroanalytical Chemistry*, **2001**, 516, 119-126.

- (36) O. Ouerghi, A. Touhami, N. Jaffrezic-renault, C. Martelet, H. Ben Ouada, S. Cosnier, *Bioelectrochemistry*, **2002**, 56, 131-133.
- (37) M. Wang, L. Wang, H. Yuan, X. Ji, C. Sun, L. Ma, Y. Bai, T. Li, J. Li, *Electroanalysis*, **2004**, 16, 757-764.
- (38) D. Tang, R. yuan, Y. Chai, J. Dai, X. Zhong, Y. Liu, *Bioelectrochemistry*, **2004**, 65, 15-22.
- (39) F. Darain, D. S. Park, J. S. Park, Y. B. Shim, *Biosensors and Bioelectronics*, **2004**, 19, 1245-1252.
- (40) I. Navratilova, P. Skladal, *Bioelectrochemistry*, **2004**, 62, 11-18.
- (41) A. Bardea, F. Patolsky, A. Dagan, I. Willner, *Chem. Commun.*, **1999**, (Issue1), 21-22.
- (42) A. Bardea, A. Dagan, I. Willner, *Anal. Chim. Acta*, **1999**, 385, 33-43.
- (43) L. Alfonta, A. Bardea, O. Khersonsky, E. Katz, I. Willner, *Biosensors and Bioelectronics*, **2001**, 16, 675-687.
- (44) Y. Xu, H. Cai, P. He, Y. Fang, *Electroanalysis*, **2004**, 16, 150-155.
- (45) L. Alfonta, E. Katz, I. Willner, *Anal. Chem.*, **2000**, 72, 927-935.
- (46) E. Katz, I. Willner, *Electroanalysis*, **2003**, 15, 913-947.
- (47) J. Guan, Y. Miao, Q. Zhang, *Journal of Biosensing and Bioengineering*, **2004**, 97, 219-226.
- (48) J. Rickert, W. Göpel, W. Beck, G. Jung, P. Heiduschka, *Biosensors and Bioelectronics*, **1996**, 11, 757-768.
- (49) R. Blonder, E. Katz, Y. Cohen, N. Itzhak, A. Riklin, I. Willner, *Anal. Chem.*, **1996**, 68, 3151-3157.
- (50) L. Alfonta, I. Willner, D. J. Throckmorton, A. K. Singh, *Anal. Chem.*, **2001**, 73, 5287-5295.
- (51) E. Katz, L. Alfonta, I. Willner, *Sens. Actuat. B*, **2001**, 76, 134-141.
- (52) H. C. Yoon, H. Yang, Y. T. Kim, *Analyst*, **2002**, 127, 1082-1087.

- (53) R. Pei, Z. Cheng, E. Wang, X. Yang, *Biosensors and Bioelectronics*, **2001**, 16, 355-361.
- (54) C. J. McNeil, D. Athey, M. Ball, W. O. Ho, S. Krause, R. D. Armstrong, J. D. Wright, K. Rawson, *Anal. Chem.*, **2001**, 73, 91-102.
- (55) W. O. Ho, S. Krause, C. J. McNeil, J. A. Pritchard, R. D. Armstrong, D. Athey, K. Rawson, *Anal. Chem.*, **1999**, 71, 1940-1946.
- (56) C. Nylander, B. Liedberg, T. Lind, *Sensors and Actuators*, **1982**, 3, 79-88.
- (57) B. Liedberg, C. Nylander, I. Lundström, *Sensors and Actuators*, **1983**, 4, 299-304.
- (58) J. Homola, S. S. Yee, G. Gauglitz, *Sensors and Actuators B*, **1999**, 54, 3-15.
- (59) D. M. Disley, J. Blyth, D. C. Cullen, H. You, S. Eapen, C. R. Lowe, *Biosensors and Bioelectronics*, **1998**, 13, 383-396.
- (60) G. Sakai, K. Ogata, T. Uda, N. Miura, N. Yamazoe, *Sensors and Actuators B: Chemical*, **1998**, 49, 5-12.
- (61) C. E. H. Berger, J. Greve, *Sensors and Actuators B: Chemical*, **2000**, 63, 103-108.
- (62) D. Song, Y. Mu, X. Liu, L. Zhao, H. Zhang, Q. Jin, *Microchemical Journal*, **2003**, 74, 93-97.
- (63) J. W. Lee, S. J. Sim, S. M. Cho, J. Lee, *Biosensors and Bioelectronics*, **2005**, 20, 1422-1427.
- (64) D. Hao, M. Ohme-Takagi, K. Yamasaki, *FEBS Letters*, **2003**, 536, 151-156.
- (65) P. Y. Tsoi, M. Yang, *Biosensors and Bioelectronics*, **2004**, 19, 1209-1218.
- (66) R. Wang, M. Minunni, S. Tombelli, Marco Mascini, *Biosensors and Bioelectronics*, **2004**, 20, 598-605.
- (67) Y. Sakao, F. Nakamura, N. Ueno, M. Hara, *Colloids and Surfaces B: Biointerfaces*, **2005**, 40, 149-152.
- (68) K. Mosbach, B. Danielsson, *Biochemical and Biophysical Acta*, **1974**, 364, 140-145.
- (69) U. Harborn, B. Xie, R. Venkatesh, B. Lelsson, *Clinica Chimica Acta*, **1997**, 267, 225-237.

- (70) M. Shimohigoshi, I. Karube, *Sensors and Actuators B*, **1996**, 30, 17-21.
- (71) Y. Zheng, T. Hua, D. Sun, J. Xiao, F. Xu, F. Wang, *Journal of Food Engineering*, **2005**, in press.
- (72) V. Lysenko, G. Delhomme, A. Soldatkin, V. Strikha, A. Dittmar, N. Jaffrezic-Renault, C. Martelet, *Talanta*, **1996**, 43, 1163-1169.
- (73) G. Z. Sauerbrey, *Phys.*, **1959**, 155, 206.
- (74) C. K. O'Sullivan, G. G. Guilbault, *Biosensors and Bioelectronics*, **1999**, 14, 663-670.
- (75) R. M. Carter, M. B. Jacobs, G. J. Lubrano, G. G. Guibault, *Anal. Lett.*, **1995**, 28, 1379-1386.
- (76) K. Yun, E. Kobatake, T. Haruyuma, M. Laukkanen, K. Keinanen, M. Aizawa, *Anal. Chem.*, **1998**, 70, 260-264.
- (77) J. S. Boveniser, M. B. Jacobs, G. G. Guilbault, C. K. O'Sullivan, *Anal. Lett.*, **1998**, 31, 1287-1295.
- (78) R. Pei, J. Hu, Y. Hu, Y. Zeng, *Chem. J. Chin. Univ.*, **1998**, 19, 363-367.
- (79) B. S. Attili, A. A. Suleiman, *Microchem. J.*, **1996**, 54, 174-179.
- (80) G. G. Guilbault, B. Hock, R. Schmid, *Biosensors and Bioelectronics*, **1992**, 7, 411-419.
- (81) S. Si, F. Ren, W. Chang, S. Yao, *J. Anal. Chem.*, **1997**, 357, 1101-1105.
- (82) H. Ebato, C. A. Gentry, J. N. Herron, W. Muller, Y. Okahata, H. Ringsdorf, P. A. Suci, *Anal. Chem.*, **1994**, 66, 1683-1689.
- (83) J. Rickert, A. Brecht, W. Gopel, *Biosensors and Bioelectronics*, **1997**, 12, 567-575.
- (84) S. Storri, T. Santorini, M. Minunni, M. Mascini, *Biosensors and Bioelectronics*, **1998**, 13, 347-357.
- (85) J. Richardson, P. Hawkins, R. Luxton, *Biosensors and Bioelectronics*, **2001**, 16, 989-993.
- (86) L. H. Mak, M. Knoll, N. Dankbar, C. Sundermeier, A. Gorschlüter, *Sensors and Actuators B*, **2005**, in press.

- (87) J. Chen, Y. Miao, N. He, X. Wu, S. Li, *Biotechnology Advances*, **2004**, 22, 505-518.
- (88) M. Seydack, *Biosensors and Bioelectronics*, **2005**, 20, 2454-2469.
- (89) M. C. Daniel, D. Astruc, *Chem. Rev.*, **2004**, 104, 293-346.
- (90) D. Maxwell, M. J. Taylor, S. Nie, *J. Am. Chem. Soc.*, **2002**, 124, 9606-9612.
- (91) J. S. Mitchell, Y. Wu, C. J. Cook, L. Main, *Analytical Biochemistry*, **2005**, 343, 125-135.
- (92) D. Hernandez-Santos, M. B. Gonzalez-Garcia, A. C. Garciz, *Electroanalysis*, **2002**, 14, 1225-1235.
- (93) H. Cai, Y. Wang, P. He, Y. Fang, *Analytica Chimica Acta*, **2002**, 469, 165-172.
- (94) H. Cai, C. Xu, P. He, Y. Fang, *J. Electroanal. Chem.*, **2001**, 510, 78-85.
- (95) L. Zhang, X. Jiang, E. Wang, S. Dong, *Biosensors and Bioelectronics*, **2005**, 21, 337-345.
- (96) F. Patolsky, C. M. Lieber, *Materialstoday*, **2005**, 8, 20-28.
- (97) Y. Cui, Q. Wei, H. Park, C. M. Lieber, *Science*, **2001**, 293, 1289-1292.
- (98) K. Sawicka, P. Gouma, S. Simon, *Sensors and Actuators B*, **2005**, 108, 585-588.
- (99) F. Zhang, X. Wang, S. Ai, Z. Su, Q. Wan, Z. Zhu, Y. Xian, L. Jin, K. Yamamoto, *Analytica Chimica Acta*, **2004**, 519, 155-160.
- (100) J. J. Gooding, *Electrochimica Acta*, **2005**, 50, 3049-3060.
- (101) J. N. Wohlstadter, J. L. Wilbur, G. B. Sigal, H. A. Biebuyck, M. A. Billadeau, L. W. Dong, A. B. Fischer, S. R. Gudibande, S. H. Jamieson, J. H. Kenten, J. Leginus, J. K. Leland, R. J. Massey, S. J. Wohlstadter, *Adv. Mater.*, **2003**, 15, 1184-1187.
- (102) J. Li, H. T. Ng, A. Cassell, W. Fan, H. Chen, Q. Ye, J. Koehne, J. Han, M. Meyyappan, *Nano Lett.*, **2003**, 3, 597-602.
- (103) C. V. Nguyen, L. Delzeit, A. M. Cassell, J. Li, J. Han, M. Meyyappan, *Nano Lett.*, **2002**, 2, 1079-1081.
- (104) J. J. Gooding, *Electroanalysis*, **2002**, 14, 1149-1156.
- (105) J. J. Davis, M. L. H. Green, H. A. O. Hill, Y. C. Leung, P. J. Sadler, J. Sloan, A. V.

- Xavier, S. C. Tsang, *Inorg. Chim. Acta*, **1998**, 272, 261-266.
- (106) S. G. Wang, Q. Zhang, R. Wang, S. F. Yoon, J. Ahn, D. J. Yang, J. Z. Tian, J. Q. Li, Q. Zhou, *Electrochem. Commun.*, **2003**, 5, 800-803.
- (107) J. Z. Xu, J. J. Zhu, Q. Wu, Z. Hu, H. Y. Chen, *Electroanalysis*, **2003**, 15, 219-224.
- (108) M. J. Schöning, A. Kurowski, M. Thust, P. Kordos, J. W. Schultze, H. Lüth, *Sensors and Actuators B: Chemical*, **2000**, 64, 59-64.
- (109) C. Steinem, A. Janshoff, V. S. Y. Lin, N. H. Völcker, M. R. Ghadiri, *Tetrahedron*, **2004**, 60, 11259-11267.
- (110) B. Lillis, C. Jungk, D. Iacopino, A. Whelton, E. Hurley, M. M. Sheehan, A. Splinter, A. Quinn, G. Redmond, W. A. Lane, *Biosensors and Bioelectronics*, **2005**, 21, 282-292.
- (111) E. Finot, E. Bourillot, R. Meunier-Prest, Y. Lacroute, G. Legay, M. Cherkaoui-Malki, N. Latruffe, O. Siri, P. Braunstein, A. Dereux, *Ultramicroscopy*, **2003**, 97, 441-449.
- (112) L. Malaquin, C. Vieu, M. Geneviève, Y. Tauran, F. Carcenac, M. L. Pourciel, V. Leberre, E. Trévisiol, *Microelectronic Engineering*, **2004**, 73-74, 887-892.
- (113) G. D. Withey, A. D. Lazareck, M. B. Tzolov, A. Yin, P. Aich, J. I. Yeh, J. M. Xu, *Biosensors and Bioelectronics*, **2005**, in press.
- (114) Y. Xia, G. M. Whitesides, *Annu. Rev. Mater. Sci.*, **1998**, 28, 153-184.
- (115) M. Mrksich, G. M. Whitesides, *Trends in Biotechnology*, **1995**, 13, 228-235.
- (116) R. S. Kane, S. Takayama, E. Ostuni, D. E. Ingber, G. M. Whitesides, *Biomaterials*, **1999**, 20, 2363-2376.
- (117) J. W. Gardner, P. N. Bartlett, *Sensors and Actuators B*, **1994**, 18-19, 211-220.
- (118) M. A. Craven, J. W. Gardner, P. N. Bartlett, *Trends in analytical chemistry*, **1996**, 15, 486-493.
- (119) J. Trihaas, L. Vognsen, P. V. Nielsen, *International Dairy Journal*, **2005**, 15, 679-691.
- (120) T. Rajamäki, H. L. Alakomi, T. Ritvanen, E. Skyttä, M. Smolander, R. Ahvenainen, *Food Control*, **2004**, 17, 5-13.
- (121) S. Ampuero, J. O. Bosset, *Sensors and Actuators B*, **2003**, 94, 1-12.

(122) A. P. F. Turner, N. Magan, *Nature reviews: Microbiology*, **2004**, 2, 161-166.

(123) <http://spaceresearch.nasa.gov>

CHAPTER II: TWO IMMOBILIZATION TECHNIQUES: LANGMUIR-BLODGETT AND SELF-ASSEMBLED MONOLAYERS

1. LANGMUIR-BLODGETT TECHNIQUE

1.1. History

When describing the history of Langmuir or Langmuir-Blodgett films one is bound to start with an American statesman, Benjamin Franklin, who showed the first interest in mono-molecular layers and reported the following to the British Royal Society in 1774: (1)

At length at Clapman where there is, on the common, a large pond, which I observed to be one day very rough with the wind, I fetched out a cruet of oil, and dropped a little of it on the water. I saw it spread itself with surprising swiftness upon the surface; but the effect of smoothing the waves was not produced; or I had applied it first on the leeward fide of the pond, where the waves were largest, and the wind drove my oil back upon the shore. I then went to the windward fide, where they began to form; and there the oil, though not more than a teaspoonful, produced an instant calm over a space several yards square, which spread amazingly and extended itself gradually until it reached the leeside, making all that quarter of the pond, perhaps half an acre, as smooth as a looking glass.

Over one hundred years later Lord Rayleigh suspected that the maximum extension of an oil film on water represents a layer with the thickness of one molecule. At the same time the foundation for our ability to characterize monolayers at an air/water interface was set by Agnes Pockels. She developed a rudimentary surface balance in her kitchen sink, which she used to determine (water) surface contamination as a function of area of the surface for different oils. Publication of Pockels's work in 1891 in *Nature* set the stage for Langmuir's quantitative work on fatty acid, ester and alcohol

monolayers. (2, 3)

Irwing Langmuir was the first one to perform systematic studies on floating monolayers on water in the late 1910's and early 1920's. He investigated the pressure-area relationship of molecules on an aqueous surface. The areas occupied by molecules such as acids, alcohols and esters were found to be independent of the hydrocarbon chain length, thus showing that only the hydrophilic head groups were immersed in the subphase. Langmuir was awarded the Nobel Prize for Chemistry in 1932 for his studies of surface chemistry, using floating monolayers to learn about the nature of intermolecular forces.

Katherine Blodgett, who worked with Langmuir on the properties of floating monolayers, developed the technique of transferring the films onto solid substrates and hence building up multilayer films. These built-up monolayer assemblies are therefore referred to as Langmuir-Blodgett films. The term "Langmuir film" is normally reserved for a floating monolayer at the air/water interface.

Interest in Langmuir-Blodgett films subsided with the outbreak of the Second World War, and remained low until the 1960's when Kuhn and Möbius showed how monolayers could be used to construct precise supermolecular structures. They used the Langmuir-Blodgett technique to demonstrate the fluorescence and quenching of dye molecules attached to fully saturated fatty acids under ultra-violet light. (4) This work and the publication of Gaines' "Insoluble Monolayers at Liquid Gas Interfaces" in 1966 initiated a revival of interest in the field. The first international conference on LB films was held in 1979 and since then the use of this technique has been increasing widely among scientists working on various different fields of research.

1.2. Langmuir films

The formation of Langmuir films consists of two fundamental steps:

(i) Spread

To form a Langmuir film, the surface-active molecule, normally amphiphile, is dissolved in a volatile organic solvent (frequently chloroform or hexane) that will not react with or dissolve into the subphase. A very small quantity of this solution is spread on the surface of the subphase with a micropipette, and as the solvent evaporates, the surfactant molecules spread.

(ii) Compress

Sweeping the barrier over the subphase surface causes the molecules to come closer together and eventually to form a compressed, ordered monolayer.

1.2.1. Amphiphilic molecules

An amphiphile is a molecule that is insoluble in water, with one hydrophilic end, which is preferentially immersed in the water; and the other hydrophobic part, which preferentially resides in the air (or in the nonpolar solvent). (5) With correct 'amphiphatic balance' namely, the balance between the hydrophilic and hydrophobic constituents within the same molecules, such amphiphilic molecules can orient themselves at an air/water interface with their hydrophobic chains upwards in the air and their hydrophilic head groups downwards into the aqueous phase.

The hydrophobic part of amphiphile molecule usually consists of hydrocarbon or fluorocarbon chains, while the hydrophilic part consists of a polar group (-OH, -COOH, -NH₃⁺, -SO₃⁻ etc.). The hydrocarbon chain of the substance used for monolayer studies has to be long enough for formation of an insoluble monolayer. A rule of thumb is that there should be more than 12 hydrocarbons or groups in the chain ((CH₂)_n, n>12). If the chain is shorter, though still insoluble in water, the amphiphile on the water surface tend to form micells. On the other hand, if the chain is too long the amphiphile is prone to crystallize on the water surface, not to form a monolayer at the air/water interface. It should be noted that the solubility of an amphiphile in water depends on the balance between the alkyl chain length and the strength of its hydrophilic part. Abraham Ulman presented the effect of different functional groups on monolayer formation of C16-compounds as shown in Table II.1.

No film	Unstable film	Stable film	Dissolve in water
Hydrocarbon	-CH ₂ OCH ₃	-CH ₂ OH	-SO ₃ ⁻
-CH ₂ I	-C ₆ H ₄ OCH ₃	-COOH	-OSO ₃ ⁻
-CH ₂ Br	-COOCH ₃	-CN	-C ₆ H ₄ SO ₄ ⁻
-CH ₂ Cl		-CONH ₂	-NR ₄ ⁺
-NO ₂		-CH=NOH	
		-C ₆ H ₄ OH	
		-CH ₂ COCH ₃	
		-NHCONH ₂	
		-NHCONH ₃	

Table II.1: The effect of different functional groups on Langmuir film formation with C16-compounds (5).

The amphiphilic molecules used in our study are behenic acid (BA) ($C_{21}H_{43}COOH$) and octadecylamine (ODA) ($C_{18}H_{37}NH_2$). Their chemical structures are shown in Figure II.1.

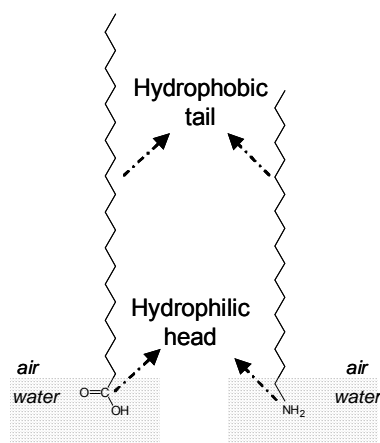


Figure II.1: Chemical structures of BA and ODA, and their spreading at the air/water interface.

1.2.2. Principle of surface tension measurement

Surface tension can be defined as the force required for increase of the surface area isothermally by an unit amount. The presence of surfactants at a air/water interface has a marked effect on the surface tension of water, since the tendency for surfactants to collect at the interface favours expansion of the interfacial area, which is balanced against the tendency for the interface to contract and minimize its surface area.

The measurement of surface tension, associated with Langmuir-Blodgett technique, is realized by a Wilhelmy balance, which is a strip of chromatography paper called Wilhelmy plate. When suspended at the air/water interface, the plate is pulled down into the bulk of the subphase by the surface tension of water.

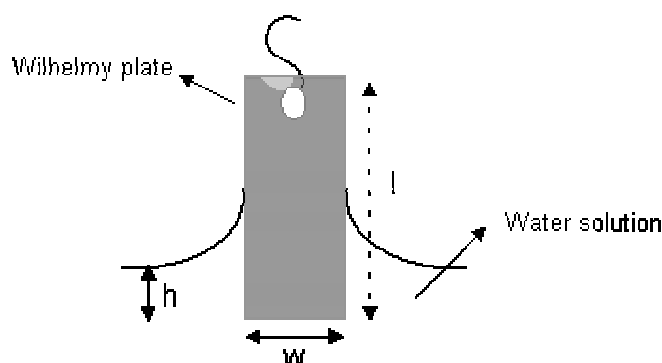


Figure II.2: Tension surface measurement with the Wilhelmy balance.

The forces upon the plate are gravity and surface tension acting downwards into the subphase, and buoyancy due to the displaced water acting upwards.

If the plate has dimensions $l \times w \times t$ (length, width, thickness), a density ρ , and it is immersed in the water to a depth h , then the net force downwards F can be described by the Equation II.1:

$$\text{Force} = \text{weight} - \text{upthrust} + \text{surface tension} \quad (\text{II.1})$$

$$F = \rho g l w t - \rho' g h w t + 2\gamma (t + w) \cos\theta \quad (\text{II.1}')$$

Where g is the acceleration due to gravity, ρ' is the density of the subphase, γ is the surface tension of the surfactant-covered subphase and θ is the contact angle (0° for a completely wetted filter paper). The weight and upthrust terms can be eliminated as the display unit is zeroed before making any measurements, leaving Equation II.2:

$$F = 2\gamma (t + w) \cos\theta \quad (\text{II.2})$$

If the plate is perfectly wetted by the subphase, therefore $\theta = 0$, the equation can be further simplified to Equation II.3:

$$F = 2\gamma (t + w) \text{ or } \gamma = F / 2(t + w) \quad (\text{II.3})$$

With Langmuir-Blodgett technique, it is not the surface tension, but the surface pressure that is measured and registered. Surface pressure π is the difference in surface tension between pure water (γ') and surfactant-covered water (γ). This is expressed as Equation II.4:

$$\pi = \gamma' - \gamma = \Delta F / 2w \quad \text{with } w \gg t \quad (\text{II.4})$$

The compression of the amphiphile layer at the air/water interface decreases the surface tension of the solution, therefore increases the surface pressure. In the Table II.2: surface tension values of different solvents are listed.

Liquid	Surface tension (mN/m)
Water	72.8
Glycerol	63.4
Diiodomethane	50.8
Bromobenzene	40.0
Octanol	27.5
Propanol	21.7

Table II.2: Surface tension values of different solvents.

1.2.3. Instrument

The formation of Langmuir and Langmuir-Blodgett films is performed in a Langmuir trough, which is equipped with a Wilhelmy balance in order to measure surface pressure of the monolayer, one or two moveable barriers to compress the monolayer at the air/water interface, a dipper mechanism permitting to transfer the monolayer onto solid substrate, as shown in Figure II.3. Usually the trough is placed in a chamber in order to prevent external contamination.

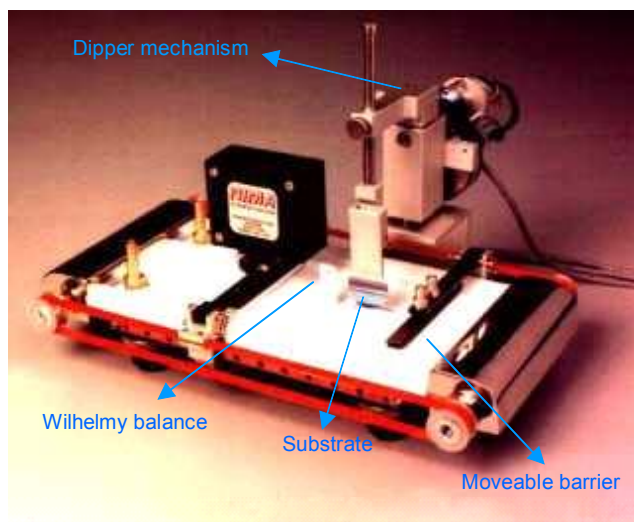


Figure II.3: Langmuir trough produced by NIMA.

1.2.4. Surface pressure-molecular area isotherm

The most important indicator of the monolayer properties is given by measuring the surface pressure as a function of the area of each molecule. This is carried out at a constant temperature and is known as the surface pressure-molecular area isotherm (referred to Π -A). Usually an isotherm is recorded by compressing the film at a constant rate while continuously monitoring the surface pressure. A schematic Π -A isotherm is shown in Figure II.4.

The surface pressure-molecular area isotherm is rich in information on stability of the monolayer at the air/water interface, the reorientation of molecules in the two-dimensional system, phase transitions, and conformational transformations.

A simple terminology used to classify different monolayer phases of fatty acids has been proposed by W. D. Harkins as early as 1952. (6) As the monolayer is compressed, it shows three phases: gas, liquid or solid one.

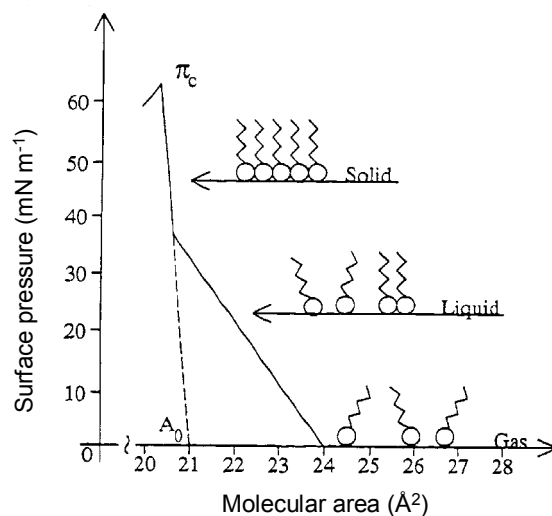


Figure II.4: Schematic Π -A isotherm.

In gas state, the area per molecule is large, and ideally there should be no interaction (lateral adhesion) between the molecules, and therefore, the surface pressure is low.

As the barriers move, the monolayers are compressed, accompanying with the intermolecular distance decrease and the surface pressure increases. A phase transition (from the gas to the liquid state) takes place. In the liquid phase, the monolayer is coherent, and the molecules have more degree of freedom and gauche conformations can be found in the alkyl chains.

When the barriers compress the film further, a second phase transition can be observed, from the liquid to the solid state. In the condensed solid phase, the molecules are closely packed and uniformly oriented. If further pressure is applied on the monolayer, it collapses due to mechanical instability, and consequently a sharp decrease in the surface pressure is observed.

1.3. Langmuir-Blodgett films

1.3.1. Principle

The term “Langmuir-Blodgett film” traditionally refers to monolayers that have been vertically transferred off the water subphase and onto a solid support. Vertical deposition is the most common method of LB films transfer, called Langmuir-Blodgett

technique. An alternative way to deposit the monolayer is the Langmuir-Schaeffer (LS) technique, which differs from the LB technique only in the sense that the solid substrate is horizontally lowered in contact with the monolayer for transferring the monolayer.

The LB deposition is traditionally carried out in the “solid” phase with surface pressure keeping constant. In this case the surface pressure is high enough to ensure sufficient cohesion in the monolayer, so that the monolayer will not fall apart during transfer to the solid support. This also ensures building up of homogeneous multilayers.

When the solid surface is hydrophobic the first layer is deposited during the first down pass. When the solid support is hydrophilic, the first layer will be deposited during the first up-stroke pass. Because the hydrophobic tails are repelled by the hydrophilic support as it is immersed in the water. Once the first layer is deposited, more layers will be deposited on each subsequent pass of the support through the air/water interface. Multilayers can therefore be deposited onto the support.

There are several parameters that can affect quality of LB films:

- Quality of the monolayer at the air/water interface, particularly the stability;
- Properties of the subphase (temperature, ingredient, pH);
- Surface pressure for transferring LB films, namely the target pressure;
- Transfer rate;
- Surface properties of support (cleanliness, surface free energy, chemical composition etc).

In order to deposit successfully LB films onto the support, usually the substrate is previously functionalised to provide favourable platform for the deposition. The pre-treatment of the support will be introduced in the next part of this chapter.

1.3.2. Type of deposition

Different film architectures can be obtained upon the deposition by Langmuir-Blodgett technique (Figure II.5). Y-type multilayers are most common and can be prepared on either hydrophilic or hydrophobic substrates with the reversed head-tail arrangement. They are the most stable architectures because of strong head-head and tail-tail interactions. X-type and Z-type films are fewer reported. In fact, with some

amphiphiles, even when films have been deliberately transferred by an X- or Z- method, the spacing between the hydrophilic headgroups shows a packing similar to that of Y-type films, implying that some molecular reorganization could occur during or shortly after deposition. (7)

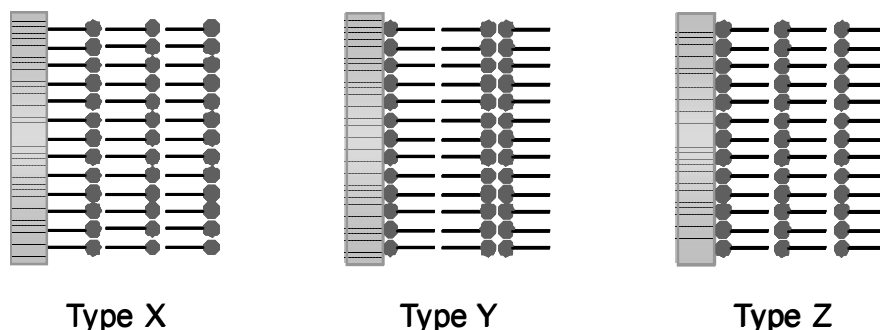


Figure II.5: Possible architectures for Langmuir-Blodgett films.

1.3.3. Transfer ratio

The quantity and the quality of the deposited monolayer on the solid support can be measured by transfer ratio (TR), given by the Equation II.5:

$$TR = A_l / A_s \quad (\text{II.5})$$

Where A_l is the area of monolayer removed from subphase at a constant pressure, A_s is the area of substrate immersed in water. Such a ratio is usually measured for each substrate pass through the air/water interface. For an ideal transfer the TR is equal to 1.

1.4. The mixed amphiphile/protein LB films

Langmuir-Blodgett films have been studied for application in a great variety of domains, such as nonlinear optics, molecular electronics, sensors etc. Since 1980s, extensive researches have been carried out to immobilize biomolecules by LB technique for elaboration of biosensor. Proteins were introduced in the amphiphile monolayer to form a mixed amphiphile/protein LB films. There are several different ways to prepare the mixed amphiphile/protein LB films.

1.4.1. Different methods for preparation of the mixed amphiphile/protein LB films

1.4.1.1. Adsorption of proteins under the compressed amphiphile monolayer

In 1971, Fromherz used this method to make the mixed layer with a multi-compartment Langmuir trough (8). As shown in Figure II.6, in the first compartment, the amphiphile was injected on the subphase of pure water and the monolayer was compressed till the surface pressure in the range of 5 to 30 mN m⁻¹. After that, under a constant surface pressure, the layer was moved towards the second compartment, in which the proteins were present in the subphase. The proteins were adsorbed onto the head groups of amphiphile molecules by electrostatic interaction and the mixed monolayer formed. Finally, the mixed layer was moved to the third compartment with pure water as subphase, where the mixed layer was transferred onto solid supports. Arisawa et al. developed a urea sensor by immobilizing urease onto an ISFET by using of this LB technique. (9)

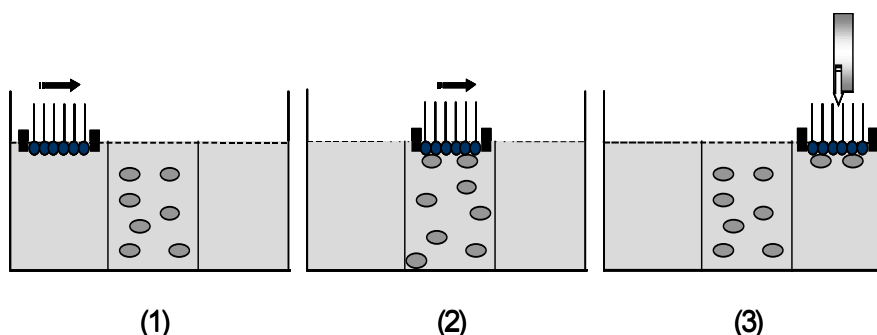


Figure II.6: Formation of the mixed LB films by adsorption of proteins under the compressed amphiphile monolayer.

1.4.1.2. Injection of proteins under the compressed amphiphile monolayer

This method was firstly developed by Zaitsev (10-11), they injected a solution of protein in the water subphase under the amphiphile layer which is previously formed at the air/water interface, as shown in Figure II.7. However, these two methods are poorly reproducible for the formation of the mixed LB films.

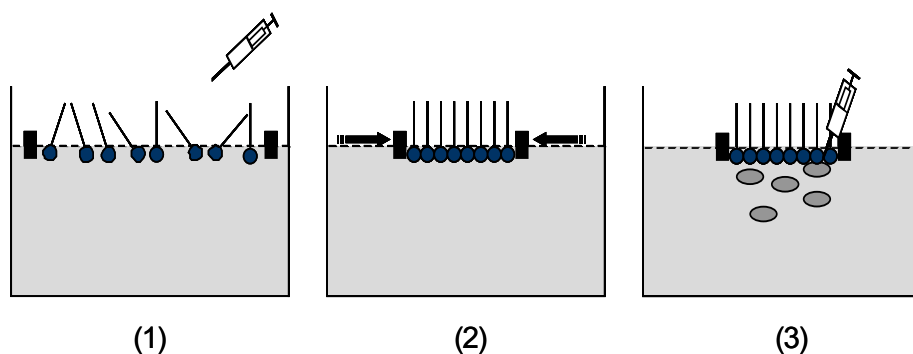


Figure II.7: Formation of the mixed LB films by injection of proteins under the compressed amphiphile monolayer.

1.4.1.3. Adsorption of proteins under non-compressed amphiphile monolayer

The most commonly used method is based on adsorption of proteins under non-compressed amphiphile monolayer. As shown in Figure II.8, firstly, the amphiphile solution is injected on the subphase of protein solution, proteins are gradually adsorbed onto amphiphile layer by the electrostatic interaction. When the adsorption reaches equilibrium, the mixed monolayer is compressed to the target pressure. And finally at this surface pressure the stable mixed layer is transferred onto solid substrates.

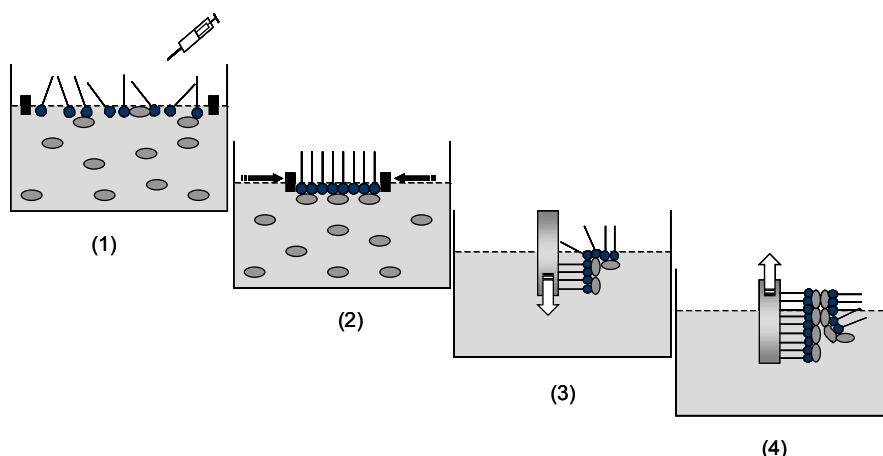


Figure II.8: Formation of the mixed LB films by adsorption of protein under the non-compressed amphiphile monolayer.

Such kind of mixed LB films have been investigated by the group of Valleton (12-20) and our laboratory (21-23). Comparing to the first two methods mentioned above, this method has several advantages: simplicity for obtaining well ordered multilayer of LB films, high reproducibility for depositing of LB films, high homogenous structure of LB films. In this thesis, considering these factors we have chosen this method to form and transfer the mixed LB films for elaborating biosensor.

There are still some other LB methods, which are not commonly used, to elaborate the mixed amphiphile/protein LB films. For example, Girard-Egrot et al. deposited first amphiphile LB films on the substrates, and then immersed the coated substrates in a solution of enzyme glutamate dehydrogenase for adsorption onto amphiphile multilayer. (24-25) Okahata et al. prepared an enzyme-lipid complex in the first step, and then transferred the monolayer of the complex onto a Pt substrate as the sensor membrane. (26)

1.4.2. Structure of the mixed monolayer at the air/water interface

Protein can be adsorbed onto amphiphile monolayer spreaded at the air/water interface by electrostatic interaction between protein and the polar heads of amphiphile molecules. Zaitsev investigated the influence of the electrostatic effect on the adsorption of protein by studying the mixed monolayer of glucose oxidase with different kinds of amphiphiles: phosphatidylcholine (neutrally charged), cetyltrimethylammonium bromide (positively charged) and stearic acid (negatively charged) (27). The results showed that the enzyme GOD, which is negatively charged in buffer solution at pH 7.0, is more strongly adsorbed on positively charged lipid monolayers than on zwitterionic ones, and only slightly adsorbed on negatively charged monolayers of stearic acid.

The dynamic formation and structure of mixed monolayer with BA/GOD at the air/water interface proposed by the group of Valleton is shown in Figure II.9. (18)

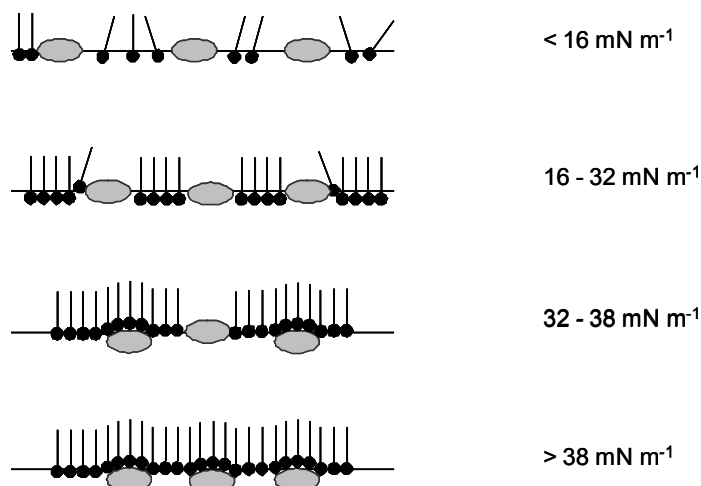


Figure II.9: Dynamic formation and structure of mixed monolayer with BA/GOD at the air/water interface.

The results showed that before spreading the amphiphile behenic acid, the surface pressure was about 2 mN m^{-1} showing that some of enzyme molecules were adsorbed at the air/water interface. Enzyme GOD was allowed to adsorb under the behenic acid film at the air/water interface. It took about 45 min to reach adsorption equilibrium and the surface pressure reached 16 mN m^{-1} . Then the monolayer was compressed at a constant rate, during the compression the surface pressure increased. In the range of surface pressure from 16 mN m^{-1} to 32 mN m^{-1} , the mixed monolayer was thought to be in a liquid phase. With further compression, the enzyme molecules were gradually expelled from the air/water interface and pushed down under the polar heads of BA molecules, the monolayer is considered to reach gradually the solid phase. At a high surface pressure (above 38 mN m^{-1}), the mixed film was constituted of a behenic

acid monolayer in a solid phase, under which GOD sublayer was adsorbed by the electrostatic interaction as shown in Figure II.9.

However, the phase change above 40 mN m^{-1} was not mentioned. If further compression were applied on the mixed monolayer, there would be a risk of overlapping of the layer and even a complete collapse of the monolayer.

1.4.3. Application of LB technique for biosensor elaboration

The quest for biosensors has brought the need for highly selective and sensitive organic layers, with tailored biological properties that can be incorporated into electronic, optical, or electrochemical devices. The molecular dimension of LB films makes the use of even highly expensive molecules economically attractive, therefore, the development of sophisticated detection systems possible. Furthermore, LB technique has other important advantages for elaboration of biosensors as referred in chapter I.

Up to now, LB technique has been widely used to immobilize enzymes (28-36), antibodies (37-44) and DNA (45) etc. on the substrate for the elaboration of various biosensors.

2. SELF-ASSEMBLED MONOLAYERS

2.1. Introduction

2.1.1. Definition of self-assembled monolayers

Self-assembled monolayers are molecular assemblies that are formed spontaneously by the immersion of an appropriate substrate into a solution of a reaction-active surfactant in a suitable solvent.

From the energetics point of view, a self-assembling surfactant molecule can be divided into three parts, as shown in Figure II.10. The first part is the head anchoring group that provides the most exothermic process while anchoring on the substrate surface by the chemisorption. The energy associated with the chemisorption is at the order of tens of kcal/mol (e.g., $\sim 40\text{--}45 \text{ kcal mol}^{-1}$ for thiolate on gold). The second part is the alkyl chain, and the energy associated with its interchain van der Waals interaction is at the order of few (<10) kcal mol^{-1} (exothermic). The third part in the surfactant is the terminal surface group, which determines the surface properties (e.g. wetting, friction, adhesion etc.) of the SAMs functionalized substrate surface. For example, in the case of a simple alkyl chain, the terminal methyl (CH_3) group provides a hydrophobic surface. The ordering of alkanethiol is driven by the strong affinity between the head groups and the substrates, the lateral van der Waals interactions between the tethered alkyl chains, and the dipole interactions between the polar end groups.

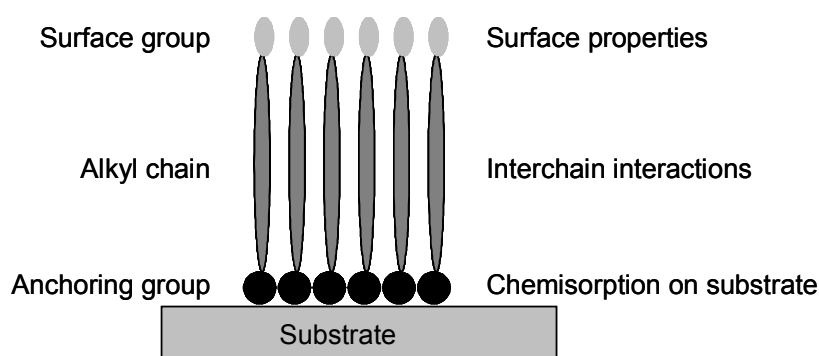


Figure II.10: A schematic view of the self-assembling surfactant molecule in SAMs.

2.1.2. Types of self-assembled monolayers on electrode

SAMs can form on many materials which possess well-defined surface chemistries, including metals, semiconductors, oxides and so on. (46) In Table II.3,

surfactants and the related substrates, on which they can form SAMs are listed.

Surface	Substrates	Surfactants
Metal	Au	R-SH, R-SS-R, R-S-R, R-NH ₂ , R-NC, R-Se, R-Te
	Ag	R-COOH, R-SH
	Pt	R-SH, R-NC
	Pd	R-SH
	Cu	R-SH
	Hg	R-SH
Semiconductor	GaAs	R-SH
	InP	R-SH
	CdSe	R-SH
	ZnSe	R-SH
Oxide	Al ₂ O ₃	R-COOH
	TiO ₂	R-COOH, R-PO ₃ H
	ITO	R-COOH, R-SH, R-Si(x) ₃
	SiO ₂	R-Si(x) ₃

Table II.3: Chemical systems of substrates and the corresponding surfactants that form SAMs.

2.1.3. Advantages of self-assembled monolayers

The advantages of SAMs arise from the chemical binding of the anchoring group at the substrate surface and the ease with which SAMs are formed.

- SAMs are very stable as mentioned above and they are able to survive prolonged exposure to vacuum.
- Different surface properties of the substrates can be provided by terminal groups of the surfactants without disrupting the self-assembly process or destabilizing the SAMs.
- SAMs provide a means of attaching the biomolecules to the electrode with a diverse set of structures ranging from modified monolayers to multilayers.

- In electrochemistry, the thiol-based SAMs survive the electrochemical treatment and experiments. The anchored sulfur atoms are believed to resist oxidation, reduction, and desorption in a range of potentials.
- A monolayer is deposited on the metal in a manner of seconds to minutes.
- Usually, this method does not require anaerobic or anhydrous conditions; nor does it require a vacuum.
- Weakly adsorbed impurities has slight effect on the formation of SAMs, since high affinity interaction between the anchoring group and the substrate enables the assembling layer to displace more weakly adsorbed impurities.
- Curvature or accessibility of the substrate surface is not a serious obstacle factor; because substrates can range from macro- to nano-scale, from smooth to porous, as well as from plane to sphere (nanoparticles).

Another advantage is the amenability to application in controlling interfacial (physical, chemical, electrochemical) properties.

Comparing to LB films SAMs are more stable. Since LB films are deposited onto the substrates by physisorption, mainly by hydrophilic and/or hydrophobic interaction, they are more sensitive to the external environment, such as temperature, pH, solvent etc.

2.2. Preparation of self-assembled monolayers

In this thesis, SAMs of alkanethiol on gold and silver were performed. Therefore, only preparations of SAMs on gold and silver substrates are discussed here.

Usually the gold and silver substrates are obtained by evaporating or sputtering gold and silver films (typically 50-200 nm thick) on glass, silicon, or cleaved mica. To improve the adhesion of the gold and silver film to the oxide surface, a thin layer of chromium or titanium is often deposited first.

2.2.1. Preparation of SAMs on gold substrates

2.2.1.1. Pretreatment of gold substrates

Gold is the most popular substrate for thiol SAMs. Owing to its noble character, gold substrate can be handled in air without the formation of an oxide surface layer, and can survive harsh chemical treatments for the removal of organic contaminants. The formation of a monolayer on gold is strongly dependent on the cleanliness and structure of gold prior to modification. (47) Since it is well known that gold is a soft metal and is readily contaminated by organic and inorganic species during manual handling. (48)

Before used, the gold substrates need to be cleaned well in order to remove the contaminants on the surface which may affect the integrity of the SAMs formation. The importance of the cleanliness of the gold surface on formation and reproducibility of SAMs has been recognized by many groups working in the field of SAMs. In the literature we can find numerous different cleaning procedures. Most of them involve gold surface oxidation to remove organic and inorganic contaminants on the gold surface: electrochemical oxidation (49), immersion into strong oxidizing solutions (50), a combination of the two (51), or exposure to reactive oxygen species formed by either UV irradiation or oxygen plasma (52, 53).

In this thesis, a strong oxidizing solution, $\text{H}_2\text{SO}_4:\text{H}_2\text{O}_2$ (7:3 v/v) (piranha solution) was used. (Caution: piranha solution reacts violently with organic materials and should be handled very carefully.) First, the gold substrates were cleaned with acetone in an ultrasonic bath for 10 min in order to remove the protection layer of polymer and dried under nitrogen flow, after they were immersed into the hot piranha solution for 1 min. Subsequently, the gold substrates were rinsed thoroughly in absolute ethanol, and dried under nitrogen flow. The immersion time in acetone and piranha was optimized.

Wetting properties of gold surface before and after pretreatment were studied with a contact angle meter. It is widely accepted that clean gold is hydrophilic. In this thesis, the contact angle of gold substrate as received is about 90° , which is due to the presence of a carbon- and oxygen-containing contaminant layer on the gold surface. (54) After cleaning, the contact angle is $<10^\circ$, which proves that the gold surface is free of contaminants. The contact angle images are shown in Table II.4.





samples	as received	after cleaning	with SAMs of ODT	with mixed SAMs
Contact angle	$90^\circ \pm 3^\circ$	$<10^\circ$	$110^\circ \pm 3^\circ$	$9^\circ \pm 3^\circ$
Contact angle image				

Table II.4: The contact angle values and images of the gold substrates before and after different treatments.

2.2.1.2. Formation of the SAMs on gold substrate

The most common approach for formation of SAMs on solid substrate is by immersing the substrate into a homogeneous solution of the self-assembling molecule at room temperature. There are a number of experimental factors that can affect the structure of the resulting SAMs: solvent, temperature, concentration of the adsorbate, immersion time, purity of the adsorbate, concentration of oxygen in solution, cleanliness of the substrate, and chain length or more generally, structure of the adsorbate.

Usually any solvent capable of dissolving the adsorbate is suitable. Ethanol is the most popular solvent because some plausible gold oxide will be reduced in ethanol, but sometimes other solvents are preferred. The thiol concentration can be varied from micromolar levels to the neat liquid thiol. However, very low concentrations of thiols are favorable for obtaining large crystalline domains of alkanethiols via slow self-assembly. Immersion time varies from several minutes to several hours for alkanethiol, while for sulfides and disulfides, immersion time of several days may be necessary.

In this thesis, gold substrates were functionalized with two kinds of SAMs. In the first case, as soon as the cleaning procedure is finished, the gold substrates were put into a 1 mM 1-octadecanethiol (ODT) ethanol solution for 21 h at room temperature to render their surfaces hydrophobic. Since such a hydrophobic surface is favourable to the deposition of LB films. Then the substrates were thoroughly cleaned with ethanol to remove physically adsorbed thiol on the surface and dried under a N_2 flow. The contact angle image of the gold substrate modified with SAMs of ODT is given in Table II.4.

In the second case, after cleaning, gold substrates were immersed immediately into a mixed solution of 16-mercaptohexadecanoic acid (MHDA) and 1,2-Dioleoyl-sn-Glycero-3-Phosphoethanolamine-N-(Biotinyl) sodium salt (biotinyl-PE) in absolute ethanol at the concentration of 1 mM and 0.1 mM, respectively, for 21 h in order

to obtain mixed self-assembled monolayers. Then the substrates were thoroughly cleaned with ethanol to remove physically adsorbed thiol and biotinyl-PE on the surface, and finally dried under a N_2 flow. The contact angle image of the gold substrate with the mixed SAMs is also shown in Table II.4. Figure II.11 shows the procedures for the functionalization of gold substrate by thiol SAMs.

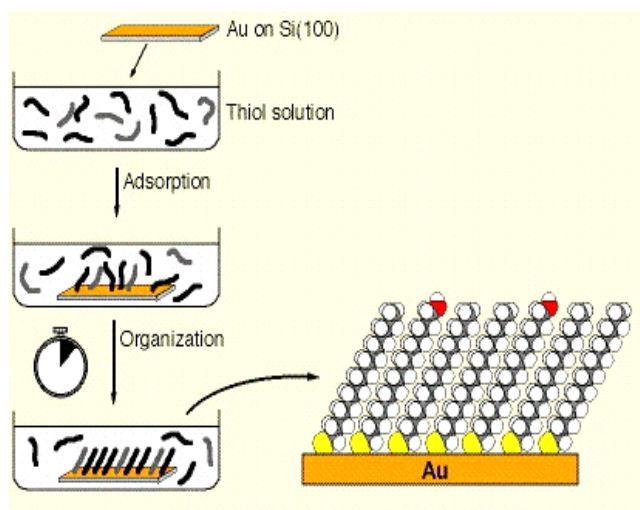


Figure II.11: Different steps of the functionalization of gold substrate by thiol SAMs.

2.2.2. Pretreatment and formation of SAMs on silver substrates

For silver substrates, mild cleaning procedures are necessary due to their high reactivity to the oxygen in air. (55) In this study, they were only cleaned with hot ethanol for 5 min, and then in order to minimize the effects of oxidation and contamination, they were immediately immersed into thiol solution of ODT with a concentration of 1 mM for 24 h. Since they are easily oxidized, the formation of SAMs was performed in the presence of N_2 flow, as shown in Figure II.12. After the substrates were thoroughly cleaned with ethanol to remove physically adsorbed thiol and dried under a N_2 flow. The contact angle of ODT-functionalized silver surface is $115 \pm 3^\circ$.

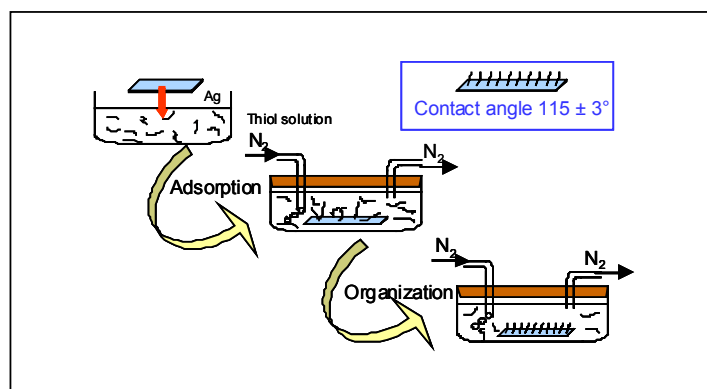


Figure II.12: SAMs functionalization of silver substrate with 1 mM ODT.

There are some other deposition methods for SAMs. When the thiol is sufficiently volatile, SAMs deposition can be performed in the vapor phase of the thiol, both in a vacuum (56) and at ambient pressures (57). SAMs deposition can also be performed in a solid phase, Whitesides et al. developed the technique of microcontact printing: It uses the relief pattern on the surface of a PDMS stamp to form patterns of self-assembled monolayers on the substrate surface by contact. (58) In μ CP of alkanethiols on gold, for example, the PDMS stamp is wetted with an “ink” (typically, ~ 2 mM solution of thiol in ethanol) and is brought into contact with the gold surface for 20 s. The thiol is transferred from the stamp to gold surface upon contact, SAMs with pre-designed patterns are stamped on the gold surface.

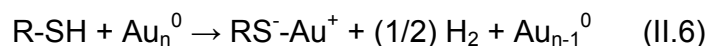
2.3. Kinetics and mechanism of formation of SAMs

There are substantial differences among reports in the literature regarding the kinetics of formation of the SAMs on the solid substrates from liquid solution. The most important factors affecting the kinetics features appear to be the presence of preadsorbed contaminants, the solution phase hydrodynamics, and solvent effects. (59)

The general kinetic of alkanethiol adsorption onto Au(111) in relatively dilute solution (10^{-3} M) is believed to have two distinct adsorption kinetics: a very fast step, which takes a few tens of seconds to minutes, by the end the contact angles are close to their desired values and the thickness about 80-90% of their maximum; a slow step, which may last several hours, at the end the thickness and contact angles will reach their final values. (60)

The initial step is a diffusion-controlled Langmuir adsorption, its kinetics is governed by the surface-head group reaction. The second step can be described as a surface reorganization process, during which the alkyl chains get a phase change from the disordered state to an ordered state and form a two-dimensional quasi crystal. Its kinetics is related to the chain disorder, different components of chain-chain interaction, and surface mobility of chains.

Extensive X-ray photoelectron spectroscopy (XPS) experiments suggest that chemisorption of alkanethiols on a gold surface yields the gold thiolate species. In the case of alkanethiols, the mechanism of alkanethiols binding to gold substrates is considered to be an oxidative addition of the S-H bond to gold substrate followed by reductive elimination of the hydrogen, thus resulting in the formation of a thiolate species, as shown in Equation II.6:



In the case of disulfides, the mechanism is thought to follow Equation II.7:



Another common SAMs system is silanization of silicon oxide. For the formation of the SAMs on the silicon oxide, for example, with octadecyltrichlorosilane (OTS), two possible monolayer growth modes were proposed by P. Dutta: island growth and uniform growth. (61, 62) In the island mode, the molecules form dense islands of (nearly) vertical molecules. Additional molecules attach at island edges or form new islands as the coverage increases. In the latter mode, molecules deposit randomly on the substrate, falling over at low coverage. As more molecules adsorb on the substrate, the molecules begin to stand up.

2.4. Structure of SAMs on gold and silver substrate

Alkanethiols on Au (111) form a $(\sqrt{3} \times \sqrt{3}) R30^\circ$ (R = rotated) structure. Sulfur atoms bond to the three-fold hollow sites on the Au surface and the extremely strong surface bond (44 kcal mol⁻¹) contributes to the stability of the SAMs. Alkanethiols on Ag (111) form a $(\sqrt{7} \times \sqrt{7}) R10.9^\circ$ structure with an S-S distance of 4.41 Å. Because of this shorter S-S distance, alkanethiols on Ag are more densely packed, which results in near-perpendicular orientation of molecules on the Ag surfaces. However, in the case of Au (111), the alkyl chain is tilted 30° from the surface normal to decrease the lattice energy. The difference in orientation is mainly due to the interchain van der Waals interaction. (63)

2.5. Protein immobilization by SAMs

As referred above, SAMs are well-ordered, once form, they are very stable due to the high affinity of adsorbates to the substrate. Moreover, the variety of terminal functionality of SAMs can provide the needed design flexibility, both at the individual molecular and at the material levels, and offer a vehicle for investigation of specific interactions at interfaces. Accordingly, such well-ordered monolayers are very suitable for protein immobilization, which allows immobilize proteins close to the electrode surface with a high degree of control over the molecular architecture of the recognition interface. In practice, SAMs have been used for fundamental investigations of the interactions of proteins with surfaces and particularly for the fabrication of a variety of biosensors including enzyme biosensors (64-66), immunosensors (67), and DNA

hybridization biosensors (68) etc.

There are two basic approaches for immobilizing proteins onto the gold substrates surface by SAMs. The proteins can be attached to thiol containing moieties and then bind to the gold surfaces by SAMs, or they can be bound to previously SAMs-functionalized gold substrates.

2.5.1. Protein modification

In this case, proteins are first tagged in the solution with an appropriate sulfur-containing molecule via reaction with specific reactive groups present on the biomolecule surface, e.g. the amino group. And then the modified proteins are self-assembled onto the gold substrate via the sulfur moiety.

It has been reported that proteins can be chemically modified by N-succinimidyl 3-(2-pyridyldithiol)propionate (SPDP) and 2-iminothiolane. During the modification, a disulfide moiety is connected to the primary amine group of the protein via an amido linkage. (69, 70) After that the modified proteins were immobilized onto the gold surface by SAMs (71), as shown in Figure II.13. Such a method allows a monolayer of protein to be attached to the electrode. In addition, single point labelling of the protein allows control over the orientation of the protein. However, Dong et al. showed that the immobilization of thiol-labelled glucose oxidase produced a less stable sensing interface than enzyme immobilized onto a pre-formed SAMs. (72)

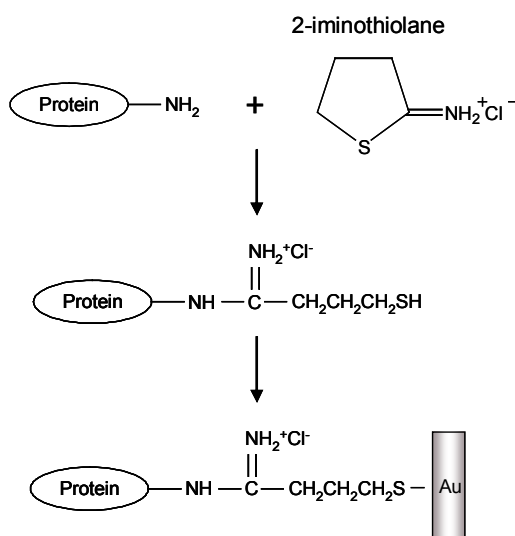
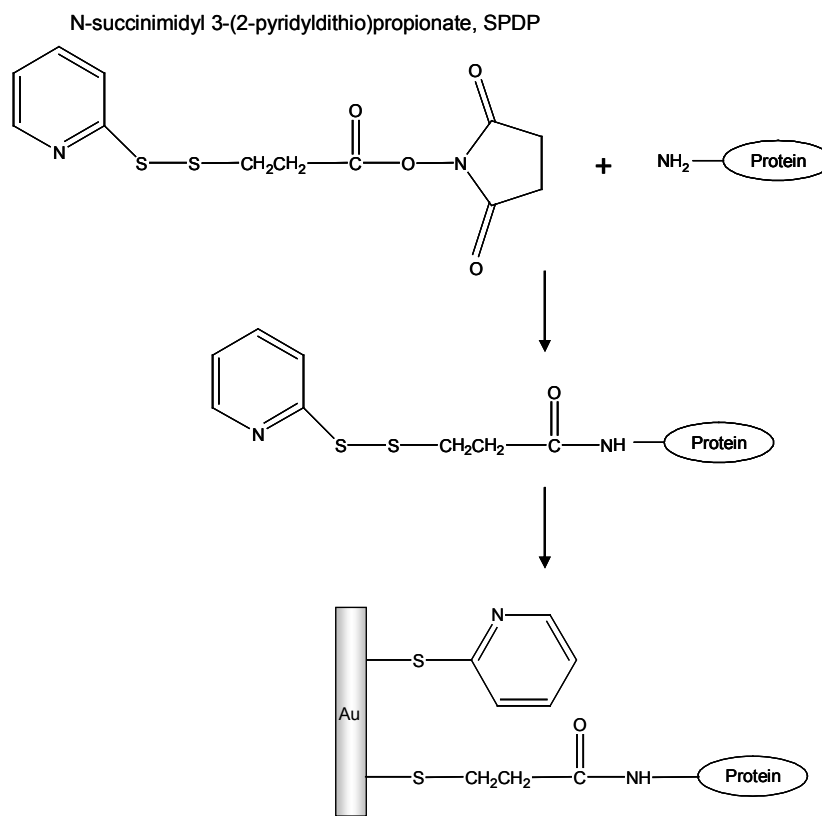


Figure II.13: Previously modified protein immobilization by SAMs.

2.5.2. Substrate modification

By this method the substrate is firstly functionalized by self-assembling one monolayer of a sulfur-containing surfactant. Proteins are then bound to the SAMs via reaction with specific moieties present on the biomolecule surface.

2.5.2.1. Non-covalent binding

One common non-covalent approach for immobilizing protein to the surface of SAMs is by electrostatic binding. This method is simple and gentle, and it can provide a potential control over the orientation of the immobilized protein molecules depending on the charge distribution on the shell of the protein.

In this thesis, mixed protein/amphiphile LB films have been transferred onto SAMs prefunctionalized gold and silver substrates by the non-covalent binding.

The major drawback of the electrostatic binding is that the strength of the bond is dependent on the solution conditions. The change in ionic strength and pH can lead to removal of proteins from the surfaces of the SAMs.

2.5.2.2. Cross-linking

Cross-linking proteins to the surfaces of SAMs with bifunctional reagent glutaraldehyde is a relatively uncontrolled method. It suffers from poor reproducibility and protein leaching. Usually multilayers of protein are produced on the substrate surface.

2.5.2.3. Direct covalent attachment

Direct covalent attachment is the most potential method for elaboration of biosensor due to the high stability of the resulting bond. The immobilization is conducted in two stages: activation of the carrier, and coupling of the biomolecule.

Usually proteins are covalently bound to COOH-terminated SAMs by using carbodiimide coupling that allow to couple amines to carboxylic acids. The most often used carbodiimide couplings is N-ethyl-N-[dimethylaminopropyl] carbodiimide (EDC) and N-hydroxysuccinimide (NHS). In the reaction EDC converts the carboxylic acids into a reactive intermediate which is susceptible to be attacked by amines. In some cases EDC and NHS or N-hydroxysulphosuccinimide (NHSS) are used together as they produce a more stable reactive intermediate which has been shown to give a greater reaction yield.

For covalently coupling proteins onto amine-terminated SAMs, a bifunctional linker glutaraldehyde is often used. GA can react with amino tails of SAMs to create $-C=N=C-$ bond, after that the proteins with the amine group are coupled with the other aldehyde group.

Mirsky et al. reviewed surface activation methods for immobilization of proteins on the monolayers of 16-mercaptohexadecanoic and 16-

mercaptohexadecylamine on the gold electrodes. (67) Here we only list the most commonly used activation methods of carboxy and amino groups for the elaboration of biosensors, as shown in Figure II.14.

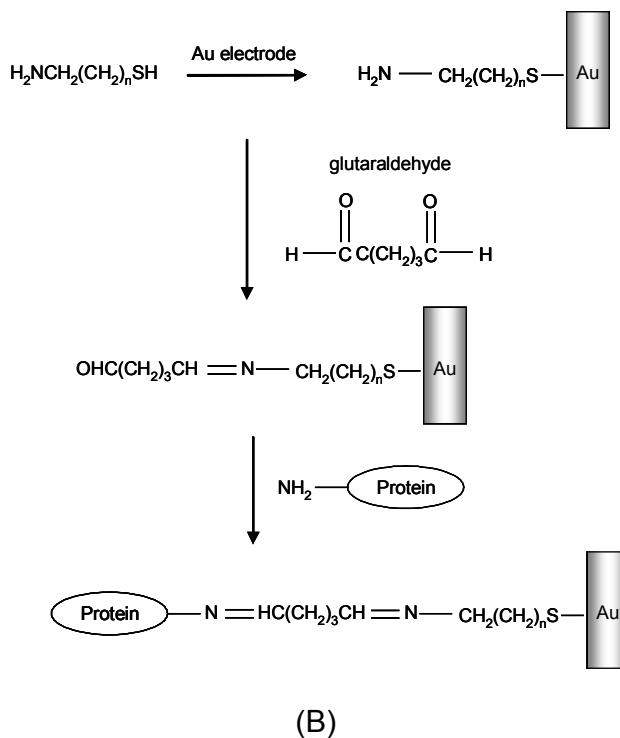
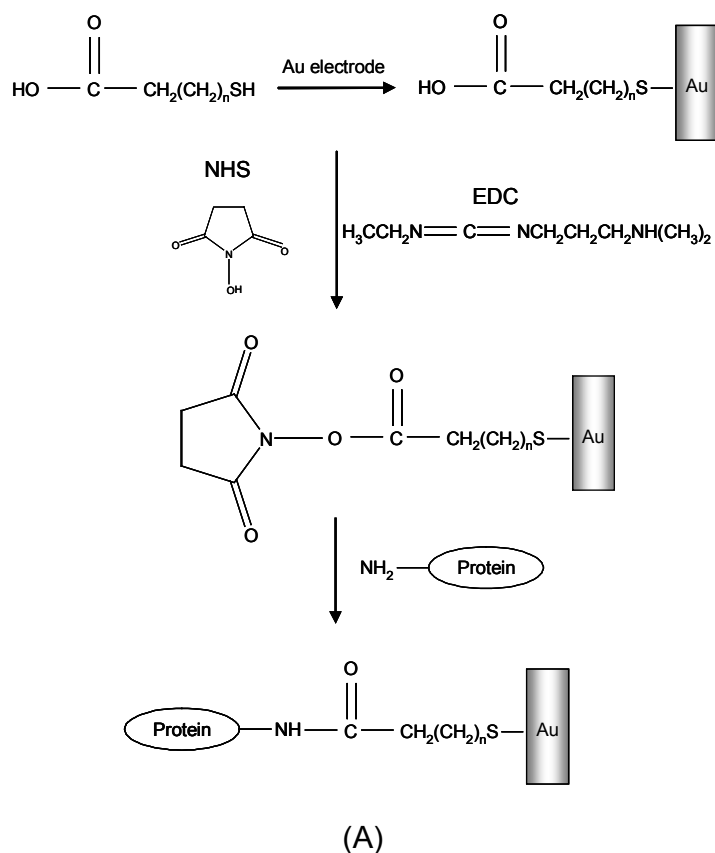


Figure II.14: Protein immobilization on previously SAMs-functionalized substrates by covalent attachment.

2.5.2.4. *Direct affinity attachment*

More recently a new strategy for more site-specific binding of biomolecules based on streptavidin/biotin pair has been extensively investigated. Streptavidin is a tetrameric protein, approximately $4.5 \times 4.5 \times 5.8$ nm, and with a molecular weight of 60 kDa. It can bind biotin at four binding sites, two binding sites on each of two opposite faces, with an extremely high binding constant ($K_d = 10^{-15}$ M), which makes the binding process effectively irreversible. (73) Moreover, diverse biomolecules can be easily functionalized by biotin with no disturbing effect on their specific sites. All these properties make the avidin/biotin binding pair highly suitable for immobilizing proteins on the substrates and for the construction of biosensor.

The formation of SAMs with biotin molecules on gold substrate can be realized either by covalently coupling biotin to previously chemisorbed ω -functionalized thiolates (74-77), or by directly self-assembling of biotinylated thiols or disulfides (78, 79). Usually in order to optimize the binding properties of the monolayer, accordingly to reduce the non-specific interaction between streptavidin and the surface, SAMs of biotinylated thiol are diluted by hydroxyalkanethiol with a spacer segment. (73, 80-83)

However, these methods suffer from the complicated chemical treatment or organic synthesis of biotinylated thiol which is almost not commercially available. In this thesis, we chose a mixed SAMs of MHDA and biotinyl-PE, which are commercially available. The mixed SAMs, in which the biotinyl-PE is inserted and bound to MHDA by the electrostatic interaction, were simply prepared by immersing the pretreated gold substrates into the mixed solution of MHDA and Biotinyl-PE in ethanol. The ratio between two components determines the density of specific biotinyl anchoring sites.

The biotin-containing SAMs are a desirable platform for construction of self-assembled multilayer of protein on biosensor, in particular, immunosensor. The structure of the system is shown in Figure II.15: the mixed SAMs containing biotinyl sites, streptavidin, biotinylated antibody and antigen in the way of a stepwise assembled system.

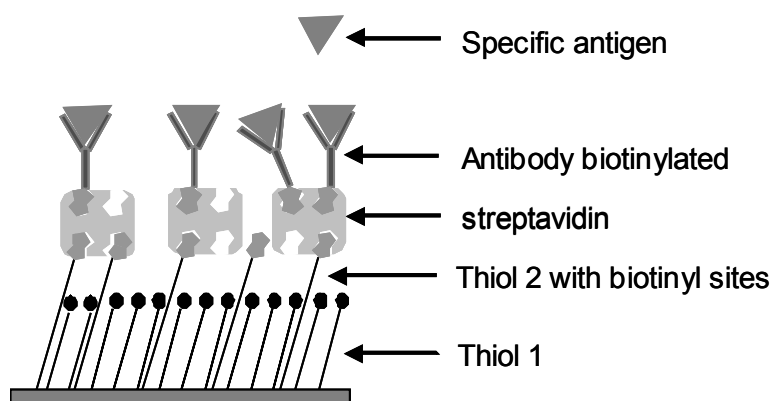


Figure II.15: Self-assembled multilayer structure based on biotin/avidin affinity interaction.

2.6. Application of SAMs to biosensor elaboration

As discussed above SAMs are effective methods for protein immobilization and they have many important advantages for the construction of biosensors, as listed as the following:

- Easy formation of ordered, pinhole free and stable monolayers;
- Flexibility to design the head group of SAMs with various functional groups in order to accomplish hydrophobic or hydrophilic surface as the requirement;
- Only minimum amount of biomolecule is needed for immobilization on the SAMs;
- Reasonable stability for extended period, allowing several reliable measurements and reproducible immobilization of the recognition molecule in a favourable microenvironment;
- Molecular level control of the interfacial chemistry can be exploited to enable ready approach of the target analyte to the interface with the limitation of the access of interfering substances.

Up to now SAMs have been used as major immobilization technique for elaboration of all kinds of biosensors, such as enzyme biosensors, immunosensors, DNA-based biosensors and so on. With the development of electronics and nanotechnology, the size of electrode is gradually minimized to micro- even nanometer scale. SAMs can be expected to become an increasingly prevalent and critical tool due to their clear advantages.

3. CHARACTERIZATION OF SAMS AND LB FILMS

To obtain accurate information on the structure of thin organic films as SAMs and LB films, it is essential to use a variety of characterization techniques that are able to determine certain properties of the layer. The most frequently used techniques are divided into five groups and listed in the Table II.5.

Analytical techniques	Structural information
<i>General</i>	
Contact angle	Hydrophobicity, order
QCM	Change in mass
<i>Optical</i>	
IR spectroscopy/FTIR	Functional groups, molecular orientation
Fluorescence spectroscopy	Density of adsorbates
Ellipsometry	Layer thickness
SPR	Layer thickness
<i>Vacuum</i>	
XPS	Elemental composition
<i>Microscopy</i>	
AFM	Molecular packing
STM	Molecular packing
<i>Electrochemical</i>	
Cyclic Voltammetry	Thickness, order/defects, electrical properties
Impedance spectroscopy	Thickness, order/defects, electrical properties

Table II.5: Analytical techniques for characterizing the ultra-thin films. (84)

Contact angle can be used to examine the general hydrophobicity or hydrophilicity of a surface, it is a simple and effective method to obtain a first impression about the structure and composition of the layer. The principle and measurement of contact angle will be introduced detailedly in Annex I.

Quartz crystal microbalance can detect mass change in a scale of several

nanograms. It can be used to study the kinetics of layer adsorption of SAMs and LB films.

Infrared (IR) spectroscopy is a very important method for characterization of SAMs and LB films. The spectra can provide not only the usual structural data, but also information about the average orientation of the molecules in the thin layer.

Fluorescence spectroscopy can be used to observe the packing of SAMs and LB films on the substrates and it can provide information on the density of adsorbates.

Ellipsometry is one of the most common optical techniques to estimate the thickness of the thin organic films. It is based on a plane-polarized laser beam that is reflected by the substrate, which results in a change of the phase and amplitude of the light. Then by comparing these two sets of parameters for an uncovered and covered substrate, the thickness of the layer can be calculated.

Surface plasmon resonance is based on the angle-dependent reflection of a p-polarized laser beam at thin metal layers and it can give important information on thickness of the layer. It is sensitive to the variation of the mean thickness and refractive index of the SAMs layer.

X-ray photoelectron spectroscopy is a useful technique for quantitative analysis of surface composition. It provides information on the chemical state of the constituents, but gives very little, or no, lateral resolution. XPS has been used to probe the chemical nature of the SAMs. Briefly, incident X-rays bombard the sample, and electrons are ejected from the core shells of the atoms within the SAMs. These electrons are collected in an analyzer; by measuring the energies of the electrons entering the analyzer, the binding energies are calculated. These are specific to each element and give indications of the oxidation states of the elements.

Atomic force microscopy and scanning tunneling microscopy (STM) allow characterize the organic thin films at a molecular resolution. The generated images are the result of the forces acting between the tip and the surface or the surface electron density for AFM and STM, respectively. In the Annex II AFM is well introduced.

The electrochemical characterization of SAMs on gold is usually performed by cyclic voltammetry (CV) and electrochemical impedance spectroscopy. For CV large potential sweeps are applied to the gold electrode and the resulting current is recorded. However, for EIS only very small sinusoidal potential sweeps with frequencies varying from 100 mHz to 10 kHz are applied to the gold electrode, which makes a less disturbing

technique than CV. By the two techniques we can know if the SAMs are well ordered, and if there are defects in the monolayers.

References

- (1) G. Roberts, Ed. Langmuir-Blodgett films, Plenum Press, New York, **1990**.
- (2) A. Pockels, *Nature*, **1891**, 43, 437.
- (3) A. Pockels, *Nature*, **1892**, 46, 418.
- (4) Langmuir-Blodgett Troughs-operating manual, 6th Edition, Nima Technology Ltd., page 21.
- (5) A. Ulman, An Introduction to Ultrathin Organic Films: From Langmuir-Blodgett to Self-Assembly; Academic Press: Boston, **1991**; Preface.
- (6) W. D. Harkins, The Physical Chemistry of Surface Films, Reinhold, New York, **1952**.
- (7) D. R. Talham, *Chem. Rev.*, **2004**, 104, 5479-5501.
- (8) P. Fromherz, *Biochimica Biophysica Acta*, **1971**, 225, 382-387.
- (9) S. Arisawa, R. Yamamoto, *Thin Solid Films*, **1992**, 210/211, 443-445.
- (10) S. Y. Zaitsev, *Colloids and surfaces A*, **1993**, 75, 211-216.
- (11) S. Y. Zaitsev, *Sensors and Actuators B*, **1995**, 24-25, 177-179.
- (12) C. Fiol, S. Alexandre, N. Delpire, J. M. Valleton, *Thin Solid Films*, **1992**, 215, 88-93.
- (13) N. Dubreuil, S. Alexandre, C. Fiol, F. Sommer, J. M. Velleton, *Langmuir*, **1995**, 11, 2098-2102.
- (14) C. Fiol, S. Alexandre, N. Dubeuil, J. M. Valleton, *Thin Solid Films*, **1995**, 261, 287-295.
- (15) N. Dubreuil, S. Alexandre, C. Fiol, J. M. Valleton, *Journal of Colloid and Interface Science*, **1996**, 181, 393-398.
- (16) S. Alexandre, N. Dubreuil, C. Fiol, D. Lair, Tran-Minh Duc, Jean-Marc Velleton, *Thin Solid Films*, **1997**, 293, 295-298.
- (17) N. Dubreuil, S. Alexandre, D. Lair, F. Sommer, T. M. Duc, J. M. Velleton, *Colloids and Surfaces B: Biointerfaces*, **1998**, 11, 95-102.
- (18) J. M. Chovelon, M. Provence, N. Jafrezic-Renault, V. Derue, D. Lair, S. Alexandre,

- J. M. Valleton, *Journal of Biological Physics and Chemistry*, **2001**, 1, 68-75.
- (19) S. Alexandre, C. Lafontaine, J. M. Velleton, *Journal of Biological Physics and Chemistry*, **2001**, 1, 21-23.
- (20) S. Alexandre, V. Dérue, J. M. Velleton, F. Sommer, T. M. Duc, *Colloids and Surfaces B: Biointerfaces*, **2002**, 23, 183-189.
- (21) A. Zhang, N. Jaffrezic-Renault, J. Wan, Y. Hou, J. M. Chovelon, *Materials Science and Engineering C*, **2002**, 21, 91-96.
- (22) J. M. Chovelon, K. Wan, N. Jaffrezic-Renault, *Langmuir*, **2000**, 16, 6223-6227.
- (23) J. M. Chovelon, F. Gaillard, K. Wan, N. Jaffrezic-Renault, *Langmuir*, **2000**, 16, 6228-6232.
- (24) A. P. Girard-Egrot, R. M. Morélis, P. R. Coulet, *Thin Solid Films*, **1997**, 292, 282-289.
- (25) A. P. Girard-Egrot, R. M. Morélis, P. R. Coulet, *Langmuir*, **1997**, 13, 6540-6546.
- (26) Y. Okahata, T. Tsuruta, K. Ijio, K. Ariga, *Langmuir*, **1988**, 4, 1373-1375.
- (27) S. Y. Zaitsev, *Colloids and Surfaces A*, **1993**, 75, 211-216.
- (28) C. Fiol, J. M. Chovelon, N. Dubreuli, G. Barbey, A. Barraud, A. Ruaudel-Teixier, *Thin Solid Films*, **1992**, 210/211, 489-491.
- (29) T. Tatsuma, H. Tsuzuki, Y. Okawa, S. Yoshida, T. Watanabe, *Thin Solid Films*, **1991**, 202, 145-150.
- (30) K. Wan, J. M. Chovelon, N. Jaffrezic-Renault, *Talanta*, **2000**, 52, 663-670.
- (31) J. W. Choi, Y. K. Kim, I. H. Lee, J. Min, W. H. Lee, *Biosensors and Bioelectronics*, **2001**, 16, 937-943.
- (32) A. Zhang, Y. Hou, N. Jaffrezic-Renault, J. Wan, A. Soldatkin, J. M. Chovelon, *Bioelectrochemistry*, **2002**, 56, 157-158.
- (33) R. Singhal, A. Gambhir, M. K. Pandey, S. Annapoorni, B. D. Malhotra, *Biosensors and Bioelectronics*, **2002**, 17, 697-703.
- (34) Y. Hou, N. Jaffrezic-Renault, A. Zhang, J. Wan, A. Errachid, J. M. Chovelon, *Sensors and Actuators B: Chemical*, **2002**, 86, 143-149.

- (35) S. K. Sharma , R. Singhal , B. D. Malhotra , N. Sehgal, A. Kumar, *Electrochimica Acta*, **2004**, 49, 2479-2485.
- (36) S. K. Sharma, R. Singhal, B. D. Malhotra, N. Sehgal, A. Kumar, *Biosensors and Bioelectronics*, **2004**, 20, 651-657.
- (37) I. Vikholm, O. Teleman, *Journal of Colloid and Interface Science*, **1994**, 168, 125-129.
- (38) A. Barraud, H. Perrot, V. Billard, C. Martelet, J. Therasse, *Biosensors and Bioelectronics*, **1993**, 8, 39-48.
- (39) T. Katsube, T. Yaji, K. Suzuki, S. Kobayashi, T. Kawaguchi, T. Shiro, *Applied Surface Science*, **1988**, 33-34, 1332-1338.
- (40) T. B. Dubrovsky, M. V. Demcheva, A. P. Savitsky, E. Yu. Mantrova, A. I. Yaropolov, V. V. Savransky, L. V. Belovolova, *Biosensors and Bioelectronics*, **1993**, 8, 377-385.
- (41) G. K. Chudinova, A. V. Chudinov, V. V. Savransky, A. M. Prokhorov, *Thin Solid Films*, **1997**, 307, 294-297.
- (42) G. I. Lepesheva, T. N. Azeva, V. N. Knyukshto, V. L. Chashchin, S. A. Usanov, *Sensors and Actuators B: Chemical*, **2000**, 68, 27-33.
- (43) B. K. Oh, B. S. Chun, K. W. Park, W. Lee, W. H. Lee, J. W. Choi, *Materials Science and Engineering: C*, **2004**, 24, 65-69.
- (44) C. Nicolini, M. Adami, T. Dubrovsky, V. Erokhin, P. Facci, P. Paschkevitsch, M. Sartore, *Sensors and Actuators B: Chemical*, **1995**, 24, 121-128.
- (45) G. B. Sukhorukov, M. M. Montrel, A. I. Petrov, L. I. Shabarchina, B. I. Sukhorukov, *Biosensors and Bioelectronics*, **1996**, 11, 913-922.
- (46) R. K. Smith, P. A. Lewis, P. S. Weiss, *Progress in Surface Science*, **2004**, 75, 1-68.
- (47) C. D. Bain, E. B. Troughton, Y. T. Tao, J. Evall, G. M. Whitesides, R. G. Nuzzo, *J. Am. Chem. Soc.*, **1989**, 111, 321 – 335.
- (48) Z. Yang, A. Gonzalez-Cortes, G. Jourquin, J. C. Viré, J. M. Kauffmann, *Biosensors and Bioelectronics*, **1995**, 10, 789-795.
- (49) L. Strong, G. M. Whitesides, *Langmuir*, **1988**, 4, 546-558.

- (50) S. D. Evans, R. Sharma, A. Ulman, *Langmuir*, **1991**, 7, 156-161.
- (51) H. O. Finklea, D. A. Snider, J. Fedyak, *Langmuir*, **1990**, 6, 371-376.
- (52) M. G. Samant, C. A. Brown, J. G. Gordon, *Langmuir*, **1991**, 7, 437 – 439.
- (53) H. Ron, I. Rubinstein, *Langmuir*, **1994**, 10, 4566 – 4573.
- (54) H. Ron, S. Matlis, I. Rubinstein, *Langmuir*, **1998**, 14, 1116 – 1121.
- (55) A. Majid, F. Bensebaa, P. L'Ecuyer, G. Pleizier, Y. Deslandes, *Rev. Adv. Mater. Sci.*, **2003**, 4, 25-31.
- (56) G. E. Poirier, E. D. Pylant, *Science*, **1996**, 272, 1145-1148.
- (57) O. Chailapakul, L. Sun, C. Xu, R. M. Crooks, *J. Am. Chem. Soc.*, **1993**, 115, 12459-12467.
- (58) Y. Xia, G. M. Whitesides, *Annu. Rev. Mater. Sci.*, **1998**, 28, 153-184.
- (59) W. Pan, C. J. Durning, N. J. Turro, *Langmuir*, **1996**, 12, 4469-4473.
- (60) A. Ulman, *Chem. Rev.*, **1996**, 96, 1533-1554.
- (61) A. G. Richter, C. J. Yu, A. Datta, J. Kmetko, P. Dutta, *Physical Review E*, **2000**, 61, 607-615.
- (62) A. G. Richter, C. J. Yu, A. Datta, J. Kmetko, P. Dutta, *Materials research-CAT, Sector 10*, 136-139.
- (63) N. Sandhyarani, T. Pradeep, *International Reviews in Physical Chemistry*, **2003**, 22, 221-262.
- (64) J. J. Gooding, D. B. Hibbert, *Trends in Analytical Chemistry*, **1999**, 18, 523-533.
- (65) S. E. Creager, K. G. Olsen, *Analytica Chimica Acta*, **1995**, 307, 277-289.
- (66) N. K. Chaki, K. Vijayamohanan, *Biosensors and Bioelectronics*, **2002**, 17, 1-12.
- (67) V. M. Mirsky, M. Riepl, O. S. Wolfbeis, *Biosensors and Bioelectronics*, **1997**, 12, 977-989.
- (68) J. J. Gooding, F. Mearns, W. Yang, J. Liu, *Electroanalysis*, **2003**, 15, 81-96.
- (69) J. W. Kenny, T. G. Fanning, J. M. Lambert, R. R. Traut, *J. Mol. Biol.*, **1979**, 135,

151.

(70) J. Carlsson, H. Drevin, R. Axén, *Biochem. J.*, **1978**, 173, 723.

(71) S. Ferretti, S. paynter, D. A. Russell, K. E. Sapsford, D. J. Richardson, *Trends in Analytical Chemistry*, **2000**, 19, 530-540.

(72) X. Dong, J. Lu, C. Cha, *Bioelectrochem. Bioenerg.*, **1997**, 42, 63.

(73) J. Spinke, M. Liley, F. J. Schmitt, H. J. Guder, L. Angermaier, W. Knoll, *J. Chem. Phys.*, **1993**, 99, 7012-7019.

(74) C. Yam, C. M. Pradier, M. Salmain, P. Marcus, G. Jaouen, *Journal of Colloid and Interface Science*, **2001**, 235, 183-189.

(75) C. Yam, C. M. Pradier, M. Salmain, N. Fischer-Durand, G. Jaouen, *Journal of Colloid and Interface Science*, **2002**, 245, 204-207.

(76) T. L. Lasseter, W. Cai, R. J. Hamers, *Analyst*, **2004**, 129, 3-8.

(77) X. Cui, R. Pei, Z. Wang, F. Yang, Y. Ma, S. Dong, X. Yang, *Biosensors and Bioelectronics*, **2003**, 18, 59-67.

(78) L. Häussling, H. Ringsdorf, F. J. Schmitt, W. Knoll, *Langmuir*, **1991**, 7, 1837-1840.

(79) J. N. Herron, W. Müller, M. Paudler, H. Riegler, H. Ringsdorf, P. A. Suci, *Langmuir*, **1992**, 8, 1413-1416.

(80) V. H. Pérez-Luna, M. J. O' Brien, K. A. Opperman, P. D. Hampton, G. P. Lopez, L. A. Klumb, P. S. Stayton, *J. Am. Chem. Soc.*, **1999**, 121, 6469-6478.

(81) L. S. Jung, K. E. Nelson, P. S. Stayton, C. T. Campbell, *Langmuir*, **2000**, 16, 9421-9432.

(82) K. E. Nelson, L. Gamble, L. S. Jung, M. S. Boeckl, D. G. Castner, C. T. Campbell, P. S. Stayton, *Langmuir*, **2001**, 17, 2807-2816.

(83) J. Spinke, M. Liley, H. J. Guder, L. Angermaier, W. Knoll, *Langmuir*, **1993**, 9, 1821-1825.

(84) S. Flink, Frank C. J. M. Van Veggel, D. N. Reinhoudt, *Adv. Mater.*, **2000**, 12, 1315-1328.

CHAPTER III: ELABORATION OF AN IMPEDIMETRIC IMMUNOSENSOR BY LANGMUIR-BLODGETT TECHNIQUE

1. GENERAL INTRODUCTION ON ANTIBODY IGG

Numerous of infections microbes exist in our surrounding environment, such as viruses, bacteria, fungi, protozoa and multicellular parasites. Most infections in normal individuals are short-lived and leave little permanent damage since the immune system resists infectious agents, which is offered by the functions of circulating antibodies and white blood cells. Antibodies are produced specifically to combine the antigens associated with different diseases, while white blood cells attack and destroy foreign particles in the blood and tissues, including antigen-antibody complexes.

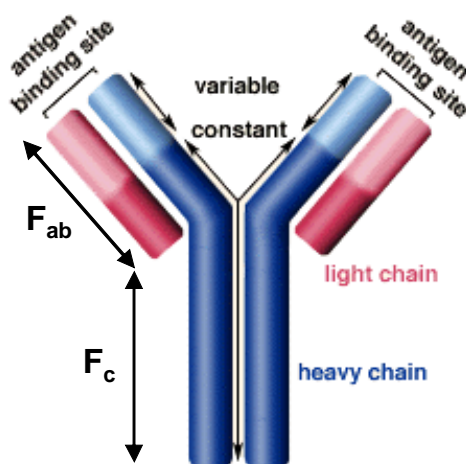
1.1. Structure of antibody IgG

Antibody molecules are immunoglobulins (Ig), which are a group of glycoproteins and present in the serum and tissue fluids of all mammals. In most higher mammals five distinct classes of immunoglobulin molecules are recognized, namely IgG, IgM, IgA, IgD and IgE. They are structurally very similar. Each antibody consists of four polypeptides— two heavy chains and two light chains joined to form a "Y" shape on the upper parts of which two antigen binding sites are located. But they are different in size, charge, amino acid composition and carbohydrate content. Since the type of antibody used in this work is IgG, only IgG's structure will be introduced here.

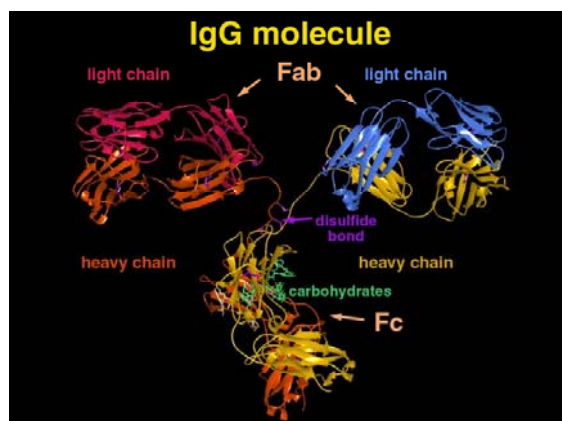
The basic structural unit of IgG (150 kDa) is composed of four polypeptide chains, as shown in Figure III.1A, two light chains (in pink), and two heavy chains (in blue), which are connected by disulfide bonds. Each light chain has a molecular weight of about 25,000 Daltons and it is composed of two domains, variable one (light pink part) and constant one. Each heavy chain has a molecular weight of about 50,000 Daltons and it consists of variable domain (light blue part) and constant one. The heavy chain

determines the functional activity of the antibody molecules. The classes of immunoglobulin are distinguished by their heavy chains. A computer simulated structure of an IgG molecule is shown in Figure III.1B. (1)

The variable regions of the heavy and light chain combine in one interaction site, which has a shape corresponding to that of an epitope of an antigen, called antigen-binding fragment (F_{ab}). As shown in Figure III.1A, the two tips of the "Y" are referred to as the F_{ab} portions. Thus an IgG molecule has two identical binding sites for the antigen. The bottom part of the "Y", namely the C terminal region of each glycoprotein chain, is called the F_c portion, which directs the biological activity of the antibody.



(A)



(B)

Figure III.1: Basic structure of an IgG molecule.

1.2. Antibody specificity and affinity

The binding of antigen to antibody involves the formation of multiple non-covalent bonds between the antigen and amino acids of the binding site in antibody, including hydrogen bonds, and other non-covalent bonds by electrostatic, Van der Waals

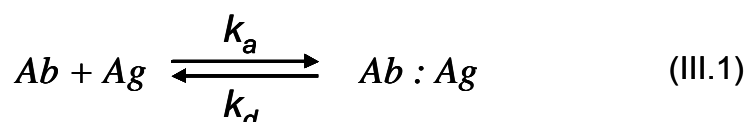
and hydrophobic forces. (2) Although they are individually weak comparing to the covalent bonds, the sum of a great number of non-covalent forces is still considerable.

The conformations of target antigen and the corresponding binding sites in the antibody are complementary to form sufficient binding forces and resist the thermodynamic disruption of the bond. Only when the interaction groups are close enough, the forces become substantial. If the shape of binding sites in antibody can not fit well with that of the antigen or there is overlap of structure, steric repulsive forces may be greater than the binding ones. In this case, the antigen is not specifically bound to the antibody and it can be separated from the antibody. Each antibody can recognize only one particular epitope of a given antigen. This is called the high specificity of the antigen-antibody reaction.

Antibody affinity indicates the strength of a single antigen-antibody bond. It is the sum of all the attractive and repulsive forces. The non-covalent bonds are dissociable, hence the overall combination of an antibody and antigen is reversible.

1.3. Kinetics of antibody-antigen interaction

As referred above, antibody and antigen proceed according to the lock-and-key principle. It is determined by relatively weak noncovalent interaction. The interaction is characterized with an association and a dissociation reaction rate constant, k_a and k_d , respectively, as shown in Equation III.1:



The association constant K_a , which ranges from 10^5 - 10^{11} M^{-1} , can be described by Equation III.2:

$$K_a = \frac{k_a}{k_d} = \frac{[Ab:Ag]}{[Ab] [Ag]} \quad (III.2)$$

Where $[Ab]$, $[Ag]$ and $[Ab:Ag]$ are the concentration of the antibody, antigen and complex in the solution, respectively.

For Equation III.2, when half of the binding sites of antibodies are occupied by antigens, $[Ab] = [Ab:Ag]$, then the equilibrium constant becomes $K_a = 1 / [Ag]$. It implies that for high-affinity antibodies it requires only low concentration of antigen to occupy half

of the binding sites of the antibodies. On the contrary, low-affinity antibody requires a much high concentration of antigen to achieve this aim.

2. STUDY OF MIXED LANGMUIR-BLODGETT FILMS OF IMMUNOGLOBULIN G/AMPHIPHILE AND THEIR APPLICATION FOR IMMUNOSENSOR ENGINEERING*

Abstract

Langmuir-Blodgett technique appears to be quite suitable for generating biospecific surfaces and it has potential application for fabricating biosensors. In this work, mixed Langmuir-Blodgett films of immunoglobulin G/amphiphile have been transferred onto hydrophobic silver surface previously modified by 1-octadecanethiol SAMs. In order to obtain stable LB films, the influences of different parameters - type of amphiphile, surface pressure and pH – on the properties of mixed IgG/amphiphile monolayer, were investigated. Electrochemical properties of the engineered immunosensor have been measured by electrochemical impedance spectroscopy. The immunosensor obtained exhibits a high sensitivity and a good specificity in a linear dynamic range from 200 to 1000 ng ml⁻¹.

* Slightly modified version of Y. Hou, C. Tlili, N. Jaffrezic-Renault, A. Zhang, C. Martelet, L. Ponsonnet, A. Errachid, J. Samitier, J. Bausells, Biosensors and Bioelectronics, 2004, 20, 1126-1133.

2.1. Introduction

Immunosensors are of great interest because of the potential utility, which is due to their main advantages, such as high sensitivity, selectivity and robustness related to the selectivity and affinity of the antibody-antigen binding reaction (3). With the development of immobilizing biomolecules techniques and analytical techniques, immunosensors have been attracting numerous researchers, and they have been investigated and employed to various fields: the environment analysis (4-6), clinical diagnostics (7), food and drink industries (8) etc.

Like other types of biosensors, immunosensors need suitable techniques to immobilize the active biocomponents and appropriate transducers. Immobilization of antibody is a crucial step for fabricating high quality immunosensor, since after immobilization the activity of antibody should remain high and binding of antigen should occur in a manner that reduces interference. The conventional methods for immobilization of biocomponents include physical adsorption, covalent binding, entrapment etc., however, they suffer from a poor spatially controlled deposition (9). Conducting polymers have been used widely as a platform for the fabrication of biosensors including immunosensors. However, it's difficult to control the amount of biocomponents in the active films, and moreover, the thickness of polymers leads to a decrease of the response time of the biosensor.

Comparing to these techniques, Langmuir-Blodgett technique is considered as a desirable immobilization method for biosensor owing to the advantages: making uniform, ordered and ultra-thin organic films; controlling the amount of biocomponents by the number of deposited layers; and in addition preserving the activities and specific recognition properties of biocomponents. Up to now this technique has been used to immobilize various biomolecules, such as enzymes (10-12), and antibodies (13-17) for the fabrication of biosensors.

The molecular recognition receptor of an immunosensor is prepared by immobilizing antibodies onto a substrate, which can be a conductor or semiconductor material. Noble metal substrates of Pt, Au, Ag seem very suitable for this purpose, since they are easy to functionalize. Gold (18) and platinum (19) have been widely used for fabricating immunosensors. In this study, we have employed silver as substrates. To the best of our knowledge, the applications of substrates of silver functionalized by the method of self-assembled monolayers to Langmuir-Blodgett films deposition and

impedimetric immunosensor have never been reported.

The other important part for fabricating immunosensor is to choose an appropriate transducer. Up to now, the available transducers for immunosensors can be broadly divided into optical, electrochemical, mass-sensitive and thermal devices. Electrochemical impedance spectroscopy is a relatively new technique for immunosensor, which is based on change of localized impedance resulting from a change in dielectric constant that can be brought on by antigen-antibody complex formation.

In this study, Langmuir-Blodgett technique was used to immobilize anti-rabbit IgG/amphiphile LB films onto the hydrophobic surface of 1-octadecanethiol-modified silver. It is worth remarking that control of the LB films deposition process depends on knowing the properties of the monolayer at the air/water interface. In order to obtain stable LB films, in this paper, the influences of different parameters - type of amphiphile, surface pressure and pH – on the properties of mixed IgG/amphiphile monolayer, were investigated. And the optimal conditions were chosen for the transfer of the LB films. On the other part, a simple impedimetric spectroscopy was used for electrochemical study of the engineered immunosensor.

2.2. Materials and methods

2.2.1. Biomaterials and chemicals

The antibody used was anti-rabbit IgG (whole molecule) developed in goats, the antigens were rabbit IgG and sheep IgG from serums (reagent grade). All of them were purchased from Sigma Chemical Company and used without any further purification.

The amphiphiles octadecylamine and behenic acid, purity higher than 99%, were purchased from Fluka. And they were dissolved in chloroform (99.8% purity) from Aldrich Chemical Company at a concentration of 1 mg ml⁻¹. 1-octadecanethiol used for modification of silver substrate was obtained from Aldrich Chemical Company. Potassium dihydrogen phosphate and potassium chloride from Merck, sodium hydroxide from Aldrich Chemical Company were used to prepare phosphate buffer solution (PBS).

Water used in the subphase was purified by an Elga system with a reverse osmosis, deionization, filtration and ultraviolet irradiation systems to have a resistance as high as 18.2 mΩ.cm. Its pH was about 5.5, and its surface tension was

71.8 mN m⁻¹ at 25 °C in air.

In our study, the antibody IgG solutions at a concentration of 4 mg l⁻¹ were prepared freshly on the day of experiment by dissolving the antibody IgG in PBS (pH 5.5-7.3) with a 5 mM concentration. All glassware that was to come into contact with the samples, solutions, or solvents was washed well with sulfochromic solution, rinsed with copious amounts of ultrapure water and then acetone, dried for overnight in a sealed oven at 100 °C.

2.2.2. The fabrication of silver substrate

The microelectronics fabrication process for the devices planar has been performed at Centro Nacional de Microelectrónica (CNM) in Spain by using <100>-oriented, 100 mm diameter, p-type silicon wafers with nominal resistivity of 4-40 Ω cm, which corresponds to a doping level of 1x10¹⁵ cm⁻³. The process started with a thermal oxidation process to grow a silicon dioxide layer (SiO₂-780 Å) on silicon wafers in a hydrox furnace at 950 °C. And then LPCVD Si₃N₄ layer (1000 Å) was deposited on the silicon dioxide at 800 °C. Finally, a 300 Å titanium layer and 1000 Å thick silver layer were sputtered on the silicon nitride surface.

2.2.3. Self-assembled monolayers and modification of silver substrates

Langmuir-Blodgett and self-assembled monolayers have been intensively studied as two major techniques for the fabrication of supramolecular structures. SAMs are ordered molecular assemblies formed by the adsorption of an active surfactant on a solid surface (20). Due to their dense and stable structure, SAMs have potential applications in corrosion prevention, wear protection, and in addition, the biomimetic and biocompatible nature of SAMs makes their applications in chemical and biochemical sensing promising. In this paper the silver substrates were modified with 1-octadecanethiol by means of SAMs, which provide a hydrophobic surface that is favourable to the deposition of Langmuir-Blodgett films.

Comparing to gold substrate, mild cleaning procedures and an O₂-free SAMs formation environment are necessary for silver substrate due to its higher reactivity to atmospheric gases (21). The preparation of SAMs of 1-octadecanethiol on silver substrate was introduced in chapter II. In brief, silver substrates were cleaned with hot ethanol for 5 min, and then they were immersed immediately into solution of 1-octadecanethiol in ethanol with a concentration 1 mM for 24 h with the presence of N₂

flow. Excess thiol was removed from the surface by rinsing the surface with plenty of ethanol. And substrates were then dried under a N_2 flow.

A contact angle meter (GBX scientific instruments, France) was used to measure the contact angle of SAMs modified silver. It has been reported that SAMs formed on Ag are dense and well-ordered (22-23). We found that the substrates were hydrophobic with contact angle $115^\circ \pm 3^\circ$ (24), which is higher than the contact angle obtained for gold substrates. This shows that thiol SAMs on silver is more compact and reproducible. By this way we can obtain a well protected silver surface and then a better transfer coefficient of Langmuir-Blodgett films can be obtained.

2.2.4. Langmuir-Blodgett films

Langmuir film experiments were operated on a Langmuir trough which is computer controlled from NIMA (model 611 with an effective film area $30\text{ cm} \times 10\text{ cm}$). The surface pressures were measured by using a Wilhelmy balance, which was equipped with a strip of chromatography paper suspended at the air-water interface.

The subphase temperature was controlled at $20 \pm 1^\circ\text{C}$ by a thermostatic system (Julabo-F25, France). The subphase was constituted of solution of antibody IgG in PBS at different pH or in ultrapure water. Before each experiment, the surface of the subphase was cleaned by aspiration. And the surface was considered as clean when the change in surface pressure of the clean subphase upon compression of the area was smaller than 0.1 mN m^{-1} .

The chloroform solution of ODA or BA, with a concentration of 1 mg ml^{-1} , was spread ($22\text{ }\mu\text{l}$ used for ODA and $25\text{ }\mu\text{l}$ for BA each time) on the subphase of antibody solution by using a microsyringe of $50\text{ }\mu\text{l}$. The spreading was achieved at the same distance above the subphase in all experiments. It took approximately 15 min to wait for chloroform evaporating.

As indicated above, control of LB films deposition process depends on knowing the properties of the monolayer at air/water interface. For studying adsorption of IgG to amphiphile monolayer at the air/water interface, surface pressure-time curves (referred to as Π -t) were recorded with opened barrier, namely without applying compressing force. The characteristics of a monolayer on the water surface were studied by measuring the changes in surface pressure upon compressing the monolayer at a given temperature, namely surface pressure-molecular area isotherm (referred to as Π -A). The shape of the isotherm is characteristic of the molecules making up the film. The

stability of the monolayers, which is an important parameter for the stability of the mixed LB films, was demonstrated by molecular area ratio-time evolution isotherms at the target pressure (referred to as A/A_0 -t).

The optimal conditions for obtaining stable monolayers of IgG/amphiphile were chosen after all experiments. Under these conditions, LB films of IgG/amphiphile were deposited onto the SAMs modified silver with the vertical dipping method at a rate of 5 mm min^{-1} . After the deposition, the substrates were placed into the vapour of glutaraldehyde for 15 min, in order to stabilize LB layers by cross-linking with this bifunctional reagent, and then they were used for the following impedance measurements.

2.2.5. Impedance measurements

The electrochemical cell for the impedance measurements was a three-electrode cell with a volume of 5 ml. The counter-electrode was made of a platinum plate with an active surface of 0.64 cm^2 , whereas the active surface of the working silver electrode was fixed by an O-ring seal at 0.07 cm^2 . The polarisation of the working electrode was fixed against a saturated calomel reference electrode (SCE), which was purchased from Radiometer Analytical SA.

The various steps of fabrication of the sensor were controlled by impedance spectroscopy. The experimental set-up (an Electrochemical Interface SI 1287 and a Frequency Response Analyser 1255B from Solartron) controlled by a computer was used to measure the total ac impedance of the electrochemical cell. These measurements were carried out by scanning the frequency from 5×10^{-2} to 10^5 Hz , acquiring five points per decade. An excitation voltage of 10 mV was superimposed. All measurements were performed in PBS (pH=7.4) at room temperature.

2.3. Results and discussion

2.3.1. Adsorption of antibody IgG to amphiphile monolayer at the air/water interface

The adsorption of IgG was strongly dependent on the type of amphiphile and pH values of the subphase. In the case of BA, as can be seen from the Figure III.2A, at pH 5.5 and 6.5 surface pressure did not increase apparently during 3 h. However, in the case of ODA, shown in Figure III.2B, IgG molecules were more easily adsorbed to ODA monolayer at the air/water interface, and higher surface pressure was obtained with

the increase of pH value.

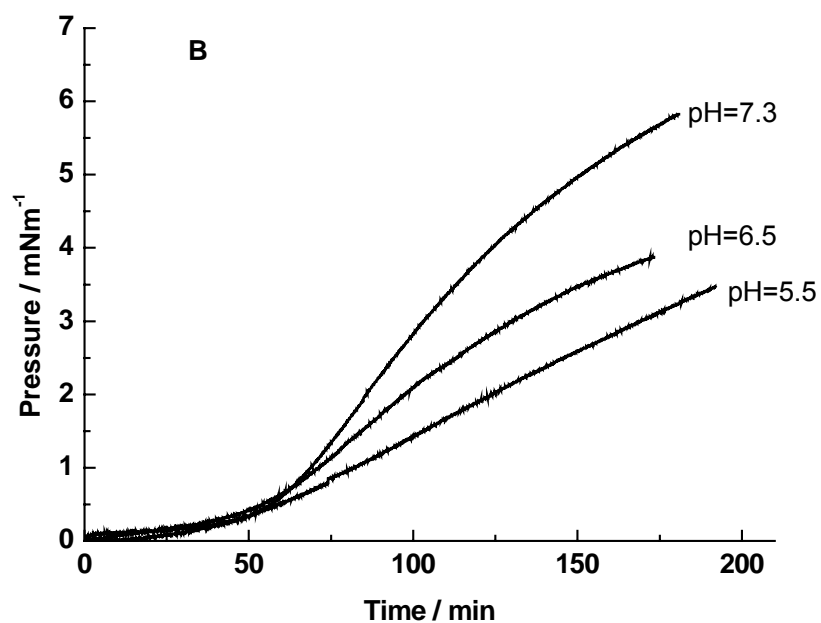
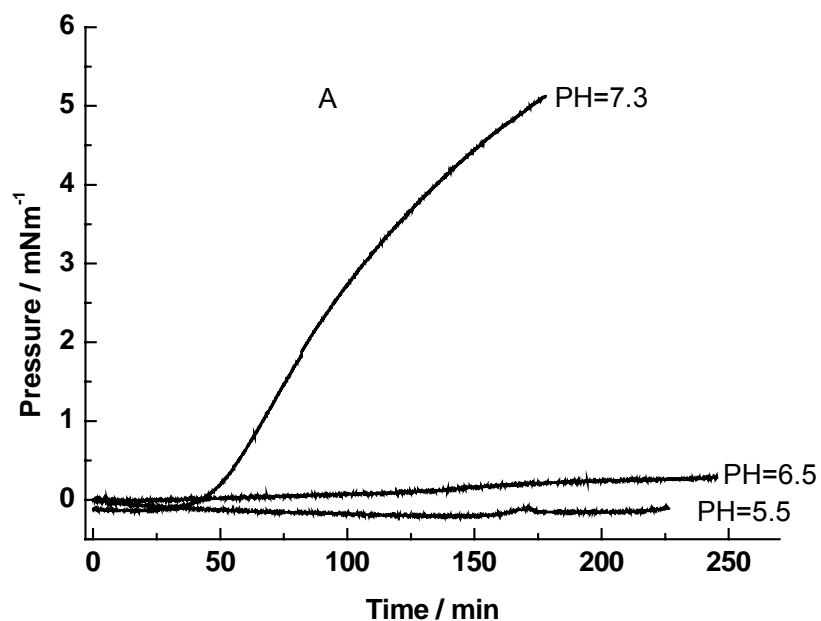


Figure III.2: Surface pressure-time isotherms with different pH in the subphase for BA (A) and ODA (B).

Electrostatic force between IgG and amphiphile molecules is expected to be the important factor for the adsorption process. For BA, whose pK_a is around 5.4

(25), at pH 5.5 it would be nearly neutrally charged, therefore, the electrostatic interaction between antibody IgG and BA is feeble. In addition, when the pH value of subphase is closer to pK_a value of BA, the strong ion-dipole interaction among the carboxyl groups of BA molecules decreases the intermolecular distance at the air/water interface (see Figure III.3) (26), which made it more difficult for big antibody IgG molecules to be entrapped into the monolayer. As a result at pH 5.5 there was nearly no increase of surface pressure during 3 h.

With the increase of pH value from 5.5 to 7.3, the ionic repulsion between polar groups of BA molecules increases the intermolecular distance, and it makes much easier for antibody IgG molecules to be entrapped into the monolayer of BA. As can be seen from the curve of pH 7.3, the surface pressure reached 5 mN m^{-1} after 3 h.

In the case of ODA, whose pK_a is close to 10 (27), when the pH value of subphase is lower than 10, ODA molecules are positively charged. For antibody IgG molecules, because their isoelectric point is about 7.0, they are globally positively charged when pH is lower than isoelectric point. It is not a priori favourable to electrostatic interactions between IgG and ODA molecules. However, it is proposed that negatively charges exist in the antibody IgG molecules and they can be adsorbed onto the monolayer of ODA by the interaction between the negatively charged part of IgG and positively charged ODA molecules. Still more, the pH values of the subphase we chose are far lower than pK_a of ODA so that intermolecular distance is in favour of the entrapment of antibody IgG into the monolayer of ODA. As is shown in the Figure III.2B, antibody IgG molecules are adsorbed onto the monolayer of ODA so easily. In the case of pH 7.3, the pH value is a little higher than the isoelectric point of antibody IgG molecules, hence it is favourable to electrostatic interactions between IgG and ODA molecules, as a result, at this pH point IgG molecules were adsorbed easily to ODA monolayer, and a much higher surface pressure was obtained after 3 h.

Comparing the two different amphiphile molecules BA and ODA, ODA is considered more suitable for the formation of the mixed IgG/amphiphile monolayer at the air/water interface, because it is easier for IgG to be adsorbed onto ODA monolayers under conditions used.

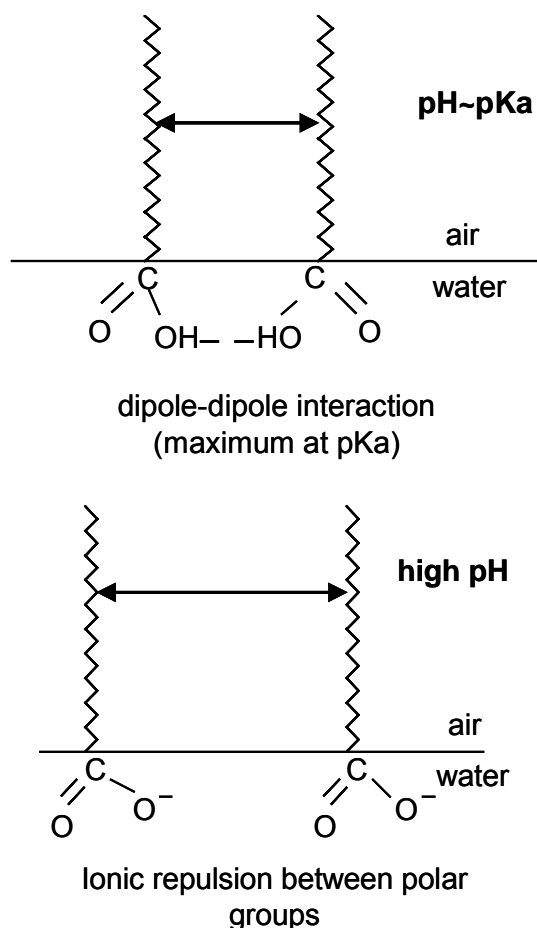


Figure III.3: Interaction between the carboxyl groups at the air/water interface for values of pH: near pKa and higher than pKa.

2.3.2. Surface pressure-molecular area isotherms

Three different subphases: ultrapure water, PBS at pH 6.5 without and with IgG, were used to investigate the characteristics of the corresponding amphiphile monolayers. The surface pressure–molecular area isotherms of amphiphile molecules on ultrapure water were considered as a reference. For the mixed film, an apparent molecular area was defined as the ratio of the film area to the number of amphiphile molecules.

We can see from the Figure III.4. the ingredients of the subphase have apparent influence on the characteristics of the amphiphile monolayers at the air/water interface. For BA, Figure III.4A, the monolayer with the subphase of ultrapure water was a little different from the one with the subphase of PBS. And molecular area of the BA monolayer in the ultrapure water subphase was a little smaller, probably because the PH value of ultrapure water 5.5 is close to pK_a value of BA, and a strong ion-dipole interaction among the carboxyl groups makes the monolayer denser.

Comparing the two curves of BA with and without IgG in PBS, it can be

seen that at the low surface pressure, the molecular area of BA in the antibody-containing subphase is greater than that obtained in the subphase without IgG, which demonstrates that the IgG molecules were entrapped into the unstructured BA monolayer at the low surface pressure. The result could prove that there is indeed interaction between IgG and BA under the condition. However, with further compression of the monolayer, IgG molecules were gradually expelled from the interface and pushed under the head of BA monolayer or into the aqueous subphase, as we remark the slopes of the two curves become more and more similar at the high surface pressure.

For ODA, Figure III.4B, the monolayers of ODA with the two different subphases of ultrapure water and PBS are comparatively different. At the pH 6.5, the amino head of ODA should be positively charged, the addition of strongly bound multivalent counter-ions, such as PO_4^{3-} in the PBS subphase have effect on the monolayer (28). We can see from Figure III.4B that at low surface pressure the molecular area of the ODA monolayer with the PBS as subphase was much larger than that of the ODA monolayer in ultrapure water. It is proposed that at low surface pressure aggregate of long-chain amine ODA around PO_4^{3-} took place. In the case of PBS subphase with IgG, the molecular area is still greater than without IgG at low surface pressure, it means that interaction exists also between antibody IgG and ODA molecules, and some of IgG molecules were inserted into the ODA monolayer.

Like BA, with compressing the monolayer, IgG molecules were gradually pushed under the head of ODA monolayer or into the solution. The surface pressure 35 mN m^{-1} indicated in Figure III.4B is chosen as target pressure. Because at this surface pressure the mixed IgG/amphiphile monolayer is in the solid phase, as we can see from Figure III.4B. It's well known that the molecules are relatively well oriented and closely packed in the solid phase.

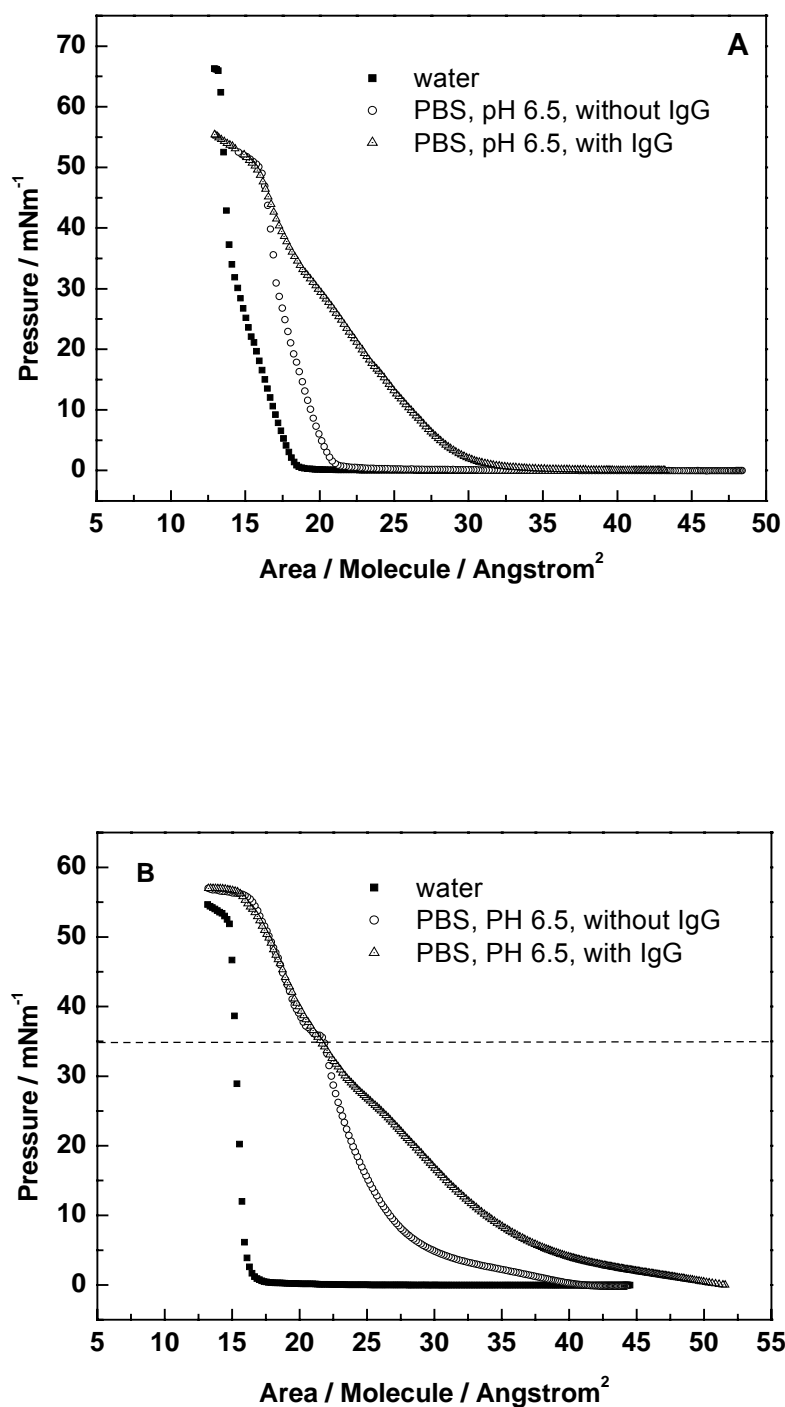


Figure III.4: Isothermal compression curves for amphiphile with different subphases: water, phosphate buffer solution (5×10^{-3} M, pH 6.5) without antibody IgG and with antibody IgG (4 mg l^{-1}) for BA (A) and ODA (B).

2.3.3. The stability of the mixed IgG/amphiphile monolayer

The stability of the mixed monolayer is very important because it is related to the transfer efficiency and the quality of deposited LB films. It can be examined

by the evolution of surface pressure with time at a fixed molecular area, or the evolution of molecular area ratio with time at a fixed surface pressure, after the monolayer has been compressed. The latter condition was chosen in this paper.

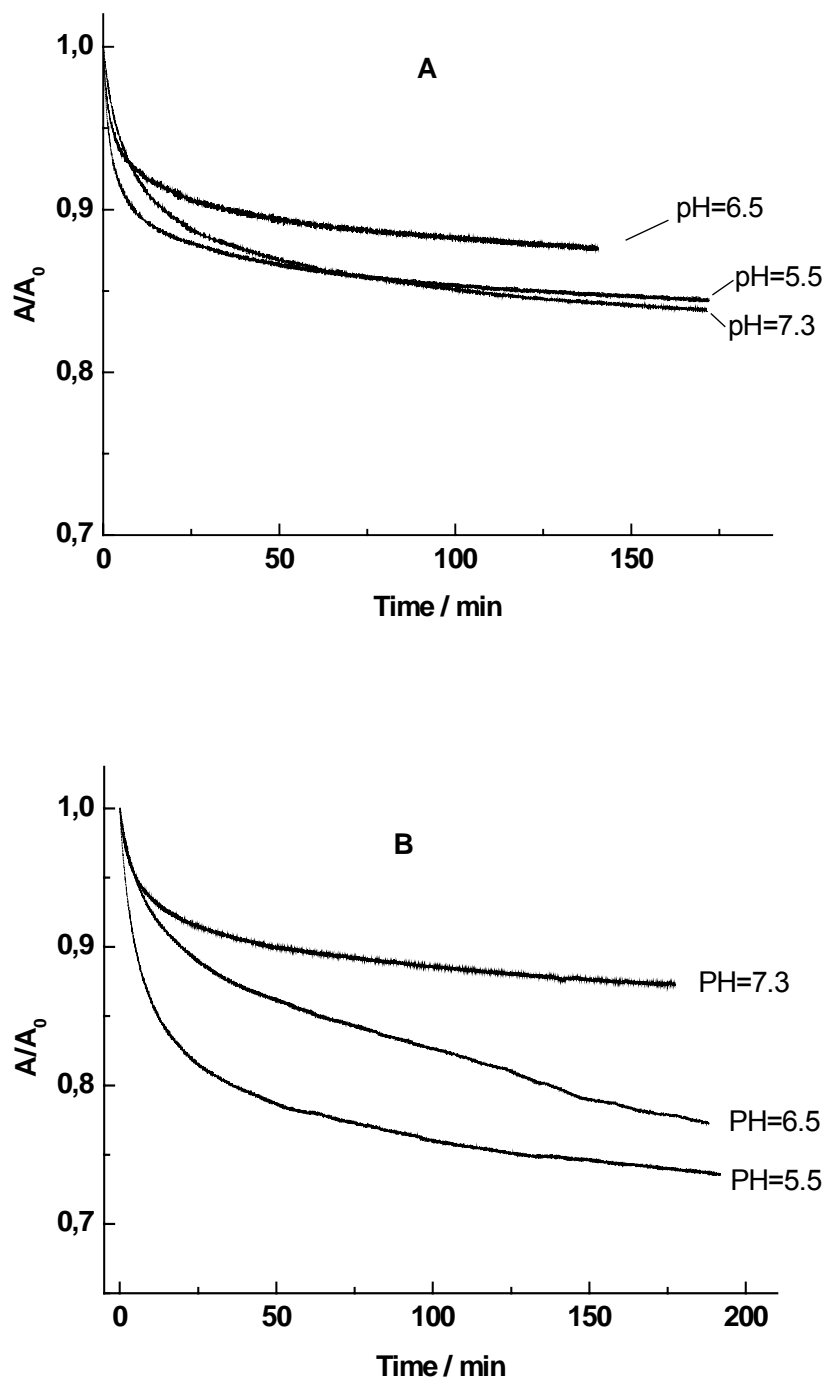


Figure III.5: Molecular area ratio-time isotherms at different pH, for BA (A) and ODA (B).

As has been reported by our group (11), the pure amphiphile monolayer is unstable because of their partial solubility in the subphase. However, we can see from

the Figure III.5A and III.5B all the monolayers with different amphiphiles and pH values are stable in the antibody-containing subphase. As stated before, this increase in stability is due to interactions between the antibody molecules and the polar heads of amphiphile. Another phenomenon can be seen from the figures is that the surface area of monolayer decreases clearly at the beginning and then keeps comparatively constant with time. This initial loss in area depends on the rate at which the monolayer is compressed and is due to a structural rearrangement occurring within the layer. And after rearrangement the monolayers become very stable, and especially the monolayer with ODA and at pH 7.3, in our study, after 3 h, the molecular ratio remained 88 %. And so pH 7.3 was chosen for the deposition of the Langmuir-Blodgett films.

Still more, we have compared the stabilities of the IgG/amphiphile monolayers at different surface pressures which correspond to different phases for the monolayers. Here we have shown them for BA in Figure III.6, and we found that at 35 mN m^{-1} the mixed monolayer of BA and IgG is more stable, as we can see from Figure III.4A, at this surface pressure the monolayer is in the solid phase. So we can conclude that the IgG/amphiphile monolayer in the solid phase is more stable than that in the liquid phase at air/water interface.

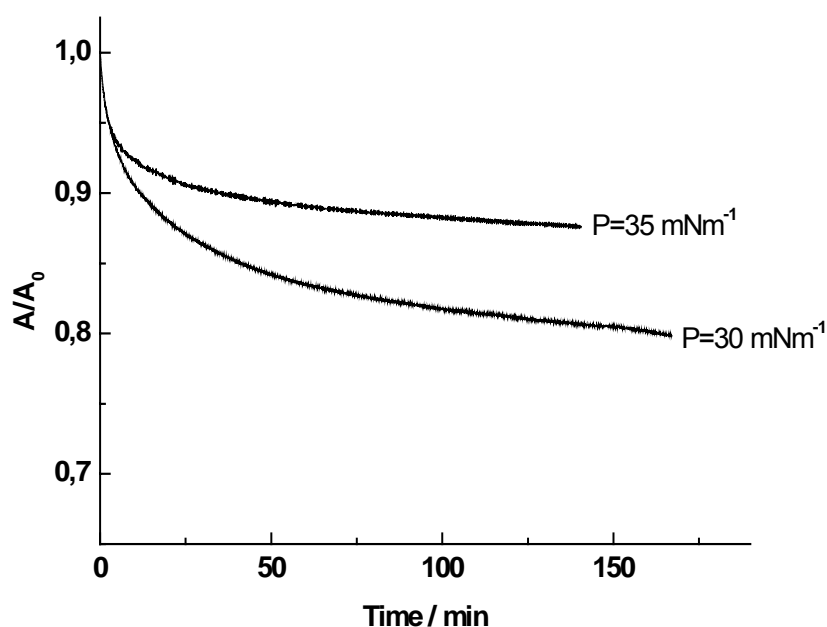


Figure III.6: Molecular area ratio-time isotherms of BA with IgG at different target pressures.

From the experimental results, we concluded optimal conditions for forming stable mixed IgG/amphiphile monolayer as the following ones: ODA as

amphiphile molecule, pH 7.3, surface target 35 mN m^{-1} and 20°C . Under these conditions, Langmuir-Blodgett films of IgG/amphiphile were deposited efficiently onto the SAMs modified silver with the vertical dipping method at a rate of 5 mm min^{-1} and were used for the study of the corresponding immunosensor.

2.3.4. Impedance measurements

After mixed LB films deposition on the sample of silver substrate which was previously modified by an ODT SAMs, it was mounted as working electrode in the cell. And different concentrations of specific antigen (rabbit IgG reagent), which was expected to react specifically with the immobilized antibody (anti-rabbit IgG), were added to the buffer solution in the cell. The impedance measurements were carried out under optimized conditions in order to minimize the influence of the Warburg impedance on the total impedance of the cell (frequency range from 5×10^{-2} to 10^5 Hz and polarisation voltage of -250 mV). As shown in Figure III.7A, the semicircle diameter in the Nyquist plot increases with increasing specific antigen concentration, especially at low frequency. However, when a non-specific antigen (sheep IgG reagent) comes in contact with the working electrode, there is quasi no modification of the initial Nyquist plot with increasing non-specific antigen concentration, as shown in Figure III.7B.

Since the more important change of impedance occurs at 0.15 Hz , it was chosen for the study of the sensor response. To obtain a calibration curve of the immunosensor, we have plotted the variations of $\log (|Z/Z_0|)$ versus the antigen concentration at a frequency 0.15 Hz (Figure III.7) for both specific antigen (rabbit IgG reagent) and non-specific antigen (sheep IgG reagent).

In this expression, $|Z_0|$ is the modulus of the impedance of the antibody modified electrode before the injection of antigen, and $|Z|$ is that of the subsequent electrode after each antigen addition. In Figure III.8, the specific signal differs significantly from the non-specific signal for concentration higher than 200 ng ml^{-1} , hence the detection limit is evaluated to be around this value.

For the specific signal curve, in the range 200 to 900 ng ml^{-1} , a slope of $0.224 \mu\text{g}^{-1} \text{ ml}$ is observed. Over 900 ng ml^{-1} the sensor is prone to reach saturation. If we compare these results to those obtained with an impedimetric immunosensor based on gold electrode functionalised with a cyano N-substituted pyrrole (18), the same type of calibration curve was obtained. For the non-specific signal curve, a slope of $0.045 \mu\text{g}^{-1} \text{ ml}$ is obtained. We think this low slope corresponds to a weak non-specific adsorption. As to experimental value presented in Figure III.8 the reproducibility is about 6×10^{-4} . And the

obtained engineered immunosensor has good specificity.

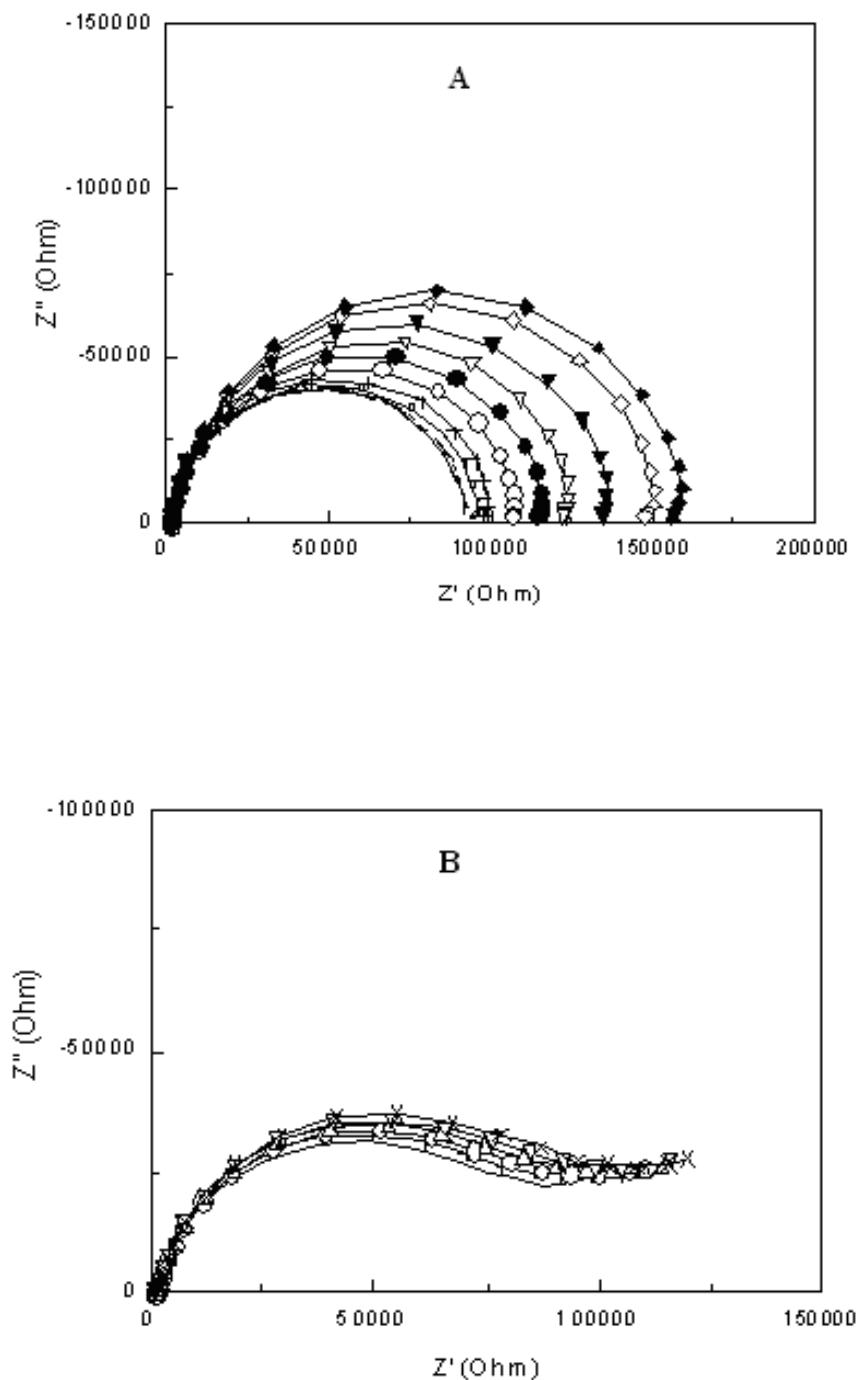


Figure III.7: Complex plane impedance plots obtained for a silver electrode modified with ODT SAMs and mixed IgG/amphiphile LB films, at a potential of -250 mV versus SCE and ac signal of 10 mV, in PBS. (A): without antigen injection (solid line) and with different concentrations of rabbit IgG: 10 (dot), 20 (dash dot), 30 (dash), (∇) 50, (+) 100, (\circ) 200, (\bullet) 300, (∇) 500, (\blacktriangledown) 700, (\square) 900 and (\blacksquare) 1200 ng ml^{-1} and the detect limit is 200 ng ml^{-1} . (B): without sheep IgG (solid line) and with different concentrations of sheep IgG: (+) 50, (\circ) 100, (Δ) 400, (∇) 800, and (\times) 1200 ng ml^{-1} .

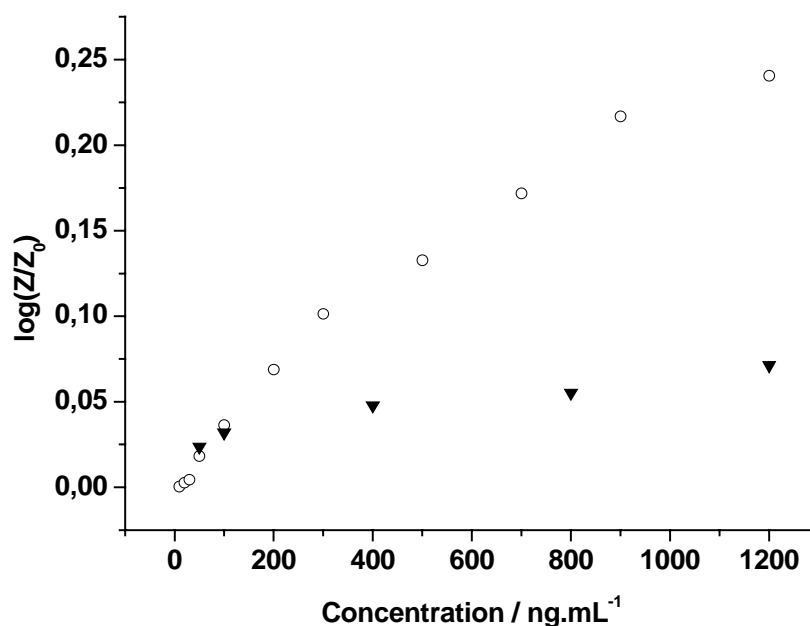


Figure III.8: Response curves for different antigens obtained for silver substrates modified with ODT SAMs and mixed IgG/amphiphile LB films: applied potential -250 mV versus SCE, at frequency 0.15 Hz, in PBS: (○) specific antigen (rabbit IgG), (▲) non-specific antigen (sheep IgG).

2.4. Conclusion

The Langmuir-Blodgett technique is a useful and suitable tool for fabrication of immunosensors. In this work under optimal conditions mixed Langmuir-Blodgett films of immunoglobulin G/amphiphile were successfully transferred onto silver surface previously modified by an ODT SAMs. Impedance measurements on these structures allow obtain a label-free detection of the specific antigen (rabbit IgG) with a detection limit of 200 ng mL^{-1} and a linear dynamic range, from 200 to 900 ng mL^{-1} . These preliminary results appear very promising for building up biomolecular structures and developing biosensors with LB technique. Further work will be devoted to the application of these types of LB films to other proteins for fabrication of odorant biosensors.

References

- (1) <http://images.google.com>
- (2) C. Luo, Detections of antibody-antigen reactions using surface acoustic wave and electrochemical immunosensors, Ph.D., *Thesis*, **2004**, University of Heidelberg, Germany.
- (3) H. Bertold, *Analytica Chimica Acta*, **1997**, 347, 177-186.
- (4) C. R. Suri, M. Raje, G. C. Varshney, *Critical Reviews in Biotechnology*, **2002**, 22, 15-32.
- (5) E. Barceló, D. Barzen, G. Gauglitz, R. Abuknesha, *TrAC Trends in Analytical Chemistry*, **2001**, 20, 124-132.
- (6) J. M. Van Emon, C. L. Gerlach, K. Bowman, *Journal of Chromatography B: Biomedical Sciences and Applications*, **1998**, 715, 211-228.
- (7) P. B. Lippa, L. J. Sokoll, D. W. Chan, *Clinica Chimica Acta*, **2001**, 314, 1-26.
- (8) L. D. Mello, L. T. Kubota, *Food Chemistry*, **2002**, 77, 237-256.
- (9) M. Gerard, A. Chaubey, B.D. Malhotra, *Biosensors and Bioelectronics*, **2002**, 17, 345-359.
- (10) J. M. Chovelon, F. Gaillard, K. Wan, N. Jaffrezic-Renault, *Langmuir*, **2000**, 16, 6228-6232.
- (11) A. Zhang, N. Jaffrezic-Renault, J. Wan, Y. Hou, J. M. Chovelon, *Materials Science and Engineering C*, **2002**, 21, 91-96.
- (12) J. M. Chovelon, M. Provence, N. Jaffrezic-Renault, V. Derue, D. Lair, S. Alexandre, J. M. Valleton, *Journal of Biological physics and Chemistry*, **2001**, 1, 68-75.
- (13) I. V. Turko, I. S. Yurkevich, V. L. Chashchin, *Thin Solid Films*, **1991**, 205, 113-116.
- (14) A. Barraud, H. Perrot, V. Billard, C. Martelet, J. Therasse, *Biosensors and Bioelectronics*, **1993**, 8, 39-48.
- (15) I. Vikholm, O. Teleman, *Journal of Colloid and Interface Science*, **1994**, 168, 125-129.

- (16) T. Dubrovsky, A. Tronin, C. Nicolini, *Thin Solid Films*, **1995**, 257, 130-133.
- (17) G. K. Chudinova, A. V. Chudinov, V. V. Savransky, A. M. Prokhorov, *Thin Solid Films*, **1997**, 307, 294-297.
- (18) O. Ouerghi, A. Senillou, N. Jafferezic-Renault, C. Martelet, H. Ben Ouada, S. Cosnier, *Journal of Electroanalytical Chemistry*, **2001**, 501, 62-69.
- (19) M. S. Desilva, Y. Zhang, P. J. Hesketh, G. Jordan Maclay, S. M. Gendel, J. R. Stetter, *Biosensors and Bioelectronics*, **1995**, 10, 675-682.
- (20) A. Ulman, *Chem. Rev.*, **1996**, 96, 1533-1554.
- (21) A. Majid, F. Bensebaa, P. L'Ecuyer, G. Pleizier, Y. Deslandes, *Rev. Adv. Mater. Sci.*, **2003**, 4, 25-31.
- (22) P. Fenter, P. Eisenberger, J. Li, N. Camillone III, S. Bernasek, G. Scoles, T. A. Ramanarayanan, K. S. Liang, *Langmuir*, **1991**, 7, 2013-2016.
- (23) M. H. Schoenfish, J. E. Pemberton, *J. Am. Chem. Soc.*, **1998**, 120, 4502-4513.
- (24) P. E. Laibinis, G. M. Whitesides, D. L. Allara, Y. Tao, A. N. Parikh, R. G. Nuzzo, *J. Am. Chem. Soc.*, **1991**, 113, 7152-7167.
- (25) C. Foil, S. Alexandre, N. Dubreuil, J. M. Valleton, *Thin Solid Films*, **1995**, 261, 287-295.
- (26) J. R. Kanicky, A. F. Poniatowski, N. R. Mehta, D. O. Shah, *Langmuir*, **2000**, 16, 172-177.
- (27) K. Wan, Etude de Differentes Methodes de Biofonctionnalisation pour la Realisation de Biocapteurs. Application a la Detection de Pesticides. Ph.D. Thesis, **1999**, Ecole Centrale de Lyon, France, p 84.
- (28) G. L. Jr Gaines, *Nature*, **1982**, 298, 544-545.

CHAPTER IV: ELABORATION OF AN ODORANT BIOSENSOR BASED ON ODORANT-BINDING PROTEINS BY LANGMUIR-BLODGETT TECHNIQUE

1. INTRODUCTION ON ODORANT-BINDING PROTEINS

Olfaction is a function widespread in the animal kingdom: for example, fishes, insects and mammals are all able to smell. Olfactory receptors were discovered by Buck and Axel in 1991 (1). It is by now widely recognized that they belong to a large multi-gene family containing ~1000 members. Thanks to the diversity of these receptors, it is possible for mammals to recognize ~10,000 different odorant molecules. The olfactory system will be discussed in detail in the Chapter VI.

In mammals, olfactory receptors are immersed in the protective nasal mucus, and are therefore not in direct contact with air. Contrary to fishes, that smell water-soluble molecules, terrestrial animals smell small volatile and mostly hydrophobic molecules (2). These molecules cannot easily cross hydrophilic barrier of the nasal mucus. While searching for olfactory receptors using tritiated odorants such as pyrazine (2-isobutyl-3-metoxypyrazine) with very low detection thresholds for humans, Pelosi et al. (3) discovered a soluble pyrazine-binding protein, which is secreted by the nasal olfactory mucosa of bovines and other mammals. The abundance of this pyrazine-binding protein in nasal mucus of these animals gave rise to the hypothesis that it may serve as an odorant carrier, it was therefore called odorant binding protein.

Odorant-binding proteins are abundant and usually soluble proteins with low molecular weight (~20 kDa). They are lipocalins secreted in the nasal mucus of vertebrates. These proteins reversibly bind odorants with dissociation constants in the micromolar range. OBPs are suspected to play a role in the transport of airborne odorants, which are commonly hydrophobic molecules towards specific olfactory receptors on sensory neurones across the aqueous nasal mucus. Although vertebrate

OBPs display low sequence similarity (usually <20% amino acid identity), they all share a conserved folding pattern, an eight-stranded β -barrel flanked by an α -helix at the C-terminal end of the polypeptide chain. The β -barrel defines a central apolar cavity, called the calyx, whose role would be to bind and transport hydrophobic odorant molecules (4, 5). The molecular structure for bovine OBP is shown in Figure IV.1 (6).

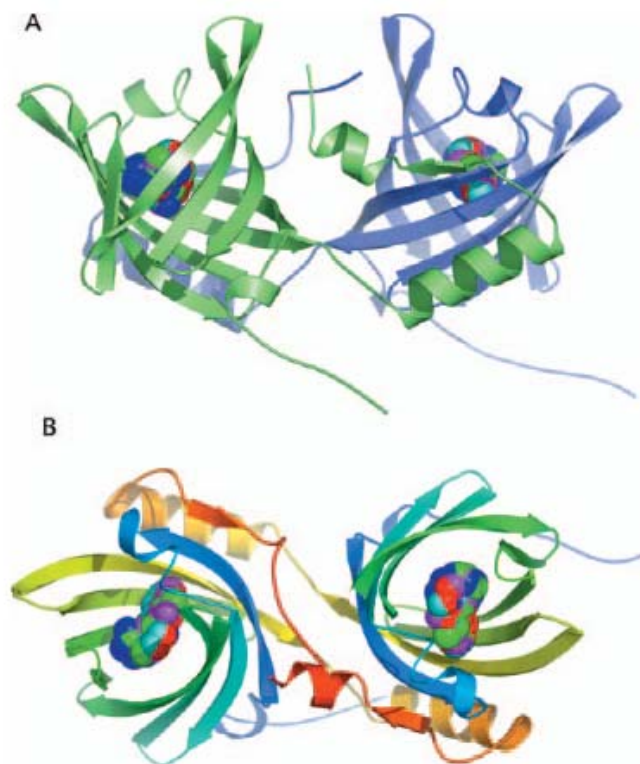


Figure IV.1: Bovine odorant-binding protein dimer (secondary structure representation) and superposition of all the ligands (sphere representation) in both cavities. (A) Monomer A (green) and monomer B (blue-grey). (B) The structure is rotated 90° towards the reader with respect to (A); both monomers are rainbow-colored.

OBPs have been identified in a variety of species, including cow, pig, rabbit, mouse and rat, and recently, elephant and human. In rat, three OBP (called OBP-1, OBP-2 and OBP-3) have been cloned with quite different sequences (7). Binding studies have demonstrated that the three OBPs are specially tuned towards distinct chemical classes of odorants. Rat OBP-1 preferentially binds heterocyclic compounds such as pyrazine derivatives (8, 9). OBP-2 appears to be more specific for long-chain aliphatic aldehydes and carboxylic acids (7), whereas OBP-3 was described to interact strongly with odorants composed of saturated or unsaturated ring structure (10).

In this study a novel rat OBP-1 variant called OBP-1F, originating from the Fisher rat strain, was used. Recombinant OBP-1F was secreted by the yeast *Pichia pastoris*.

Recombinant OBP-1F was shown to exist as a homodimer exhibiting two disulfide bonds (C44-C48 and C63-C155), a pairing close to that of hamster aphrodisin. One odorant molecule can be bound per dimer of OBP-1F molecule, and the binding of odorant molecules was found to induce local conformation changes. It's suggested that one binding site is located in one of the two β -barrels of the OBP-1F dimer and a subtle conformational change correlated with binding of an odorant molecule, which hampers uptake of a second odorant by the other hydrophobic pocket (7). Molecular model of rat OBP-1F is shown in Figure IV.2.

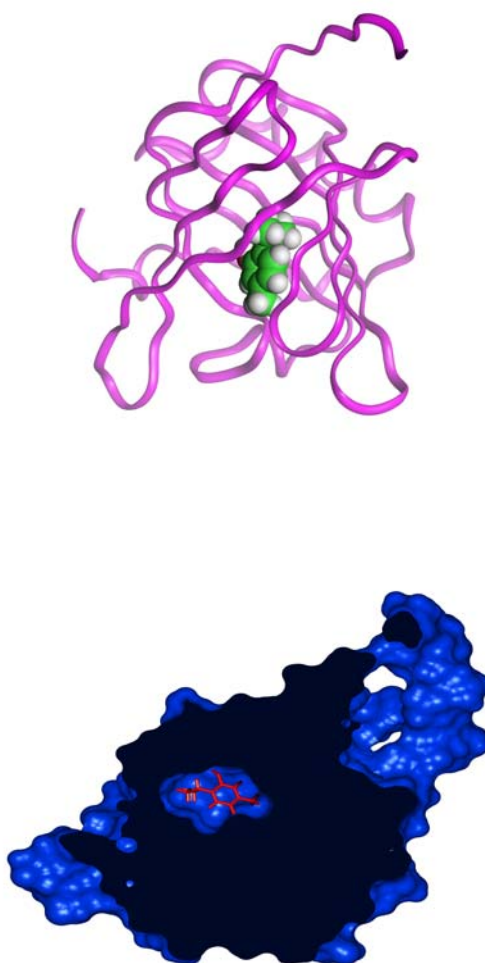


Figure IV.2: (A) Molecular model of rat OBP-1F with thymol molecule located in the binding pocket of the protein; (B) Vertical section of the molecular model of rat OBP-1F through the binding pocket containing a thymol molecule shown in red.

2. STUDY OF LANGMUIR AND LANGMUIR-BLODGETT FILMS OF ODORANT-BINDING PROTEIN/AMPHIPHILE FOR ODORANT BIOSENSORS*

Abstract

In order to make ultrathin films for the fabrication of artificial olfactory systems, odorant biosensors, we have investigated mixed Langmuir and Langmuir-Blodgett films of odorant-binding protein/amphiphile. Under optimized experimental conditions (phosphate buffer solution, pH 7.5, OBP-1F concentration of 4 mg L^{-1} , target pressure 35 mN m^{-1}), the mixed monolayer at the air/water interface is very stable and has been efficiently transferred onto gold supports, which were previously functionalized by self-assembled monolayers with 1-octadecanethiol. Atomic force microscopy and electrochemical impedance spectroscopy were used to characterize mixed Langmuir-Blodgett films before and after contact with a specific odorant molecule, isoamyl acetate. AFM phase images show a higher contrast after contact with the odorant molecule due to the new structure of the OBP-1F/ODA LB film. Non-Faradaic electrochemical spectroscopy is used to quantify the effect of the odorant based on the electrical properties of the OBP-1F/ODA LB film, as its resistance strongly decreases from $1.18 \text{ M}\Omega$ (before contact) to $25 \text{ k}\Omega$ (after contact).

* Slightly modified version of Y. Hou, N. Jaffrezic-Renault, C. Martelet, C. Tlili, A. Zhang, J. C. Pernollet, L. Briand, G. Gomila, A. Errachid, J. Samitier, L. Salvagnac, B. Torbi  ro, P. Temple-Boyer, *Langmuir*, 2005, 21, 4058-4065.

2.1. Introduction

Many fundamental and central biological recognition and transduction processes occur at biological surfaces. To investigate the molecular behaviour of biomolecules at biological surfaces, a well defined and flexible model system is required. LB and SAMs may provide the desired control on the order at a molecular level and thus may be considered desirable techniques for the construction of future organic materials. (11)

So far, extensive researches have been devoted to either simple Langmuir-Blodgett films systems (12-14) and self-assembled monolayers (15-17) or complex ones, which combine these two techniques with biocomponents. Both techniques are important for their potential application in the fabrication of biosensors. The Langmuir-Blodgett technique has already shown its efficiency for depositing well-defined films of enzymes (18-26) and antibodies (27-29) etc. for manufacturing biosensors and it presents numerous advantages such as: speed, reproducibility, good control of the quantity of biocomponents, and preservation of the activities and specific recognition properties of biomolecules. Since Nuzzo and Allara showed in 1983 that SAMs of alkanethiolates on gold could be prepared from dilute solutions of dialkyl disulfides (30), interest in SAMs has rapidly expanded and the use of SAMs in various fields of research is rapidly growing. Recent developments show that SAMs play an important role in the construction of biosensors due to advantages such as simplicity, adaptability, stability and the control of biomolecule surface orientation. (31-33)

This study deals with the preparation of ultra-thin films in which odorant-binding proteins were incorporated by the combination of LB films and SAMs, with the aim of drawing up a preliminary design for an artificial olfactory system to detect specific odorant molecules.

OBPs are abundant low-molecular weight soluble proteins secreted by the olfactory epithelium in the nasal mucus of vertebrates. Although their functions are still unclear, OBPs are suspected of playing a carrier role for conveying odorants, which are commonly hydrophobic molecules, to their neuronal receptors through the aqueous nasal mucus. (7) Rat OBP-1 binding properties have been investigated by spectroscopic approaches using fluorescent probe competitive assays and by isothermal titration calorimetry, demonstrating that this dimeric OBP is capable of reversibly binding to distinct chemical classes of odorants with dissociation constants in the micromolar range.

(9) In the present report a recombinant OBP rat variant OBP-1F was used for the preparation of mixed protein/amphiphile LB films. The experiments were performed in the subphase of PBS at a pH of 7.5. Considering that OBP-1F is perfectly soluble in the pH range from 6.5 to 8.5, and the protein denatures at a pH value below 3 and above 9.5. OBP-1F dissolves perfectly and keeps active in the subphase at pH 7.5. Fatty amine octadecylamine was chosen as the amphiphile because at this pH, OBP-1F could be considerably better adsorbed onto positively charged amphiphile monolayers such as amine than onto neutral or negatively charged ones. Because the calculated isoelectric point of OBP-1F is 5.20, the protein molecules are mainly negatively charged at a pH value of 7.5. In addition, the use of fatty amines allowed us to carry out a cross-linking step between amine terminal moieties (from protein and fatty amine) and glutaraldehyde molecules in order to improve the stability of the transferred LB films as reported by Sun et al. (19) and Chovelon et al. (25). The presence of the protein and counter-ions of hydrogen phosphate in the subphase was expected to be favorable for the stability of the fatty amine monolayer at the air/water interface. (34)

The basic LB technique is known to consist of the formation of a monolayer of amphiphile molecules on the surface of the subphase containing soluble protein and then the transfer of the monolayer onto the solid substrate using a vertical dipping procedure (Langmuir-Blodgett) or a horizontal one (Langmuir-Schfäer). To obtain high-quality LB films, the properties of the monolayer, especially its stability, were investigated here, because they play a key role in obtaining stable and reproducible LB films, which are essential for biosensor applications. LB films of odorant-binding protein/amphiphile, OBP-1F/ODA in our case, were deposited onto gold substrates using the vertical dipping procedure, which had been previously functionalized with 1-octadecanethiol SAMs to provide a hydrophobic surface favorable for the deposition of OBP-1F/ODA LB films.

As a practical application, the LB films obtained were exposed to isoamyl acetate, an odorant molecule that has previously been shown to interact with OBP-1F. (9) In this study, several techniques including scanning electron microscopy (SEM), atomic force microscopy and electrochemical impedance spectroscopy have been applied to characterize LB films designed for odorant biosensor applications. AFM is considered as a powerful tool in microbiology (35, 36) and is also an interesting tool for the characterization of LB films (20, 26, 37, 38) because it could give access to the molecular architecture. A complementary technique, EIS, is a rapidly developing electrochemical technique for the characterization of films containing biomolecules at the

electrode surface and has potential applications in biosensing. (39-42)

2.2. Materials and methods

2.2.1. Materials

Recombinant rat OBP-1F (wt 18.5 KDa) provided by INRA was produced using the yeast *Pichia pastoris* and purified by reversed phase liquid chromatography as described previously. (7) Purified protein was dialysed extensively against MilliQ H₂O and lyophilized. Isoamyl acetate was obtained from Sigma. Octadecylamine (purity > 99%) and 1-octadecanethiol (purity 98%) were purchased from Fluka and Aldrich, respectively. Solvent chloroform (purity 99.8%) bought from Aldrich was used to dissolve ODA at a concentration of 1 mg/ml, and ODT was dissolved at a concentration of 1 mM in ethanol (purity > 99.8%) obtained from Fluka, for modification of the gold substrate. Potassium dihydrogen phosphate and sodium chloride (from Prolabo), and sodium hydroxide from Aldrich were used to prepare 10 mM phosphate buffer solution containing 100 mM NaCl, pH 7.5, which was used for all LB film preparation and impedance measurements. All reagents were of analytical grade (>99%).

In the present study, OBP-1F solutions were prepared freshly on the day of the experiment by dissolving the lyophilized protein in 10 mM PBS (pH 7.5). Water used throughout all experiments was purified by an Elga system with reverse osmosis, deionization, filtration and ultraviolet irradiation systems to have a resistance as high as 18.2 mΩ.cm. Its pH was about 5.5, and its surface tension was 71.8 mN.m⁻¹ at 25 °C in air. All glassware that was to come into contact with samples, solutions, or solvents was washed well with sulfochromic solution, rinsed with copious amounts of ultrapure water and then acetone, and finally dried overnight in a sealed oven at 100 °C.

2.2.2. Gold substrate and monolayer preparation

Gold substrates, provided by Laboratoire d'Analyse et d'Architecture des Systèmes (LAAS), Toulouse, were fabricated using standard silicon technologies. <100>-oriented, P-type (3-5 Ω.cm) silicon wafers were thermally oxidized to grow an 800 nm-thick field oxide. Then, a 30 nm-thick titanium layer and a 300 nm-thick gold top layer were deposited by evaporation under vacuum.

The formation of a monolayer on gold was seen to be strongly

dependent on several factors, such as the structure of the gold and its cleanliness prior to modification. Gold is known to be a soft metal, readily contaminated by organic and inorganic species during manual handling. (43) Consequently the fabrication process and the pre-treatment, namely cleanliness, of gold substrates are of paramount importance for the reproducibility of the following steps.

In the present study, the whole metallization process was optimized so that the Ti/Au layer would adhere well onto the field oxide, and the gold upper surface would therefore have good properties. This optimization was obtained by using low deposition rates (around 1 nm.s^{-1}) for both evaporation processes, and by eliminating the Ti/Au annealing process ($250^\circ\text{C} - 20 \text{ min}$).

Likewise, the cleaning procedure was optimized as well. As referred in chapter II, the gold substrates were first cleaned with acetone in an ultrasonic bath for 10 min, then immersed in a 7:3 (v/v) $\text{H}_2\text{SO}_4\text{:H}_2\text{O}_2$ (piranha solution) for 1 min. Gold substrates were subsequently rinsed thoroughly in absolute ethanol and finally dried under nitrogen flow. As soon as the cleaning procedure was finished, the substrates were put into a 1 mM ODT ethanol solution for 21 h. After the formation of well-ordered SAMs, the contact angle of the gold electrode is $110^\circ \pm 3^\circ$.

2.2.3. Langmuir and Langmuir-Blodgett films

The same Langmuir trough described in chapter III was used. The subphase temperature was controlled at $10 \pm 1^\circ\text{C}$ by a thermostatic system (Julabo-F25, France) to obtain a well-organized and stable monolayer, because it has been reported that lowering the temperature of subphase can increase the stability of the monolayer at the air/water interface. (24) Before each experiment, the trough was washed several times with ultrapure water, and the surface of the subphase was cleaned by aspiration. The surface was considered clean when changes in the surface pressure of the subphase upon compression of the area were smaller than 0.1 mN m^{-1} . After that the subphase, which was composed of a solution of OBP-1F in PBS at different concentrations or in ultrapure water, was introduced into the trough.

To elaborate the mixed layer of octadecylamine and protein OBP-1F, the protein solution in PBS was used as the subphase, and $22 \mu\text{L}$ of ODA in chloroform (1 mg ml^{-1}) was injected and spread onto the interface using a micropipette. It was spread from the same distance above the subphase in all experiments. After spreading, the monolayers were left for at least 15 min to allow the solvent to evaporate. Proteins

were allowed to adsorb from the subphase to the air/water interface. Our study found that it took more than 10 hours to reach adsorption equilibrium. As such a long adsorption time may result in water evaporating from the subphase, thereby unfavourably affecting the accuracy of the experimental results, proteins were allowed to adsorb from the subphase for about 3 h, representing 70% of the steady state equilibrium.

The apparent molecular area was defined as the ratio of the film area to the number of spread ODA molecules. The film was then compressed at a rate of $5 \text{ cm}^2 \text{ min}^{-1}$ until the target surface pressure was reached. Such a low rate of compression was chosen to avoid too much disturbance of the equilibrium of the monolayer. A relaxation time of 3 h was required before the onset of dipping. While the surface pressure remained constant and the monolayer was stable, the monolayer was transferred onto hydrophobic gold substrates by a vertical dipping method at a rate of 3 mm min^{-1} . After each upstroke, the substrate was kept in air for 5 min to dry the films. The transfer ratio, expressed as the ratio of area of film transferred onto the coated monolayer area on the substrates, was used as a parameter to characterize the LB deposition process. After transfer, film functionalized gold substrates were put into glutaraldehyde vapour for 15 min to stabilize the LB layers by cross-linking with this bifunctional reagent. Samples were then ready for further experiments.

To understand the proper formation of Langmuir and Langmuir-Blodgett films, first the properties of the monolayer at the air/water interface were studied. The adsorption of protein onto the amphiphile monolayer at the air/water interface was studied by recording surface pressure-time curves (referred to as Π -t) with barriers opened, namely without any compressing force. The characteristics of the monolayer at the air/water interface were studied by measuring the changes in surface pressure when the monolayer was compressed at a given temperature, namely surface pressure-molecular area isotherm (referred to as Π -A). The shape of the isotherm is characteristic of the molecular build-up of the film. The stability of the monolayer, which is an important parameter for the stability of mixed LB films, can be shown by molecular area ratio-time evolution isotherms at the target pressure (referred to as A/A_0 -t) or the surface pressure-time evolution over a constant molecular area (referred to as P_b -t).

2.2.4. Equilibrium with volatile odorant

Once the OBP-1F/ODA LB films had been deposited and stabilized,

functionalised gold substrates were placed in a 2-L sealed glass chamber containing pure undiluted odorant isoamyl acetate (10 μ L in the chamber) which evaporated freely for 16 h at room temperature ($20 \pm 1^\circ\text{C}$). The samples were then used for AFM and EIS measurements.

2.2.5. Langmuir-Blodgett films characterization

2.2.5.1. Scanning Electron Microscopy

SEM images were taken using a scanning electron microscope (Philips XL20). The accelerating voltage was 10 kV.

2.2.5.2. Atomic Force Microscopy

Atomic force microscopy measurements were performed by Laboratory of NanoBioEngineering (Barcelona Science Park), they were obtained in air at room temperature using a Pico+ Microscope (Molecular Imaging). The tapping mode was used to avoid damaging the surface of the sample. Silicon rectangular cantilevers (NCL, Nanoworld) with a normal spring constant of 48 N m^{-1} and resonance frequency of 190 kHz were used (typical curvature radius of the tip 10 nm).

For the purpose of AFM imaging, two different sets of samples were prepared under the same conditions: one set corresponding to OBP-1F/ODA LB films before exposure to odorant molecules and the other set corresponding to OBP-1F/ODA LB films after exposure to odorant molecules. Imaging of both sets of samples were performed under the same conditions.

2.2.6. Electrochemical Impedance Spectroscopy

Impedance measurements were performed in a conventional electrochemical cell containing a three-electrode system with an Electrochemical Interface SI 1287 and a Frequency Response Analyzer 1255B from Solartron. A Pt plate and a saturated calomel electrode were used as counter and reference electrodes, respectively. Gold substrates with LB films deposited act as working electrodes with an effective surface of 0.07 cm^2 . Non Faradaic impedance measurements were performed in contact with a PBS solution, at ambient temperature ($20 \pm 1^\circ\text{C}$), in a frequency range from 50 mHz to 100 kHz, at a polarization potential of -600 mV/SCE with a frequency modulation of 10 mV.

2.3. Results and discussion

2.3.1. Adsorption of protein at the air/water interface

The surface pressure vs time (Π -t) curves presented in Figure IV.3 were measured during adsorption of protein onto the amphiphile monolayer at the air/water interface with three different protein concentrations: 4, 6 and 10 mg L⁻¹. The data were acquired without any compressing force. We also tried to study the adsorption of protein in the absence of amphiphile. However, hardly any increase of surface pressure was observed over 3 h.

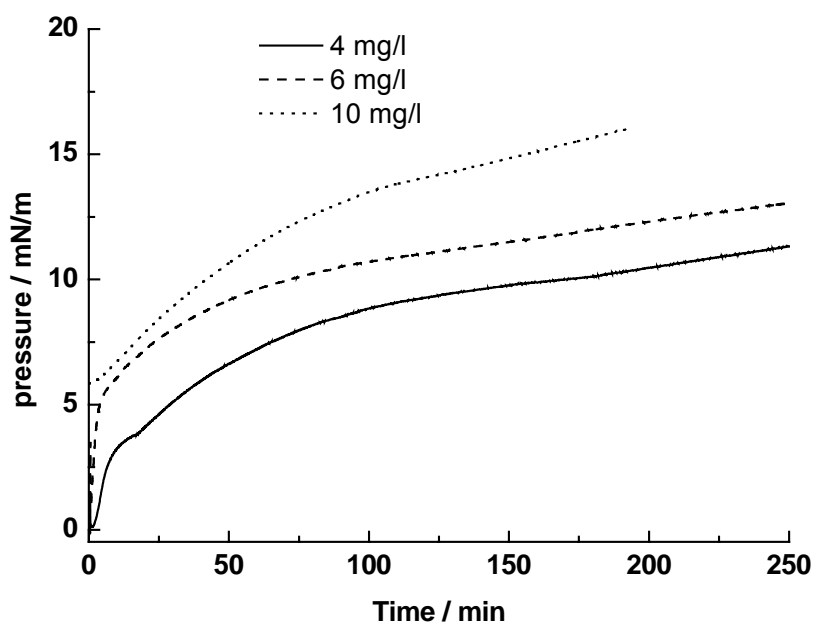


Figure IV.3: Adsorption of OBP-1F at the air/water interface as a function of time.

It can be seen from Figure IV.3 that the increase of the surface pressure was strongly dependent on the concentration of protein in the subphase, and on time; higher concentrations of OBP-1F protein resulted in higher surface pressures. Such behaviour is in accordance with the kinetics of adsorption. This figure also shows that after 250 min the surface pressure continues to increase but very slowly, which means that the adsorption process of protein molecules almost reaches equilibrium. There are probably still a few protein molecules that are prone to penetrate lipid layers and adsorb between the head group of amphiphiles at the air/water interface, or there is a change in the secondary structure of the protein over the time. Because of the unfavourable effect on the accuracy of the experimental results produced by a long adsorption time, proteins

were allowed to adsorb from the subphase for about 3 h only.

As compared to the results of the adsorption of protein butyrylcholinesterase (BuChE) (wt 44.4 KDa) at an air/water interface studied by Chovelon et al., (25) the surface pressure in the case of OBP-1F (18.5 KDa) is found to be comparatively low. For example, at a protein concentration of 4 mg L^{-1} for both cases, the surface pressure was approximately 25 mN m^{-1} for BuChE with an adsorption time of 250 min, but only about 11 mN m^{-1} for OBP-1F.

In fact, proteins follow a diffusion-controlled adsorption mechanism at the air/water interface. They are prone to penetrate the lipid layer and expose their hydrophobic part to the air phase at the interface, and this can proceed for as long and as far as there is time and space available at the interface. (45) Furthermore, with the presence of an ionic surfactant such as ODA in this work, proteins can be adsorbed onto or between the head group of amphiphiles via electrostatic interactions. At a low surface pressure without any compressing force, diffusion-controlled adsorption plays a predominant role in the increment of surface pressure. However, it has already been reported that the rate of desorption of proteins increases markedly with decreasing molecular weight at a given surface pressure. (46) So if their mass weights are considered, it is rational that the surface pressure for BuChE is higher than that for OBP-1F. At low surface pressure, molecules of BuChE are more prone to spread at the air/water interface. However for OBP-1F the rate of desorption of protein OBP-1F was so high in the subphase that the increase of surface pressure arose mainly from the adsorption of protein onto the amphiphile molecules. This point has been confirmed by the fact that for OBP-1F, there is hardly any increase of surface pressure over 3 h in the absence of amphiphile ODA, as referred to above.

2.3.2. Surface pressure-molecular area isotherms

Three different subphases: ultrapure water, PBS at pH 7.5 without and with OBP-1F, were used to investigate the characteristics of the corresponding amphiphilic monolayers. The surface pressure-molecular area isotherms of ODA molecules on ultrapure water were considered as a reference. For the mixed film, an apparent molecular area was defined as the ratio of the film area to the number of spread amphiphile molecules.

It can be seen from Figure IV.4 that ingredients in the subphase have an apparent influence on the characteristics of the amphiphilic monolayers at the air/water

interface. When ultrapure water is used as the subphase, extrapolated to 0 mN m^{-1} from the linear portion of the compression curve, it gives an apparent surface area of only $15 \text{ \AA}^2/\text{ODA}$, which is lower than the theoretical value of $21 \text{ \AA}^2/\text{ODA}$. It results most likely from the partial dissolution of ODA molecules in water, which demonstrates that the ODA monolayer at the air/water interface is not very stable with ultrapure water as the subphase.

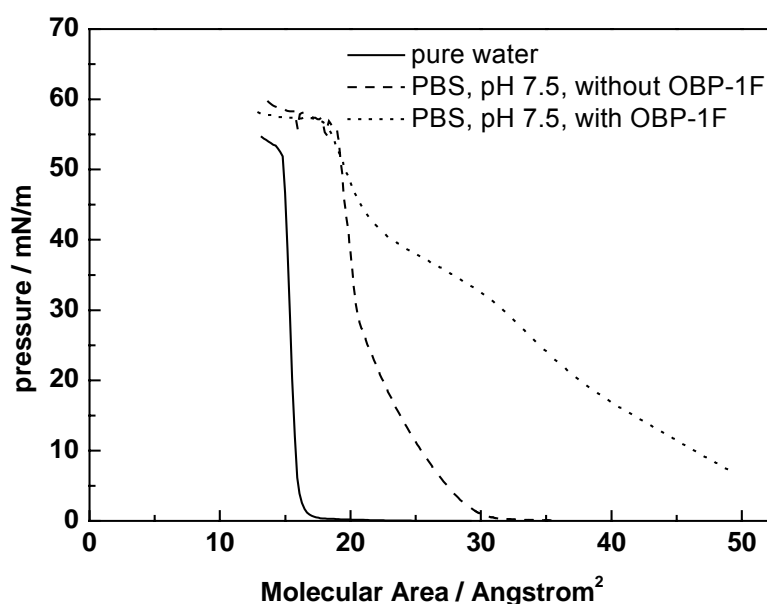


Figure IV.4: Surface pressure-area isotherms for amphiphile ODA with different subphases: water, phosphate buffer solution (pH 7.5) without and with protein OBP-1F (4 mg L^{-1}).

However, for PBS as the subphase, the curve is considerably different from that obtained with ultrapure water as the subphase. We can see from Figure IV.4 that at low surface pressure the molecular area of the ODA monolayer with the PBS as the subphase was much greater than that of the ODA monolayer in ultrapure water. For ODA, whose pK_a is close to 10, (40) at pH 7.5, the amino head of ODA can be assumed to be positively charged. Therefore, the addition of strongly bound multivalent counterions, such as PO_4^{3-} to the PBS subphase has some effect on the monolayer. Probably, at low surface pressure, long-chain amine ODA around PO_4^{3-} aggregated. The extrapolation to 0 mN m^{-1} of the linear portion of the compression curve gives an apparent surface area of $20 \text{ \AA}^2/\text{ODA}$, which is quite close to the theoretical value. It can be concluded that there is hardly any dissolution of ODA molecules under such conditions. The increased stability of the monolayer, as expected, is attributed to the

addition of counter ions in the subphase, which induced an interaction between anions and positively charged amines.

In the case of a PBS subphase with OBP-1F protein, the apparent molecular area is still greater than without OBP-1F at low surface pressures, which means that interactions also take place between protein and ODA molecules, and some protein molecules were inserted into the ODA monolayer.

With surface pressures below 10 mN m^{-1} , there is no lateral adhesion between ODA molecules, it is the so-called gas state. In this state protein can not only penetrate the amphiphile monolayer and spread at the air/water interface by diffusion, but can also be adsorbed onto or between heads of amphiphile molecules by electrostatic interaction.

With compression, the intermolecular distance then decreases, and the surface pressure increases. The increase of surface pressure leads protein and amphiphile molecules to come closer and consequently form the mixed protein/amphiphile monolayer. For surface pressures between 10 and 30 mN m^{-1} , the monolayer is considered to be in the liquid state, where the amphiphile monolayer is coherent with protein molecules partially slipping between the headgroup of amphiphiles and partially adsorbing onto the amphiphile monolayer.

With a further compression, the monolayer changes from liquid to solid, between 30 and 40 mN m^{-1} as shown in Figure IV.4, where the slope of the Π -A curve decreases. In this surface pressure range, the mixed monolayer is reorganized, protein molecules inserted between the headgroup of amphiphiles are gradually expelled from the interface and pushed under the positively charged head of ODA molecules. Consequently, the surface pressure does not increase significantly. A more marked effect in this range of surface pressure is that a relatively stable monolayer including a relatively high amount of protein can be obtained, which is important for the formation of stable and homogeneous Langmuir-Blodgett films and the elaboration of biosensors.

Above 40 mN m^{-1} , if further pressure is applied on the monolayer, there is a risk of overlapping of the layer at the air/water interface and even the completely collapse of the mixed monolayer due to its mechanical instability.

As a further step, the stabilities of the monolayers in the solid-liquid transition state were investigated with the aim of obtaining an optimal target pressure for the deposition of LB films.

2.3.3. Stability of the mixed protein/amphiphile monolayer

The stability of the mixed monolayer is very important because it is related to the transfer efficiency and the quality of deposited LB films. It can be examined by the evolution of surface pressure with time at a fixed molecular area, or the evolution of molecular area ratio with time at a fixed surface pressure, after the monolayer has been compressed.

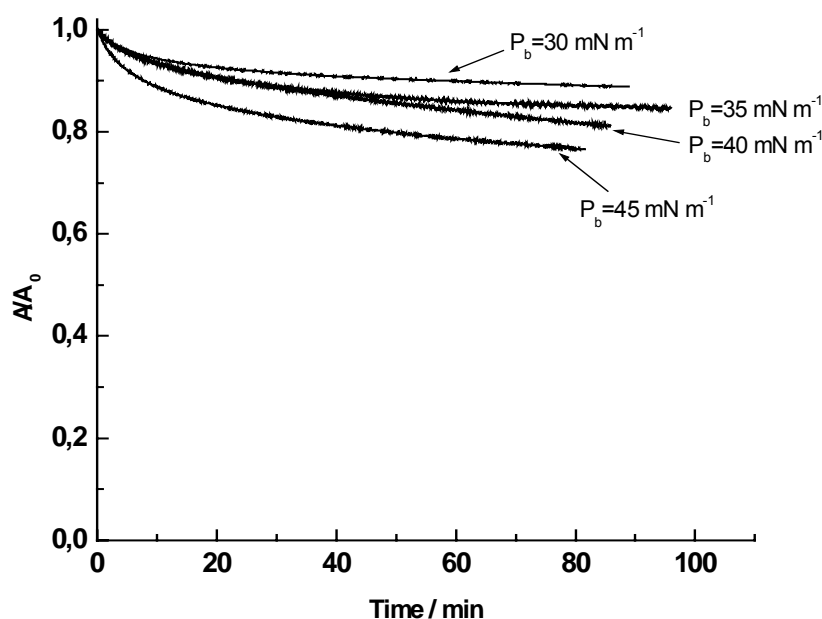


Figure IV.5: Evolution of the molecular area for the mixed monolayer at constant surface pressures of 30, 35, 40 and 43 mN m^{-1} with protein concentration of 4 mg L^{-1} .

As has been reported by our group, (24) the pure amphiphile monolayer is unstable because of its partial solubility in the subphase. In this paper, the stabilities of the mixed protein/amphiphile monolayers were studied with different surface pressures (30, 35, 40 and 43 mN m^{-1}), as shown in Figure IV.5. We found that the surface area of the monolayers decreases in the first 10 min, and after that relatively stable monolayers are obtained. This initial loss in area depends on the rate at which the monolayer is compressed and is due to a structural rearrangement occurring within the layer. After 80 min, the molecular area ratio (A/A_0) with time at different surface pressures (30, 35, 40 and 43 mN m^{-1}) is 0.89, 0.85, 0.82, and 0.77, respectively. The mixed monolayers at these surface pressures are quite stable. This confirms that the addition of protein to the subphase indeed increases the stability of the monolayer at the air/water interface. In fact, as stated by Miller, the electrostatic interaction between protein and surfactant

induces the formation of a protein/surfactant complex which is much less soluble than the protein. (45) This complex can then be concentrated at the air/water interface.

In addition, we have investigated the stabilities of the mixed protein/amphiphile monolayers at 35 mN m^{-1} with different concentrations (4, 6 and 10 mg L^{-1}) of the proteins, shown in Figure IV.6. The results show that the stabilities do not seem to depend on the concentration of protein, which is consistent with the fact that at this surface pressure the proteins were mostly expelled from the interface and were adsorbed onto the ODA monolayer.

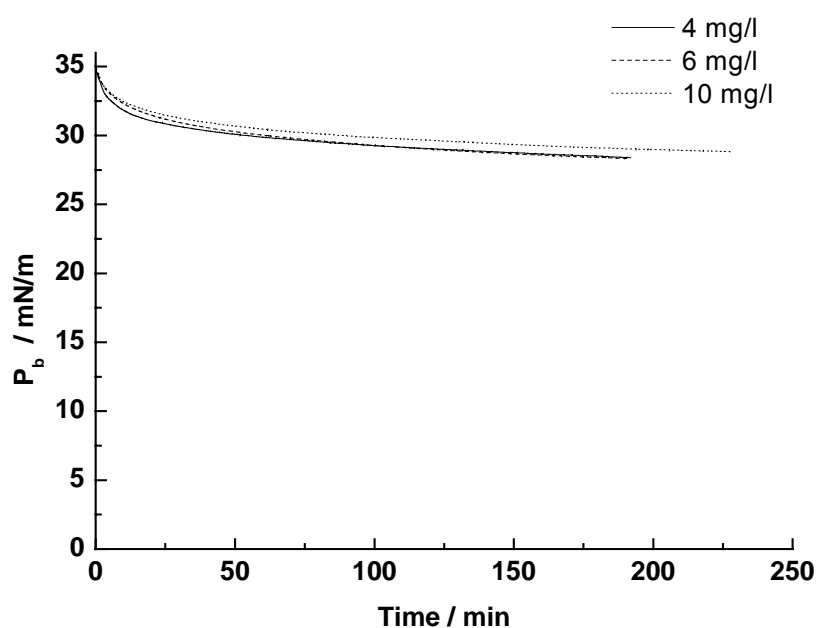


Figure IV.6: Evolution of the surface pressure for the mixed monolayer at constant molecular areas with the different concentrations of OBP-1F (4, 6, 10 mg L^{-1}).

2.3.4. Transfer of Langmuir-Blodgett films

The stable mixed protein/amphiphile monolayers were transferred from the air/water interface onto solid substrates of gold under different target pressures (30, 35, 40 and 43 mN m^{-1}). Because the gold substrates had been functionalized with SAMs of ODT to be hydrophobic, LB films should be deposited during the first downstroke of the substrate through the air/water interface.

For 4 mg L^{-1} OBP-1F in the subphase, at the target pressure of 35 mN m^{-1} , two layers of LB films can be transferred successfully onto ODT functionalised gold substrates with good reproducibility and quite a high transfer ratio (96%, 110%,

respectively), shown in Figure IV.7, which corresponds to a Y-type deposition. However, for the higher target pressures 40 and 43 mN m^{-1} , the transfer of LB films was not so effective. Probably at these surface pressures the phase transition of the monolayer from liquid to solid has nearly ended and the molecules are closely packed. In this state, the monolayer is much more fragile and sensitive to any external force. It can be assumed that the vertical passage of the solid substrate could probably damage the monolayer, resulting in overlapping or partial collapse of the monolayer, and so the transfer ratios for LB films at these surface pressures are lower.

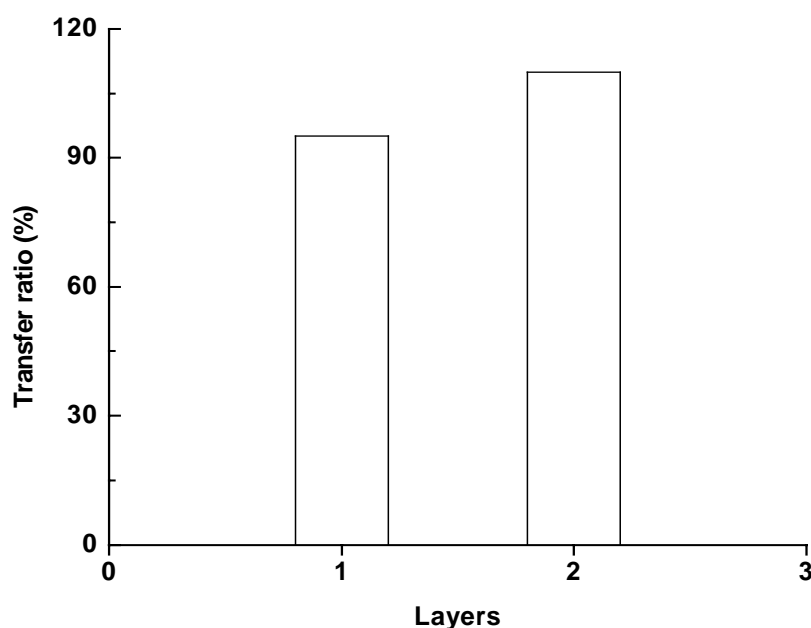


Figure IV.7: Transfer ratio for two layers of mixed OBP-1F/ODA LB films deposition at target pressure 35 mN m^{-1} .

From the results discussed above we can see that at 35 mN m^{-1} , the mixed protein/amphiphile monolayer is very stable at the air/water interface and it can be more effectively transferred onto functionalized gold substrate. Furthermore, we have mentioned that at a target pressure of 35 mN m^{-1} the proteins were mostly expelled from the interface and were adsorbed onto the ODA monolayer. This is why this surface pressure has been chosen as the target pressure for LB deposition and AFM and EIS studies.

Scanning electron microscopy was used to characterize LB films obtained at different target pressures on a submillimeter scale, to obtain some general topographic information. As shown in Figure IV.8, the structures appeared to be

heterogeneous, as important rearrangements probably occur during and/or after the transfer. This kind of protein/amphiphile LB films structure has been reported by Sommer et al. (38) and Chovelon et al. (26, 47) with AFM. In addition, when the four images are compared, at higher surface pressures (40 and 43 mN m^{-1}), the structures of LB films on the gold substrates seem to be more heterogeneous with small domains. Because of the poor transfer at these over-high surface pressures, their films were not used in the following studies.

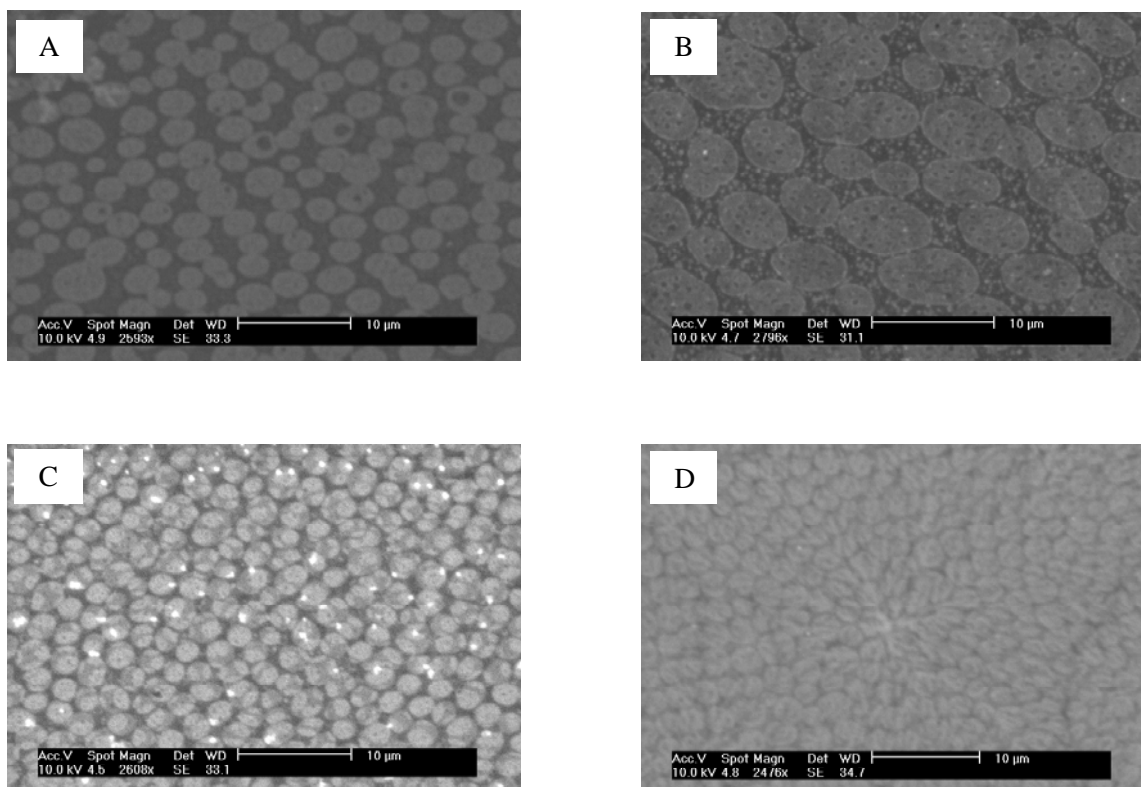


Figure IV.8: SEM images of two layers of mixed OBP-1F/ODA LB films transferred on gold substrates at different surface pressures: (A) 30, (B) 35, (C) 40 and (D) 43 mN m^{-1} .

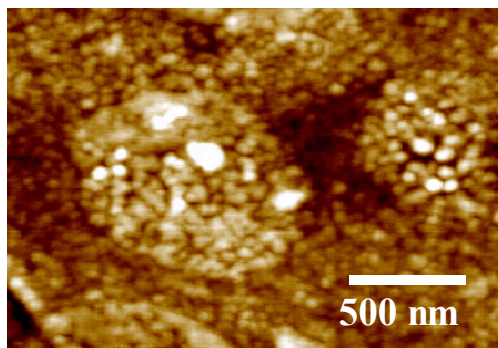
2.3.5. Characterization of Langmuir-Blodgett films for odorant biosensor applications

Two layers of mixed OBP-1F/ODA LB films were efficiently transferred onto ODT functionalized gold substrates at 35 mN m^{-1} . AFM and EIS measurements were made on these structures (gold/thiol/ODA/OBP LB films) before and after exposure to the vapour of the odorant molecule, isoamyl acetate.

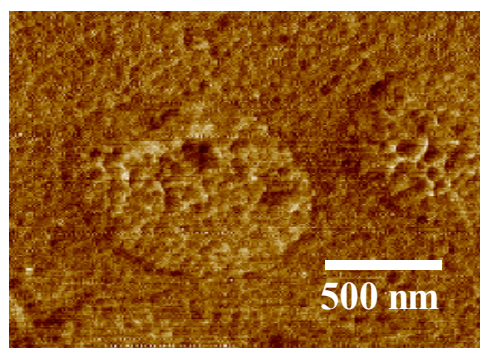
2.3.5.1. Atomic force microscopy

Topographic images (Figures IV.9a and 9b) of the mixed OBP-1F/ODA LB films remain almost unchanged within the resolution of the imaging conditions of

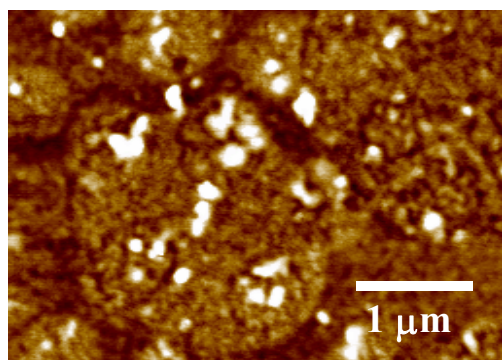
experiments after exposure to a small, hydrophobic odorant molecule, isoamyl acetate. The white spots on the topographic images are probably due to dust or salts remaining after the rinsing process.



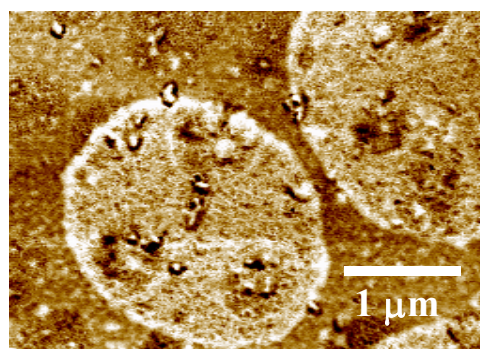
(a) topographic images



(a') phase images



(b) topographic images



(b') Phase images

Figure IV.9: AFM topographic (a) and phase (a') images of two layers of mixed OBP-1F/ODA LB film transferred onto functionalized gold substrate at 35 mN m^{-1} before exposure to odorant. Scan area $2.1 \times 2.1 \mu\text{m}^2$. Vertical scale (a) 10 nm, (a') 1.3° . AFM topographic (b) and phase (b') images of a mixed OBP-1F/ODA LB film transferred onto functionalized gold substrate at 35 mN m^{-1} after exposure to odorant. Scan area $4 \times 4 \mu\text{m}^2$. Vertical scale (b) 10 nm, (b') 9.4° .

However a strong change in the AFM phase images was induced by the exposure to the odorant (Figures IV.9a' and 9b'). Before exposure to the odorant molecule, the sample surface is almost uniform (variations of $\sim 1^\circ$ maximum are observed), there is no phase contrast between the oval domains and the rest. It proves that the LB films obtained are well-ordered and uniform, and OBP-1F aggregates are well covered with ODA molecules. After exposure to the odorant, a sharp contrast was observed between the aggregates and the other sample constituents, with phase variations of up to $\sim 9^\circ$. Because phase atomic force microscopy images by recording the phase lag between the signal that drives the cantilever and the cantilever oscillation

output signal, it provides information about surface properties such as elasticity, adhesion and friction, and it can be concluded that one or all of these mechanical properties in the aggregates were modified.

Small odorant molecules can be assumed to penetrate the outer lipid layer to reach the OBP-1F aggregates. Interaction between the odorant molecules and OBP-1F can induce a conformational change of the protein, as observed by Nespoulous et al., (7) and consequently a stronger interaction between the hydrophilic part of OBP-1F and ODA polar heads, leading to a partial break-down of LB films. Even slight modifications in the build-up of layers induce strong changes in electrical properties, as discussed in the next section.

2.3.5.2. Non Faradaic electrochemical impedance spectroscopy

The impedance modulus ($|Z|$) and the phase angle theta *versus* potential modulation frequency (Figure IV.10a and 10b, respectively) show the behaviour over the entire frequency range explored, while the Nyquist plot (Figure IV.10c) more clearly emphasizes the impedance changes at low frequencies where experimental results show there is better sensitivity to odorant molecules.

The physical origin of the observed response can be understood from electrical circuit modelling, in which the electrical response of the physical interface is modelled using various discrete electrical circuit elements. The model that provides the best fit for the data over the entire frequency range is shown in Figure IV.10d.

This model represents the physical structure of the interface in terms of three layers, each having its own unique electrical properties. The inner layer corresponds to SAMs on gold substrates, which has no critical sensitivity to odorant binding; R_{SAMs} and C_{SAMs} represent respectively the resistance and capacity of octadecanethiol-SAMs. The outer layer physically represents OBP-1F/ODA LB films and is represented by a constant phase element Q_{LB} and a parallel resistor R_{LB} ; the impedance of the constant phase element is defined as $Z = A(j\omega)^{-n}$, where A is the modulus, ω the angular phase and n the phase ($0 \leq n \leq 1$). The solution resistance is represented by a simple resistor R_s , which is dependent upon the ionic strength of the used buffer solution.

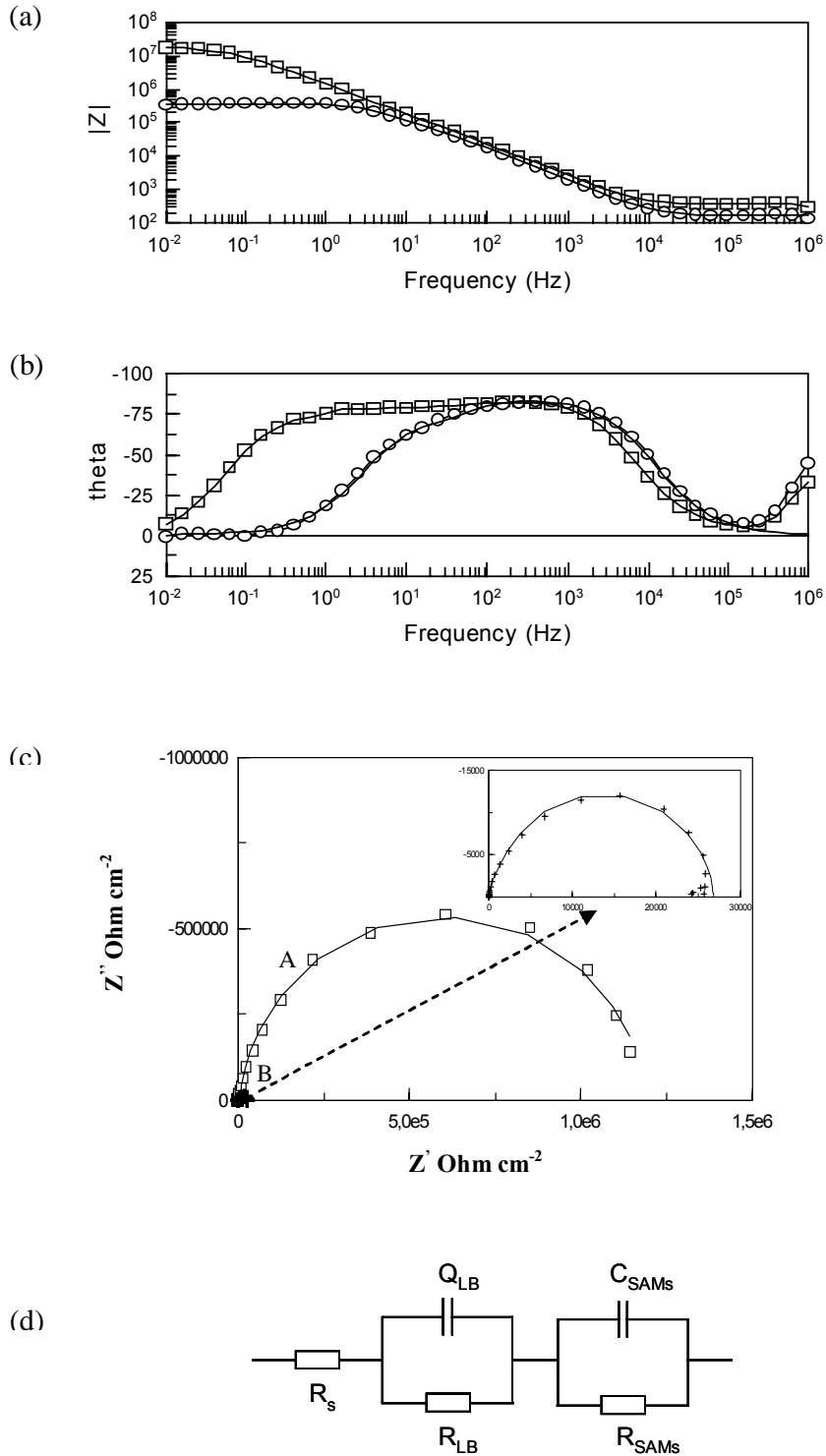


Figure IV.10: Electrochemical impedance spectroscopy: bode diagrams are shown in (a) the impedance modulus ($|Z|$) versus potential modulation frequency and (b) the phase angle theta versus potential modulation frequency, in which the symbols represent experimental values and the straight lines represent fitted data: (\square) before exposure to odorant molecules, (\circ) after exposure to odorant molecules. (c) Nyquist (Z'' vs. Z') plots measured for gold/thiol/ODA/OBP-1F LB films before (A) and after (B) exposure to odorant molecules. Inset: enlarged curve for (B). (d) The equivalent circuit model used to fit the impedance data, the electrical circuit elements were described in the text.

The fitting data in Table IV.1 show that after contact with the odorant, the most important modification is to resistance R_{LB} , which decreases significantly. This further confirms the supposition that small odorant molecules could penetrate the outer lipid layer to reach OBP-1F aggregates, which leads to a rearrangement of the aggregates and of the LB films. These aggregates seem to be more individualized, tightly surrounded by amphiphilic molecules. This molecular reorganization can induce defined interstitial spaces where buffer species can diffuse more easily, which could provoke electrical shortening between solution and gold substrate, and provides an explanation for a strong decrease in the value of electrical resistance R_{LB} .

	R_s (Ω)	R_{SAMS} (Ω)	C_{SAMS} (μF)	$R_{LB}(M\Omega)$	$Q_{LB}(\mu F)$	n
Before odorant	24.50	3634.54	5.23	1.18	1.86	0.93
After odorant	11.40	751.59	5.57	0.025	2.35	0.95

Table IV.1: Values of circuit elements in the equivalent circuit obtained by matching the experimental data from Figure IV.10c to the circuit model shown in Figure IV.10d.

On the other hand, we can see from Table 1 that n is rather close to 1, hence, Q_{LB} can be considered as pure capacitance. After the binding of odorant molecules, capacitance Q_{LB} increases. All vertebrate odorant-binding proteins share a conserved folding pattern, an eight-stranded β -barrel flanked by an α -helix at the C-terminal end of the polypeptide chain. The β -barrel defines a central apolar cavity, whose role is to bind and transport hydrophobic odorant molecules. (4, 5) Molecular modelling of OBP-1F revealed that no charged amino acids are present in the binding cavity. All charged amino acids are located on the surface of the protein. (7) We can therefore speculate that after the binding of odorant molecules, all charged amino acids are oriented towards the OBP-1F outside, and that increasing the charge density therefore leads to an increase of the dielectric constant of the LB films.

We propose a theoretical model, based on all results discussed above, for the two layers of mixed OBP-1F/ODA LB films transferred onto gold substrate with a hydrophobic surface, at 35 mN m^{-1} . It is shown in Figure IV.11, on the left. Because the gold surface is hydrophobic, LB films are deposited during the first downstroke of the

substrate through the air/water interface. It has been found that, before the transfer step, protein molecules are mostly pushed under the polar heads of ODA molecules during compression, resulting in the formation of well-ordered mixed LB films on the substrates, which is confirmed by AFM images.

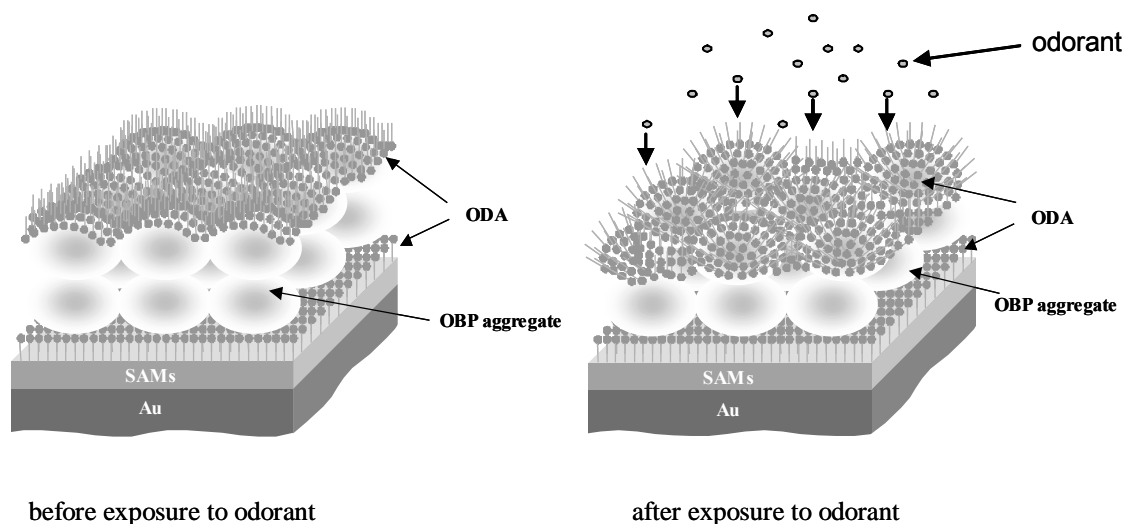


Figure IV.11: Left: theoretical model for the two layers of mixed OBP-1F/ODA LB films transferred onto functionalized gold substrate at 35 mN m^{-1} before exposure to odorant molecules; Right: the model for the two layers of mixed OBP-1F/ODA LB films after exposure to odorant molecules.

During exposure of the substrate to odorant molecules, these small odorant molecules could penetrate the outer lipid layer to reach OBP-1F aggregates. The interaction leads to a rearrangement of the OBP-1F aggregates and the LB films, which is confirmed by AFM and EIS measurements. So the model proposed for the mixed LB films after binding odorant molecules is shown in Figure IV.11, on the right. Phase contrast modification of the mixed LB films is observed during the recognition processes, and the OBP-1F aggregates seem more individualized, surrounded by amphiphilic molecules.

2.4. Conclusion

Stable mixed Langmuir films incorporating odorant-binding protein can be formed at the air/water interface and can be efficiently transferred onto functionalized gold supports at the target pressure of 35 mN m^{-1} for the construction of reproducible, stable and well-ordered mixed LB films. In addition, non Faradaic EIS allows the sensing characteristics of LB based recognizing devices to be quantified, and allows us to put forward a hypothesis concerning the topographic modification of the engineered layers, which occurs during the recognition processes. In further steps sensor arrays are

expected to be produced for designing versatile electronic noses, which could easily be mass-produced, on a LB technique basis, and applied to the detection of mixtures of odorants in various environmental conditions.

References

- (1) L. Buck and R. Axel, *Cell*, **1991**, 65, 175-187.
- (2) P. Pelosi, *Crit. Rev. Molec. Biol.*, **1994**, 29, 199-228.
- (3) P. Pelosi, N. E. Baldaccini, A. M. Pisanelli, *Biochem. J.*, **1982**, 201, 245-248.
- (4) M. A. Bianchet, G. Bains, P. Pelosi, J. Pevsner, S. H. Snyder, H. L. Monaco, L. M. Amzel, *Nature Structural Biology*, **1996**, 3, 934-939.
- (5) M. Tegoni, R. Ramoni, E. Bignetti, S. Spinelli, C. Cambillau, *Nature Structural Biology*, **1996**, 3, 863-867.
- (6) F. Vincent, R. Ramoni, S. Spenelli, S. Grolli, M. Tegoni, C. Cambillau, *Eur. J. Biochem*, **2004**, 271, 3832-3842.
- (7) C. Nespoulous, L. Briand, M. M. Delage, V. Tran, J. C. Pernollet, *Chemical Senses*, **2004**, 29, 189-198.
- (8) D. Löbel, S. Marchese, J. Krieger, P. Pelosi, H. Breer, *Eur. J. Biochem.*, **1998**, 254, 318-324.
- (9) L. Briand, C. Nespoulous, V. Perez, J. J. Rémy, J. C. Huet, J. C. Pernollet, *Eur. J. Biochem.*, **2000**, 267, 3079-3089.
- (10) D. Löbel, J. Strotmann, M. Jacob, H. Breer, *Chemical Senses*, **2001**, 26, 673-680.
- (11) A. Ulman, *An Introduction to Ultrathin Organic Films: From Langmuir-Blodgett to Self-Assembly*; Academic Press: Boston, **1991**, Preface.
- (12) M. C. Petty, *Langmuir-Blodgett films: An introduction*; Cambridge University Press: Cambridge, **1996**, Chapter 4.
- (13) M. Bardosova, R. H. Tredgold, Z. Ali-Adib, *Langmuir*, **1995**, 11, 1273-1276.
- (14) A. Datta, J. Kmetko, C. Yu, A. G. Richter, K. Chung, J. Bai, P. Dutta, *J. Phys. Chem. B*, **2000**, 104, 5797-5802.
- (15) A. Ulman, *Chem. Rev.*, **1996**, 96, 1533-1554.
- (16) M. H. Schoenfish, J. E. Pemberton, *J. Am. Chem. Soc.*, **1998**, 120, 4502-4513.

- (17) P. E. Laibinis, G. M. Whitesides, D. L. Allara, Y. Tao, A. N. Parikh, R. G. Nuzzo, *J. Am. Chem. Soc.*, **1991**, 113, 7152-7167.
- (18) Y. Okahata, T. Tsuruta, K. Ijio, K. Ariga, *Langmuir*, **1988**, 4, 1373-1375.
- (19) S. Sun, P. H. Ho-Si, D. J. Harrison, *Langmuir*, **1991**, 7, 727-737.
- (20) N. Dubreuil, S. Alexandre, C. Fiol, F. Sommer, J. M. Valleton, *Langmuir*, **1995**, 11, 2098-2102.
- (21) A. P. Girard-Egrot, R. M. Morélis, P. R. Coulet, *Langmuir*, **1997**, 13, 6540-6546.
- (22) V. Rosilio, M. M. Boissonnade, J. Zhang, L. Jiang, A. Baszkin, *Langmuir*, **1997**, 13, 4669-6475.
- (23) C. Fiol, J. M. Valleton, N. Delpire, G. Barbey, A. Barraud, A. Ruaudel-Teixier, *Thin Solid Films*, **1992**, 210/211, 489.
- (24) A. Zhang, N. Jaffrezic-Renault, J. Wan, Y. Hou, J. M. Chovelon, *Materials Science and Engineering C*, **2002**, 21, 91-96.
- (25) J. M. Chovelon, K. Wan, N. Jaffrezic-Renault, *Langmuir*, **2000**, 16, 6223-6227.
- (26) J. M. Chovelon, F. Gaillard, K. Wan, N. Jaffrezic-Renault, *Langmuir*, **2000**, 16, 6228-6232.
- (27) A. Tronin, T. Dubrovsky, C. Nicolini, *Thin Solid Films*, **1996**, 284/285, 894-897.
- (28) I. Vikholm, O. J. Teleman, *Colloid Interf. Sci.*, **1994**, 168, 125-129.
- (29) A. Barraud, H. Perrot, V. Billard, C. Martelet, J. Therasse, *Biosensors and Bioelectronics*, **1993**, 8, 39-48.
- (30) R. G. Nuzzo, D. L. Allara, *J. Am. Chem. Soc.*, **1983**, 105, 4481-4483.
- (31) Th. Wink, S. J. V. Zuilen, A. Bult, W. P. V. Bennekomp, *Analyst*, **1997**, 122, 43R-50R.
- (32) S. Ferretti, S. Paynter, D. A. Russell, K. E. Sapsford, D. J. Richardson, *Trends in Analytical Chemistry*, **2000**, 19, 530-540.
- (33) J. Spinke, M. Liley, H. J. Guder, L. Angermaier, W. Knoll, *Langmuir*, **1993**, 9, 1821-1825.

- (34) G. L. Jr Gaines, *Nature*, **1982**, 298, 544-545.
- (35) Y. F. Dufrêne, *Journal of Bacteriology*, **2002**, 184, 5205-5213.
- (36) D. Fotiadis, S. Scheuring, S. A. Müller, A. Engel, D. J. Müller, *Micron*, **2002**, 33, 385-397.
- (37) I. Fujiwara, M. Ohnishi, J. Seto, *Langmuir*, **1992**, 8, 2219-2222.
- (38) F. Sommer, S. Alexandre, N. Dubreuil, D. Lair, T. Duc, J. M. Valleton, *Langmuir*, **1997**, 13, 791-795.
- (39) E. Katz, I. Willner, *Electroanalysis*, **2003**, 15, 913-947.
- (40) Y. Hou, C. Tlili, N. Jaffrezic-Renault, A. Zhang, C. Martelet, L. Ponsonnet, A. Errachid, J. Samitier, J. Bausells, *Biosens. Bioelectron.*, **2004**, 20, 1126-1133.
- (41) J. Janata, *Critical Reviews in Analytical Chemistry*, **2002**, 32, 109-120.
- (42) T. L. Lasseter, W. Cai, R. J. Hamers, *Analyst*, **2004**, 129, 3-8.
- (43) Z. Yang, A. Gonzalez-Cortes, G. Jourquin, J. C. Viré, J. M. Kauffmann, J. L. Delplancke, *Biosens. Bioelectron*, **1995**, 10, 789-795.
- (44) H. Ron, S. Matlis, I. Rubinstein, *Langmuir*, **1998**, 14, 1116-1121.
- (45) R. Miller, V. B. Fainerman, A. V. Makievski, J. Krägel, D. O. Grigoriev, V. N. Kazakov, O. V. Sinyachenko, *Advances in Colloid and Interface Science*, **2000**, 86, 39-82.
- (46) L. Dziri, K. Puppala, R. M. Leblanc, *J. Colloid Interf. Sci.*, **1997**, 194, 37-43.
- (47) J. M. Chovelon, M. Provence, N. Jaffrezic-Renault, S. Alexandre, J. M. Valleton, *Materials Science and Engineering C*, **2002**, 22, 79-85.

CHAPTER V: DEVELOPMENT OF A NEW IMMOBILIZATION TECHNIQUE BASED ON SELF- ASSEMBLED MULTILAYER FOR G PROTEIN-COUPLED RECEPTORS

1. INTRODUCTION ON RHODOPSIN

G protein-coupled receptors, characterized by their common structure of a membrane-spanning seven-helix bundle (1), comprise the largest gene family in the human genome and the largest single class of cell-surface receptors. They transmit signals from the outside to the inside of the cell and they are involved in many important physiological processes, including the detection of light, smell, sound and taste. Among them, rhodopsin is the primary molecule in the visual signaling cascade. It is the only GPCRs whose crystal structure has been determined, and it was chosen as the bioreceptor in this study.

Firstly, vision process is introduced to help us understand the function of rhodopsin.

1.1. Vision

The eyes behave similarly, in some respects, to a camera. Light enters the pupil, it is focused by the lens and strikes a light-sensitive detector (called the retina) located along the inner surface of the back of the eyes (Figure V.1).

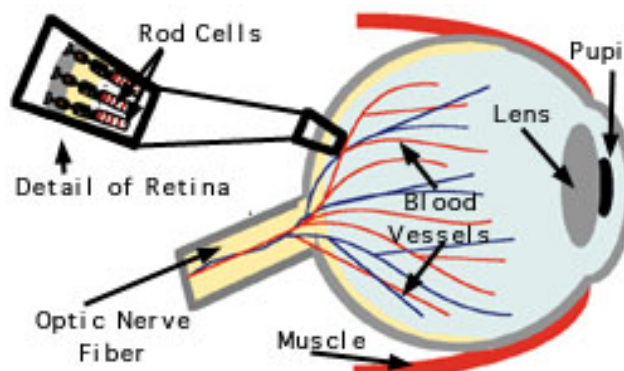


Figure V.1: A schematic drawing of the human eye. (2)

The retina is lined with many millions of photoreceptor cells that consist of two types: 7 million cones providing color information and sharpness of images, and 120 million rods (Figure V.2, left), which are extremely sensitive detectors for white light to provide night vision. The outer segments (tops) of the rods and cones contain a region filled with membrane-bound discs that contain proteins bound to the chromophore 11-*cis*-retinal. A chromophore is a molecule that can absorb light at a specific wavelength, and thus typically displays a characteristic color. In rod cells, the protein which binds the chromophore retinal is opsin, and the bound complex of 11-*cis*-retinal plus opsin is known as rhodopsin, or visual purple.

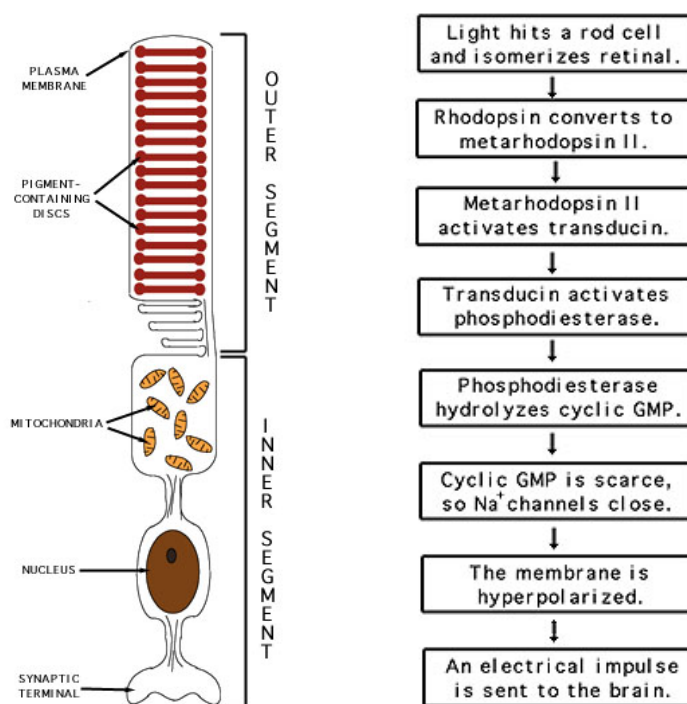


Figure V.2: Left: This is a schematic diagram of a rod cell. The stacked disks contain rhodopsin, the complex of opsin protein and 11-*cis*-retinal. Right: A flowchart outlining the major steps in the vision signal transduction cascade. (2)

When visible light hits the chromophore, the chromophore undergoes an isomerization, or change in molecular arrangement to all-*trans*-retinal. The new form of retinal does not fit well into the protein, and leads to a series of conformational changes in the protein. The conformation changes initiate a cascade of biochemical reactions that result in the closing of Na^+ channels in the cell membrane, as outlined in Figure V.2 on the right. Prior to this event, Na^+ ions flow freely into the cell to compensate for the lower potential (more negative charge) which exists inside the cell. When the Na^+ channels are closed, a large potential difference builds up across the plasma membrane (inside the cell becomes more negative and outside the cell becomes more positive). This potential difference is passed along to an adjoining nerve cell as an electrical impulse at the synaptic terminal, the place where these two cells meet. The nerve cell carries this impulse to the brain, where the visual information is interpreted.

Rhodopsin also absorbs in the ultraviolet region of the spectrum. However, the lens of the eye absorbs ultraviolet light, preventing it from reaching rhodopsin in the retina. This is why we cannot see ultraviolet light.

1.2. Structure of rhodopsin

Rhodopsin is composed of the protein opsin (~40 kDa) covalently linked to 11-*cis*-retinal (a derivative of vitamin A) through Lys²⁹⁶. (1) The structure model of rhodopsin is shown in Figure V.3. Opsin consists of 348 amino acids, covalently linked together to form a single chain. This chain has seven hydrophobic, or water-repelling, alpha-helical regions that pass through the lipid membrane of the pigment-containing discs. The retinal is situated among these alpha helices in the hydrophobic region.

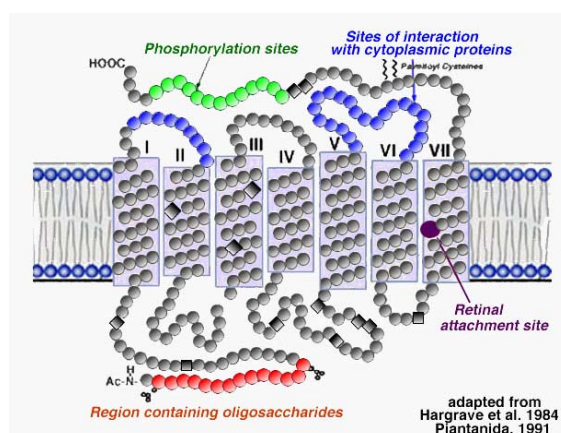


Figure V.3: Structure model of rhodopsin showing seven transmembrane components and the attachment site for retinal. (3)

After light hits the rod cell, the first step in the monochrome vision process is for the chromophore 11-*cis*-retinal to isomerize to all-*trans*-retinal. This isomerization occurs in a few picoseconds (10^{-12} s) or less. Energy from light is crucial for this isomerization process: absorption of a photon leads to isomerization about half the time; in contrast, spontaneous isomerization in the dark occurs only once in 1000 years! The molecule resulting from the isomerization is called all-*trans*-retinal. In the *cis* configuration, both of the attached hydrogens are on the same side of the double bond; in the *trans* configuration, the hydrogens are on opposite sides of the double bond. Figure V.4 shows the schematic diagrams of rhodopsin before and after light stimulation.

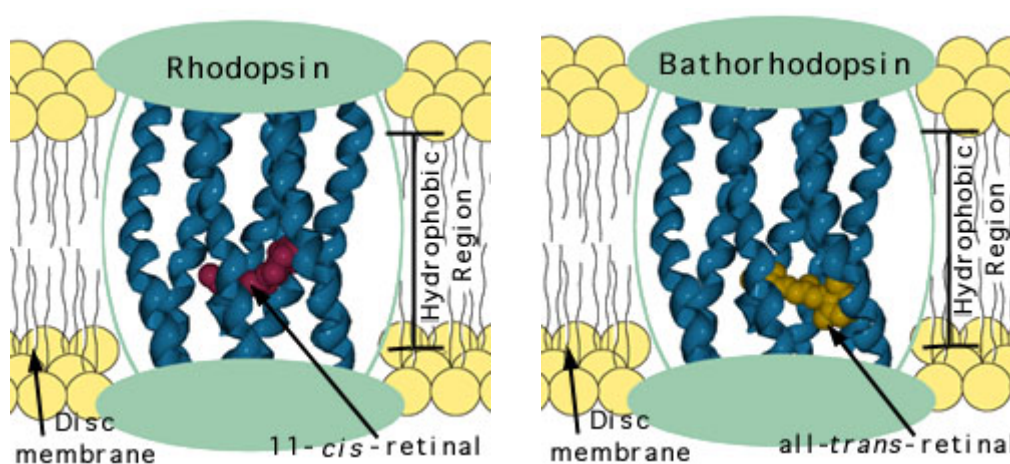


Figure V.4: The schematic diagrams of rhodopsin (11-*cis*-retinal bound to opsin) and bathorhodopsin (all-*trans*-retinal bound to opsin) in the membrane of a pigment-containing disc in the rod cell. (2)

2. IMMOBILIZATION OF RHODOPSIN ON A SELF-ASSEMBLED MULTILAYER AND ITS SPECIFIC DETECTION BY ELECTROCHEMICAL IMPEDANCE SPECTROSCOPY*

Abstract

Rhodopsin, the G protein-coupled receptor which mediates the sense of vision, was immobilized onto gold electrode by two different techniques: Langmuir-Blodgett and a strategy based on a self-assembled multilayer. We demonstrated that LB films of rhodopsin are not stable on gold electrode. Thus in this study a new protein multilayer was prepared on gold electrode by building up layer-by-layer a self-assembled multilayer. It is composed of a mixed self-assembled monolayer formed by MHDA and biotinyl-PE, followed by a biotin-avidin system which allows binding of biotinylated antibody specific to rhodopsin. Such a self-assembled multilayer was characterized by electrochemical measurements and by AFM. The immobilization of rhodopsin by the specific antibody bound previously on self-assembled multilayer was monitored with electrochemical impedance spectroscopy. In addition, the specificity and sensitivity of this self-assembled multilayer system to the presence of rhodopsin were investigated. All these results demonstrate that rhodopsin can be immobilized efficiently, specifically, quantitatively and stably on gold electrode through the self-assembled multilayer.

* Slightly modified version of Y. Hou, S. Helali, A. Zhang, N. Jaffrezic-Renault, C. Martelet, J. Minic, T. Gorjankina, M. A. Persuy, E. Pajot-Augy, R. Salesse, F. Bessueille, J. Samitier, A. Errachid, V. Akinov, L. Reggiani, C. Pennetta, E. Alfinito, *Biosensors and Bioelectronics*, **2005**, in press.

2.1. Introduction

Membrane proteins, encoded by about 20% of genes in almost all organisms, including humans, are critical for cellular communication, electrical and ion balances, structural integrity of the cells adhesions and other functions (4). Among membrane proteins, G protein-coupled receptors are of special importance because they form one of the largest and the most diverse groups of receptor proteins. They mediate the sense of vision, smell, taste, and pain (1). In our study, rhodopsin, the dim light receptor of rod outer segments of the retina, was chosen as representative GPCRs, since it is the only GPCRs whose crystal structure is known and which is naturally highly available. It contains seven transmembrane α -helices, and its chromophore, 11-*cis* retinal, is covalently bound to lysine 296 through a Schiff base linkage (5).

For immobilization of this bioreceptor, two techniques, Langmuir-Blodgett and self-assembled multilayer, were employed in this study, since they can provide the required control at a molecular level and they have potential application for the construction of well-ordered and ultra-thin organic films.

Langmuir-Blodgett technique has already shown its efficiency for depositing well-defined films of enzymes (6-10) and antibodies (11-13) to elaborate biosensors.

Properties of Langmuir and Langmuir-Blodgett films of rhodopsin have already been investigated by Lavoie et al. (5) and group of Nicolini (14-17). Lavoie et al. studied structure of rhodopsin in monolayers at the air/water interface, and they reported that experimental conditions can be found where the secondary structure of rhodopsin can be retained when spread in monolayers. Nicolini et al. investigated the properties of LB films of purified bovine rhodopsin and they found that bleached rhodopsin in LB films has high thermal stability. In this study, we investigated the property and stability of monolayer of rhodopsin membrane fraction at the air/water interface. We used the rhodopsin in its membrane fraction because the presence of lipids surrounding rhodopsin prevents its unfolding and maintains its activity.

Since Nuzzo and Allara, pioneers in the assembly of sulfur-containing molecules in 1983, noticed that dialkane sulfides form highly ordered monolayers on metal surfaces (18), the field of self-assembled monolayers has witnessed tremendous growth (19). The simplicity and adaptability of self-assembled monolayers and control over biomolecule surface orientation suggest that SAMs play an important role in the

construction of artificial biomolecular recognition surfaces and particularly in the development of biosensors (20-22).

More recently the construction of self-assembled multilayer from biological components has been investigated intensively owing to its potential application for biosensors (23-26). For this purpose avidin-biotin system can work perfectly as a bridge to anchor bioreceptor, since the biotinylation of a biomolecule does not affect its biological activity. And still more, the non-covalent complex between avidin and biotin is characterized by an affinity constant of $10^{15} \text{ mol}^{-1} \text{ L}$. Once formed, the bond is stable even if the pH of the solution is changed and it can easily survive multiple washing (27).

In the present study, we used mixed self-assembled monolayers on gold electrodes, formed by MHDA and biotinyl-PE which is inserted and bound to MHDA by electrostatic interaction, as the basis for the formation of a multilayer structure. We investigated a multilayer system of relevance for biosensor research to anchor membrane protein rhodopsin, using neutravidin and a biotin-labelled antibody specific to rhodopsin.

Among the various transduction techniques, such as quartz crystal microbalance, surface plasmon resonance, ellipsometry etc., electrochemical impedance spectroscopy is a rapidly developing and effective electrochemical technique for the characterization of biomaterial-functionalized electrodes and biocatalytic transformations at electrode surfaces, and specifically for the transduction of biosensing events at electrodes. Compared to other electrochemical techniques, one of the advantages of EIS is the small amplitude perturbation from steady state, which makes it possible to treat the response theoretically by linearized or otherwise simplified current-potential characteristics. Up to now EIS has been extensively performed to characterize the fabrication of biosensors and to monitor the biomolecular recognition (28-33). In our study, it was used to monitor the formation of the multilayer structure and the recognition of rhodopsin membrane fraction by self-assembled multilayer. AFM is a powerful tool in structural biology (34) since it could gives access to the molecular architecture, and it was used to characterize the multilayer film in this study.

2.2. Materials and methods

2.2.1. Biomaterials and chemicals

Rhodopsin provided by INRA was prepared from calf eyes according to

the procedure of Papermaster (35), and used as receptor enriched membrane fraction. In brief, retinae were dissected and homogenized in 20 % sucrose in 10 mM Tris-acetate buffer, pH 7.2. A fraction enriched in rod outer segment membranes containing rhodopsin as a major component was obtained by sucrose gradient centrifugation. After isolation, it was resuspended in 137 mM NaCl, 8 mM Na₂HPO₄, 2.7 mM KCl, 1.5 mM KH₂PO₄, buffer (pH 7.2), with 1.5 % octylglucoside, aliquoted and frozen at -80°C.

For the control of the non-specific response of the functionalized gold electrode, tests were performed using I7 olfactory receptor, which belongs to the same family of GPCRs as rhodopsin. The I7 olfactory receptor was expressed in yeast *Saccharomyces cerevisiae* and prepared as membrane fraction as previously reported (36). The total protein concentration in membrane fraction was determined using the BCA reagent (Pierce, Brebieres, France) with bovine serum albumin as a standard.

The specific monoclonal Rho-1D4 antibody raised against the rhodopsin C-terminal nanopeptide was purchased from National Cell Culture Center (Minneapolis, MN, USA). The antibody was biotinylated using DSB-X™ Biotin Protein Labeling Kit (Molecular Probes, Leiden, Netherlands).

16-mercaptohexadecanoic acid and biotinyl-PE were purchased respectively from Aldrich Chemical Company and Avanti. IgG from goat, which was used as blocking reagent, was bought from Sigma. Neutravidin was obtained commercially from PIERCE. And solvents ethanol and acetone were both bought from Fluka (purity > 99.8%).

Potassium dihydrogen phosphate, di-sodium hydrogen phosphate and sodium chloride all from PROLABO, potassium chloride from Fluka and sodium hydroxide from Aldrich Chemical Company were used to prepare phosphate buffer solution, consisting of 1.8 mM KH₂PO₄, 0.1 mM Na₂HPO₄, 140 mM NaCl and 2.7 mM KCl, pH 7.0. All of them are analytical grade reagents (>99%). Solutions were prepared with water that has been purified by an ultrapure water system Elga. This buffer solution was used for all experiments.

2.2.2. Fabrication and pre-treatment of gold substrate

Gold substrates were provided by LAAS in Toulouse, their fabrication and pre-treatment were given in the chapter IV.

2.2.3. Formation and deposition of LB films of rhodopsin

Langmuir experiments were performed with the Langmuir trough from NIMA (model 611). The subphase temperature was controlled at 5 ± 1 °C by a thermostatic system (Julabo-F25, France). The surface pressure was measured by a Wilhelmy balance and the trough was filled with a subphase of PBS.

A small amount (40 μ l) of rhodopsin membrane fraction (1.5 mg ml⁻¹ total protein concentration) was spread at the air/water interface for formation of rhodopsin monolayer. The surface pressure-molecular area isotherm was studied to characterize the monolayer at the air/water interface. In addition, the stability of the monolayer at the air/water interface was investigated. They were recorded as molecular area ratio-time evolution isotherms at the target pressure (referred to as A/A_0 -t). The film was transferred onto bare gold electrode, which has a hydrophilic surface after cleaning, by a vertical dipping procedure at target pressure 30 mN m⁻¹.

2.2.4. Preparation of self-assembled multilayer

After cleaning, gold substrates were immersed immediately into a mixed solution of MHDA and biotinyl-PE in absolute ethanol at the concentration of 1 mM and 0.1 mM, respectively, for 21 h (Step I). The ratio between components determines the density of specific anchoring sites. Then gold substrates were removed from the mixed solution and thoroughly rinsed with ethanol and dried under N₂ flow. Subsequently, gold substrates functionalized with mixed SAMs were put into 1×10^{-7} M goat IgG solution in PBS (pH=7.0) for 2 h for blocking free space inside of the mixed SAMs (Step II). Next, they were placed in a 1×10^{-7} M neutravidin solution for 90 min (Step III), followed by deposition of biotinylated specific monoclonal anti-rhodopsin antibody (Biot-Rho-1D4) at 1×10^{-7} M for 1 h (Step IV). Finally, rhodopsin membrane fraction was anchored on the self-assembled multilayer systems (V).

In this study, neutravidin is used as an alternative to streptavidin which is often used to provide avidin-biotin system, under consideration of several key features, such as carbohydrate free and neutral isoelectric point that provide exceptionally low nonspecific binding properties. In addition, neutravidin can bind at four binding sites like streptavidin, two binding sites on each of two opposite faces, which permits its binding onto biotin-containing SAMs on one side and anchor Biot-Rho-1D4 on the other side in the following step. After each step, substrates were rinsed well with PBS to remove the excess of material which was physically adsorbed onto the surface.

2.2.5. Electrochemical measurements

The electrochemical characteristics of the modified electrode were measured using cyclic voltammetry and non-faradaic impedance. Electrochemical measurements were performed in a conventional electrochemical cell containing a three-electrode system with a Voltalab 80 impedance analyser. A Pt plate and a saturated calomel electrode were used as counter and reference electrode, respectively. Functionalized gold electrodes act as working electrodes with an effective surface of 0.2122 cm^2 .

Cyclic voltammetry measurements were performed in the presence of 2 mM $\text{K}_4[\text{Fe}(\text{CN})_6]$ + 2 mM $\text{K}_3[\text{Fe}(\text{CN})_6]$ in PBS (pH=7.0) and the potential was swept between -0.3 and 0.6 V (vs. SCE) at a rate of 50 mV s^{-1} .

Impedance measurements were carried out in absence of any redox probe in the PBS at ambient temperature in a frequency range from 500 mHz to 100 kHz, at a polarization potential of 0 V/SCE with a frequency modulation of 10 mV. All electrochemical measurements were performed in a faraday cage.

2.2.6. Atomic force microscopy

Atomic force microscopy measurements were carried out in Laboratory of NanoBioEngineering (Barcelona Science Park), they were performed with a commercial microscopy instrument (PicoSPM Molecular Imaging). A pyramidal silicon tip with spring constant of approximately 3 N m^{-1} was used. The cantilever was oscillated at its free resonance frequency (75 kHz) with a free amplitude, $A_0 = 1.6 \text{ V}$. All the experiments were performed under ambient conditions with relative humidity of about 60%. The image presented in this paper was taken in tapping mode. Since it minimizes potentially destructive shear and adhesive forces on the sample compared to contact mode, which is a particularly valuable property when imaging cells or biological molecules. The image was first-order flattened.

2.3. Results and discussion

2.3.1. Study of Langmuir films of rhodopsin

2.3.1.1. Characteristics of rhodopsin monolayer at the air/water interface

The characteristics of rhodopsin membrane fraction monolayer at the air/water interface were studied by measuring the changes in surface pressure upon compressing the monolayer at a given temperature (5°C), namely surface pressure-molecular area isotherm (shown in Figure V.5). In this study, the film was spread at an initial surface pressure of 0 mN m⁻¹. It was incubated for 20 min, and finally compressed at the rate of 3 cm² min⁻¹. Extrapolated to 0 mN m⁻¹ from the linear portion of the compression curve gives an apparent surface area of 4500 Å²/molecule. It is greater than the molecular area occupied by rhodopsin surrounding by lipids in the disc membrane reported by Lavoie et al. (5) (3400 Å²) and Pepe et al. (15) (3710 Å²). Such a difference in size is probably induced by the procedure of preparation of rhodopsin samples i.e. different lipidic molecules or presence of detergent to solubilize rhodopsin molecules.

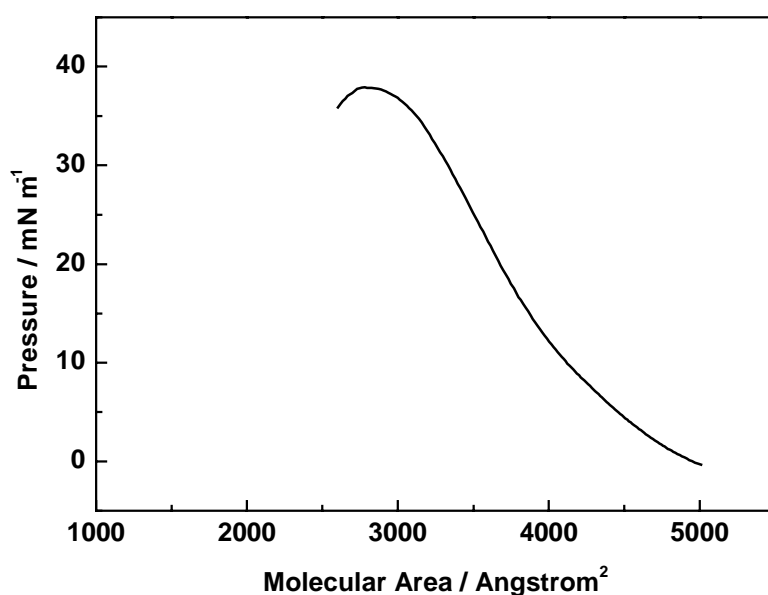


Figure V.5: Surface pressure-area isotherm of rhodopsin monolayer at the air/water interface on a subphase of PBS.

2.3.1.2. Stability of rhodopsin monolayer at the air/water interface

Since the stability of the LB films is dependent, to a great extent, upon the stability of the monolayer at the air/water interface, we have investigated the stability of monolayer of rhodopsin at different surface pressures (30 and 35 mN m⁻¹). They are recorded as molecular area ratio-time evolution isotherms at constant surface pressure, as shown in Figure V.6. It can be seen that the monolayers of rhodopsin are not stable.

In particular, at the surface pressure 35 mN m^{-1} , after 70 min, molecular area ratio A/A_0 reaches nearly 0.5, which means that about 50% rhodopsin molecules were expelled from interface and turned into the subphase at such a surface pressure.

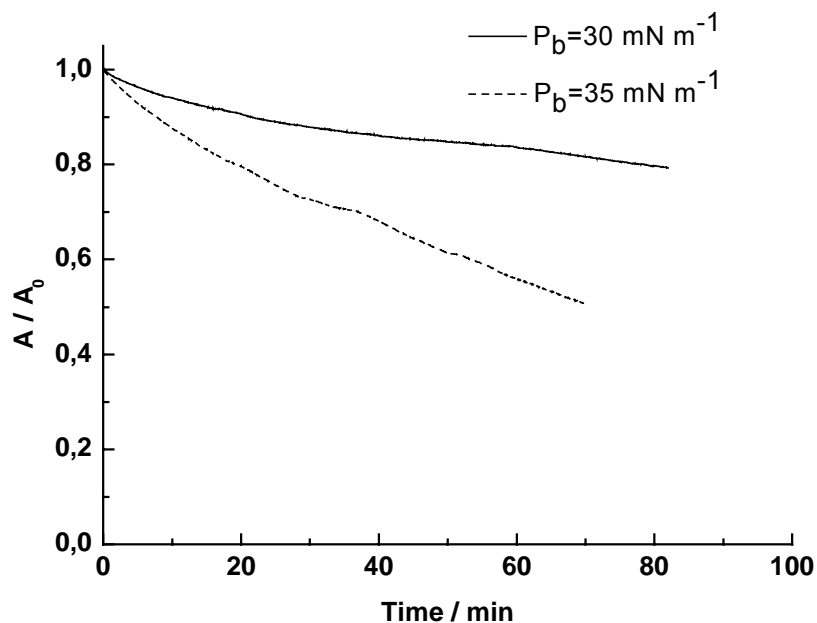


Figure V.6: Stability of rhodopsin monolayers at the air/water interface for two different surface pressures (30 mN m^{-1} and 35 mN m^{-1}).

In the previous studies, we showed that an enzyme (10), or an antibody (13) can form stable Langmuir and Langmuir-Blodgett films in presence of amphiphile. They can form protein/surfactant complex with amphiphile after optimizing experimental conditions, especially pH of subphase. Such a complex can strengthen the stability of at the air/water interface. Rhodopsin is a transmembrane protein and thus extremely hydrophobic. Under the conditions used the Langmuir film formed at the air/water interface is not stable.

In addition, we transferred the monolayer of rhodopsin onto bare gold electrode, which was freshly cleaned before use, at a target pressure of 30 mN m^{-1} . Then by electrochemical impedance measurements we investigated the gold electrode, on which the LB films of rhodopsin are deposited. It was observed that there was a continuous variation of impedance with time. It means that the obtained LB films are quite unstable, which confirms that the stability of the LB films is dependent upon the stability of the monolayer at the air/water interface. Therefore, it is quite difficult to elaborate a biosensor with such unstable system. So in this study we investigated

another immobilization technique based on a self-assembled multilayer, in which rhodopsin is anchored and bound on gold electrode by affinity interaction with its specific antibody which is biotin-labelled.

2.3.2. Study of self-assembled multilayer formation

Figure V.7 shows the schematic diagram for self-assembled multilayer formation on gold electrode. Electrochemical characteristics of the stepwise formation of self-assembled multilayer were studied by CV and EIS.

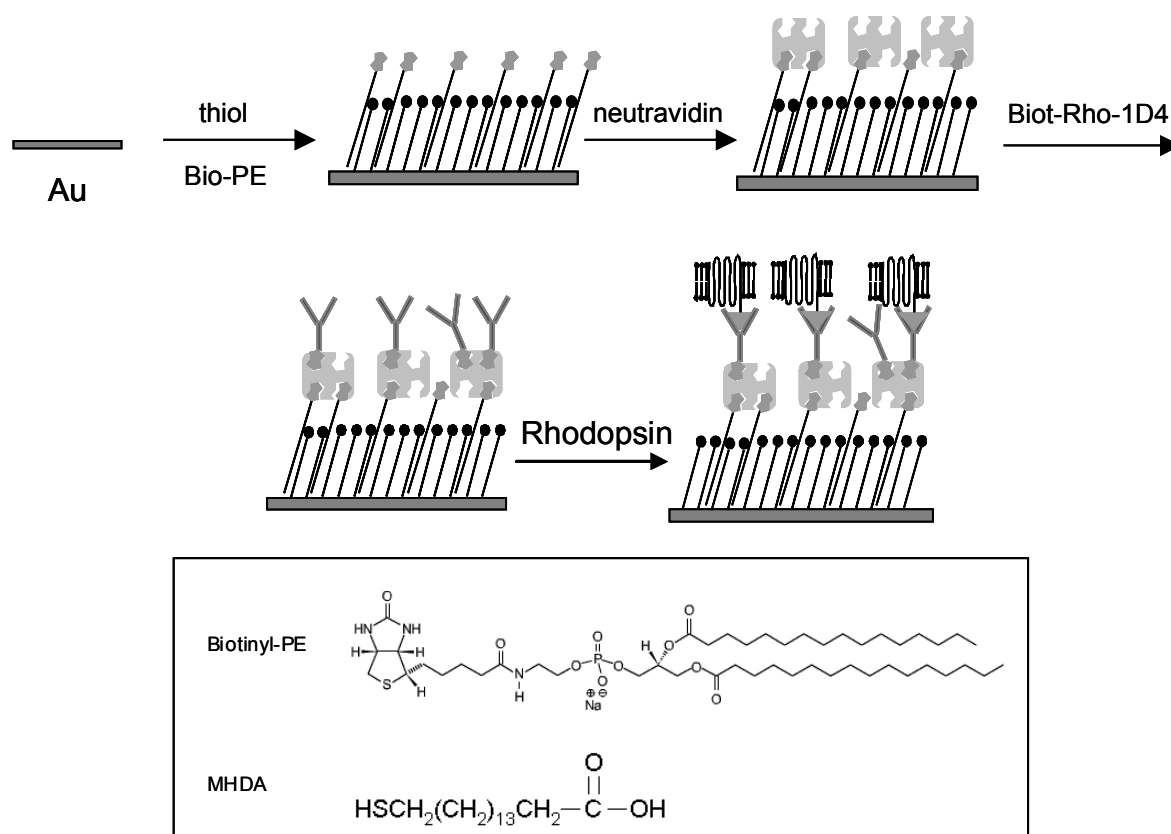


Figure V.7: Schematic diagram for self-assembled multilayer formation via biotin/avidin pairs on gold electrode.

2.3.2.1. Electrochemical characteristics of self-assembled multilayer formation by CV

In the presence of a fairly reversible redox couple $[\text{Fe}(\text{CN})_6]^{4-/3-}$, cyclic voltammetry was used to monitor the formation of self-assembled multilayer. As it is shown in Figure V.8, the pretreated bare gold electrode gives a reversible cyclic voltammogram (curve a). The formation of mixed SAMs on gold electrode is accompanied by a considerable decrease in the amperometric response of the electrode and an increase in the peak to peak separation between the cathodic and anodic waves

of the redox probe (curve b). This confirms that the formation of mixed SAMs resulted in an insulating surface and the electron transfer kinetics of $[\text{Fe}(\text{CN})_6]^{4-/3-}$ are perturbed. After blocking the free space inside SAMs with goat IgG, a slight increase of current response is observed (curve c). The increase of current response is probably due to structural rearrangement of the mixed SAMs with insertion and adsorption of goat IgG molecules. Another possibility is adsorption of goat IgG on the terminal carboxylic group of MHDA which is negatively charged in the pH 7.0, reduces the electrostatic repulsion to negative redox ions $[\text{Fe}(\text{CN})_6]^{4-/3-}$. The increase of current response confirms that goat IgG molecules are indeed inserted inside of the mixed SAMs so that they can block the free space between biotinyl-PE molecules in the mixed SAMs. The binding of neutravidin on the electrode reduces slightly the penetration of the redox pair and decreases the current response. In the subsequent step, the immobilization of Biot-Rho-1D4 decreases the current response slightly further.

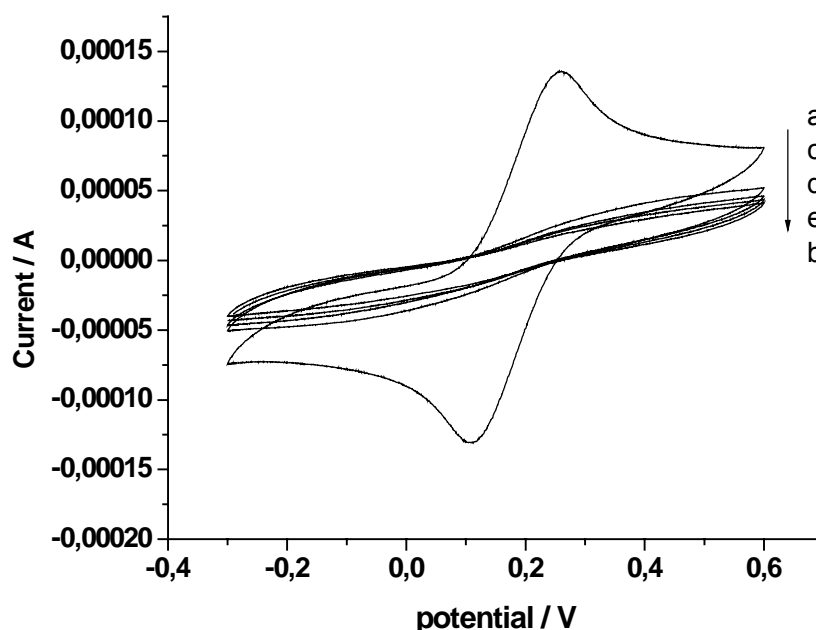


Figure V.8: Electrochemical characteristics of self-assembled multilayer formation by cyclic voltametric. CVs recorded in PBS solution in the presence of 4 mM $[\text{Fe}(\text{CN})_6]^{4-/3-}$. (a) Bare gold electrode; (b) Step I: mixed SAMs modified gold electrode; (c) Step II: blockage with goat IgG; (d) Step III: binding of neutravidin; (e) Step IV: immobilization of biotinylated antibody Biot-Rho-1D4. The scan rate is 50 mV s⁻¹.

2.3.2.2. Electrochemical characteristics of self-assembled multilayer formation by EIS

The EIS measurements were performed in PBS either in the presence

or absence of redox probe $[\text{Fe}(\text{CN})_6]^{4-/3-}$. However, we found that the presence of such redox probe has effects on rhodopsin immobilization, the binding efficiency of biotinylated specific antibody to rhodopsin seemed to decrease. Such a phenomenon was also observed by Rickert et al. (31). Therefore, the redox couple $[\text{Fe}(\text{CN})_6]^{4-/3-}$ is omitted in all electrochemical impedance measurements.

Non-faradaic impedance measurements were carried out in the frequency range from 500 mHz to 100 kHz. Nyquist plots of impedance spectra of layer-by-layer self-assembled multilayer are shown in Figure V.9 significant difference in the impedance spectra is observed upon the stepwise formation of the multilayers and upon rhodopsin deposition. Moreover, by EIS measurements we observed that such self-assembled multilayers are very stable.

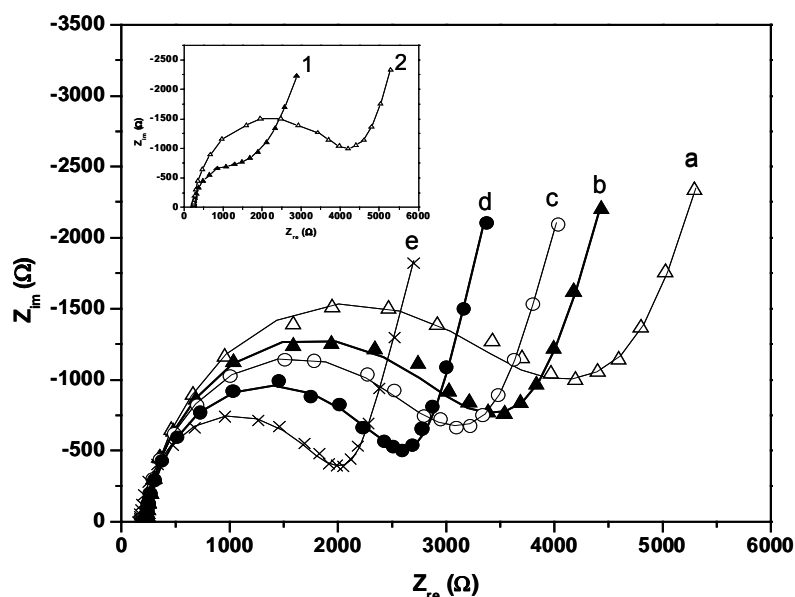


Figure V.9: Electrochemical characteristics of self-assembled multilayer formation by EIS. Nyquist plots of impedance spectra taken in PBS without redox couple in the frequency range from 500 mHz to 100 kHz. (a) Step I: mixed SAMs modified gold electrode; (b) Step II: blockage with goat IgG; (c) Step III: binding of neutravidin; (d) Step IV: immobilization of biotinylated antibody Biot-Rho-1D4. (e) after injection of 80 ng ml^{-1} rhodopsin membrane fraction. Inset: Nyquist plots for bare gold electrode (1) and gold electrode modified with the mixed SAMs (2). The symbols are the experimental data and the line represents the simulated spectra with the parameters calculated by Zplot/Zview software using the equivalent circuit shown in Figure V.10. The calculated parameters are given in Table V.1.

The impedance data were analyzed with the help of National Nanotechnology Laboratory, Lecce. They were fitted with a commercially available software Zplot/Zview (Scibner Associates Inc.). The equivalent circuit, shown in Figure

V.10, was found to fit adequately the data over the entire frequency range.

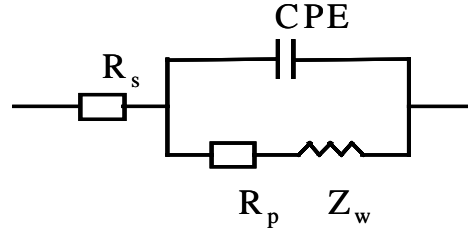


Figure V.10: The equivalent circuit.

The circuit follows a standard Randles cell and includes the following four elements:

- (i) The ohmic resistance of the electrolyte solution, R_s .
- (ii) The constant phase element impedance, Z_{CPE1} , whose expression is given by Equation V.1.

$$Z_{CPE1} = 1 / [T(i\omega)^P] \quad (V.1)$$

Where i is the imaginary unit, ω is the circular frequency, and $CPE1-T$ ($F(\text{rad/s})^{1-CPE1-P}$) and $CPE1-P$ are the two fitting parameters which model the double layer capacitance and its phase angle, respectively.

- (iii) The generalized finite Warburg impedance in the open circuit model, Z_{W1o} , whose expression is given by Equation V.2.

$$Z_{W1o} = R \times \text{ctnh}([i \times T \times \omega]^P) / (i \times T \times \omega)^P \quad (V.2)$$

Where $W1o-R$ (Ohm), $W1o-T$, (s), and $W1o-P$ are the associated three fitting parameters.

- (iv) The polarization resistance R_p .

The fitting values for the stepwise formation of the multilayers are reported in Table V.1.

Starting from the bare gold, the deposition of the mixed SAM monolayer is found to produce a significant increase of the polarization resistance together with a significant decrease of the double layer capacitance which confirms the good insulating properties of the mixed monolayer already found in the CV characterization. In all the successive steps we found a systematic decrease of the polarization resistance and of the Warburg resistance which indicate a recovery in the efficiency of the mass transfer

phenomenon and/or difference in the dielectric or conductive properties of the electrode surface with formation of new layer. The value of the solution resistance is found to remain practically constant. The deviation of CPE1-P and W_0 -P from the ideal values 1 and 0.5, respectively, is taken as a measure of the presence of spurious effects like the roughness of the electrode surface and some anomalies of the mass transfer to follow the standard diffusion equation.

	R_s (Ω)	CPE1-T ($\mu F(rad/s)^{1-n}$)	CPE1-P (n)	R_p (Ω)	W_0 -R (Ω)	W_0 -T (s)	W_0 -P	Chi-squared (10^{-4})
Bare gold	238.8	3.63	0.94	774.5	2433	0.236	0.33	10
Step I	230.4	0.744	0.91	3150	4079	0.521	0.40	9.8
Step II	233.9	0.655	0.92	2623	2875	0.345	0.40	9.9
Step III	219.7	0.681	0.92	2376	2487	0.304	0.40	9.8
Step IV	231.5	0.698	0.92	2011	1607	0.172	0.41	8.1
After 80 ng/ml rhodopsin	165.8	0.661	0.93	1550	1257	0.149	0.40	9.9

Table V.1: The fitting values of the equivalent circuit elements for stepwise formation of the multilayer films by Zplot/Zview software.

2.3.2.3. Self-assembled multilayer formation characterized by AFM

In order to characterize the formation of the multilayer film and to obtain information on its architecture, AFM measurements were taken in tapping mode. After the rhodopsin membrane fraction was immobilized on the self-assembled multilayers, AFM image was taken, as presented in the image Figure V.11, which reveals randomly located grainy features that range in size from 30-100 nm and are about 5 nm high. These sizes are consistent with those observed by negative staining of the rhodopsin membrane fraction preparation using electron microscopy (37). In addition, the thickness of the rhodopsin-containing layer is approximately equivalent to the thickness of the cell membrane, indicating that membrane vesicles open upon immobilization. Further, during the scanning, we found that on some areas of fraction membrane, the tip interaction with the surface increased, which confirms that the rhodopsin is present as membrane fraction.

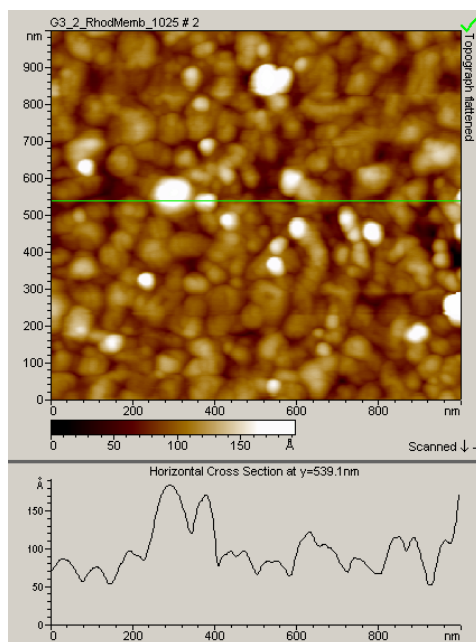


Figure V.11: Topographic AFM image (1 μm x 1 μm) obtained in tapping mode: after immobilization of rhodopsin membrane fraction on the self-assembled multilayers.

2.3.2.4. Recognition properties of the self-assembled multilayer

In order to evaluate the recognition properties of the system, in terms of sensitivity and selectivity, we exposed the gold electrode with self-assembled multilayers to various concentrations of rhodopsin after immobilization of Biot-Rho-1D4. The corresponding Nyquist plots of impedance spectra are shown in Figure V.12A. The fitting values are presented in Table V.2.

Concentration (ng ml^{-1})	R_p (Ω)	CPE1-T ($\mu\text{F}(\text{rad/s})^{1-n}$)	CPE1-P (n)	$R_p(\Omega)$	$W_o-R(\Omega)$	$W_o-T(\text{s})$	W_o-P
0	231.5	0.698	0.92	2011	1607	0.172	0.41
10	195.1	0.662	0.92	1825	1515	0.172	0.40
20	185.3	0.690	0.92	1736	1351	0.152	0.40
30	179.5	0.671	0.92	1669	1315	0.153	0.40
50	169.1	0.700	0.92	1615	1231	0.144	0.40
80	165.8	0.661	0.93	1550	1257	0.149	0.40
120	158.1	0.693	0.92	1533	1161	0.137	0.40

Table V.2: The fitting values of the equivalent circuit elements for specific binding of rhodopsin at various concentrations by Zplot/Zview software.

We found that both the polarization resistance and the Warburg resistance decrease with the addition of rhodopsin. At low concentration, the decrease is

very sensitive in magnitude, and for concentration above 80 ng ml^{-1} , the system is prone to be saturated. The solution resistance is also found to decrease systematically in an analogous but less significant way, probably due to the addition of rhodopsin membrane fraction in the cell. All other parameters determined by the fitting procedure do not exhibit significant change.

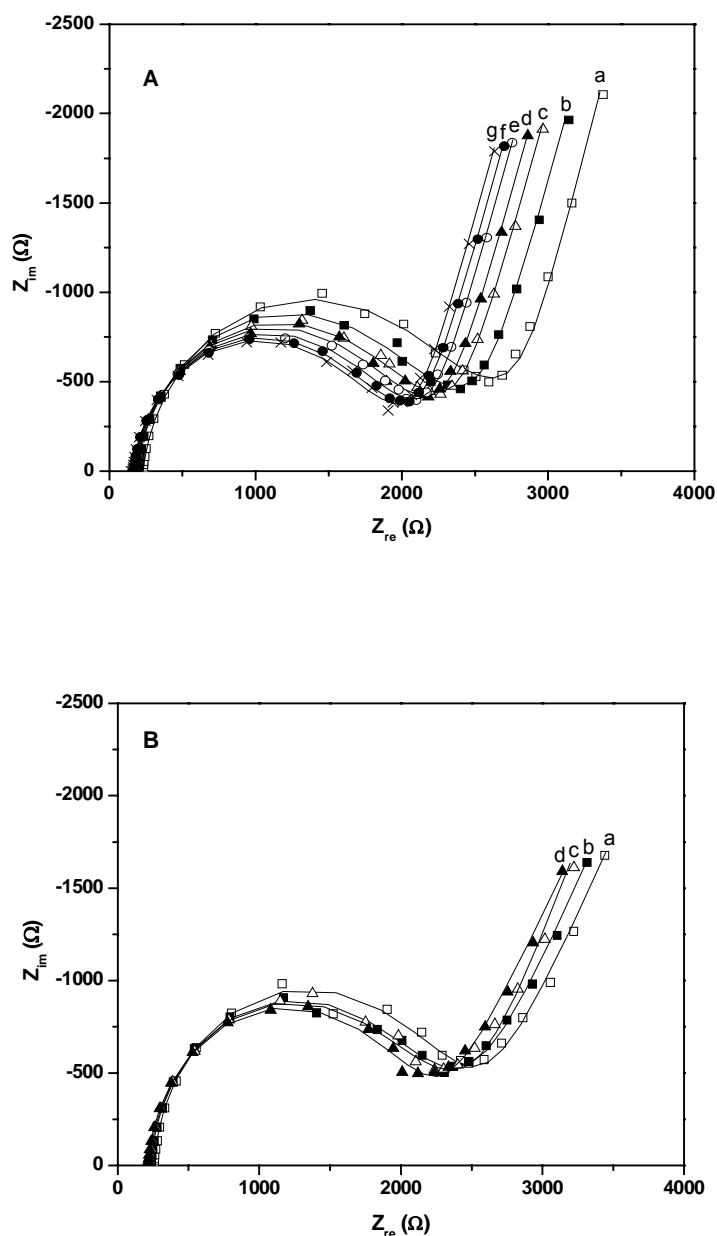


Figure V.12: Nyquist plots of impedance spectra taken in PBS without redox couple (A) with various concentrations of rhodopsin membrane fraction: (a) 0; (b) 10; (c) 20; (d) 30; (e) 50; (f) 80 and (g) 120 ng ml^{-1} . (B) with various concentrations of unrelated analyte: (a) 0; (b) 20; c 50; (d) 100 ng ml^{-1} . Applied frequency was from 500 mHz to 100 kHz. The symbols are the experimental data and the line represents the simulated spectra calculated by Zplot/Zview software using the same equivalent circuit as shown in the Figure V.10.

To confirm that the above-observed impedance changes arise from the specific interaction between Biot-Rho-1D4 and rhodopsin, and to reveal the selectivity of the binding, control experiments were performed. After immobilization of Biot-Rho-1D4, the gold electrode was exposed to various concentrations of an unrelated membrane protein (I7 olfactory receptor in its membrane fraction), which is also a member of the GPCR family. The corresponding Nyquist plots of impedance spectra obtained are shown in Figure V.12B. It can be seen that there is only a slight variation on the impedance with the increase of I7 concentration.

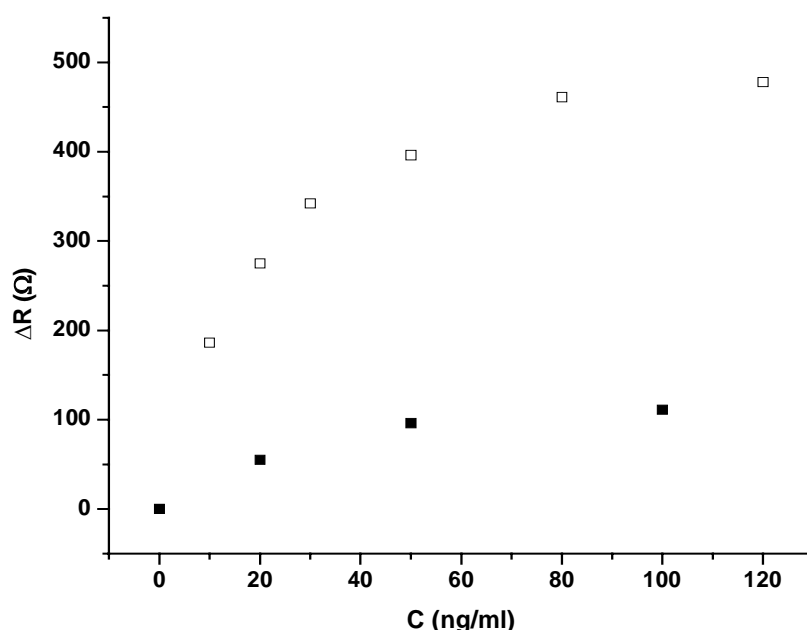


Figure V.13: Calibration plots showing the change of polarization resistance as a function of the different concentrations of specific (□) or unrelated analytes (■).

Figure V.13 shows calibration plots that correspond to the resistance change (ΔR) with different concentrations of the specific analyte (rhodopsin membrane fraction) and non-specific analyte (I7 membrane fraction). The changes of resistance are calculated by the Equation V.3 and V.4:

$$\Delta R = R_{Ab} - R_{Ab-Rho} \quad (V.3)$$

and

$$\Delta R = R_{Ab} - R_{Ab-I7} \quad (V.4)$$

Where R_{Ab} is the value of the resistance when biotinylated Biot-Rho-1D4 antibody is immobilized on the electrode, R_{Ab-Rho} is the value of resistance after injection

of specific rhodopsin analyte, R_{Ab-I7} is the value of resistance after injection of the unrelated analyte I7.

From Figure V.13 it can be observed that there is only a slight response to unrelated analyte addition, which is due to non-specific adsorption. However, compared with the specific response, we can see that the response for unrelated analyte I7 at the concentration of 100 ng ml^{-1} is even lower than that for specific rhodopsin at the concentration of 10 ng ml^{-1} . We thus confirm that impedance change in Figure V.12A. is not due to non-specific adsorption but it arises from specific interaction. So we can conclude that the self-assembled multilayer system has high sensitivity and selectivity for grafting of rhodopsin, and thus represents an efficient means to constitute a biosensor for detection of rhodopsin or with rhodopsin as the sensing element. Taking into account the blank and the signal fluctuation (noise), the detection limit for the binding of rhodopsin on the self-assembled multilayer is 10 ng ml^{-1} .

2.4. Conclusion

In this study, rhodopsin membrane fraction was immobilized on gold electrode by Langmuir-Blodgett or a self-assembled multilayer method. In a first step, we showed that LB films of rhodopsin deposited on bare gold electrode are not stable. In a second step, we realized a multilayer system, based on mixed self-assembled monolayers and biotin/avidin pairs acting as binding agents, and it proved to be an efficient immobilization method. Electrochemical impedance measurements demonstrated that such self-assembled multilayer system is sensitive and selective for the specific grafting of rhodopsin membrane fraction.

The objective of our project is to explore the possibility to develop a nanobiosensor array based on the electrical properties of a single GPCR protein, such as olfactory receptors. In the future work we will immobilize olfactory receptors in their membrane fraction by this self-assembled multilayer method on micro- and nano-electrodes to investigate electrical properties of the system in the presence of odorants.

References

- (1) N. Vaidehi, W. B. Floriano, R. Trabanino, S. E. Hall, P. Freddolino, E. J. Choi, G. Zamanakos, W. A. Goddard III, *Proc. Natl. Acad. Sci.*, **2002**, 99, 12622-12627.
- (2) <http://www.chemistry.wustl.edu/~edudev/LabTutorials/Vision/Vision.html>
- (3) <http://images.google.fr>
- (4) D. C. Teller, T. Okada, C. A. Behnke, K. Palczewski, R. E. Stenkamp, *Biochemistry*, **2001**, 40, 7761-7772.
- (5) H. Lavoie, B. Desbat, D. Vaknin, C. Salesse, *Biochemistry*, **2002**, 41, 13424-13434.
- (6) Y. Okahata, T. Tsuruta, K. Ijro, K. Ariga, *Langmuir*, **1988**, 4, 1373-1375.
- (7) C. Fiol, J. M. Valleton, N. Delpire, G. Barbey, A. Barraud, A. Ruaudel-Teixier, *Thin Solid Films*, **1992**, 210/211, 489-491.
- (8) J. M. Chovelon, F. Gaillard, K. Wan, N. Jaffrezic-Renault, *Langmuir*, **2000**, 16, 6228-6232.
- (9) N. Dubreuil, S. Alexandre, C. Fiol, F. Sommer, J. M. Valleton, *Langmuir*, **1995**, 11, 2098-2102.
- (10) A. Zhang, N. Jaffrezic, J. Wan, Y. Hou, J. M. Chovelon, *Materials Science and Engineering C*, **2002**, 21, 91-96.
- (11) A. Tronin, T. Dubrovsky, C. Nicolini, *Thin Solid Films*, **1996**, 284/285, 894-897.
- (12) A. Barraud, H. Perrot, V. Billard, C. Martelet, J. Therasse, *Biosensors and Bioelectronics*, **1993**, 8, 39-48.
- (13) Y. Hou, C. Tlili, N. Jaffrezic-Renault, A. Zhang, C. Martelet, L. Ponsonnet, A. Errachid, J. Samitier, J. Bausells, *Biosensors and Bioelectronics*, **2004**, 20, 1126-1133.
- (14) L. Maxia, G. Radicchi, I. M. Pepe, C. Nicolini, *Biophysical Journal*, **1995**, 69, 1440-1446.
- (15) I. M. Pepe, L. Maxia, C. Nicolini, *Thin Solid Films*, **1996**, 284-285, 739-742.
- (16) I. M. Pepe, C. Nicolini, *Journal of Photochemistry and Photobiology B: Biology*,

1996, 33, 191-200.

(17) I. M. Pepe, M. K. Ram, S. Paddeu, C. Nicolini, *Thin Solid Films*, **1998**, 327-329, 118-122.

(18) R. G. Nuzzo, D. L. Allara, *J. Am. Chem. Soc.*, **1983**, 105, 4481 – 4483.

(19) A. Ulman, *Chem. Rev.*, **1996**, 96, 1533-1554.

(20) T. Wink, S. J. V. Zuilen, A. Bult, W. P. V. Bennekomp, *Analyst*, **1997**, 122, 43R-50R.

(21) S. Ferretti, S. Paynter, D. A. Russell, K. E. Sapsford, *Trends in Analytical Chemistry*, **2000**, 19, 530-540.

(22) J. J. Gooding, D. B. Hibbert, *Trends in Analytical Chemistry*, **1999**, 18, 525-533.

(23) J. Spinke, M. Liley, H. J. Guder, L. Angermaier, W. Knoll, *Langmuir*, **1993**, 9, 1821-1825.

(24) X. Cui, R. Pei, Z. Wang, F. Yang, Y. Ma, S. Dong, X. Yang, *Biosensors and Bioelectronics*, **2003**, 18, 59-67.

(25) C. Boozer, Q. Yu, S. Chen, C. Lee, J. Homola, S. S. Yee, S. Jiang, *Sensors and Actuators B*, **2003**, 90, 22-30.

(26) J. Ladd, C. Boozer, Q. Yu, S. Chen, J. Homola, S. Jiang, *Langmuir*, **2004**, 20, 8090-8095.

(27) S. Storri, T. Santoni, M. Minunni, M. Mascini, *Biosensors and Bioelectronics*, **1998**, 13, 347-357.

(28) E. Katz, I. Willner, *Electroanalysis*, **2003**, 15, 913-947.

(29) J. Guan, Y. Miao, Q. Zhang, *Journal of Bioscience and Bioengineering*, **2004**, 97, 219-226.

(30) L. Alfonta, A. Bardea, O. Khersonsky, E. Katz, I. Willner, *Biosensors and Bioelectronics*, **2001**, 16, 675-687.

(31) J. Rickert, W. Göpel, W. Beck, G. Jung, P. Heiduschka, *Biosensors and Bioelectronics*, **1996**, 11, 757-768.

(32) R. Pei, Z. Cheng, E. Wang, X. Yang, *Biosensors and Bioelectronics*, **2001**, 16, 355-

361.

(33) M. Wang, L. Wang, G. Wang, X. Ji, Y. Bai, T. Li, S. Gong, J. Li, *Biosensors and Bioelectronics*, **2004**, 19, 575-582.

(34) D. Fotiadis, S. Scheuring, S. A. Müller, A. Engel, D. J. Müller, *Micron*, **2002**, 33, 385-397.

(35) D. S. Papermaster, *Methods Enzymol*, **1982**, 81, 48-52.

(36) J. Minic, M. A. Persuy, E. Godel, J. Aioun, I. Connerton, R. Salesse, E. Pajot-Augy, *FEBS J*, **2005**, 272, 524-537.

(37) J. Minic, J. Grosclaude, J. Aioun, M. A. Persuy, T. Gorojankina, R. Salesse, E. Pajot-Augy, Y. Hou, S. Helali, N. Jaffrezic, F. Bessueille, A. Errachid, G. Gomila, O. Ruiz, J. Samitier, *BBA*, **2005**, 1724, 324-332.

CHAPTER VI: A NOVEL DETECTION STRATEGY OF ODORANTS BASED ON OLFACTORY RECEPTORS IMMOBILIZED ON IMPEDIMETRIC BIOSENSORS

1. INTRODUCTION ON OLFACTORY RECEPTORS

Olfactory receptors constitute the largest family of GPCRs, with up to about 1000 different genes per species. They are located in the membrane of cilia of the olfactory sensory neurons where the initial steps of the olfactory transduction cascade occur and detect the inhaled odorant molecules. (1)

Although crystal structure of ORs are not available, they are widely thought to have seven transmembrane α -helices separated by three extracellular and three intracellular loops, with an extracellular amino-terminus and an intracellular carboxy-terminus like all members of GPCRs family, as shown in Figure V.3.

Here we will first introduce how we can smell in order to understand better the function of ORs. Then rat olfactory receptor I7 (OR I7) used in this thesis will be introduced.

1.1. Smell

The sense of smell informs an organism about the chemical composition of the external environment. From an evolutionary standpoint it is one of the most ancient senses. Smell (or olfaction) allows vertebrates and other organisms with olfactory receptors to identify food, mates, predators, and provides both sensual pleasure (the odor of flowers and perfume) as well as warnings of danger (e.g., spoiled food, chemical dangers). For both humans and animals, it is one of important means by which we communicate with the environment.

1.1.1. Olfactory system

The odorant molecules from an object (e.g. a rose) are inhaled through the nostrils and enter the nasal cavity. They then come in contact with the olfactory neurones located in the olfactory epithelium high up in the nose. These olfactory neurones are terminated in cilia (hairs) which lie in a thin, aqueous, mucous layer covering the epithelium. Special olfactory proteins located in these cell membranes interact with odorant molecules and cause excitation in the neurone. (2)

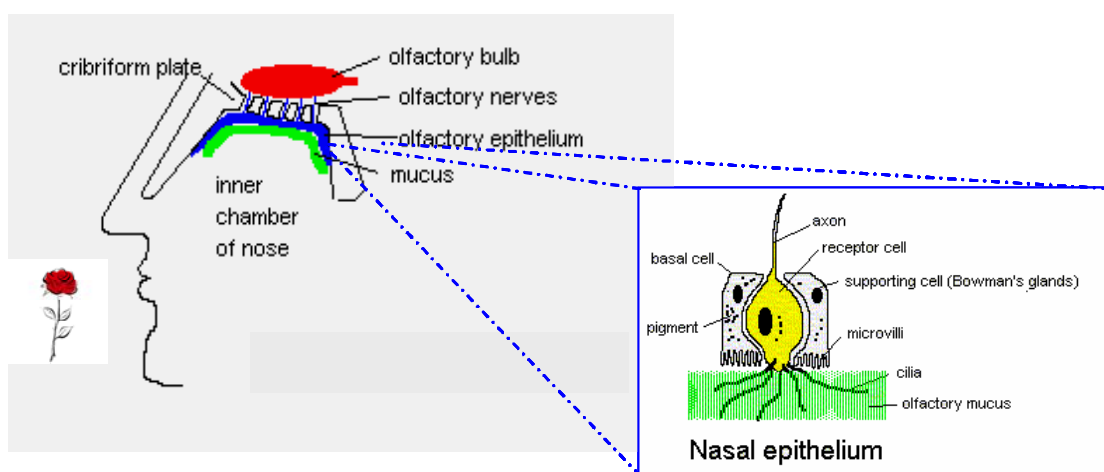


Figure VI.1: The location of the olfactory system in the human nose.

1.1.2. Olfactory signal transduction

With the help of odorant binding proteins, hydrophobic odorants can more easily cross the mucus layer to contact with the olfactory receptors. In mammals, once the olfactory receptors bind the odorant molecule, a cascade of events (shown in Figure VI.2) is initiated that transforms the chemical energy of binding into a neural signal (that is, a change in the membrane potential of the olfactory sensory neurons (OSNs)). (3) The ligand-bound receptor activates a G protein (an olfactory specific subtype, G_{olf}), which in turn activates an adenylate cyclase. The cyclase converts the abundant intracellular molecule ATP into cyclic AMP, a molecule that has numerous signalling roles in cells. The cyclic AMP binds to the intracellular face of an ion channel (a cyclic nucleotide-gated channel), enabling it to conduct cations such as Na^+ and Ca^{2+} . The influx of Na^+ and Ca^{2+} ions causes the potential inside of the cell to become less negative. If enough channels are open for long enough, the cell can reach threshold and generate an action potential. The action potential is then transmitted to the olfactory bulb via OSN axons, which synapse with the dendrites of second-order neurons and interneurons within structures called glomeruli, leading ultimately to recognition of 'smell'.

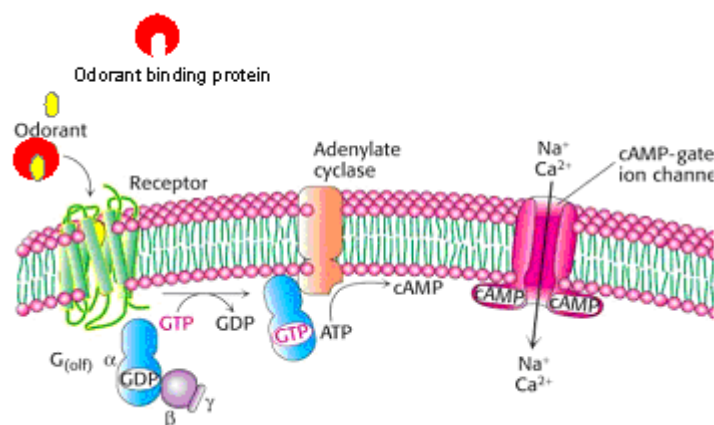


Figure VI.2: Olfactory signal transduction pathway in higher vertebrates.

1.2. OR I7 and structural characteristics of its specific ligands

In this study rat OR I7 is chosen since it is the first mammalian olfactory receptor whose preferential ligand (octanal) was identified by Zhao et al. (4). They first determined and reported the ligand specificity of olfactory receptor I7. To do that, they developed a panel of 74 odorants, including aromatic and short-chain aliphatic compounds with various functional groups. They found that the OR I7 is activated by saturated aliphatic aldehydes with backbone chains of 7 to 10 carbons, centred on octyl aldehyde (octanal).

Afterwards, Araneda et al. performed more full-scale investigations (5). They used octanal as a template, and tested 90 odorants chosen to represent alterations in functional group, backbone chain length, degree of unsaturation and side chain substitution.

They found that for the OR I7 the aldehyde carbonyl is absolute requirement. The importance of the aldehyde carbonyl has been suggested in modelling studies, which have provided evidence that the carbonyl may form electrostatic bonds with lysine 164 within the I7 binding pocket. (6)

The study on the importance of molecular length showed that only molecules with 7-11 carbons are active. The relationship between receptor activity and chain length suggests some molecular constraints imposed by the dimension of the binding site. Longer molecules (longer than 12 Å, more than 11 carbons) may simply not fit into the restricted binding region. Shorter molecules (shorter than 8 Å, fewer than 7 carbons) are also inactive. Probably because they occupy only partially the binding site and fail to activate the receptor, or they are not able to reside stably in the binding site at all.

In addition, they found that within the acceptable length range for active molecules, structural variations toward the tail end were more tolerated. This might indicate the participation of a flexible hydrophobic binding pocket, where provided that the length of the ligand is correct, the tail could assume various conformations.

In contrast to the flexible nature of the interactions at the tail end of the molecule, there are very prominent structural constraints in the immediate environment around the aldehyde group.

Therefore, they concluded that the OR I7 is highly specific for an aldehyde group, has strict steric prerequisites around the carbonyl carbon, but is rather indiscriminate regarding structural variations at the tail of the molecule. In this study we chose two related odorants octanal and heptanal and an unrelated odorant helional for study.

2. A NOVEL DETECTION STRATEGY FOR ODORANT MOLECULES BASED ON A CONTROLLED BIOENGINEERING OF RAT OLFACTORY RECEPTOR I7

Abstract:

In this study, bioreceptor OR I7 was immobilized onto specific locations on a gold electrode by multilayer bioengineering based on a successive building up of a mixed self-assembled monolayer, and based on the biotin/avidin system for binding of specific antibody, which allows well controlled binding of the bioreceptor within its lipid environment. The efficiency of this approach was probed through electrochemical impedance spectroscopy measurements. The self-assembled multilayer system that we developed allows discrimination between the specific immobilization of a given receptor and the non-specific adsorption of other proteins, and indeed represents a highly selective support for receptor immobilization. Here for the first time we reported a dose-dependent detection of olfactory receptor I7 in its membrane fraction for odorant molecules (octanal, heptanal) by EIS.

2.1. Introduction

G protein-coupled receptors are a large and ubiquitous class of membrane receptors, and they mediate senses such as odor, taste, vision and pain in mammals (7). Olfactory receptors constitute the largest family of GPCRs, with up to about 1000 different genes per species. They are located in the cilia membrane of the olfactory sensory neurons and detect inhaled odorant molecules. (1)

The mammalian nose is the gold standard for odour detection, displaying both an unmatched chemical space and the highest sensitivity. A large proportion of these properties is expected to stem from the olfactory receptors themselves, as they support combinatorial detection of odors (8) and are capable of detection at very low concentrations, e.g. 10^{-7} M to 10^{-11} M in humans (9, 10). It is thus tempting to harness these receptors to some electronic devices in order to design a new family of bio-electronic noses.

However, since the pioneering work of Buck and Axel who first identified olfactory receptors in 1991 (11), little progress has been made in the biotechnology of olfactory receptors, mainly due to the difficulty in producing recombinant cells (12), despite significant new insights (13, 14). In the meantime, physicochemical electronic noses have fulfilled some of the expectations of early predictions (15) in such application as health (16), the environment, process monitoring (17), and even security control.

Animal olfactory receptors provide us with a wealth of individual molecular detectors. With the advent of nanotechnology (18), it should become feasible to design miniaturised devices that could closely mimic the olfactory system by arraying a large number of different receptors on a single chip. Such devices could be used for high-throughput screening of ligands for receptors, since the large majority of olfactory receptors are still orphan. A first requirement to reach this goal is to demonstrate the activity of olfactory receptors outside living cells.

We assumed that a convenient, olfactory receptor-based biosensor should detect a signal intrinsic to the receptor. We thus endeavoured to immobilise an olfactory receptor on the surface of a gold electrode in order to detect an odorant-dependent signal change by EIS, a powerful technique for the transduction of biosensing events on electrodes. (19-21) In this study, this technique was applied first to evaluate the efficiency of the specific immobilization of OR I7 onto the functionalized electrode

surface, and then to detect the dose-dependent response of OR I7 to odorants.

The rat olfactory receptor I7 was chosen as the bioreceptor since its odorant ligands are well documented (4-6). Like all other GPCRs, OR I7 is structurally characterized by seven transmembrane-spanning α -helices (22), which makes the receptor extremely hydrophobic, and therefore requires a lipidic environment to maintain its native conformation and functionality (23). In this study, the OR I7 was prepared and used in its membrane fraction.

Efficient immobilization of membrane receptors at specific sites on functionalized surfaces is crucial to maintain their biological function for the construction of bioelectronic devices. (24) To satisfy this requirement, mixed self-assembled monolayers containing biotin sites were used for protein assembly, then neutravidin was introduced by high affinity avidin-biotin interaction to allow the further binding of the biotinylated anti-receptor antibody. Finally the olfactory receptors were specifically immobilized, which also constitutes in-situ selection of the receptors within their lipidic bilayer. Figure VI.3 shows our global strategy to immobilize OR I7.

2.2. Materials and methods

2.2.1. Biomaterials and chemicals

The I7 olfactory receptor provided by INRA was expressed from the yeast *Saccharomyces cerevisiae* and the membrane fraction was prepared as previously reported (25). The total protein concentration in the membrane fraction was determined using the BCA reagent (Pierce, Brebieres, France) with bovine serum albumin as a standard. Rabbit anti-I7 polyclonal antibody raised against its N-terminal 15 aminoacids was custom made by Neosystem (Strasbourg, France). The antibody was biotinylated using a DSB-X™ Biotin Protein Labeling Kit (Molecular Probes, Leiden, Netherlands). Rhodopsin (membrane fraction) used for control experiments was prepared from calf eyes according to the Papermaster's procedure (26). The monoclonal Rho-1D4 antibody, directed against the C-terminus of rhodopsin, was purchased from National Cell Culture Center (Minneapolis, MN, USA). The antibody was biotinylated using the procedure described above, and it was used for control experiments.

Odorants octanal (purity 99%) and heptanal (purity 95%) were purchased from Aldrich, helional was a generous gift from Givaudan-Roure, courtesy of Boris Schilling (CH-Dubendorf), dimethylsulfoxide (DMSO) (purity $\geq 99.9\%$) was

purchased from Sigma.

2.2.2. Preparation of odorant solutions

Stock solutions of odorants (10^{-1} M) were prepared freshly on the day of experiment in DMSO, and 10^{-4} M dilutions in ultrapure water were made extemporaneously, directly from the 10^{-1} M stock solution. Further dilutions were prepared by successive 1:10 dilutions in ultrapure water. To study the effect of solvent DMSO on odorant detection, the solution was prepared in exactly the same way as for the octanal solution, with octanal replaced by the same volume of ultrapure water.

2.2.3. Experimental setup

Electrochemical impedance measurements were performed in a conventional electrochemical cell containing a three-electrode system with a Voltalab 80 impedance analyser. A Pt plate and a saturated calomel electrode were used as counter and reference electrodes, respectively. Functionalized gold electrodes acted as working electrodes with an effective surface of 0.2122 cm^2 .

The measurements were carried out in the absence of any redox probe in PBS at ambient temperature in a frequency range of 500 mHz to 100 kHz, at a polarization potential of 0 V/SCE with a frequency modulation of 10 mV. All electrochemical measurements were performed in a Faraday cage.

For the detection of odorants, the odorant solution at different concentrations prepared in the solvent DMSO was added to the PBS solution in the electrochemical cell. For example, to obtain a final odorant concentration in the cell of 10^{-4} M, 10^{-7} M, 10^{-9} M, 10^{-11} M, 10^{-13} M, calculated volume of the odorant solution at a concentration of 10^{-1} M, 10^{-4} M, 10^{-6} M, 10^{-8} M, 10^{-10} M respectively was added. At each odorant concentration, an EIS measurement was performed and recorded. After each EIS measurement, the solution in the cell was removed and PBS solution was then introduced.

The impedance data were fitted with the commercially available software Zplot/Zview (Scibner Associates Inc.). The equivalent circuit, shown in the inset of Figure VI.4, was found to fit the data adequately over the entire frequency range.

2.3. Results and discussion

The stepwise formation of the self-assembled multilayer has been

investigated in our previous study, and we have demonstrated that the SAM is an efficient method to specifically and stably immobilize rhodopsin, a representative G protein-coupled receptor. (27)

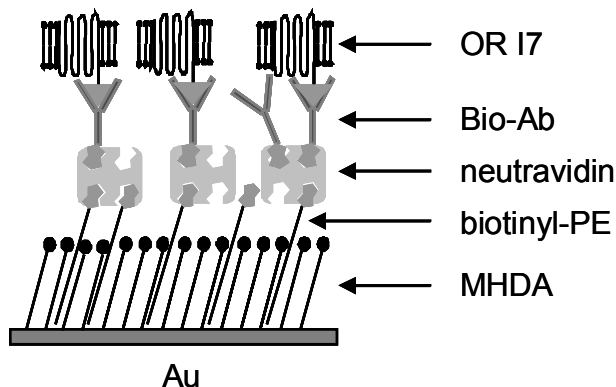


Figure VI.3: Schematic illustration of the self-assembled multilayer system.

2.3.1. Efficiency of binding bioreceptor OR I7

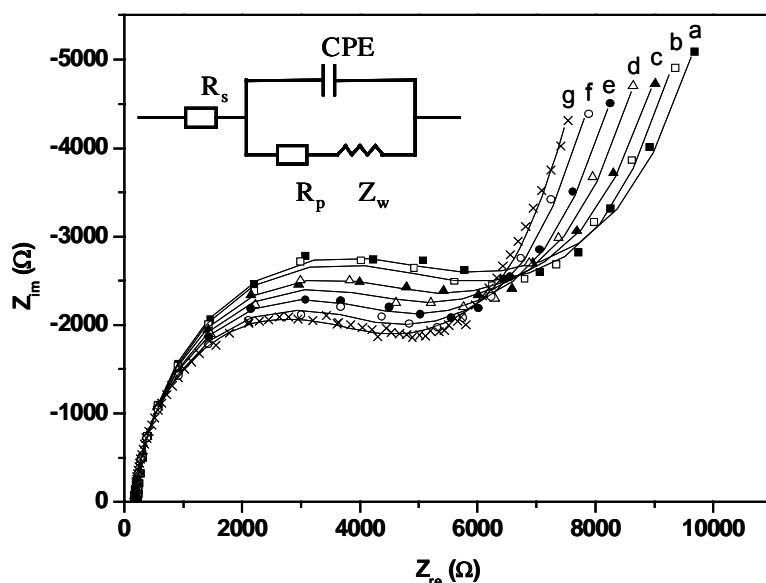


Figure VI.4: Nyquist plots of impedance spectra for test 1: detection of OR I7 (in its membrane fraction) at various concentrations with its specific biotinylated antibody: (a) 0 ng ml^{-1} ; (b) 20 ng ml^{-1} ; (c) 40 ng ml^{-1} ; (d) 60 ng ml^{-1} ; (e) 80 ng ml^{-1} ; (f) 120 ng ml^{-1} ; (g) 150 ng ml^{-1} . The symbols are the experimental data and the line represents the simulated spectra with the parameters calculated by Zplot/Zview software using the equivalent circuit shown in the inset.

In the present study, we first investigated the efficiency of binding of OR I7 on the SAM. In test 1, the gold electrode was functionalized with the biotinylated, OR

I7-specific antibody (Bio-Ab), then exposed to increasing concentrations of OR I7 in its membrane fraction. The corresponding Nyquist plots of impedance spectra are given in Figure VI.4. In test 2 (control test), the Bio-Ab coated electrode was prepared under the same conditions and was exposed to increasing concentrations of an unrelated analyte, rhodopsin in its membrane fraction. Another control experiment (test 3) was performed with biotinylated anti-rhodopsin antibody (Biot-Rho-1D4) coated gold electrode, which is exposed to OR I7 in its membrane fraction. At each concentration, EIS was used to monitor the changes occurring in the equivalent circuit parameters.

The experimental impedance spectra were fitted with computer simulated spectra using an electronic circuit shown in the inset of Figure VI.4, which satisfactorily fits the data over the entire frequency range. The circuit adopts a standard Randles cell and includes four fitting parameters: the ohmic resistance of electrolyte solution, R_s , the constant phase element, CPE, reflecting the nonhomogeneity of the layer in the presence of the large protein molecules, the Warburg impedance, Z_w , resulting from ion diffusion, and polarization resistance R_p . Of these, R_p and CPE depend on the dielectric and insulating features at the electrode/electrolyte interface, and are controlled by modifying the electrode's surface. The fitting parameters are displayed in the Table VI.1.

Test 1			Test 2			Test 3		
Concentration (ng/ml)	CPE μF	R_p (Ω)	Concentration (ng/ml)	CPE μF	R_p (Ω)	Concentration (ng/ml)	CPE μF	R_p (Ω)
0	0.486	4599	0	0.401	1542	0	0.4109	1727
20	0.521	4181	50	0.411	1500	20	0.419	1672
40	0.489	3970	100	0.393	1395	50	0.456	1631
60	0.481	3927	200	0.407	1396	100	0.470	1616
80	0.478	3800				200	0.436	1560
120	0.485	3630						
150	0.481	3466						

Table VI.1: The fitting values of the equivalent circuit elements for the three tests.

The fitting parameters show that for the three tests there is only a very slight change of CPE with increasing membrane concentration, the major change being a decrease of the polarization resistance R_p , which could indicate a recovery in the efficiency of the mass transfer phenomenon and/or a difference in the dielectric or conductive properties of the biofilm on the electrode surface due to the binding of the receptor. The change of polarization resistance versus concentrations of the analytes was plotted as calibration curves, shown in Figure VI.5.

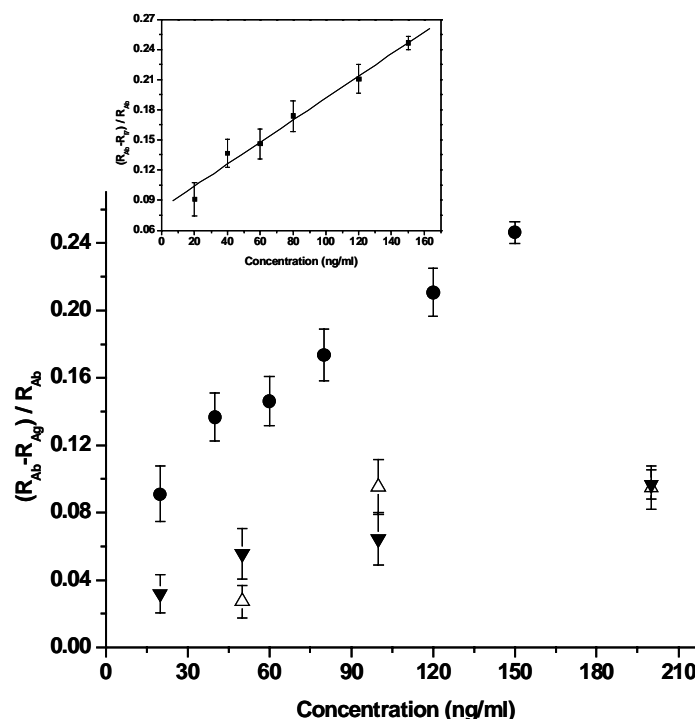


Figure VI.5: Calibration plots showing how polarization resistance changes with function of different concentrations of analytes detected by antibody previously immobilized on gold electrode: (Test 1) detection of OR I7 (in its membrane fraction) with its specific biotinylated antibody (●); (Test 2) detection of rhodopsin (in its membrane fraction) with biotinylated antibody specific to OR I7 (△); (Test 3) detection of OR I7 (in its membrane fraction) with non-specific biotinylated antibody Rho-1D4 (▼). R_{Ab} represents the polarization resistance when biotinylated antibody is immobilized on the electrode. R_{Ag} corresponds to the polarization resistance with injection of specific (OR I7) and non-specific analytes (rhodopsin) at different concentrations. Inset: Linear calibration curve for test 1.

It can be seen that R_p decreases significantly only where the specific Bio-Ab captures bioreceptor OR I7. Moreover, it can be seen from the inset of Figure VI.5 that for test 1 the response is linear, in the range of 20-150 ng/ml ($Y = 0.081 + 0.0011X$, $R = 0.995$, S.D. = 0.58), which supports the conclusion that the olfactory receptor is specifically captured on the surface of the electrode in test 1. The controls in tests 2 and 3 indicate that $35 \pm 3\%$ of the signal may be due to non-specific physical adsorption.

Thus, the self-assembled multilayer system that we have developed allows discrimination between the specific immobilization of a given receptor and the non-specific adsorption of other proteins, and indeed represents a highly selective support for receptor immobilization.

2.3.2. Detection of odorants

The preliminary determination of OR I7 odorant ligands reported by Zhao et al. (4), followed by more extensive investigations performed by Araneda et al. (5), concluded that OR I7 is highly specific for an aldehyde group, has strict steric prerequisites around carbonyl carbon, but is rather indiscriminate regarding structural variations at the tail of the molecule. We chose 2 related odorants, heptanal and octanal, commonly used as specific OR I7 ligands, for this preliminary study. Helional, which is effective to a human olfactory receptor protein (OR17-40) (9) and has a completely different chemical structure, was chosen as an unrelated odorant for control tests.

After OR I7 was immobilized, the ORI7-functionalised gold electrodes were used as working electrodes for the detection of different odorants: octanal and heptanal (specific) and helional (non specific). The most important parameter modified when a related odorant is recognized by the ORI7 receptor is the electrode's polarization resistance, so that was chosen as the sensing element (response of the biosensor). Figure VI.6 reports the variation of the polarization resistance of the OR I7-functionalised electrode as a function of odorant concentration, together with the chemical structures of the corresponding odorants.

At very low concentration (e. g. 10^{-13} M) the signal for the non-specific odorant helional is even higher than that for octanal. At such low concentration, the response resulting from the specific binding of odorants to the olfactory receptor is probably weak, therefore the effect of the physical adsorption and/or penetration of helional, which has a comparatively high molecular weight, onto/into the SAM is relatively important. As the odorant concentration increases, specific binding gradually becomes dominant. Such a non-specific response for helional is prone to saturate above 10^{-7} M. In addition, we can see from Figure VI.6, for concentrations of odorant above about 10^{-12} M, the response for the detection of specific odorants is systematically higher than that for non-specific ones. Interestingly enough, at relatively low concentrations (10^{-12} - 10^{-9} M), the system is slightly more sensitive to heptanal than to octanal, and at higher concentrations this sensitivity is reversed with the tendency for heptanal to saturate, which is consistent with the results previously reported (10).

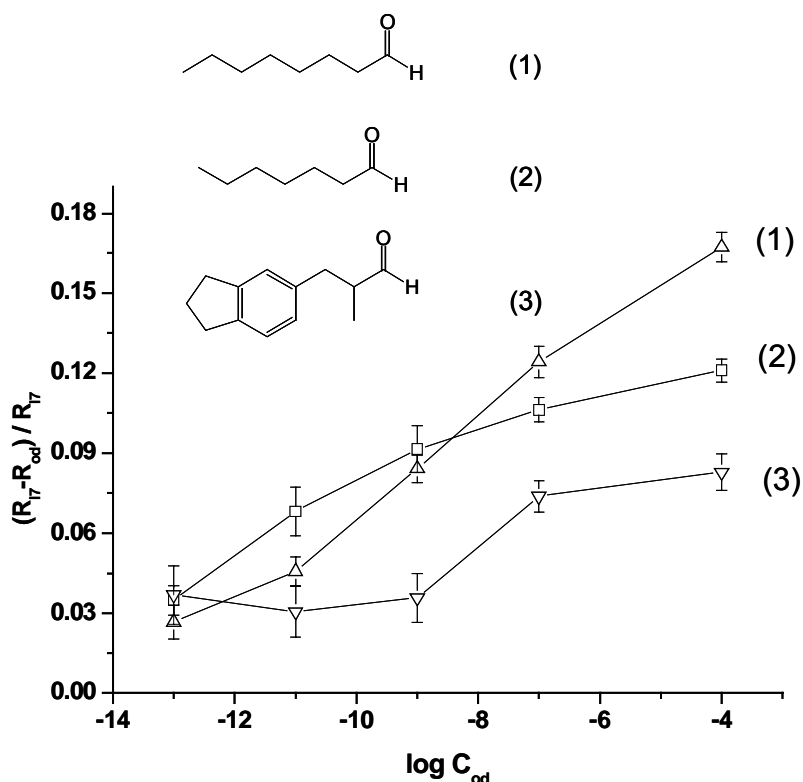


Figure VI.6: Dose-response of rat I7 receptor (in its membrane fraction) to (1) octanal (Δ), (2) heptanal (\square) and (3) helional (∇). The chemical structures of odorants are also given. R_{I7} represents the polarization resistance before injection of odorants. R_{od} corresponds to the polarization resistance with injection of specific and non-specific odorants at different concentrations.

In the following test, we studied the detection of odorant octanal with the unrelated bioreceptor rhodopsin as a control. In this case, rhodopsin was anchored specifically onto the gold electrode which had been previously functionalized by Biot-Rho-1D4, and then it was used to detect different concentrations of octanal. For further control, we tried to detect odorants in the presence of the underlayer only, namely the layer of biotinylated antibody specific to OR I7, where no OR I7 was yet anchored. Heptanal was chosen since it has a comparatively low molecular weight and yields the highest response in the complete Biot-Ab + OR I7 membrane fraction system at low and intermediate concentrations.

As the non-specific adsorption is relatively important at very low and very high concentrations, we compared the response to odorant in all tests at an intermediate concentration 10^{-11} M, shown in Figure VI.7. We can see that the responses for the specific detection of odorants are clearly higher than those obtained in the control tests. We found that for the detection of octanal, the ratio of the response of the unrelated bioreceptor rhodopsin to the response of OR I7 at an octanal concentration of

10^{-11} M is $30 \pm 3\%$. For heptanal detection the ratio of the response without OR I7 to the response with OR I7 is $15 \pm 3\%$ for a heptanal concentration of 10^{-11} M.

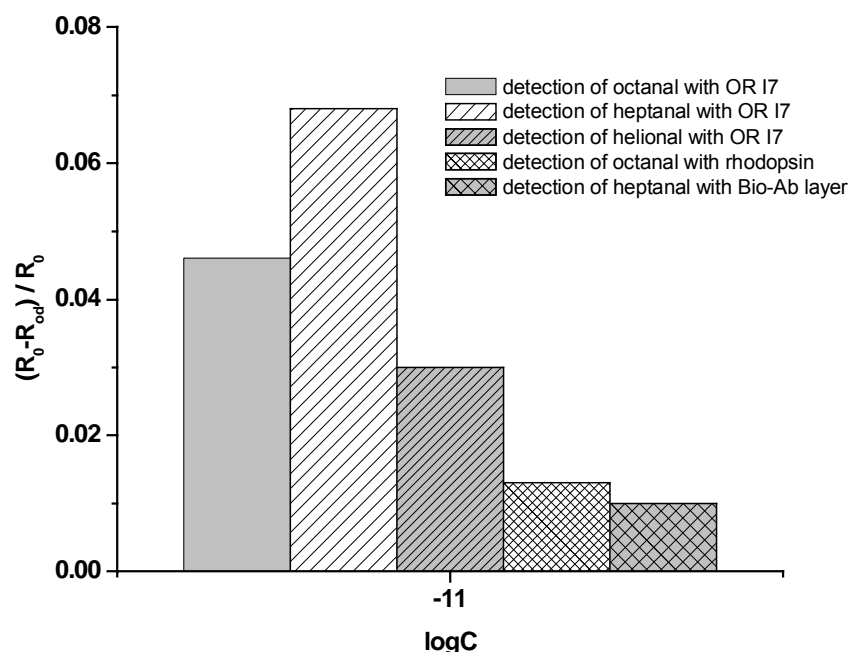


Figure VI.7: The response of odorant at 10^{-11} M under different conditions. R_0 represents the polarization resistance before injection of odorants. R_{0d} corresponds to the polarization resistance with injection of odorant at a concentration of 10^{-11} M.

In addition, we performed a blank test in order to study the effect of the solvent DMSO which is used for dissolving the odorants. The solution was prepared in exactly the same way as octanal solutions except that octanal was replaced by ultrapure water. The result showed that DMSO has only slight effect: even at 10^{-4} M, where there is the biggest effect, the response ratio is less than 10%.

The non-specific effect is most likely due to the non-specific adsorption of odorant and DMSO molecules on the self-assembled multilayer. The multilayer, based on a mixed self-assembled monolayer, is neither dense nor homogenous. It has been referred in previous chapter that the bioreceptor rhodopsin, prepared in exactly the same way as OR I7, is not densely located on such a multilayer (27). Therefore it is possible that some odorant molecules and DMSO molecules can be adsorbed and/or entrapped onto or inside the multilayer, which could result in some variation of the dielectric and insulating features at the electrode/electrolyte interface. This variation can then be detected by the sensitive transduction technique EIS. However, in the cases of the specific detection of odorants with OR I7, the variation of impedance is more significant

and is mainly due to the specific binding of odorants to the bioreceptor OR 17.

3. MICROELECTRODE

It is referred above that the objective of the project is to develop olfactory nano-biosensor. Therefore, after we validated the feasibility of elaboration of olfactory biosensor by self-assembled multilayer on gold electrode at the scale of centimeter, we tried to immobilize the olfactory receptors on microelectrodes. Two kinds of microelectrodes fabricated in Centro Nacional de Microelectronica were used for preliminary tests. This part of work was done in Laboratory of NanoBioEngineering, Barcelona Science Park, during my one-month stage.

3.1. Microelectrode 1

3.1.1. Structure of the microelectrode 1

The microelectrode 1 comprises three gold electrodes in parallel with surface area of $300\ \mu\text{m} \times 300\ \mu\text{m}$, as shown in Figure VI.8.

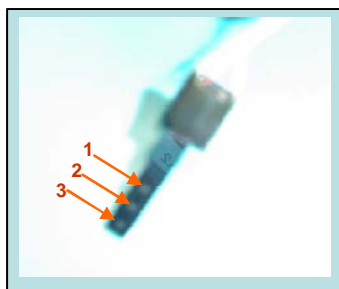
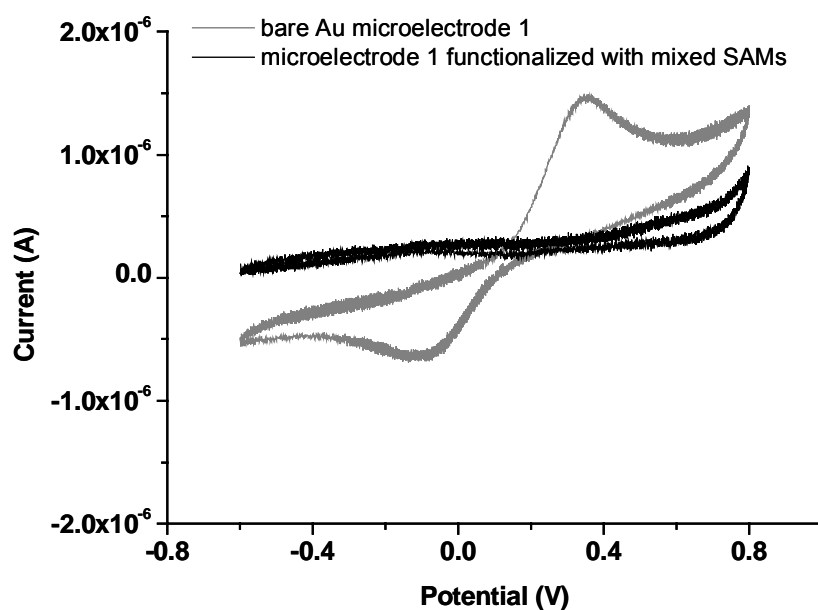


Figure VI.8: The structure of microelectrode 1.

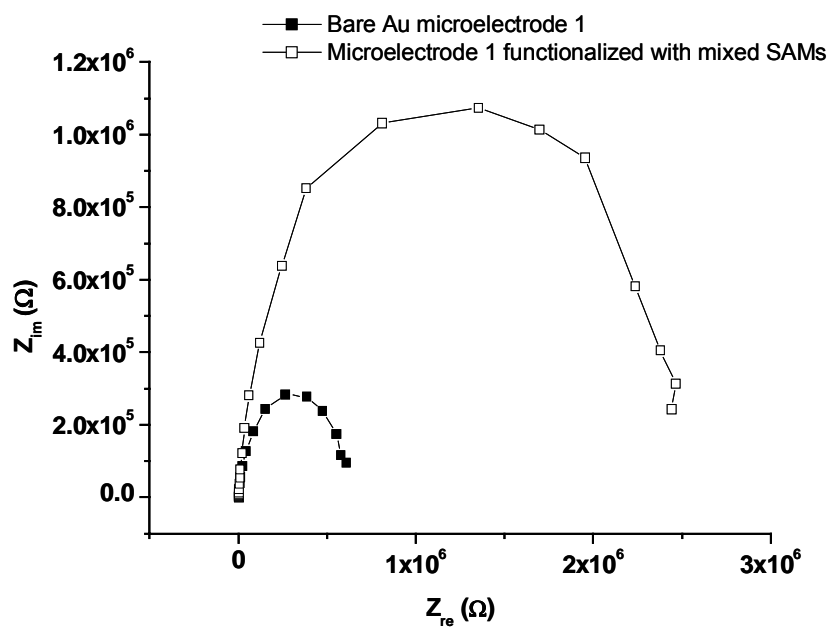
3.1.2. Electrochemical characteristics of the microelectrode 1

In the presence of the redox couple $[\text{Fe}(\text{CN})_6]^{4-/3-}$, cyclic voltammetry and impedance measurements were performed to study electrochemical properties of the microelectrode before and after functionalization with the mixed self-assembled monolayers.

We can see in Figure VI.9A that a reversible cyclic voltammogram is obtained for the bare microelectrode. With the formation of the mixed SAMs, the electron transfer kinetics of the redox probe is blocked and the amperometric response decreases. EIS measurements confirm further the formation of the mixed SAMs on the microelectrode 1, which produces a significant increase of electron transfer resistance, as shown in Figure VI.9B.



(A)



(B)

Figure VI.9: Electrochemical characteristics of the microelectrode 1 before and after functionalization with the mixed self-assembled monolayers. (A): Cyclic voltammetry, recorded in PBS solution with 4 mM $[\text{Fe}(\text{CN})_6]^{4-/3-}$. The scan rate is 50 mV s^{-1} . (B): Electrochemical impedance spectroscopy, performed at a polarization potential of 0 V/SCE.

3.2. Microelectrode 2

3.2.1. Structure of the microelectrode 2

The microelectrode 2 is composed of one gold electrode as working one with smaller surface area, and two platinum ones that can be used as counter electrodes. Semidiameter of the gold electrode is 40 μm .

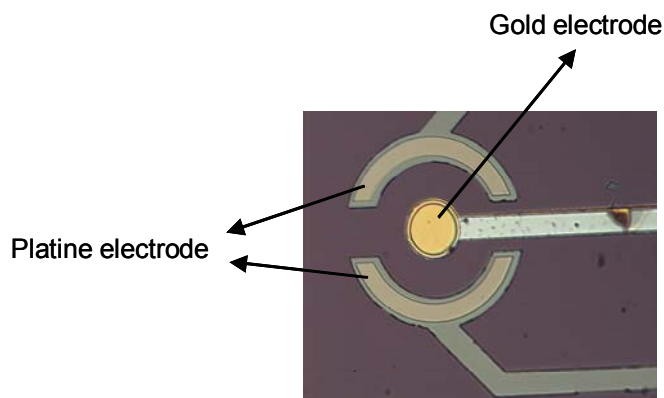


Figure VI.10: The structure of microelectrode 2.

3.2.2. Electrochemical characteristics of self-assembled multilayer formation on microelectrode 2 by EIS

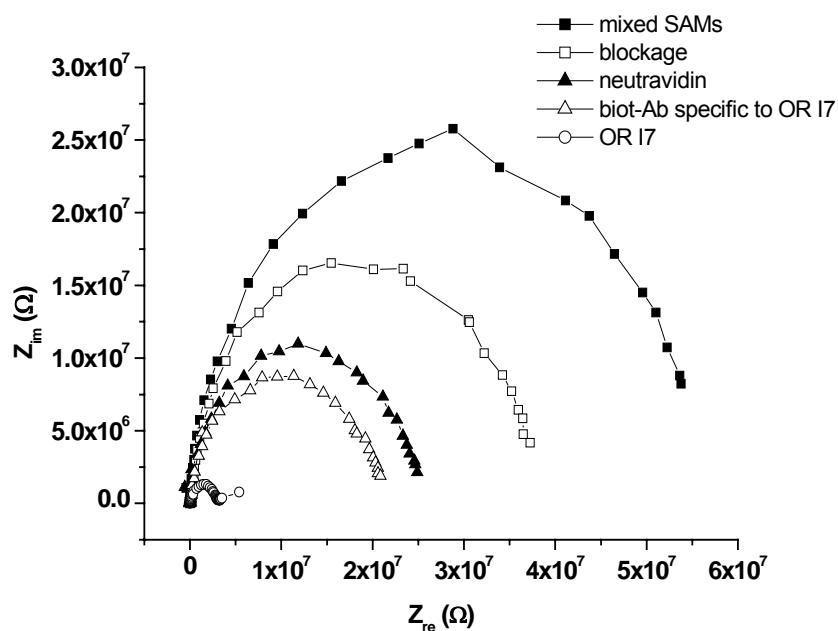


Figure VI.11: Electrochemical characteristics of self-assembled multilayer formation on the microelectrode 2 by EIS at a polarization potential of 0 V/SCE.

As the preliminary study, we investigated the layer-by-layer formation of self-assembled multilayer on the microelectrode 2 by EIS in order to validate the construction of this new microelectrode. The gold and platinum electrodes of the microelectrode were used as working and counter electrode, respectively. The Nyquist plots of impedance spectra were given in Figure VI.11. We can see that with the stepwise formation of the multilayer, the impedance decreases gradually, which is consistent with the results we have obtained with gold electrodes shown in Figure V.9.

Therefore, such a microelectrode could be used in further study for elaboration of odorant microbiosensor combining with the immobilization technique we developed. This part of work will be completed by other copartners in the project.

3.3. Conclusion

In summary, the validity of the concept that olfactory receptors can retain their activity outside their living environment has been proved. Innovative bioengineering of receptors at a molecular level can mimic the natural environment needed for them to function properly. The bioreceptor remains reactive and specific to related odorants, heptanal and octanal. In the future using a nanotechnology approach, further arraying and multiplexing of various olfactory receptors should lead to real operational artificial noses.

References:

- (1) L. Dryer, A. Berghard, *TiPS*, **1999**, 20, 413-417.
- (2) M. A. Craven, J. W. Gardner, P. N. Bartlett, *Trends in Analytical Chemistry*, **1996**, 15, 486-493.
- (3) S. Firestein, *Nature*, **2001**, 413, 211-218.
- (4) H. Zhao, L. Ivic, J. M. Otaki, M. Hashimoto, K. Mikoshiba, S. Firestein, *Science*, **1998**, 279, 237-242.
- (5) R. C. Araneda, A. D. Kini, S. Firestein, *Nature Neuroscience*, **2000**, 3, 1248-1255.
- (6) M. S. Singer, *Chem. Senses*, **2000**, 25, 155-165.
- (7) N. Vaidehi, W. B. Floriano, R. Trabanino, S. E. Hall, P. Freddolino, E. J. Choi, G. Zamanakos, W.A. Goddard III, *Proc. Natl. Acad. Sci.*, **2002**, 99, 12622-12627.
- (8) B. Malnic, J. Hirono, T. Sato, L. B. Buck, *Cell*, **1999**, 96, 713-723.
- (9) C. H. Wetzel, M. Oles, C. Wellerdieck, M. Kuczkowiak, G. Gisselmann, H. Hatt, *The Journal of Neuroscience*, **1999**, 19, 7426-7433.
- (10) G. Levasseur, M. A. Persuy, D. Grebert, J. J. Remy, R. Salesse, E. Pajot-Augy, *Eur. J. Biochem.*, **2003**, 270, 2905-2912.
- (11) L. Buck, R. Axel, *Cell*, **1991**, 65, 175-181.
- (12) M. Lu, F. Echeverri, B. D. Moyer, *Traffic*, **2003**, 4, 416-433.
- (13) H. Saito, M. Kubota, R. W. Roberts, Q. Chi, H. Matsunami, *Cell*, **2004**, 119, 679-691.
- (14) S. Katada, M. Tanaka, K. Touhara, *Journal of Neurochemistry*, **2004**, 90, 1453-1463.
- (15) K. C. Persaud, G. H. Dodd, *Nature*, **1982**, 299, 352-355.
- (16) A. P. F. Turner, N. Magan, *Nature Reviews (Microbiology)*, **2004**, 2, 161-166.
- (17) W. J. Harper, *Adv Exp Med Biol.*, **2001**, 488, 59-71.

- (18) M. Sarikaya, C. Tamerler, Alex K. Y. Jen, K. Schulten, F. Baneyx, *Nature Materials*, **2003**, 2, 577-585.
- (19) A. Bardea, E. Katz, I. Willner, *Electroanalysis*, **2000**, 12, 1097-1106.
- (20) E. Katz, I. Willner, *Electroanalysis*, **2003**, 15, 913-947.
- (21) L. Alfonta, A. Bardea, O. Khersonsky, E. Katz, I. Willner, *Biosensors and Bioelectronics*, **2001**, 16, 675-687.
- (22) C. Crasto, M. S. Singer, G. M. Shepherd, *Genome Biology*, **2001**, 2, 1027.1-1027.4.
- (23) P. Stenlund, G. J. Babcock, J. Sodroski, D. G. Myszka, *Analytical Biochemistry*, **2003**, 316, 243-250.
- (24) C. Bieri, O. P. Ernst, S. Heyse, K. P. Hofmann, H. Vogel, *Nature Biotechnology*, **1999**, 17, 1105-1108.
- (25) J. Minic, M. A. Persuy, E. Godel, J. Aioun, I. Connerton, R. Salesse, E. Pajot-Augy, *FEBS J*, **2005**, 272, 524-537.
- (26) D. S. Papermaster, *Methods Enzymol*, **1982**, 81, 48-52.
- (27) Y. Hou, S. Helali, A. Zhang, N. Jaffrezic-Renault, C. Martelet, J. Minic, T. Gorojankina, M. A. Persuy, E. Pajot-Augy, R. Salesse, F. Bessueille, J. Samitier, A. Errachid, V. Akinov, L. Reggiani, C. Pennetta, E. Alfinito, *Biosensors and Bioelectronics*, **2005**, in press.

CONCLUSION

The overall objective of the thesis was to elaborate and characterize biofilms of odorant-binding proteins and olfactory receptors on electrode for construction of olfactory micro- and nanobiosensors.

At first, with antibody IgG chosen as the bioreceptor, we have studied the mixed IgG/amphiphile LB films and the corresponding immunosensor. Under the optimal conditions (ODA as amphiphile, pH 7.3, surface target 35 mN m⁻¹ and 20 °C.), the mixed Langmuir films were quite stable at the air/water interface and were successfully transferred onto silver substrate which had been previously functionalized by the ODT SAMs. The immunosensor obtained exhibits a high sensitivity and a good specificity for the antigen in a linear dynamic range from 200 to 1000 ng ml⁻¹. These preliminary results prove that LB technique is very promising for building up biomolecular structures and developing affinity biosensors.

In the following study, LB technique was used to investigate the mixed OBP-1F/amphiphile LB films for elaboration of odorant biosensors. Under optimized conditions (pH 7.5, OBP-1F concentration of 4 mg L⁻¹, target pressure 35 mN m⁻¹), the mixed OBP-1F/amphiphile Langmuir and LB films were quite stable and well-ordered. The sensing of the obtained system for the specific odorant molecules, isoamyl acetate, was performed by AFM and non-Faradaic EIS. The efficiency of the corresponding odorant biosensor was proved by a sharp phase contrast observed with AFM and a strong decrease of resistance for LB films from 1.18 MΩ (before binding odorant) to 25 kΩ (after binding odorant) obtained with EIS.

These results showed that LB technique is suitable for elaboration of odorant biosensors. However, for G-protein coupled receptors, such as rhodopsin (in its membrane fraction), Langmuir and LB films are unstable due to its special structure and non-solubility in water.

In order to improve the stability, we have developed a new immobilization method based on a self-assembled multilayer, which is composed of a mixed self-assembled

monolayer formed by MHDA and biotinyl-PE, followed by a biotin-avidin system allowing the binding of biotinylated antibody specific to rhodopsin or olfactory receptors. By AFM we have observed grainy features on the gold electrode with size ranging from 30 to 100 nm and about 5 nm high, which correspond to rhodopsin membrane fraction. By EIS we have confirmed that rhodopsin can be immobilized efficiently, specifically, quantitatively with high stability on gold electrode by the self-assembled multilayer system with a detection limit of 10 ng ml^{-1} .

At last, we have demonstrated that the new developed immobilization method is also suitable for transferring the olfactory receptors OR 17 on the macro- and microelectrode. For the first time we performed the dose-dependent detection of OR 17 in its membrane fraction for odorant molecules by EIS. We have shown that the immobilized olfactory receptors remain reactive and specific to related odorants octanal and heptanal. In the project "SPOT-NOSED", olfactory nanobiosensors will be elaborated based on this immobilization method as soon as the nanoelectrode will be available.

A more generic immobilization technique will be developed. It will be based on the self-assembled multilayer including the biotinylated antibody specific to the tag genetically introduced to all the newly produced olfactory receptors. This way will allow the development of an array of olfactory biosensors. The electronic nose being based on this array associated with a specific signal processing and statistic data mining.

(Français)

L'objectif de ce travail était de réaliser et de caractériser des biofilms à partir des protéines spécifiques d'espèces odorantes et de récepteurs olfactifs sur électrodes pour la réalisation de micro- et nanocapteurs olfactifs.

Dans un premier temps, avec l'anticorps IgG comme biorécepteur, nous avons étudié les couches mixtes de LB composées d'IgG et d'amphiphile et l'immunocapteur correspondant. Dans des conditions optimales (amphiphile ODA, pH 7.3, pression cible 35 mN m^{-1} et $20 \text{ }^{\circ}\text{C}.$), les couches de Langmuir sont stables à l'interface air/eau, et ont été transférées avec succès sur substrat d'argent préalablement fonctionnalisé par ODT SAMs. L'immunocapteur obtenu présente une sensibilité élevée et une bonne spécificité pour l'antigène avec une gamme dynamique linéaire de 200 à 1000 ng ml^{-1} . Ces résultats préliminaires ont montré que la technique LB était prometteuse pour la fabrication de structures moléculaires et le développement de biocapteurs d'affinité.

Dans l'étude suivante, la technique LB a été utilisée avec les couches mixtes composées d'OBP-1F et d'amphiphile pour l'élaboration de biocapteurs d'odorant. Sous des conditions optimales (pH 7.5, concentration d'OBP-1F : 4 mg L^{-1} , cible pression de surface 35 mN m^{-1}), les couches de LB sont stables et bien ordonnées. L'affinité du système obtenu pour les molécules d'odorant spécifique, isoamyl acétate, a été évaluée par AFM et EIS. L'efficacité du biocapteur d'odorant correspondant a été montrée par des différences de contraste de phase en AFM et une nette diminution de la résistance des films LB passant de $1.18 \text{ M}\Omega$ (avant la mise en présence d'odorant) à $25 \text{ k}\Omega$ (après la mise en présence d'odorant) observée par EIS.

Ces résultats ont permis de montrer que la technique LB est adaptée à l'élaboration de biocapteurs olfactifs. Cependant, pour les récepteurs couplés à des protéines G comme la rhodopsine (dans sa fraction membranaire), les couches de LB ne sont pas stables en raison de son insolubilité dans l'eau et de sa structure particulière.

Afin d'améliorer la stabilité, nous avons développé une nouvelle méthode d'immobilisation basée sur une multicouche auto-assemblée, composée de monocouches auto-assemblées formées de MHDA et biotinyl-PE, suivi d'un système biotine-avidine permettant de fixer des anticorps biotinylés spécifiques à la rhodopsine ou aux récepteurs olfactifs. Nous avons observé par AFM, sur électrode d'or, des agrégats de 30 à 100 nm de largeur et d'environ 5 nm de hauteur, témoins de la présence de la rhodopsine dans sa fraction membranaire. Nous avons également confirmé par EIS que la rhodopsine peut être immobilisée de manière efficace,

spécifique, quantitative et stable sur électrode d'or, avec cette technique de multicouche auto-assemblée, avec une limite de détection de 10 ng ml^{-1} .

Pour terminer, nous avons démontré que cette nouvelle technique est également appropriée au transfert de récepteurs olfactifs OR I7 sur macro- et microélectrode. Pour la première fois, nous avons réalisé la détection des molécules d'odorant par les OR I7 (dans leur fraction membranaire) par EIS. Nous avons montré que les récepteurs immobilisés restaient réactifs et spécifiques aux odorants octanal et heptanal. Dans le cadre du projet SPOT-NOSED, les nanobiocapteurs seront élaborés suivant cette technique d'immobilisation dès que la nanoélectrode sera disponible.

Une technique d'immobilisation plus générique sera développée. Elle est basée sur la multicouche auto-assemblée incluant l'anticorps biotinylé spécifique du tag introduit génétiquement sur tous les récepteurs olfactifs qui seront produits. Cette voie permettra de préparer les nanoélectrodes pour obtenir un réseau de biocapteurs olfactifs. Le nez électronique sera basé sur ce réseau associé à un traitement du signal spécifique et un traitement statistique des données.

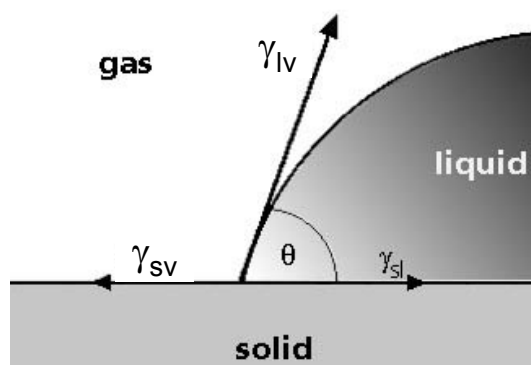
ANNEXES

ANNEXE I: CONTACT ANGLE

Contact angle measurement is a simple, rapid and sensitive method to characterize the properties of a solid surface. It is a well-known technique in many fields such as contamination control, adhesion, surface treatments, and polymer film modification.

1. Definition and principle

Contact angle θ is a quantitative measure of the wetting of a solid by a liquid. It is defined geometrically as the angle on the liquid side of the tangential line drawn through the three phase boundary where liquid, gas and solid phases intersect, or two immiscible liquids and solid phases intersect.



$\theta = 0$	complete wetting
$0 < \theta < 90^\circ$	hydrophilic
$\theta > 90^\circ$	hydrophobic

Figure A.I.1: Contact angle formation on a solid surface according to Young's equation.

The shape of the drop and the magnitude of the contact angle are controlled by three interaction forces of interfacial tension of each participating phase (gas, liquid, and solid). In an ideal situation the relation between these forces and the contact angle can be described by the Young's equation (Equation A.I.1) and contact angle is often referred to as Young's contact angle.

$$\gamma_{lv} \cos \theta = \gamma_{sv} - \gamma_{sl} \quad (\text{A.I.1})$$

Where γ_{lv} , γ_{sv} and γ_{sl} refer to the interfacial energies of the liquid/vapor, solid/vapor and solid/liquid interfaces, respectively.

However, often non-ideal conditions due to environmental, roughness and chemical heterogeneity effects lead to deviations from this relationship. Many other theoretical approaches based on the Young's equation have therefore been developed to account for these non-ideal contributions. They are not discussed here.

2. Measurement of contact angle

Two different approaches are commonly used to measure contact angles of non-porous solids, goniometry and tensiometry. Goniometry involves the observation of a sessile drop of test liquid on a solid substrate. Tensiometry involves measuring the forces of interaction as a solid is contacted with a test liquid. In this thesis, the former was used to measure the contact angle. Therefore, only goniometry is introduced here.

The basic elements of a goniometer include a light source, sample stage, lens and image capture, as shown in Figure A.I.2. Contact angle can be assessed directly by measuring the angle formed between the solid and the tangent to the drop surface. Figure A.I.3 shows a contact angle meter.

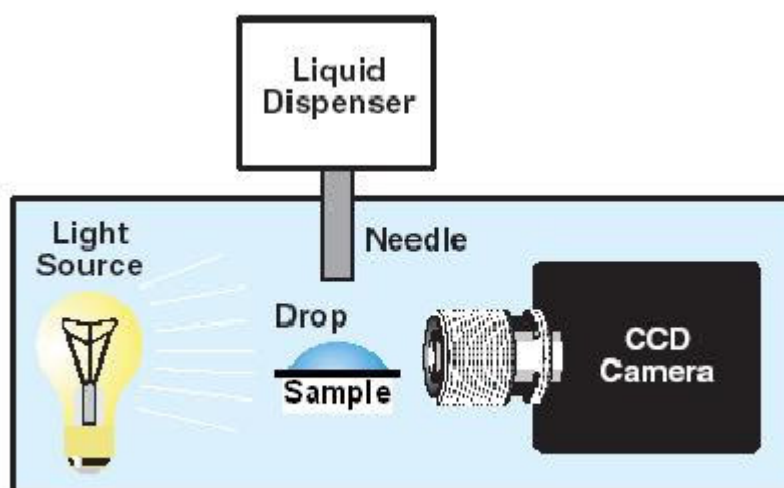


Figure A.I.2: The basic elements of a goniometer.

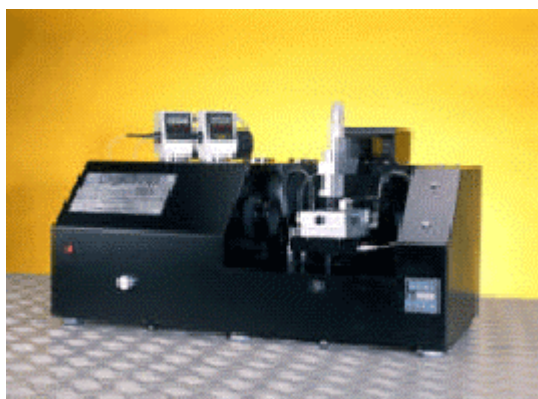


Figure A.I.3: Contact angle meter (DIGIDROP, GBX).

The shape of a drop of liquid is determined from the balance of forces, which includes the surface tension of the liquid. The surface or interfacial tension at the liquid interface can be related to the drop shape through the Equation A.I.2:

$$\gamma = \Delta\rho g R_0^2 / \beta \quad (\text{A.I.2})$$

Where γ = surface tension

$\Delta\rho$ = difference in density between fluids at interfaces

g = gravitational constant

R_0 = radius of drop curvature at apex

β = shape factor

Modern computational methods allow measurement of the surface tension for any pendant drop where the densities of the two fluids in contact are known upon the Young-Laplace equation.

Goniometry has many advantages, it can be used in many situations where tensiometry cannot. A great variety of solid substrates can be used provided that they have relatively flat portion for testing and they can fit on the stage of the instrument. Substrates with regular curvature, such as contact lenses are also easily analyzed. Testing can be done using very small quantities of liquid. Moreover, it is also easy to test high temperature liquids such as polymer melts.

However, it has also some limitations, for example, the assignment of the tangent line that will define the contact angle, is a factor which can limit the reproducibility of contact angle measurements. In addition, the amount of surface sampled for each measurement is limited and multiple measurements should be used to characterize the same surface. Fibers are not easily studied by goniometry.

ANNEXE II: ATOMIC FORCE MICROSCOPE

The atomic force microscope, invented by Binnig in 1986 (1), uses a sharp probe to magnify surface features. Compared to optical microscope, the AFM provides unambiguous measurement of step heights, independent of reflectivity differences between materials. With the AFM, it is possible to image the surface topography of an object with extremely high magnifications, up to 1,000,000 \times . Furthermore, the magnification of AFM is made in three dimensions, the horizontal X-Y plane and the vertical Z dimension.

Since its invention, AFM is being used to solve processing and materials problems in a wide range of technologies that affect the electronics, telecommunications, biological, chemical, automotive, aerospace, and energy industries. The materials being investigated include thin and thick film coatings, synthetic and biological membranes, metals, polymers, and semiconductors. (2) AFM is considered as a powerful tool for characterizing the topographic properties of the ultrathin films such as Langmuir-Blodgett films and self-assembled monolayers. (3-5)

1. The principle of AFM

The principles on how the AFM works are very simple. An atomically sharp tip is scanned over a surface with feedback mechanisms that enable the piezo-electric scanners to maintain the tip at a constant force (to obtain height information), or height (to obtain force information) above the sample surface. Tips are typically made of Si_3N_4 or Si, and extended down from the end of a cantilever. The nanoscope AFM head employs an optical detection system in which the tip is attached to the underside of a reflective cantilever. A diode laser is focused onto the back of a reflective cantilever. As the tip scans the surface of the sample, moving up and down with the contour of the surface, the laser beam is deflected off the attached cantilever into a dual element photodiode. The photodetector measures the difference in light intensities between the upper and lower photodetectors, and then converts to voltage. Feedback from the photodiode difference signal, through software control from the computer, enables the tip to maintain either a constant force or constant height above the sample. In the constant force mode the piezo-electric transducer monitors real time height deviation. In the constant height mode the deflection force on the sample is recorded. The latter mode of operation requires calibration parameters of the scanning tip to be inserted in the sensitivity of the AFM head during force calibration of the microscope.

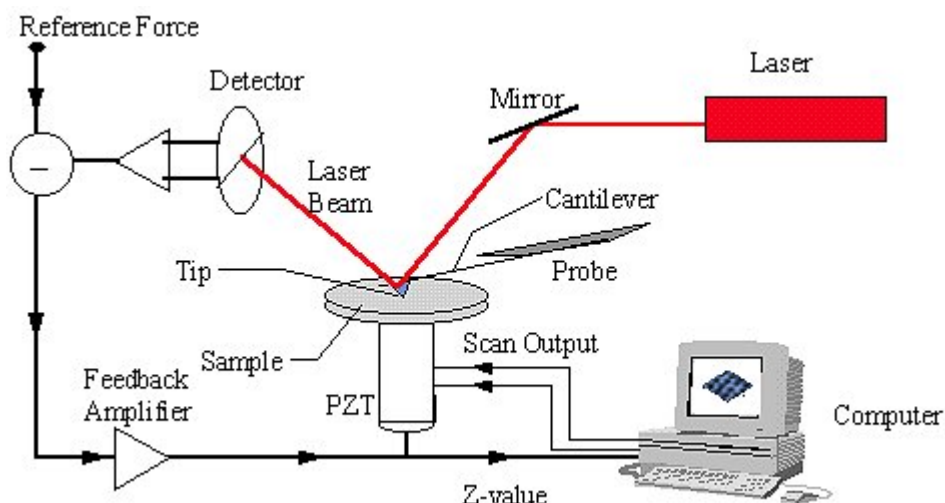


Figure A.II.1: Essential elements of atomic force microscope.

2. The common AFM modes

A number of AFM imaging modes are available for special purposes. Here three commonly used techniques, contact mode, non-contact mode and tapping mode are introduced.

2. 1. Contact mode

The contact mode, by which the tip scans the sample in close contact with the surface, is the common mode used in the force microscope. With this mode the deflection of the cantilever is sensed and compared in a DC feedback amplifier to some desired value of deflection. If the measured deflection is different from the desired value, the feedback amplifier applies a voltage to the piezo to raise or lower the sample relative to the cantilever in order to restore the desired value of deflection. The voltage that the feedback amplifier applies to the piezo is a measure of the height of features on the sample surface. It is displayed as a function of the lateral position of the sample.

By this mode, the tip is rastered over the surface while in constant contact with it. Therefore, it is more damaging for soft surfaces. Another disadvantage of this mode is the distortion of the image of the surface topography when areas of different friction coefficients are present on the surface, which induce a lateral torsion of the cantilever.

2. 2. Non-contact mode

The non-contact mode is used in situations where tip contact might alter the sample in subtle ways. With this mode the tip hovers 50 - 150 Angstrom above the sample surface. Attractive Van der Waals forces between the tip and the sample are detected, and topographic images are constructed by scanning the tip above the surface.

Unfortunately, the attractive forces from the sample are substantially weaker than the forces used by contact mode. Therefore the tip must be given a small oscillation so that AC detection methods can be used to detect the small forces between the tip and the sample by measuring the change in amplitude, phase, or frequency of the oscillating cantilever in response to force gradients from the sample.

2. 3. Tapping mode

Tapping mode is a key advance in AFM. It allows high resolution topographic imaging of sample surfaces that are easily damaged, loosely hold to their substrate, or difficult to image by other AFM techniques. Tapping mode overcomes problems associated with friction, adhesion, electrostatic forces, and other difficulties that plague conventional AFM scanning methods by alternately placing the tip in contact with the surface to provide high resolution and then lifting the tip off the surface to avoid dragging the tip across the surface.

Tapping mode inherently prevents the tip from sticking to the surface and causing damage during scanning. When the tip contacts the surface, unlike contact and non-contact modes, the high frequency (50 kHz – 500 kHz) makes the surfaces stiff (viscoelastic). Also, the surface material is not pulled sideways by shear forces since the applied force is always vertical. Another advantage of the tapping mode is its large, linear operating range. This makes the vertical feedback system highly stable, allowing routine reproducible sample measurements. In this thesis, it was used to characterize the mixed OBP/amphiphile LB films and the self-assembled multilayers for the immobilization of membrane protein including G-protein coupled receptors.

References

- (1) G. Binning, Atomic force microscope and method for imaging surface with atomic resolution, US Patent 4, **1986**, 724, 318.
- (2) <http://www.chembio.uoguelph.ca/educmat/chm729/afm/firstpag.htm>
- (3) I. Fujiwara, M. Ohnishi, J. Seto, *Langmuir*, **1992**, 9, 2219-2222.
- (4) C. Fiol, S. Alexandre, N. Delpire, J. M. Valleton, *Thin Solid Films*, **1992**, 215, 88-93.
- (5) A. Ulman, An Introduction to Ultrathin Organic Films: From Langmuir-Blodgett to Self-Assembly; Academic Press: Boston, **1991**.

ANNEXE III: SCANNING ELECTRON MICROSCOPE

An electron microscope uses a focused beam of electrons to obtain much higher magnification than that obtained with a conventional light microscope. The increase in magnification is possible because the wavelength of a high-speed electron is much lower than that of visible light, and so much higher resolution can be obtained. The scanning electron microscope is an instrument that produces an enlarged image by restering an electron beam over the sample. It has been widely used for visualization of organic surfaces, especially in the study of surface morphology, domains, pinholes and defects, and patterns.

Electron microscopes function exactly as their optical counterparts except that they use a focused beam of electrons instead of light to "image" the specimen and provide information on structure and composition of the sample.

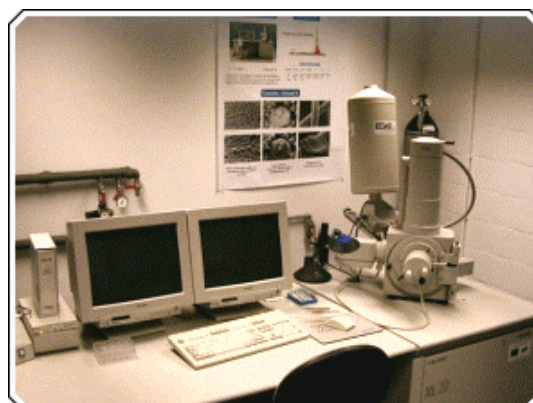
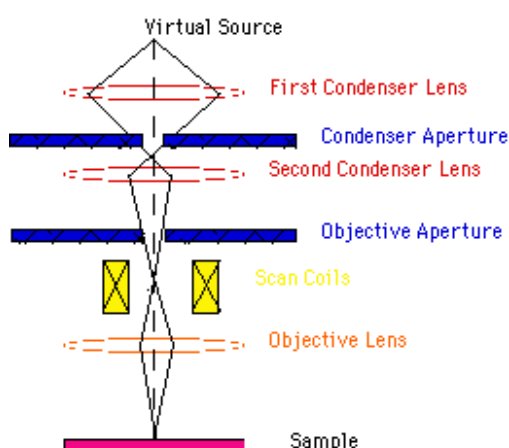


Figure A.III.1: Left: Essential elements of SEM (1); Right: An instrument of SEM (Philips XL20) (2).

As shown in the Figure A.III.1, on the left, the "virtual source" at the top represents the electron gun, producing a stream of monochromatic electrons which is accelerated towards the specimen using a positive electrical potential. This stream is confined and focused using metal apertures and magnetic lenses into a thin, focused, monochromatic beam. The electron beam is focused onto the sample using a magnetic lens and is either backscattered or ejected from the sample toward electron detectors. These detectors absorb the electrons and measure their trajectory and intensity. This data appears on a screen or photographic film as a magnified 3D image of the sample surface. The resolution far exceeds that of any light microscope, and information can also be gathered to determine the composition and microstructure of the sample.

References

- (1) <http://www.unl.edu/CMRAcfem/semoptic.htm>
- (2) <http://images.google.fr>

ANNEXE IV: LIST OF PUBLICATIONS

Yanxia Hou, Nicole Jaffrezic-Renault, Claude Martelet, Aidong Zhang, Jasmina Minic, Tatiana Gorjankina, Marie-Annick Persuy, Edith Pajot-Augy, Roland Salesse, Vladimir Akimov, Lino Reggiani, Cecilia Pennetta, Eleonora Alfinito, Oscar Ruiz, Gabriel Gomila, Josep Samitier, Abdelhamid Errachid, *A novel detection strategy for odorant molecules based on a controlled bioengineering of rat olfactory receptor 17 (OR 17)*, in preparation.

Yanxia Hou, Salwa Helali, Aidong Zhang, Nicole Jaffrezic-Renault, Claude Martelet, Jasmina Minic, Tatiana Gorjankina, Marie-Annick Persuy, Edith Pajot-Augy, Roland Salesse, Francois Bessueille, Josep Samitier, Abdelhamid Errachid, Vladimir Akinov, Lino Reggiani, Cecilia Pennetta, Eleonora Alfinito, *Immobilization of Rhodopsin on a self-assembled multilayer and its specific detection by electrochemical impedance spectroscopy*, **Biosensors and Bioelectronics**, 2005, in press.

Jasmina Minic, Jeanne Grosclaude, Josiane Aioun, Marie-Annick Persuy, Tatiana Gorjankina, Roland Salesse, Edith Pajot-Augy, Salwa Helali, **Yanxia Hou**, Nicole Jaffrezic-Renault, François Bessueille, Abdelhamid Errachid, Gabriel Gomila, Oscar Ruiz, Josep Samitier, *Immobilization of native membrane-bound rhodopsin on biosensor surfaces*, **BBA**, 2005, 1724, 324-332.

Gabriel Gomila, Ignacio Casuso, Abdelhamid Errachid, Oscar Ruiz, Edith Pajot, Jasmina Minic, Tatiana Gorjankina, Roland Salesse, Joan Bausells, Guillerilo Villanueva, **Yanxia Hou**, Nicole Jaffrezic, Cecilia Pennetta, Eleonora Alfinito, Vladimir Akimov, Lino Reggiani, Giorgio Ferrari, Laura Fumagalli, Marco Sampietro, Josep Samitier, *Artificial nose integrating biological olfactory receptors and NEMS*, 2005, in submission.

Yanxia Hou, Nicole Jaffrezic-Renault, Claude Martelet, Chaker Tlili, Aidong Zhang, Jean-Claude Pernollet, Loïc Briand, Gabriel Gomila, Abdelhamid Errachid, Josep Samitier, Ludovic Salvagnac, Benoit Torbiéro, Pierre Temple-Boyer, *Study of Langmuir and Langmuir-Blodgett films of odorant-binding protein/amphiphile for odorant biosensor*, **Langmuir**, 2005, 21, 4058-4065.

Yanxia Hou, Nicole Jaffrezic-Renault, Claude Martelet, Chaker Tlili, Aidong Zhang, *Elaboration of odorant biosensors based on Langmuir-Blodgett technique*, **Journal of Advanced Science**, 2005, 17, 49-54.

Tlili Chaker, **Yanxia Hou**, Hafsa Korri-Youssfi, Laurence Ponsonnet, Claude Martelet,

Abdelhamid Errachid, Nicole Jaffrezic-Renault, *Impedancemetric probing of mixed amphiphile-antibody films transferred onto silver electrodes*, **Sensor letters**, 2005, 2, 1-6.

Ziying Guo, Feng Feng, **Yanxia Hou**, Nicole Jaffrezic-Renault, Quantitative Determination of Zinc in Milkvech by Anodic Stripping Voltammetry with Bismuth Film Electrodes, **Talanta**, 2005, 65, 1052-1055.

Yanxia Hou, Chaker Tlili, Nicole Jaffrezic-Renault, Aidong Zhang, Claude Martelet, Laurence Ponsonnet, Abdelhamid Errachid, Josep samitier, Joan Bausells, *Study of mixed Langmuir-Blodgett films of immunoglobulin G/amphiphile and their application for immunosensor engineering*, **Biosensors and Bioelectronics**, 2004, 20, 1126-1133.

Yanxia Hou, Nicole Jaffrezic-Renault, Aidong Zhang, Jialiang Wan, Abdelhamid Errachid, Jean-Marc Chovelon, *Study of pure urease Langmuir-Blodgett film and application for biosensor development*, **Sensors and Actuators B**, 2002, 86, 143-149

Aidong Zhang, **Yanxia Hou**, Nicole Jaffrezic-Renault, Jialiang Wan, Alexey Soldatkin, Jean-Marc Chovelon, *Mixed urease/amphiphile LB films and their application for biosensor development*, **Bioelectrochemistry**, 2002, 56, 157-158.

Aidong Zhang, Nicole Jaffrezic-Renault, Jialiang Wan, **Yanxia Hou**, Jean-Marc Chovelon, *Optimization of the mixed urease/amphiphile Langmuir-Blodgett film and its application for biosensor development*, **Material Science and Engineering C**, 2002, 21, 91-96.